Thesis

Role of the Finite Replica Analysis in the Mean-Field Theory of Spin Glasses

Tomoyuki Obuchi

Department of Physics, Tokyo Institute of Technology

February, 2010

Abstract

In this thesis, we review and examine the replica method from several viewpoints. The replica method is a mathematical technique to calculate general moments of stochastic variables. This method provides a systematic way to evaluate physical quantities and becomes one of the most important tools in the theory of spin glasses and in the related discipline including information processing tasks.

In spite of the effectiveness of the replica method, it is known that several problems exist in the procedures of the method itself. The replica symmetry breaking is the central topic of those problems and is the main issue of this thesis. To elucidate this point, we first review the recent progress about the replica symmetry breaking including its physical and mathematical descriptions in detail.

Second, we accept the recent descriptions of the replica symmetry breaking and investigate the Ising perceptron, which is a model of a neuron, by intensively utilizing those descriptions, to examine the consequence of the replica symmetry breaking. Our result is consistent to the replica symmetry breaking description, but shows that the replica method cannot correctly describe the phase-space structure of this system. This is because the phase space of this system constitutes an exceptional structure which violates the usual assumption of the replica method, but it is also explained that this problem is not directly related to the replica symmetry breaking itself.

Next, without employing the replica symmetry breaking, we investigate the zeros of the averaged nth moment of the partition function with respect to the complex replica number n for the purpose of investigating the analyticity breaking of the generating function, which is related to the replica symmetry breaking, appearing in the replica procedures. For this purpose, we employ the $\pm J$ model on some tree systems and ladders. Our result implies that the zeros actually signal a certain kind of analyticity breaking, but is irrelevant to any replica symmetry breaking.

To investigate the origin of the irrelevance of zeros of the nth moment to the replica symmetry breaking, we finally study the partition function zeros with respect to the external field and temperature for the tree systems. The result shows that the two dimensional part of the zeros density continuously touches the real axis in a certain range of the objective parameters. This result implies that the invisibility of the replica symmetry breaking by the previous formulation is not due to the peculiarity of the tree systems but due to the problem of the formulation itself. Another interesting implication of the result is that it leads to the instability of the system against deviations with respect to the external field and temperature in the spin-glass phase. This is the first direct evidence that the system shows singular behavior in the spin-glass phase.

The above results reveal several aspects and problems of the replica method and contribute to underpinning this method and the mean-field theory of spin glasses, which consequently inspire future study and understanding of spin glasses and the related topics.

Acknowledgment

First of all, I would like to express my sincerest gratitude to my supervisor, Professor Hidetoshi Nishimori for his guidance, continuous encouragements and spiritual support. I also greatly acknowledge Professor Yoshiyuki Kabashima for his guidance, fruitful discussions and collaborations on my studies.

I express my gratitude to the members of the Nishimori group and the condensed matter theory group of Tokyo Institute of Technology for stimulating discussions and warm atmosphere by them. Especially, Yoshiki Matsuda kindly taught me some technical details of numerical calculations and I am particularly appreciative of him.

I also thank Doctor Antonello Scardicchio, Doctor Markus Müller, and Professor Federico Ricci-Tersenghi for fruitful discussions and kindness when I visited Italy for research collaborations. Professor Eric Vincent kindly taught me some experimental properties of spin glasses and discussed my studies. I am also grateful to him.

This work was supported by the Japan Society for the Promotion of Science (JSPS) Research Fellowship for Young Scientists program, CREST(JST), the 21th Century COE Program 'Nanometer-Scale Quantum Physics' and the Global COE Program 'Nanoscience and Quantum Physics' at Tokyo Institute of Technology, and by the Grant-in-Aid for Scientific Research on the Priority Area "Deepening and Expansion of Statistical Mechanical Informatics" by the Ministry of Education, Culture, Sports, Science and Technology. A portion of the numerical calculations have been performed on the TSUBAME Grid Cluster at the Global Scientific Information and Computing Center (GSIC), Tokyo Institute of Technology.

Finally, I thank my family for spiritual support.

Contents

1 Introduction **7**

1.1 Spin glasses 7
1.2 Mean-field theory 10
1.3 Pure state and its implications 11
1.3.1 A simple introduction to the concept of pure states 11
1.3.2 Relations between pure states and dynamical behaviors 12
1.3.3 Hierarchical structure of pure states in the mean-field model 13
1.3.4 Experimental supports of the hierarchical structure 17
1.3.5 The mean-field theory and more 19
1.4 The replica method 20
1.5 Overview of thesis 22

2 Review of the replica method and its interpretations **25**

2.1 Replica calculations for the fully-connected p-spin interacting model 25
2.1.1 Replica symmetric ansatz 27
2.2 The solution in the limit $p \to \infty$ 29
2.2.1 Failure of the RS solution 29
2.2.2 Microcanonical approach 29
2.3 Replica symmetry breaking 32
2.3.1 The 1RSB solution for the p-spin interacting model 33
2.3.2 The 1RSB solution in the $p \to \infty$ limit 34
2.4 Pure state statistics of the 1RSB level 35
2.4.1 Pure states of the limit $p \to \infty$ 37
2.5 Viewpoint from the large deviation theory 39
2.5.1 Re-derivation of the 1RSB transition 40
2.6 Finite p cases 43
2.6.1 de Almeida-Thouless instability 43
2.6.2 Phase diagrams for the $p = 2, 3$ cases 49
2.7 Microscopic description of pure states 51
2.7.1 TAP method 51
2.7.2 Zero temperature limit 53
2.8 Summary 54

3 Analyses of weight space structure and rare events in the Ising perceptron 55
3.1 Model . . . 56
3.2 Formalism . . . 57
3.2.1 The replica symmetric solution . . . 58
3.2.2 The 1RSB solution . . . 59
3.2.3 The complexity and 1RSB formulation revisited . . . 61
3.3 Theoretical predictions . . . 64
3.3.1 Complexity for $\alpha < \alpha_{\rm s} = 0.833\ldots$ . . . 64
3.3.2 Rate function for $\alpha > \alpha_{\rm s} = 0.833\ldots$ and a transition at $\alpha_{\rm GD} = 1.245\ldots$ . . . 65
3.3.3 Phase diagram on the n-α plane . . . 67
3.4 Numerical validation . . . 68
3.5 Summary . . . 72

4 The replica zeros of $\pm J$ Ising spin glass at zero temperature 74
4.1 Fundamental knowledge about models and formulations . . . 75
4.1.1 Definition of the Cayley tree and the properties . . . 75
4.1.2 Bulk properties of Cayley trees . . . 78
4.1.3 Zeros and singularities . . . 80
4.1.4 Energetic zero-temperature limit for replica zeros . . . 81
4.2 General formula for ladders and Cayley trees . . . 82
4.2.1 The cavity method . . . 82
4.2.2 Use of the replica method . . . 84
4.2.3 Energetic zero-temperature limit in the cavity recursions . . . 86
4.2.4 Uniqueness of the analytic continuation . . . 89
4.3 Results for the ladders . . . 89
4.4 Results for the CTs . . . 91
4.4.1 Plots of the replica zeros for CTs . . . 91
4.4.2 The thermodynamic limit and phase transitions of BLs . . . 92
4.4.3 Possibility of the full-step replica symmetry breaking . . . 98
4.4.4 Physical implications of the obtained solutions . . . 101
4.5 RZs for RRGs . . . 102
4.6 Summary . . . 102

5 The replica symmetry breaking and the partition function zeros for Bethe lattice spin glasses 104
5.1 Phase boundaries and critical properties of Bethe lattice spin glasses . . . 105
5.2 Formulations . . . 107
5.2.1 The partition function zeros of Bethe lattices . . . 107
5.2.2 Population method to evaluate the CFD . . . 109
5.2.3 Numerical procedures . . . 111

5.3 Result . . . 112
5.3.1 Zeros on the complex field plane . . . 112
5.3.2 Zeros on the complex temperature plane . . . 114
5.3.3 Phase diagram . . . 115
5.3.4 The divergence of the spin-glass susceptibility . . . 116
5.4 Summary . . . 118

6 Conclusion **120**

A Calculations for chapter 3 **124**
A.1 Derivation of the RS saddle-point equations and the limit $q \to 1$. . . . 124
A.2 Derivation of the AT condition . . . 125
A.2.1 AT instability of the RS2 solution . . . 129

B Calculations for chapter 4 **131**
B.1 Derivation of the generating function $\phi(n)$ and free energy of regular random graphs . . . 131
B.2 Location of replica zeros of the width-2 ladder . . . 135
B.3 Rate function for a CT with $c = 3$ . . . 137
B.4 AT condition for the $(k, c) = (2, 3)$ Bethe lattice . . . 137

C Calculations for chapter 5 **141**
C.1 Divergence point of the spin-glass susceptibility at zero temperature . . . 141

Chapter 1

Introduction

Random spin systems are one of the major research subjects in statistical physics. The spatial randomness of conflicting interactions introduces random frustration into the system. The frustration can produce many metastable states and the system becomes affected by such states. If the structure of the metastable states is highly complex, the system shows strange behaviors like the extraordinary susceptibility against external fields, the extremely slow dynamics, and so on. Spin systems with such behaviors are called spin glasses.

At present time, one of the most important progresses of the theory of spin glasses is its mean-field description. The mean-field theory is constructed by several mathematical tools. The replica method is one of the most powerful tools and the main purpose of this thesis is to review and examine this method. Because of the intricacy of the replica theory, there still remain many problems in the theory itself. We review recent progress about this topic and provide some new approaches to reveal the mysteries related to the replica method. Before going into the details, we start with reviewing histories and topics on spin glasses and related subjects.

1.1 Spin glasses

A simple description of spin glasses is by its low temperature state. For ferro and anti-ferro magnets, the low temperature states are uniform or periodic, but those of spin glasses are spatially disordered and frozen ones. The existence of such states usually needs two requirements; one is the existence of competing interactions among spins which leads to no single configuration favored by all the interactions (this is called the frustration). Second is the spatial randomness of the interactions, which is necessary for disordered configurations stable at low temperatures.

Experimentally, materials satisfying the above two requirements are found in several alloys consisting of noble metals (Au, Ag, Cu, etc.) weakly diluted with transition metals (Fe, Mn, etc.). Interactions between the moments of the impurity atoms (spins) effectively appear through the interactions with the conducting electrons. The effective interaction

is called the RKKY interaction [1, 2]

$$J_{ij} \propto \frac{1}{r_{ij}^3} \cos(2k_F r_{ij}), \tag{1.1}$$

where r_{ij} is the distance between two impurity atoms and k_F is the Fermi wave number. The RKKY interaction takes both positive and negative values of J_{ij} due to randomness in the position of impurities and random frustration is introduced between the localized spins.

One of the important problems is how to characterize these disordered frozen states. To characterize a ferromagnetic state, the averaged magnetization $m = (\sum_i \langle S_i \rangle)/N$ is sufficient, where the brackets $\langle \cdots \rangle$ denote the thermal average over the Boltzmann factor $\exp(-\beta \mathscr{H})$ and i denotes the site index, and β is the inverse temperature $\beta = 1/T$, where we put the Boltzmann constant to unity $k_B = 1$. Meanwhile, to precisely describe the disordered frozen states, more detailed information about the local spontaneous magnetization $m_i = \langle S_i \rangle$ is required. If the spin-glass phase exists, the characteristic property that spins randomly freeze should be reflected in that phase. The local magnetization $m_i = \langle S_i \rangle$ is expected to take a non-zero value in such a situation but the sign is randomly distributed from site to site, which implies that the global magnetization vanishes $m = (\sum_i \langle S_i \rangle)/N = 0$. Hence, to detect the spin-glass ordering, the square value of the local magnetization m_i^2 is useful. This speculation leads to an order parameter q defined as

$$q = \frac{1}{N} \sum_i m_i^2. \tag{1.2}$$

This quantity q was first introduced by Edwards and Anderson [3] and is called the spin-glass order parameter. The disordered frozen phase at low temperatures is called the spin-glass phase and is characterized by $m = 0, q > 0$, while the paramagnetic phase has $m = q = 0$ and the ferromagnetic phase is characterized by $m, q > 0$.

In a ferromagnet, the ferromagnetic phase transition is accompanied by a rapid increase of the spin-correlation length which diverges at the critical temperature. This can be observed in the divergence of the linear susceptibility χ

$$\frac{\chi}{\beta} = \frac{\partial m(H)}{\partial(\beta H)} = \frac{1}{N} \sum_{i,j} \frac{\partial m_i}{\partial(\beta h_j)} = \frac{1}{N} \sum_{i,j} \left(\langle S_i S_j \rangle - \langle S_i \rangle \langle S_j \rangle \right) = \frac{1}{N} \sum_{i,j} \chi_{ij}, \tag{1.3}$$

where h_j denotes the local field applied to the site j. For the spin-glass problem we can also expect a similar phenomenon coming from the spin-glass ordering, but the simple spin-correlation function χ_{ij} does not show the long range correlation because of the frustration. Instead, the square of χ_{ij} can diverge at the critical temperature of the spin-glass ordering, which leads to the spin-glass susceptibility χ_{SG} the definition of which is given by

$$\chi_{SG} = \frac{1}{N} \sum_{i,j} (\chi_{ij})^2 = \frac{1}{N} \sum_{i,j} \left(\frac{\partial m_i}{\partial(\beta h_j)} \right)^2 = \frac{1}{N} \sum_{i,j} \left(\langle S_i S_j \rangle - \langle S_i \rangle \langle S_j \rangle \right)^2. \tag{1.4}$$

Although the spin-glass susceptibility χ_{SG} is a suitable quantity to detect the spin-glass ordering, it cannot be directly observed in experiments. A more tractable quantity in experiments is the nonlinear susceptibility whose definition and the relation with χ_{SG} is given as

$$\chi_{\rm nl} \equiv -\left.\frac{\partial^3 m(H)}{\partial H^3}\right|_{H=0} = \beta^3 \left(\chi_{SG} - \frac{2}{3}\right), \tag{1.5}$$

where H is the uniform external field. This equation shows that the divergence of χ_{SG} also leads to the divergence of $\chi_{\rm nl}$. For example, a plot of $\chi_{\rm nl}$ for AuFe near the transition point is given in fig. 1.1.

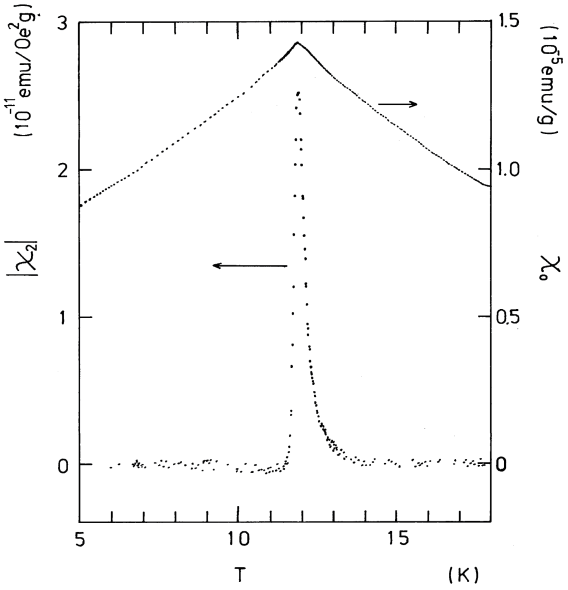

Figure 1.1: Temperature dependence of the linear $\chi_0 = (\partial m/\partial H)|_{H=0}$ and nonlinear $\chi_2 = \chi_{\rm nl}$ susceptibilities for AuFe (1.5-at. % Fe). A cusp and divergence are observed in χ_0 and χ_2, respectively, at a critical temperature T_c. From [4].

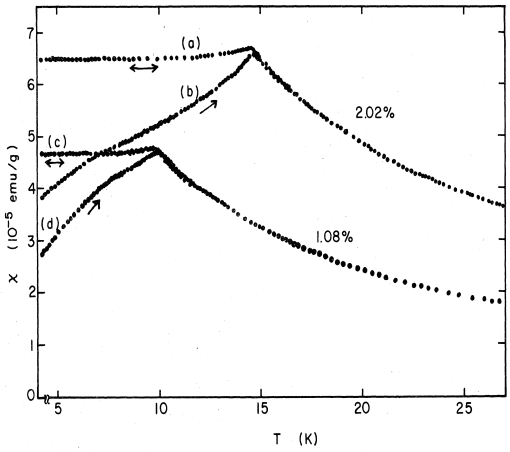

Figure 1.2: Linear susceptibility χ of CuMn vs temperature for 1.08-, 2.02-at. % Mn. After zero-field cooling ($H < 0.05$G), the susceptibilities in a field $H = 5.90$G (b) and (d) increase as the temperature grows, while the susceptibilities (a) and (c) in the field $H = 5.90$G, which applied above the critical temperature T_c before cooling, are almost constants. From [5].

Another characteristic property of spin glasses is the strong hysteresis phenomena. We depict an example of the linear susceptibility of CuMn alloys in fig. 1.2. To obtain this figure, the linear susceptibility was observed in two different situations. One is the so-called zero-field cooling. In this situation, the system is first cooled down below the critical temperature T_c in the absence of the external field. After that, a constant field ($H = 5.90$G in this experiment) is applied and the linear susceptibility is observed at several temperatures with increasing temperature. The other is the field cooling, in which a constant field ($H = 5.90$G) is applied to the system above T_c and the linear susceptibility is observed at several temperatures with decreasing temperature. Figure 1.2 shows clear differences in those two situations, which implies the ergodicity breaking of the spin-glass system at low temperatures. The ergodicity breaking means that the system cannot

explore all the states and the state of the system even after a long time depends on the initial condition. Once the spin-glass transition occurs, the ergodicity breaks and the system shows the strong dependence on the initial condition, which can be observed in the hysteresis of the linear susceptibility as fig. 1.2. This interesting behavior of spin glasses strongly motivated the researchers in the 1970-80's, and theoretical interpretations were intensively explored. In the next section, we will briefly see the mean-field description of spin glasses.

1.2 Mean-field theory

In the previous section, we have seen some concepts and quantities to characterize the spin-glass behaviors, and some experimental observations were provided. The next step for understanding spin glasses is to define a model of spin glasses to deal with the problem in theoretical ways. The so-called EA model introduced by Edwards and Anderson [3] is the first model of spin glasses. In this model, the interactions are introduced between the nearest neighbor spins and are assumed to be the random variables drawn from an identical independent distribution. The EA Hamiltonian takes the following form

$$\mathscr{H} = -\sum_{\langle i,j \rangle} J_{ij} S_i S_j, \tag{1.6}$$

where S denotes an Ising variable and J_{ij} is the random interaction. The symbol $\langle i, j \rangle$ means that the summation runs over all the pairs of neighboring spins. Edwards and Anderson solved this model within a mean-field scheme, but the detailed properties were unclear. Then, to investigate the EA model in more detail, Sherrington and Kirkpatrick introduced the infinite-range version of the EA model, which is called the SK model [6]. The SK Hamiltonian is

$$\mathscr{H} = -\sum_{i<j} J_{ij} S_i S_j, \tag{1.7}$$

where the summation runs over all pairs. The SK model is more tractable than the EA model because all the spins are fully connected and are symmetric. By analyses of the SK model, it was shown that a second order phase transition occurs and the spin-glass phase appears at a finite temperature T_c. In the SK model, the cusp of the linear susceptibility and the divergence of the spin-glass susceptibility are observed, and some aging phenomena are also confirmed by some analytical and numerical results [7–9]. Because of this good agreement with experimental results, it is considered that the mean-field model extracts some essence of spin-glass behaviors and nowadays the SK model is regarded as a standard model of spin glasses.

An especially remarkable property of the SK model is the coexistence of a huge number of thermodynamical states. These states are called "pure states" and the properties are considered as the essence of the mean-field description of spin glasses. In the next section, the notion of pure states and some related properties are explained.

1.3 Pure state and its implications

1.3.1 A simple introduction to the concept of pure states

A pure state is a somewhat abstract concept and represents a certain unit of the state of the system in the thermodynamic limit. To explain this concept, let us first review a pure ferromagnetic system as an example. In a ferromagnetic system, there are two possible thermodynamic states at low temperatures. The first one is the state for which the magnetization is positive, and for the other one the magnetization is negative. If there is no element favoring one of signs of the magnetization (i.e. boundary condition, magnetic field etc.), the partition function of the system includes both contributions equally and we can express this statement symbolically

$$Z = Z_+ + Z-,\ (Z_+ = Z_-), \tag{1.8}$$

where Z_+ is the summation of $e^{-\beta H}$ over the spin configurations for which the magnetization is positive, and similarly for Z_-. However, when a perturbation favoring a direction of the magnetization is applied to the system, e.g. the positive magnetic field, the value of Z_+ exceeds Z_-. This difference becomes larger and larger in the thermodynamic limit even when the magnetic field is a positive infinitesimal, and the partition function converges to

$$Z \to Z_+. \tag{1.9}$$

If the magnetic field is negative, the partition function Z converges to Z_-. These facts indicate that there are two distinguishable states in the thermodynamic limit. These distinguishable states are the 'pure states', and the number of pure states for this system is two.

Meanwhile, the present mean-field theory of spin glasses, which was mainly constructed by Sherrington and Kirkpatrick [6] and solved by Parisi [12, 13], tells that the number of pure states of spin glasses increases exponentially as the system size grows. Let us assume that an index γ denotes a pure state and the corresponding partition function is expressed by Z_γ. Each pure state has its own free energy $f_\gamma = -T \log Z_\gamma$. In the large system limit $N \to \infty$, the mean-field description tells us that the number of pure states with the free energy value f, $\mathscr{N}(f)$, is scaled as

$$\mathscr{N}(f) = \sum_\gamma \delta(f - f_\gamma) \sim e^{N\Sigma(f)}, \tag{1.10}$$

where the characteristic exponent $\Sigma(f)$ is called the 'complexity' or 'configurational entropy'. For the ferromagnetic case, the unbiased partition function (1.8) includes two pure states, Z_+ and Z_-, and both of them give the same value of the free energy. For spin-glass systems, however, each pure state can yield a different value of the free energy. From a naive speculation of thermodynamics, it seems that the actual system prefers the lowest free energy state than the other states with higher values of free energy, but it is not the case. A reasonable explanation to this fact is to remember that each pure state

cannot access each other because of infinitely high free energy barrier. This is the same situation as in the ferromagnetic case. Thus, when the system is once stuck in a pure state, the system never reaches other pure states without external forces. In the statistical mechanical model, all of such states are included in the partition function, and both the free energy value and the number of pure states are important. For general spin-glass systems, using eq. (1.10), we can write the partition function as

$$Z = \sum_{\gamma} Z_{\gamma} = \sum_{\gamma} e^{-N\beta f_{\gamma}} = \int df \mathcal{N}(f) e^{-N\beta f} \sim \int df e^{N(-\beta f + \Sigma(f))}. \tag{1.11}$$

This equation indicates that the equilibrium value of free energy $-\beta f_{\rm eq} = \lim_{N\to\infty} \log Z/N$ is equal to the saddle point value $\max_f\{-\beta f + \Sigma(f)\}$. This relation is quite similar to the conventional microcanonical one $-\beta f = \max_u\{-\beta u + s(u)\}$, where u is the internal energy and $s(u)$ is the corresponding entropy, and implies that the complexity $\Sigma(f)$ plays the role as the effective 'entropy' for the 'internal' free energy f.

Before ending this subsection, we note that the notion of the pure state is different from that of the metastable state. Intuitively, metastable states are simply local minima of the free energy in the phase space. The system with many metastable states shows the slow dynamics at low temperatures but it ultimately relaxes to its equilibrium state because the metastable states are not completely separated by free energy barriers and can be accessed each other in a sufficiently long term. On the other hand, pure states are also minima but they are separated by infinitely high free energy barriers. The system with many pure states also shows slow relaxation but never reaches its equilibrium state due to those infinitely high free energy barriers. Hence, pure states are very stable in comparison with simple metastable states, and the discrimination of pure and metastable states is the key concept of the mean-field theory of spin glasses.

However, when we perform real and numerical experiments, we can only treat finite size systems in a finite time scale. This leads to a difficulty in identifying the origin of the slow dynamics of spin glasses, because the phase spaces are never completely separated in finite size systems and the observation in a finite time scale cannot reject the possibility that the observed slow dynamics is due to the shortness of the observing time. Hence, we cannot easily distinguish pure and metastable states. This difficulty is an essential problem for studying spin glasses. To support the mean-field description, we should examine more detailed properties predicted from the mean-field theory. In the following subsections, we present some numerical and real experiments supporting the mean-field description.

1.3.2 Relations between pure states and dynamical behaviors

Existence of many pure states directly explains the ergodicity breaking of spin glasses. At high temperatures, the system has only one pure state and the system relaxes to the pure state without depending on the initial state. Below the critical temperature, however, the system goes into the spin-glass phase and many pure states appear. Since each pure state

has different properties (order parameters) and is separated by infinitely high free energy barriers, once the system is stuck in one of the pure states, properties of the system is determined only by that state and the system never reaches other states without external perturbations.

This description can be examined by some numerical experiments for the theoretical models of spin glasses. We here elucidate a simple example of such experiments. To this end, let us consider an annealing experiment of glassy and non-glassy spin systems. Such numerical experiments are called simulated annealing. The actual procedures are as follows:

1. Set the temperature so high that the system is in the equilibrium state.
2. Decrease the temperature to zero gradually.
3. Observe the energy of the system at zero temperature.

When the decreasing rate v_c is too large, the system cannot follow the equilibrium state and cannot reach the ground state at zero temperature. On the other hand, if the decreasing rate v_c is sufficiently small, we can find that a typical non-glassy spin system is always in the equilibrium state and finally reaches the ground state at zero temperature. For a typical spin-glass system, however, this procedure does not work and the system cannot reach the ground state. In an idealized situation (the system is infinitely large), this is the case even in the slow cooling limit $v_c \to 0$. An important point is that we can qualitatively predict the value of the energy which the spin-glass system takes in the slow cooling limit $v_c \to 0$, by accepting the description of pure states. For the typical spin-glass system, the complexity $\Sigma(f)$ takes finite values in a range $f_- \leq f \leq f_+$, and can be assessed in the statistical mechanical framework without any considerations about the dynamics. In the zero temperature limit, contributions from entropy vanish and the complexity becomes a function of the energy u, $\Sigma(u)$, defined in a range $u_- \leq u \leq u_+$. The typical functional form of $\Sigma(u)$ is given in fig. 1.3. As in fig. 1.3, the complexity usually takes its maximum at the maximum of the energy range, which means that it is highly possible that the system is trapped by the pure states with the energy u_+. Actually, for the annealing experiments conducted in some infinite range models, it is observed that the energy which the system finally takes is equal to u_+ as in fig. 1.4 [10,11]. This accordance in the qualitative level between the analysis of pure states and the dynamical behavior in annealing experiments strongly supports the validation of the present mean-field theory of spin glasses in a certain kind of spin-glass models.

1.3.3 Hierarchical structure of pure states in the mean-field model

A fact that many pure states coexist in a system also implies that the values of a certain kind of order parameters can vary from sample to sample of materials, or from trial to trial of experiments. To precisely explain this matter, let us consider a situation that we

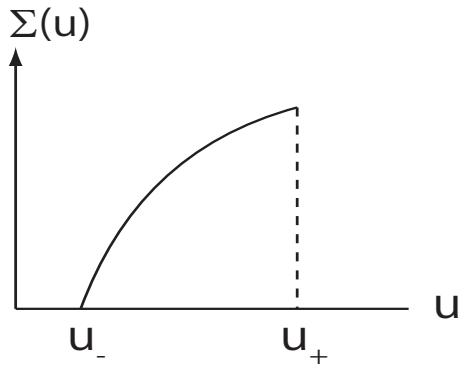

Figure 1.3: The complexity at zero temperature for the typical spin-glass system. The complexity $\Sigma(u)$ takes the maximum at the highest energy u_+, which implies that the pure states at u_+ dominate the dynamical behavior of the system.

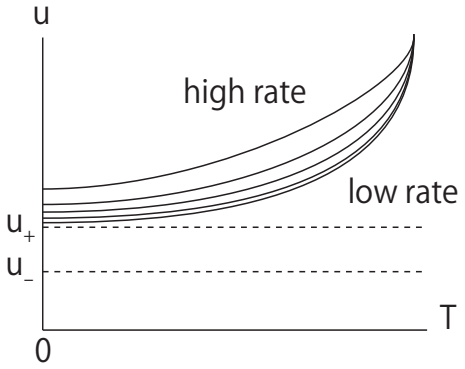

Figure 1.4: Schematic diagram of the internal energy for a temperature range in the simulated annealing. The actual ground-state energy is given by u_- but the system cannot reach the state, since many pure states with higher energies exist. Consequently, in decreasing the cooling rate v_c, the energy seems to converge the highest energy u_+ where pure states exist.

have two replicated spin-glass systems, where these systems share the same interactions $\{J_{ij}\}$ but the states of spins independently vary, and compare the behaviors of these systems. This situation is unfeasible in real experiments but is easily realizable in numerical experiments. In this situation, the following quantity, which observes the mutual overlap between the two replicated systems labeled by (1) and (2), becomes important for revealing the emergence of many pure states

$$q^{12} = \frac{1}{N}\sum_{i}^{N} S_i^{(1)} S_i^{(2)}, \tag{1.12}$$

where $S_i^{(k)}$ denotes the ith spin of the system (k). If there is only one pure state, the systems (1) and (2) are in the same pure state at equilibrium and q^{12} always takes the value independent of the initial conditions and trials of experiments. Hence, the typical distribution of q^{12}, $P(q) = [\langle\delta(q - q^{12})\rangle]_{\boldsymbol{J}}$ where the brackets $[\cdots]_{\boldsymbol{J}}$ denote the average over the random interactions $\boldsymbol{J}$ and are called the configurational average, shows a delta function $P(q) = \delta(q - q_0)$ with a certain average value q_0. However, if there are many pure states, each system will be trapped in a different state since the dynamics of the systems (1) and (2) are independent each other. Hence, q^{12} takes a different value at every experiment and the distribution $P(q)$ becomes a broad function. Interestingly, this $P(q)$ can be analytically assessed in the mean-field theory [12, 13] and the schematic diagram of $P(q)$ is presented in fig. 1.5. Of course, the distribution $P(q)$ can also be assessed in numerical experiments and we refer to a numerical result in fig. 1.6. The correspondence between the analytical and numerical results is good and this fact justifies the present mean-field solution for the SK model.

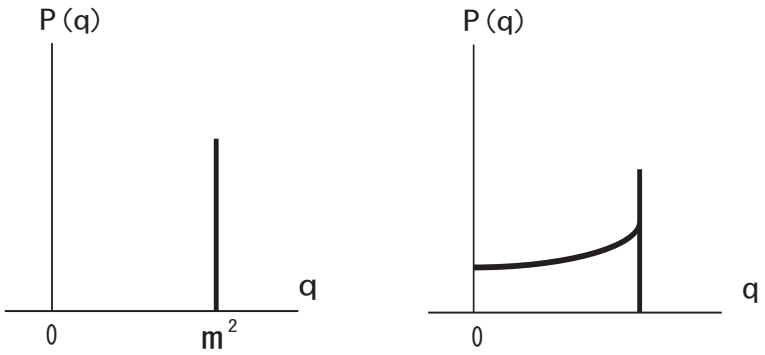

Figure 1.5: Schematic diagram of $P(q)$ for normal ferromagnetic systems (left) and the SK model (right).

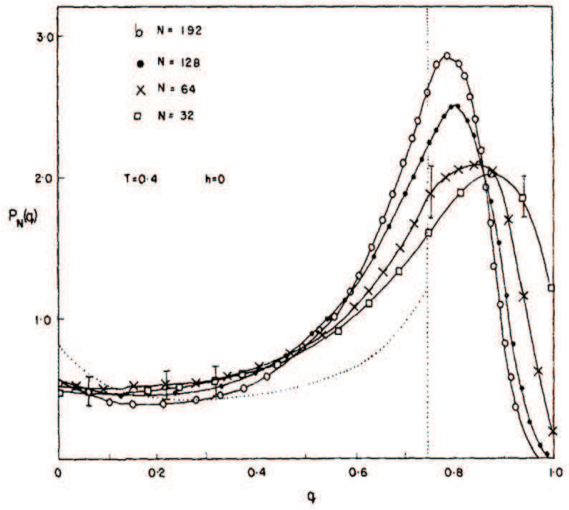

Figure 1.6: The distribution of spin-glass order parameter $P_N(q)$ for finite N of the SK model with $T = 0.4$ and zero external field $h = 0$. The dotted line is the analytical prediction given in [12, 13]. From [14].

The broad $P(q)$ implies that the overlap between two pure states α and β, i.e. $q^{\alpha\beta} = (1/N)\sum_i \langle S_i\rangle_\alpha \langle S_i\rangle_\beta$ where $\langle(\cdots)\rangle_\alpha = (1/Z_\alpha)\,\mathrm{Tr}_\alpha(\cdots)e^{-\beta H}$ denotes the thermal average over the pure state α, takes different values depending on the selection of two pure states. The mean-field theory can provide not only the behavior of $P(q)$ but also some useful information of the structure of the pure states. Let us consider a three-point probability distribution $P(q_1, q_2, q_3)$, which represents a joint probability of the overlaps between three arbitrary pure states; for three arbitrary pure states α, β and γ, $P(q_1, q_2, q_3)$ represents the probability that their mutual overlaps $q^{\alpha\beta}, q^{\alpha\gamma}$ and $q^{\beta\gamma}$ take the values q_1, q_2 and q_3:

$$P(q_1, q_2, q_3) = \left[\sum_{\alpha,\beta,\gamma} \omega_\alpha\omega_\beta\omega_\gamma \delta(q_1 - q^{\alpha\beta})\delta(q_2 - q^{\alpha\gamma})\delta(q_3 - q^{\beta\gamma})\right]_{\boldsymbol{J}} \tag{1.13}$$

where ω_α denotes the probability weight of the pure state α. In the mean-field solution of the SK model, it is known that this distribution shows a characteristic behavior

$$\begin{aligned} P(q_1, q_2, q_3) &= \frac{1}{2}P(q_1)x(q_1)\delta(q_1 - q_2)\delta(q_1 - q_3) \\ &+\frac{1}{2}\left\{P(q_1)P(q_2)\Theta(q_1 - q_2)\delta(q_2 - q_3) + (\text{two terms with } 1,2,3 \text{ permuted})\right\} \end{aligned} \tag{1.14}$$

where $x(q) = \int_0^q dq' P(q')$ and $\Theta(x)$ is the step function which takes $\Theta(x) = 1$ for $x > 0$ and $\Theta(x) = 0$ otherwise. The first term on the right hand side is non-vanishing only if the three overlaps are equal to each other, and the second term requires that the overlaps be the edges of an isosceles triangle ($q_1 > q_2, q_2 = q_3$). This means that the distances between three pure states should form either equilateral or isosceles triangles. This property is called the ultrametricity, and the ultrametricity implies that the pure states consist a hierarchical structure as in fig. 1.7.

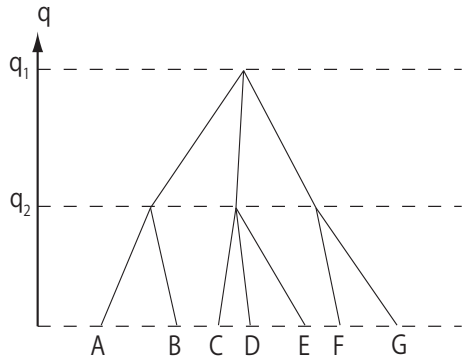

Figure 1.7: A schematic diagram of the hierarchical structure in the space of pure states labeled by A-G. The distance between C and D equals q_2 being equal to that between C and E and to that D and E, which is smaller than q_1 being equal to that between A and C and to that C and F. This hierarchical structure satisfies the ultrametricity.

The ultrametricity seems to be highly mathematical and to have no useful information about real experiments. However, there are some experiments indicating that real spin

glasses have hidden hierarchical structures in the phase space. Next, we present some examples of such experiments.

1.3.4 Experimental supports of the hierarchical structure

Two characteristic effects are observed in spin-glass materials. One is the 'rejuvenation' effect and the other is the 'memory' effect. These are considered to be the evidence that the states of real spin glasses constitute the hierarchical structures in their phase spaces. We here give a simple explanation about these two effects.

Consider an experimental situation that a small *ac* field is applied to a spin-glass material. The magnetic *ac* response is observed. If the *ac* response is delayed, the susceptibility has two components; an in-phase one χ' and an out-of-phase one χ''. This out-of-phase χ'' is zero in the paramagnetic phase but becomes finite in the spin-glass phase and relaxes slowly as fig. 1.8, which signals the aging of the system.

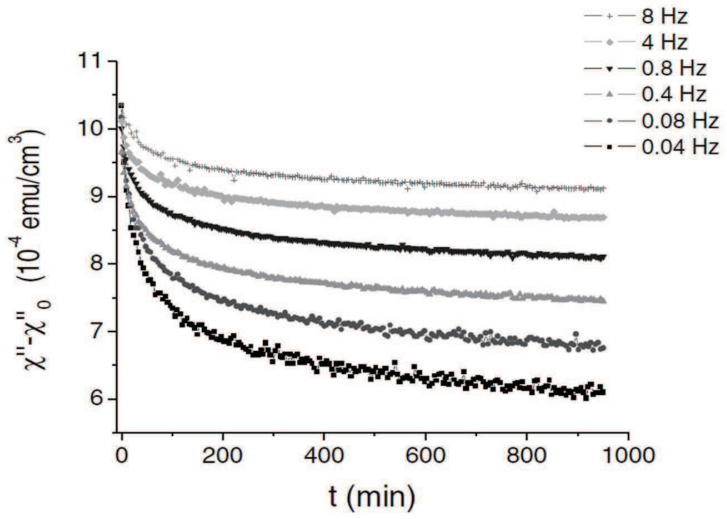

Figure 1.8: Relaxation of the out-of phase susceptibility χ'' of $CdCr_{1.7}In_{0.3}S_4$ for different frequencies. The curves are shifted vertically by an amount χ''_0 for the sake of clarity. From [15].

In the above experiment, we can change the temperature and observe the response of the system. Figure 1.9 shows the behavior of χ'' in a cycle of temperature; the temperature is kept a constant $T = 12\text{K} < T_c$ for $t_1 = 350\text{min}.$. During in the aging, the temperature is suddenly decreased from 12 to 10K and kept at $T = 10\text{K}$ for $t_2 = 350\text{min}.$, and the temperature is increased to the initial temperature $T = 12\text{K}$ and χ'' is observed for $t_3 = 350\text{min}.$. This figure 1.9 clearly shows two extraordinary behaviors. One is that the relaxation of χ'' shows a sudden jump when the temperature is decreased, which implies that the aging restarts from a 'younger state'. This is the rejuvenation effect. The other is the continuity of the two separated curves at $T = 12\text{K}$, although the system has

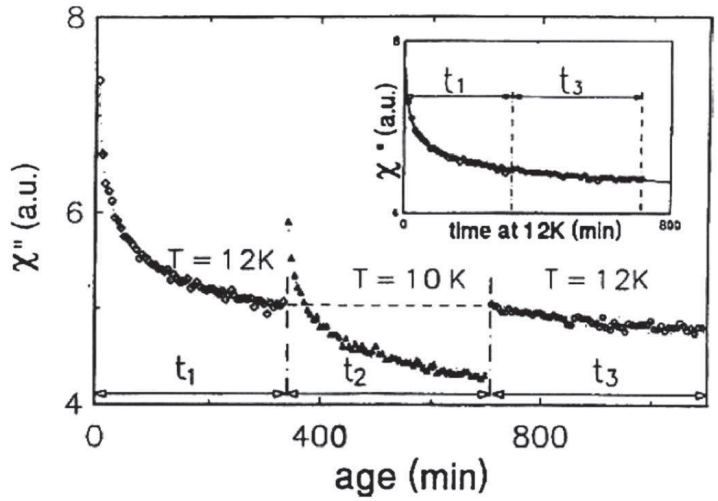

Figure 1.9: Relaxation of the out-of phase susceptibility χ'' (frequency 0.01 Hz) of $CdCr_{1.7}In_{0.3}S_4$ during the temperature cycle given in the text. The rejuvenation effect occurs at the point where the temperature is suddenly changed from $T = 12$K to 10K, and the memory effect is observed at $T = 12$K, despite of the rejuvenation at 10K. The inset is the jointed figure of both parts of 12K, which clearly shows the memory effect. From [16].

experienced the rejuvenation along the way. This phenomenon indicates that the spin glass has held the perfect memory about the past state at $T = 12$K. This is the memory effect.

These phenomena are characteristic behaviors of spin glasses, and can be interpreted by assuming that the metastable states of a spin glass constitute a hierarchical structure. This structure splits into many states as the temperature decreases and becomes more and more complicated as fig. 1.10. According to this description, the rejuvenation effect occurs as the result of splitting of the metastable states when the temperature decreases. Decreasing temperature produces new more stable states by splitting the space of the states and the system restarts relaxing to those stable states. On the other hand, the memory effect is due to the vanishing of the metastable states by increasing temperature. The states which the system explores at a low temperature are integrated into the same state when the temperature increases. This means that the process of the system at the low temperature does not influence the state at the high temperature, which causes the memory effect of the temperature. This hierarchical structure of the metastable states is considered to be related to the hierarchical structure of pure states in the mean-field theory.

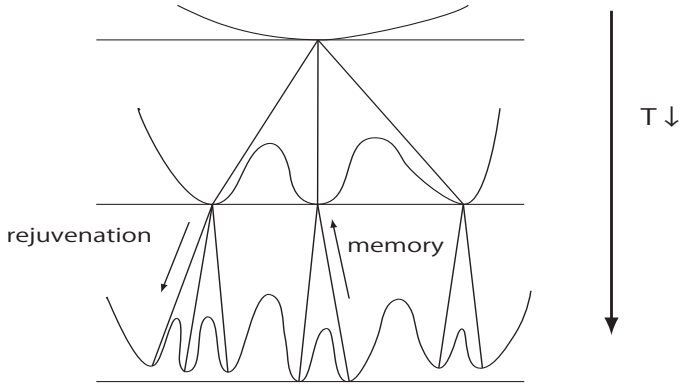

Figure 1.10: Schematic picture of the hierarchical structure of the metastable states of a spin glass

1.3.5 The mean-field theory and more

In the previous subsections, we have seen some evidence supporting the mean-field theory of spin glasses. In addition, a recent mathematical study [17] shows that the mean-field solution constructed by Parisi [12,13] is rigorous for the SK model. These facts constitute the firm foundation of the mean-field description of spin glasses.

At this point, there are some ways to proceed with the spin glass theory further.

One way is to go beyond the mean-field theory. Treating more realistic models, e.g. finite dimensional systems or systems with correlated interactions $\{J_{ij}\}$ etc., is a naive one to better understand real spin-glass systems. However, in spite of the success of the SK model, direct knowledge on finite-dimensional spin glasses or correlated systems is yet limited. Analytical approaches in finite dimensions are rather difficult and many researches rely on numerical calculations. However, even numerical approaches often do not work well for spin glasses because of the slow dynamics at and below the critical temperature. Frustrated systems like spin glasses often have many metastable states, and these metastable states prevent the system from relaxing to the equilibrium states, which means that the correct sampling of equilibrium states for frustrated systems at low temperatures often fails. Although the spin-glass transition of the SK model is definitely the equilibrium one and the phase space splits into many pure states at the transition point, the numerical simulations cannot identify the appearance of the pure states as the origin of the slow dynamics. Consequently, we do not have sufficient theoretical descriptions of finite dimensional spin glasses and there are some different arguments about their low-temperature behaviors [18–20]. These are very important and interesting problems, but we do not treat them in this thesis.

Another way is to refine the mean-field theory of spin glasses and to apply it to other subjects. Actually, in the last two decades, the spin-glass theory has been applied to many subjects and compared with other approaches in different disciplines [21]. The notion of pure states can be generalized to other problems and many research areas are included in the scope of the mean-field theory of spin glasses. For example, structural glasses [22],

super-cooled liquids [23], information processing tasks [24, 25] and so on. Especially, a statistical mechanical approach based on the spin-glass theory to the information tasks has provided many fruitful results which influence not only the informatics but also the spin-glass theory itself.

As the basis of such interdisciplinary researches, the mean-field theory of spin glasses provides some useful concepts and mathematical tools. The replica method is the most powerful one of such tools. Expressing in a simple term, we can identify the replica method as a mathematical technique to calculate the averaged quantities which are hard to assess by other usual methods. Many problems can be treated in a unified way in the framework of the replica method [24]. On the other hand, in spite of many successes of the replica method, the mathematical foundation and the physical interpretation of this method still have some mysterious parts. Such mysteries of the replica method are the main subject of this thesis. Next, we briefly explain the basic concept of the replica method and how it is used in actual situations, and eventually state the objective of this thesis.

1.4 The replica method

For the study of spin-glass models, the exchange interactions $\boldsymbol{J}$ between spins should be treated as the random variables. There are some ways to treat the randomness based on the time scales of the spins and the exchange interactions. The time scale of spins are determined by how often the spin flipping occurs in the system, while the time scale of the exchange interactions is dominated by the spatial motion of the atoms (impurities in alloys). If time scales of spins and interactions are almost the same, we should take both the averaging simultaneously. This situation is called the annealed case. The annealed partition function becomes

$$Z_{\text{anne}} = \left[\operatorname*{Tr}_{\boldsymbol{S}} e^{-\beta \mathscr{H}(\boldsymbol{S},\boldsymbol{J})} \right]_{\boldsymbol{J}}, \tag{1.15}$$

where $\operatorname{Tr}_{\boldsymbol{S}}$ means the summation over the spins. The angular brackets $[\cdots]_{\boldsymbol{J}}$ denote the average over the random interactions $\boldsymbol{J}$ and are called the configurational average. Some frustrated systems like spin glasses are, however, not correctly described by the annealed average, because the frustration is relaxed by motions of the atoms. To correctly describe spin glass behaviors, we must consider a situation that the time scale of spins is drastically shorter than that of interactions. This situation is called the quenched case, in which the interactions are fixed as constants, and the partition function becomes

$$Z(\boldsymbol{J}) = \operatorname*{Tr}_{S} e^{-\beta \mathscr{H}(\boldsymbol{S}|\boldsymbol{J})}. \tag{1.16}$$

In quenched systems, we should treat the partition function leaving the random variable dependence $\boldsymbol{J}$, but this treatment is quite difficult. For a class of quantities, however, the values of the quantities depending on random variables converge to the averaged values with the probability 1 in the large system size limit $N \to \infty$. These quantities are called

the self-averaging quantities, and an important point is that the free energy is also one of such quantities. Accordingly, we just calculate the averaged free energy f as

$$-\beta f = \lim_{N\to\infty}\left[\frac{1}{N}\log Z(\boldsymbol{J})\right]_{\boldsymbol{J}}. \tag{1.17}$$

Assessing eq. (1.17) is, however, seriously difficult. The replica method is employed to overcome this difficulty. To precisely state the details, we here define the generating function $\phi(n)$ as

$$\phi_N(n) = \frac{1}{N}\log[(Z(\boldsymbol{J}))^n]_{\boldsymbol{J}}, \tag{1.18}$$

$$\phi(n) = \lim_{N\to\infty}\phi_N(n). \tag{1.19}$$

The basic idea of the replica method is the following identity expressed in terms of $\phi_N(n)$ as

$$-\beta f = \lim_{N\to\infty}\frac{1}{N}[\log Z(\boldsymbol{J})]_{\boldsymbol{J}} = \lim_{N\to\infty}\lim_{n\to 0}\frac{\partial}{\partial n}\phi_N(n). \tag{1.20}$$

Thanks to this identity, the average of the logarithm $[\log Z(\boldsymbol{J})]_{\boldsymbol{J}}$ is replaced by the average of the nth moment $[Z^n]_{\boldsymbol{J}}$. Unfortunately, assessing the average $[Z^n]_{\boldsymbol{J}}$ for general $n \in \mathbb{R}$ is still difficult. To avoid this difficulty, the replica method additionally performs the following procedures;

- The asymptotic behavior of $[(Z(\boldsymbol{J}))^n]_{\boldsymbol{J}}$ in the limit $N \to \infty$ is calculated for natural numbers $n = 1, 2, \cdots \in \mathbb{N}$ by using some analytical techniques like the saddle-point method.

- The obtained solution of $[(Z(\boldsymbol{J}))^n]_{\boldsymbol{J}}$ for $n \in \mathbb{N}$ is extended to $n \in \mathbb{R}$ by using their analytical continuation.

The first step is necessary because the direct assessment of $[(Z(\boldsymbol{J}))^n]_{\boldsymbol{J}}$ is unfeasible even for $n \in \mathbb{N}$, and the second one is inevitable to take the $n \to 0$ limit.

The procedures of the replica method mentioned above are necessary but appear rather mysterious. Actually, these procedures cause two possible problems:

1. The uniqueness of the analytical continuation from natural to real numbers. Even if all the moments of $[(Z(\boldsymbol{J}))^n]_{\boldsymbol{J}}$ are given for $n \in \mathbb{N}$, it is impossible to uniquely continue the analytical expressions for $n \in \mathbb{N}$ to $n \in \mathbb{R}$ (or $\mathbb{C}$).

2. The analyticity breaking of $\phi(n) = \lim_{N\to\infty}\phi_N(n)$. In general, even if $\phi_N(n)$ is analytic with respect to n for finite N, the analyticity of $\phi(n) = \lim_{N\to\infty}\phi_N(n)$ can be broken.

Especially, the second problem is essentially related to the complex behavior of spin glasses. It is known that the analyticity breaking with respect to n actually occurs in some spin-glass models and such analyticity breaking relates to the replica symmetry breaking (RSB). Nowadays, we have some prescriptions to handle the RSB and we can

obtain a correct solution, which is proposed by Parisi in 1979 [12,13], even though the RSB occurs. Unfortunately, however, the Parisi solution requires some mysterious procedures in the evaluation of the free energy, and its full comprehension is not still obtained.

The subject of this thesis is to investigate the problems related to the RSB from some perspectives. We have mainly two results; one is about the interpretation of the RSB. The RSB is considered to correspond to the emergence of many pure states. We reexamine this description by treating a specific model and resolve some new aspects of the replica method. Second is a proposition of a new method to detect the RSB as singularities with respect to n. This method is based on the Lee-Yang description of phase transitions [26] and is applicable to any singularities with respect to n. Our results will be useful for supporting the correctness of the replica method and making the meaning of the RSB clearer.

1.5 Overview of thesis

In this thesis, we treat the problems related to the replica method and the RSB. Some considerations and new methods are proposed to reveal the mysteries of the RSB.

To state the problem precisely, we introduce the replica method with a detailed explanation in the next chapter. Its practical applications are also presented by treating some typical models. To reconsider the replica result from a microscopic viewpoint, we also present the so-called TAP equation [27]. This method reproduces the replica result and is useful to understand the microscopic properties of pure states.

In chapter 3, we reexamine recent progresses about the replica method. Particular ingredients of the progresses are summarized as follows:

1. Relationship between the generating function $\phi(n)$ and the probability $P(f)$ that the free energy $-\log Z/N\beta$ takes a value f.

2. Connection with complex structures of phase spaces (pure states) and a formalism of the RSB.

To extensively investigate these two statements, we concentrate on the investigation of the Ising perceptron [24] by using the replica method with the RSB. The Ising perceptron is a model of a neuron which generates a map from $\mathbb{R}^N$ to $\{+1, -1\}$, and is characterized by the value of ratio $\alpha = M/N$, where M is the number of random patterns stored in the perceptron. The reason why we treat this model is that the meaning of complexity for the perceptrons of finite size is clearer than that for other systems. For the fully connected models, including the Ising perceptrons, a pure state at zero temperature can be identified with a stable cluster, the detailed definition of which will be given in the same chapter, with respect to single spin flips [28, 29]. For samples of small systems, the size of the clusters can be numerically evaluated by exhaustive enumeration without any ambiguity. This property is extremely useful for justifying theoretical predictions through numerical experiments. Investigating the Ising perceptron analytically and numerically, we have

found that the replica method cannot correctly detect the phase-space structure of the Ising perceptron, which is due to the strange distribution of the cluster size. This also affects the probability distribution of the free energy $P(f)$ and the replica method cannot correctly calculate $P(f)$ in a certain region. The origin of this failure is also explained in the same chapter.

In chapter 4, apart from the notion of pure states, we concentrate on the analyticity of $\phi(n)$ with respect to the replica number n. For this purpose, we propose a new scheme based on the Lee-Yang theory about phase transitions [26]. In particular, we observe zeros with respect to n of the averaged nth moment $[Z^n] = 0$. In terms of the analyticity, the RSB can be regarded as an analyticity breaking of $\phi(n)$. This motivates us to observe the zeros of $[Z^n]$ to obtain useful information about the RSB. To investigate these zeros, we treat some tractable systems, i.e. the $\pm J$ models with a symmetric distribution on two types of lattices, ladder systems and Cayley trees with random fields on the boundary. There are two reasons for using these models: Firstly, these models can be investigated in a feasible computational time by the cavity method [30,31]. Especially, at zero temperature this approach gives a simple iterative formula to yield the partition function. Employing the replica method and the cavity method, we can perform symbolic calculations of the nth moment of the partition function $[Z^n]$, which enables us to directly solve the equation of the objective zeros $[Z^n] = 0$. The second reason is the existence of the spin-glass phase. It is known that the spin-glass phase is present for Cayley trees [32–35] and is absent for ladder systems. Therefore, we can compare the behavior of the zeros, which are considered to be dependent on the spin-glass ordering. Our results indicate that the zeros approach the real axis of n for some Cayley trees but not for ladder systems, which seems to be consistent with the presence and absence of spin glass ordering. However, further investigations reveal that the singularities speculated from the zeros of Cayley trees are not related to the RSB. This topic is quite complicated and the details are given in the main texts of chapter 4. We also discuss a general possibility that the zeros of $[Z^n]$ with respect to n cannot examine the full-step RSB, but this argument has some uncertainties and we cannot give a reliable conclusion. To investigate this point futher, we also examine the zeros of $[Z^n]$ with respect to n for the so-called regular random graph. The regular random graph is locally similar to the Cayley tree, which enables us to treat this system in a manner similar to the Cayley tree in the large system limit, but has some global loops, which introduce nontrivial correlations into the system and is considered to lead to the RSB at low temperatures. However, any appealing result cannot be obtained by this investigation because of the computational difficulty for assessing $[Z^n]$ of the regular random graph. The RSB is still a great mystery both from mathematical and physical points of view.

To remove some ambiguities of the discussions given in chapter 4, we tackle the RSB by investigating some tree-like systems in another way in chapter 5. In this chapter, we observe the zeros of the partition function with respect to the external field H and temperature T for the $\pm J$ model on Bethe lattices. A Bethe lattice is an interior part of the infinitely-large Cayley tree and shares similar properties to those of the Cayley tree.

The result shows that an extraordinary response to deviations of the external field and temperature exists for spin glasses on Bethe lattices, which is often identified with the RSB and implies the existence of the RSB in these models. This observation supports our previous discussion that the zeros of $[Z^n]$ with respect to n cannot detect the full-step RSB, which means that we need some modifications to obtain information about the RSB from the zeros with respect to n. Investigation along this line is an important future work.

The last chapter is devoted to a conclusion of this thesis.

Chapter 2

Review of the replica method and its interpretations

In this chapter, we review the replica method in detail. This method requires some complicated and mysterious prescriptions in the calculations. Hence, the meaning of the mathematical manipulations and physical interpretations have been examined from various perspectives for a long time. Our review in this chapter includes the recent progress in this point. In particular, a relation between the replica symmetry breaking and pure state statistics, and a relation with the large deviation theory, are quite important for the interpretations of the replica method. We will explain these topics by demonstrating the actual calculations for some typical models.

2.1 Replica calculations for the fully-connected p-spin interacting model

The SK model presented in the previous chapter is the basic model of spin glasses. This model has long-range interactions and each spin is connected to all the other spins. This property is useful for the exact treatment of the model because all the spins are symmetric and can be equally treated. The detailed analyses of the SK model developed many useful concepts and analytical tools, and eventually provided a comprehensive view of spin glasses.

When investigating spin systems, we only treat the two-spin interactions usually. This is because the interactions between the nearest neighboring spins are considered to be sufficient to capture the behavior of many physical systems. Actually, the SK model also has only the two-spin interactions. However, to demonstrate the replica method, we here treat the fully-connected p-spin interacting model as an example. The reason is the following:

1. The SK model ($p = 2$) is naturally included.

2. It is known that there are qualitatively different phase transitions for $p \geq 3$.

3. A particular limit ($p \to \infty$) makes the analysis easier, which is suitable for the demonstration of the replica method.

Thus, we hereafter concentrate on the analysis of the fully-connected p-spin interacting model. The Hamiltonian of this system can be written as

$$\mathscr{H}(\boldsymbol{S}|\boldsymbol{J}) = -\sum_{i_1<\ldots<i_p} J_{i_1\ldots i_p} S_{i_1}\ldots S_{i_p}, \tag{2.1}$$

where i is the site index and S is the Ising spin variable. The interaction $J_{i_1\ldots i_p}$ is a quenched random variable, the distribution function of which is given by

$$P(J_{i_1\ldots i_p}) = \left(\frac{N^{p-1}}{J^2\pi p!}\right)^{\frac{1}{2}} \exp\left\{-\frac{N^{p-1}}{J^2 p!}\left(J_{i_1\ldots i_p}\right)^2\right\}. \tag{2.2}$$

We adopt appropriate normalizations N^{p-1} and $p!$. This is because the physical quantities should be appropriately scaled, e.g. the average of the Hamiltonian is extensive, in the limits $N \to \infty$ and $p \to \infty$ which we will take afterward. If we set $p = 2$, this model is reduced to the SK model. Following the prescription of the replica method, we calculate the generating function $\phi(n) = \lim_{N\to\infty}(\log[Z^n]_{\boldsymbol{J}})/N$. Assuming $n \in \mathbb{N}$, the nth moment of the partition function can be assessed as

$$\begin{aligned}[Z^n]_{\boldsymbol{J}} &= \int \prod_{i_1<\ldots<i_p} dJ_{i_1\ldots i_p} P(J_{i_1\ldots i_p}) Z^n = \mathrm{Tr}\exp\left\{\frac{\beta^2 J^2 p!}{4N^{p-1}} \sum_{i_1<\ldots<i_p}\left(\sum_{\mu=1}^{n} S_{i_1}^{\mu}\ldots S_{i_p}^{\mu}\right)^2\right\} \\ &= \mathrm{Tr}\exp\left\{\frac{\beta^2 J^2 N}{2}\sum_{\mu<\nu}\left(\frac{1}{N}\sum_i S_i^{\mu} S_i^{\nu}\right)^p + \frac{1}{4}\beta^2 J^2 N n\right\},\end{aligned} \tag{2.3}$$

where the symbol Tr denotes the trace over all the spins and μ and ν represent the replica indices. In deriving the final expression in eq. (2.3), we have used the following relation

$$\frac{1}{N^{p-1}}\sum_{i_1<\ldots<i_p} S_{i_1}\ldots S_{i_p} = \frac{N}{p!}\left(\frac{1}{N}\sum_i S_i\right)^p + O(N^0), \tag{2.4}$$

and left only the leading term. It is convenient to introduce the variables

$$q^{\mu\nu} = \frac{1}{N}\sum_i S_i^{\mu} S_i^{\nu} = \frac{\boldsymbol{S}^{\mu}\cdot\boldsymbol{S}^{\nu}}{N}. \tag{2.5}$$

to replace the spin product terms $\sum_i S_i^{\mu} S_i^{\nu}/N$ in eq. (2.3). We treat $q^{\mu\nu}$ as a dummy integrating variable and use delta functions $\delta\left(\boldsymbol{S}^{\mu}\cdot\boldsymbol{S}^{\nu} - Nq^{\mu\nu}\right)$ to satisfy the constraint (2.5). We also use the Fourier-transformed expression of the delta function

$$\delta\left(\boldsymbol{S}^{\mu}\cdot\boldsymbol{S}^{\nu} - Nq^{\mu\nu}\right) = \int_{-\mathrm{i}\infty}^{+\mathrm{i}\infty}\frac{d\widehat{q}^{\mu\nu}}{2\pi}\exp\left(\widehat{q}^{\mu\nu}(\boldsymbol{S}^{\mu}\cdot\boldsymbol{S}^{\nu} - Nq^{\mu\nu})\right). \tag{2.6}$$

Substituting these expressions, we rewrite eq. (2.3) as

$$[Z^n]_{\boldsymbol{J}} = \mathrm{Tr} \int \prod_{\mu<\nu} dq^{\mu\nu} d\widehat{q}^{\mu\nu} \exp\left\{ \frac{\beta^2 J^2 N}{2} \sum_{\mu<\nu} (q^{\mu\nu})^p - N \sum_{\mu<\nu} q^{\mu\nu}\widehat{q}^{\mu\nu} + \sum_{\mu<\nu} \widehat{q}^{\mu\nu} \left(\sum_i S_i^\mu S_i^\nu \right) + \frac{1}{4}\beta^2 J^2 N n \right\}. \tag{2.7}$$

The spin trace can now be independently taken at each i

$$\mathrm{Tr}\, e^{\sum_{\mu<\nu} \widehat{q}^{\mu\nu} \left(\sum_i S_i^\mu S_i^\nu\right)} = \left(\mathrm{Tr}\, e^{\sum_{\mu<\nu} \widehat{q}^{\mu\nu} S^\mu S^\nu} \right)^N = \exp\left\{ N \log \mathrm{Tr}\, e^{\sum_{\mu<\nu} \widehat{q}^{\mu\nu} S^\mu S^\nu} \right\}. \tag{2.8}$$

Using the saddle point method, we obtain the generating function $\phi(n) = \lim_{N\to\infty} \log[Z^n]_{\boldsymbol{J}}/N$ for $n \in \mathbb{N}$ as

$$\phi(n) = \underset{q^{\mu\nu}, \widehat{q}^{\mu\nu}}{\mathrm{Extr}} \left\{ \frac{\beta^2 J^2}{2} \sum_{\mu<\nu} (q^{\mu\nu})^p - \sum_{\mu<\nu} q^{\mu\nu}\widehat{q}^{\mu\nu} + \frac{1}{4}\beta^2 J^2 n + \log \mathrm{Tr}\, e^{\sum_{\mu<\nu} \widehat{q}^{\mu\nu} S^\mu S^\nu} \right\}, \tag{2.9}$$

where the symbol Extr_x represents to take the extremization with respect to x. The extremization condition yields

$$q^{\mu\nu} = \frac{\mathrm{Tr}\, S^\mu S^\nu e^{\sum_{\mu<\nu} \widehat{q}^{\mu\nu} S^\mu S^\nu}}{\mathrm{Tr}\, e^{\sum_{\mu<\nu} \widehat{q}^{\mu\nu} S^\mu S^\nu}}, \ \widehat{q}^{\mu\nu} = \frac{1}{2} p \beta^2 J^2 (q^{\mu\nu})^{p-1}. \tag{2.10}$$

Taking this extremization condition is, however, quite difficult in the general form. Hence, we need some ansatz to reduce this extremization problem to a tractable one.

2.1.1 Replica symmetric ansatz

To proceed further, we are required to determine the explicit dependence of $q^{\mu\nu}$ on the replica indices μ and ν at the saddle point. For $n \in \mathbb{N}$, an equality $[\langle S_i^\mu S_i^\nu \rangle_n]_{\boldsymbol{J}} = [\langle S_i^\gamma S_i^\omega \rangle_n]_{\boldsymbol{J}}$, where $\langle \cdots \rangle_n$ denotes the average over the replicated Boltzmann factor $e^{-\beta \sum_\mu \mathscr{H}(\boldsymbol{S}^\mu|\boldsymbol{J})}$, holds for any different combinations of replicas ($\mu \neq \nu$ and $\gamma \neq \omega$), which is due to the permutation symmetry of $\sum_\mu \mathscr{H}(\boldsymbol{S}^\mu|\boldsymbol{J})$ with respect to the replica indices. This observation naturally leads to an ansatz that the saddle point of eq. (2.9) has also the same symmetry, which is the so-called replica symmetry (RS). Under the RS, the order parameter matrix $q^{\mu\nu}$ becomes

$$q^{\mu\nu} = q, \ \widehat{q}^{\mu\nu} = \widehat{q}, \tag{2.11}$$

and the physical meaning of $q^{\mu\nu}$ is easily understood. To see this, we note that eq. (2.10) can be written as

$$q^{\mu\nu} = [\langle S_i^\mu S_i^\nu \rangle_n]_{\boldsymbol{J}}, \tag{2.12}$$

which is almost clear from the definition of $q^{\mu\nu}$ (2.5). In the RS ansatz, each replica is independent and equivalent, which means that the contributions from replicas $\gamma \neq \mu, \nu$

are canceled out and the averaged quantity belonging to different replicas gives the same value

$$q^{\mu\nu} = [\langle S_i^\mu S_i^\nu \rangle_n]_{\boldsymbol{J}} = \left[\frac{\mathrm{Tr}\, S_i^\mu e^{-\beta\mathscr{H}(\boldsymbol{S}^\mu|\boldsymbol{J})}}{\mathrm{Tr}\, e^{-\beta\mathscr{H}(\boldsymbol{S}^\mu|\boldsymbol{J})}} \frac{\mathrm{Tr}\, S_i^\nu e^{-\beta\mathscr{H}(\boldsymbol{S}^\nu|\boldsymbol{J})}}{\mathrm{Tr}\, e^{-\beta\mathscr{H}(\boldsymbol{S}^\nu|\boldsymbol{J})}} \right]_{\boldsymbol{J}} = [\langle S_i \rangle^2], \tag{2.13}$$

which is the spin-glass order parameter explained in chapter 1.

Using the RS, we can easily calculate the terms in eq. (2.9) to derive

$$\sum_{\mu<\nu} q^{\mu\nu}\widehat{q}^{\mu\nu} = \frac{1}{2}n(n-1)\widehat{q}q, \tag{2.14}$$

$$\mathrm{Tr}\, e^{\sum_{\mu<\nu}\widehat{q}^{\mu\nu}S^\mu S^\nu} = \mathrm{Tr}\, e^{\widehat{q}/2\left\{\left(\sum_\mu S^\mu\right)^2 - n\right\}} = e^{-\frac{1}{2}n\widehat{q}} \int Dz \left(2\cosh\sqrt{\widehat{q}}z\right)^n, \tag{2.15}$$

where the last equation is derived by using the Hubbard-Stratonovich transformation

$$\exp\left(\frac{1}{2}x^2\right) = \int_{-\infty}^{\infty} \frac{dz}{\sqrt{2\pi}} \exp\left(-\frac{z^2}{2} + zx\right) = \int Dz \exp\left(zx\right), \tag{2.16}$$

where Dz is the Gaussian measure $dze^{-\frac{z^2}{2}}/\sqrt{2\pi}$ and we hereafter assume that the domain of integration of $\int Dz$ is $]-\infty,\infty[$ if there is no explicit indication. Substituting the above expressions, we can reduce $\phi(n)$ in eq. (2.9) to $\phi_{\mathrm{RS}}(n)$ as

$$\phi_{\mathrm{RS}}(n) = \underset{q,\widehat{q}}{\mathrm{Extr}} \Bigg\{ \frac{n(n-1)}{4}\beta^2 q^p - \frac{n(n-1)}{2}q\widehat{q} + \frac{1}{4}\beta^2 n \\ -\frac{1}{2}n\widehat{q} + \log \int Dz \left(2\cosh\sqrt{\widehat{q}}z\right)^n \Bigg\}, \tag{2.17}$$

where we hereinafter put $J = 1$ for simplicity of the notation. Taking the extremization condition with respect to q and $\widehat{q}$, we get

$$q = \frac{\int Dz \left(\cosh\sqrt{\widehat{q}}z\right)^n \left(\tanh\sqrt{\widehat{q}}z\right)^2}{\int Dz \left(\cosh\sqrt{\widehat{q}}z\right)^n}, \ \widehat{q} = \frac{1}{2}p\beta^2 q^{p-1}. \tag{2.18}$$

Fortunately, under the RS the expression of $\phi_{\mathrm{RS}}(n)$ can be extended to $n \in \mathbb{R}$, which enables us to take the $n \to 0$ limit. The resultant free energy f_{RS} can be derived as

$$\begin{aligned} -\beta f_{\mathrm{RS}} &= \lim_{n\to 0} \frac{\partial \phi_{\mathrm{RS}}(n)}{\partial n} \\ &= \underset{q,\widehat{q}}{\mathrm{Extr}} \left\{ -\frac{1}{4}\beta^2 q^p + \frac{1}{2}q\widehat{q} + \frac{1}{4}\beta^2 - \frac{1}{2}\widehat{q} + \int Dz \log 2\cosh(\sqrt{\widehat{q}}z) \right\}. \end{aligned} \tag{2.19}$$

The extremization condition gives the state equations (2.18) in the limit $n \to 0$, and now the problem is solved in the RS level. Unfortunately, this RS solution gives unphysical behaviors, e.g. negative entropy, at low temperatures. Next, we study this point in more detail by treating the particular limit $p \to \infty$.

2.2 The solution in the limit $p \to \infty$

2.2.1 Failure of the RS solution

To demonstrate the failure of the RS ansatz, we here analyze the $p \to \infty$ limit. In this limit, the system becomes rather simple and we can derive the exact solution without employing the replica method. First, let us study the RS solutions. In the limit $p \to \infty$, there are two possible solutions to eqs. (2.18), namely the paramagnetic solution $(q, \widehat{q}) = (0, 0)$ and the spin-glass solution $(q, \widehat{q}) = (1, +\infty)$. Substituting these solutions into eq. (2.19), we obtain the paramagnetic and spin-glass free energies, f_P and $f_{\mathrm{RS}SG}$ respectively, as

$$-\beta f_P = \frac{1}{4}\beta^2 + \log 2, \tag{2.20}$$

$$-\beta f_{\mathrm{RS}SG} \to \sqrt{\frac{2\widehat{q}}{\pi}} \to +\infty. \tag{2.21}$$

The divergence of $f_{\mathrm{RS}SG}$ clearly shows an inconsistency of this spin-glass solution. On the other hand, the paramagnetic solution also shows the unphysical behavior at low temperatures. The entropy of the paramagnetic solution s_P is

$$s_P = \log 2 - \frac{1}{4}\beta^2. \tag{2.22}$$

This clearly becomes negative below $T_c = 1/(2\sqrt{\log 2})$, which implies that there should be a phase transition above T_c. At least in the RS level, we do not have any candidate to correctly express the low temperature behavior of this system. Before seeing the correct solution in the framework of the replica theory, we employ the microcanonical approach in order to obtain the correct low temperature behavior.

2.2.2 Microcanonical approach

The microcanonical approach starts from calculations of the energy distribution of the system (2.1) in the limit $p \to \infty$ as the microcanonical ensemble

$$P(E(\boldsymbol{S})) = [\delta(E - H(\boldsymbol{S}|\boldsymbol{J}))]_{\boldsymbol{J}}. \tag{2.23}$$

The configurational average can be carried out by using the Fourier expression of the delta function. The result becomes a Gaussian distribution and does not depend on the spin configuration

$$P(E(\boldsymbol{S})) = P(E) = \frac{1}{\sqrt{N\pi}} \exp\left(-\frac{E^2}{N}\right). \tag{2.24}$$

The two-point probability distribution $P(E_1(\boldsymbol{S}_1), E_2(\boldsymbol{S}_1))$ for two independent configurations of spins $\boldsymbol{S}^1$ and $\boldsymbol{S}^2$ is similarly calculated

$$\begin{aligned} &P(E_1(\boldsymbol{S}^1), E_2(\boldsymbol{S}^2)) = [\delta(E_1 - \mathscr{H}(\boldsymbol{S}^1|\boldsymbol{J}))\delta(E_2 - \mathscr{H}(\boldsymbol{S}^2|\boldsymbol{J}))]_{\boldsymbol{J}} \\ &= \frac{1}{N\pi\sqrt{(1+q^p)(1-q^p)}} \exp\left(-\frac{E_1^2 + E_2^2}{2N(1+q^p)} - \frac{E_1^2 - E_2^2}{2N(1-q^p)}\right), \end{aligned} \tag{2.25}$$

where $q = \boldsymbol{S}^1 \cdot \boldsymbol{S}^2/N$. Under the assumption that the spin configurations $\boldsymbol{S}^1$ and $\boldsymbol{S}^2$ are thermodynamically distinguishable, the value of $|q|$ is smaller than 1, which means that q^p goes to 0 in the limit $p \to \infty$ and

$$P(E_1(\boldsymbol{S}^1), E_2(\boldsymbol{S}^2)) \to P(E_1)P(E_2). \tag{2.26}$$

Hence, the energy distribution of two different spin configurations is completely independent for each configuration. We can prove that the same property holds for any multi-point distributions by following similar discussions. Consequently, each energy level for each spin configuration can be treated as an identically independently distributed (i.i.d.) Gaussian random variable, the distribution of which is given by eq. (2.24). Due to this property, this model is called the random energy model (REM) [36] and the free energy of the REM can be assessed by the microcanonical approach.

The microcanonical approach utilizes the entropy to yield the thermodynamical behavior of the system. Because each energy level is i.i.d. for the REM, the number of states with energy E can be calculated as

$$n(u) = 2^N P(Nu) = \frac{1}{\sqrt{N\pi}} e^{N\left(\log 2 - u^2\right)}. \tag{2.27}$$

where we put $u = E/N$, which represents the energy per spin. This relation implies that in the limit $N \to \infty$, there are very many states for the range $|u| < \sqrt{\log 2} \equiv u_0$ but none in the other range $|u| \geq u_0$, and the entropy for $|u| < u_0$ is given by

$$s(u) = \frac{1}{N} \log n(E) = \log 2 - u^2. \tag{2.28}$$

An illustration of the entropy $s(u)$ of the REM is given in fig. 2.1. Using this entropy

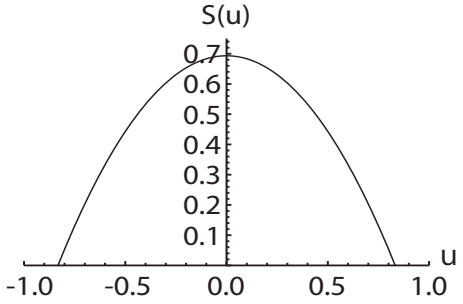

Figure 2.1: The shape of entropy $s(u)$ of the REM.

function $s(u)$, we can construct the free energy $f(T)$ from the definition

$$f(T) = \max_{|u|<u_0} \{u - Ts(u)\} = \max_{|u|<u_0} \left\{u - T(\log 2 - u^2)\right\}. \tag{2.29}$$

where T is the temperature. In the usual case, the temperature T is equal to $(\partial s(u)/\partial u)^{-1}$ as the definition of temperature in the microcanonical ensemble. This is actually the case for $T > T_c = 1/(2\sqrt{\log 2})$. In this region, eq. (2.29) gives

$$f_P = -\frac{1}{4}\beta - T\log 2 \quad (T > T_c). \tag{2.30}$$

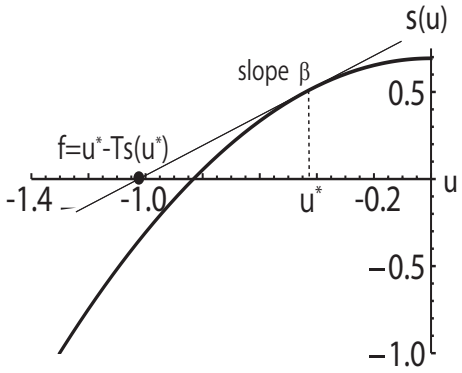

Figure 2.2: A pictorial expression of the derivation of the free energy for $T > T_c$. The free energy is given by the u-intercept of the tangent to the curve $s(u)$ with slope β.

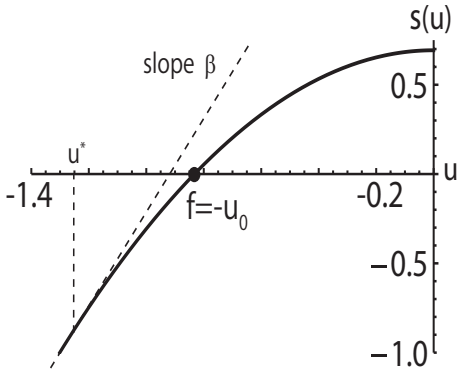

Figure 2.3: A pictorial expression of the derivation of the free energy for $T \leq T_c$. The free energy is given by the nearest value of u to the tangent of $s(u)$ with slope β.

On the other hand, for $T \leq T_c$, the maximum of eq. (2.29) is given by $u = -u_0$ and the free energy is

$$f_{SG} = -\sqrt{\log 2} = -u_0 \quad (T < T_c). \tag{2.31}$$

These free energies (2.30) and (2.31) are the exact solution of the REM.

The above discussion is easily understood by using pictorial expressions given in figs. 2.2 and 2.3. What we should do is to find a tangent to the curve $s(u)$ with slope β. We denote the abscissa of the tangent point as u^*. For $T > T_c$, this abscissa $u^* = -\beta/2$ is in the range $|u| < u_0$, and then the maximum in eq. (2.29) is given by u^*. The figure corresponding to this situation is fig. 2.2. On the other hand, for $T \leq T_c$, this value u^* is out of the range $|u| < u_0$, which means that there is no physical state for the energy level u^*. In such a situation, the maximum of eq. (2.29) is the nearest value of u to u^* under the condition $|u| < u_0$, which leads to $f = -u_0 - Ts(-u_0) = -u_0$.

Before ending of this subsection, let us consider relations between the microcanonical solution (2.29) and the RS result. As we can see easily, for $T > T_c$ the paramagnetic solution of the RS (2.20) is identical to the microcanonical solution. As the temperature decreases, the entropy of the paramagnetic solution decreases and vanishes at $T = T_c$, and below T_c the free energy is kept as a constant at the value of $T = T_c$. These observations imply that the spin glass transition of the REM is due to the vanishing entropy of the paramagnetic phase. This is a characteristic feature of the REM and this transition is sometimes called the frozen transition.

To obtain the correct solution in the replica theory, it is known that the so-called replica symmetry breaking (RSB), which allows $q^{\mu\nu}$ to depend on the replica indices, is required. Next we introduce the RSB in a general framework.

2.3 Replica symmetry breaking

In order to obtain the low temperature spin-glass phase, we must treat $q^{\mu\nu}$ in more general forms. Although the correct form of $q^{\mu\nu}$ is unknown, Parisi has proposed a particular ansatz which describes a hierarchical breaking of replica symmetry [12, 13]. The Parisi scheme is constructed from the following recursive algorithm:

(i) First step: The n replicas are grouped in n/m_1 clusters of m_1 replicas. Within the same cluster, each $q^{\mu\nu}$ $(\mu \neq \nu)$ has a value q_1. Two replicas in different clusters have an overlap $q^{\mu\nu} = q_0 \leq q_1$.

(ii) Second step: Each cluster of size m_1 is broken up into m_1/m_2 sub-clusters of m_2 replicas. Any two replicas in the same sub-cluster have overlap $q^{\mu\nu} = q_2 \geq q_1$. The other overlaps remain unchanged.

Continuing this procedure, we obtain the general k-step RSB (kRSB) situation

$$n \geq m_1 \geq m_2 \cdots \geq m_k \geq 1, \ q_k \geq q_{k-1} \geq \cdots \geq q_1 \geq q_0. \tag{2.32}$$

Each q_k is interpreted as a hierarchically constructed spin-glass order parameter and m_k is called the breaking parameter. The following example is for the case of the 2-step RSB such that $n = 12, m_1 = 6, m_2 = 3$,

$$\{q^{\mu\nu}\} = \left(\begin{array}{ccc|ccc|cccccc} 0 & q_2 & q_2 & & & & & & & & & \\ q_2 & 0 & q_2 & & q_1 & & & & & & & \\ q_2 & q_2 & 0 & & & & & & & & & \\ \hline & & & 0 & q_2 & q_2 & & & & & & \\ & q_1 & & q_2 & 0 & q_2 & & & q_0 & & & \\ & & & q_2 & q_2 & 0 & & & & & & \\ \hline & & & & & & 0 & q_2 & q_2 & & & \\ & & & & & & q_2 & 0 & q_2 & & q_1 & \\ & & q_0 & & & & q_2 & q_2 & 0 & & & \\ \hline & & & & & & & & & 0 & q_2 & q_2 \\ & & & & & & & q_1 & & q_2 & 0 & q_2 \\ & & & & & & & & & q_2 & q_2 & 0 \end{array}\right). \tag{2.33}$$

Taking the limit $n \to 0$, we assume that the parameters $\{m_k\}$ become continuous and the following inequalities hold;

$$n \leq m_1 \leq m_2 \leq \cdots \leq 1, \tag{2.34}$$

which are the inverse relations of eq. (2.32). All the parameters $\{m_k\}, \{q_k\}$ are determined by taking the extremization condition of $\phi(n)$. The above procedures are all the ingredients of the Parisi scheme. The full-step ($k = \infty$-step) RSB (FRSB) is also constructed in a similar manner but the concrete procedure is quite complicated and we here only refer to [24].

Physically, the RSB is considered to be related to the emergence of enormous number of pure states. According to this speculation, the RS ansatz describes situations that only a small number (subexponential number of the system size N) of pure states exist, and

the failure of the RS solution at low temperatures is due to the neglect of many pure states in the spin-glass phase.

Curiously, it is known that most models only show two types of RSB: The 1RSB and FRSB. In either case, it is considered that there are many pure states but the intricacy of the phase space structure is different depending on the step of RSB. Generally speaking, as the step of RSB becomes higher and higher, the phase space structure is considered to become more and more complicated.

Although our knowledge about the FRSB is still rather poor because of intricacy of the FRSB construction, the 1RSB solution has been intensively studied and its relation to pure states is well understood nowadays [37]. In the following, we mainly treat the 1RSB solution and explain the relation with many pure states in detail.

2.3.1 The 1RSB solution for the p-spin interacting model

Under the 1RSB ansatz, the replica indices are divided into n/m groups of identical size m, and $q^{\mu\nu}$ and $\widehat{q}^{\mu\nu}$ are parameterized as

$$(q^{\mu\nu}, \widehat{q}^{\mu\nu}) = \begin{cases} (q_1, \widehat{q}_1) & (\ \mu \text{ and } \nu \text{ belong to the same group }\ ) \\ (q_0, \widehat{q}_0) & (\ \text{otherwise}\ ) \end{cases} \tag{2.35}$$

Under this assumption, we can transform the term $\sum_{\mu<\nu} \widehat{q}^{\mu\nu} S^\mu S^\nu$ as

$$\sum_{\mu<\nu} \widehat{q}^{\mu\nu} S^\mu S^\nu = \frac{1}{2} \left\{ \widehat{q}_0 \left(\sum_\mu^n S^\mu \right)^2 + (\widehat{q}_1 - \widehat{q}_0) \sum_{\text{block}}^{n/m} \left(\sum_{\mu \in \text{block}}^m S^\mu \right)^2 - n\widehat{q}_1 \right\}, \tag{2.36}$$

where the first term on the right-hand side fills up all matrix elements of $\{q^{\mu\nu}\}$ with q_0. The second term replaces the elements in the block part with q_1 and the last term sets the diagonal elements to zero. Similarly, we derive

$$\sum_{\mu<\nu} (q^{\mu\nu})^p = \frac{1}{2} n(m-1) q_1^p + \frac{1}{2} n(n-m) q_0^p, \tag{2.37}$$

$$\sum_{\mu<\nu} q^{\mu\nu} \widehat{q}^{\mu\nu} = \frac{1}{2} n(m-1) \widehat{q}_1 q_1 + \frac{1}{2} n(n-m) \widehat{q}_0 q_0. \tag{2.38}$$

Combining the Hubbard-Stratonobich transformation and eq. (2.36), we obtain

$$e^{\sum_{\mu<\nu} \widehat{q}^{\mu\nu} S^\mu S^\nu} = e^{-\widehat{q}_1 n/2} \int Dz_0 \prod_{\text{block}}^{n/m} \left\{ \int Dz_1 \prod_{\mu \in \text{block}}^m e^{\left(\sqrt{\widehat{q}_0} z_0 + \sqrt{\widehat{q}_1 - \widehat{q}_0} z_1 \right) S^\mu} \right\}. \tag{2.39}$$

In this expression, we can perform the spin trace for each replica spin independently. Substituting all the results into eq. (2.9), we get

$$\phi_{\text{1RSB}}(n,m) = \underset{q_1, q_0, \widehat{q}_1, \widehat{q}_0}{\text{Extr}} \left\{ \frac{\beta^2}{4} (n(m-1) q_1^p + n(n-m) q_0^p) + \frac{\beta^2}{4} n - \frac{1}{2} n \widehat{q}_1 \right.$$
$$\left. - \frac{1}{2} n(m-1) \widehat{q}_1 q_1 - \frac{1}{2} n(n-m) \widehat{q}_0 q_0 + \log \int Dz_0 \left(\int Dz_1 (2 \cosh h)^m \right)^{n/m} \right\}. \tag{2.40}$$

where we put $h = \sqrt{\widehat{q}_0} z_0 + \sqrt{\widehat{q}_1 - \widehat{q}_0} z_1$. Taking the extremization condition, we get the following equations of states:

$$q_1 = \frac{\int Dz_0 \left(\int Dz_1 (\cosh h)^m \right)^{n/m} \frac{\int Dz_1 (\tanh h)^2 (\cosh h)^m}{\int Dz_1 (\cosh h)^m}}{\int Dz_0 \left(\int Dz_1 (\cosh h)^m \right)^{n/m}} \tag{2.41}$$

$$q_0 = \frac{\int Dz_0 \left(\int Dz_1 (\cosh h)^m \right)^{n/m} \left(\frac{\int Dz_1 \tanh h (\cosh h)^m}{\int Dz_1 (\cosh h)^m} \right)^2}{\int Dz_0 \left(\int Dz_1 (\cosh h)^m \right)^{n/m}} \tag{2.42}$$

$$\widehat{q}_1 = \frac{1}{2} p \beta^2 q_1^{p-1}, \ \widehat{q}_0 = \frac{1}{2} p \beta^2 p q_0^{p-1}. \tag{2.43}$$

If we set $q_0 = q_1 = q$, the RS solution (2.17) and (2.18) is reproduced. In the limit $n \to 0$, we can derive the free energy parameterized by m

$$-\beta f_{\rm 1RSB}(m) = \lim_{n \to 0} \frac{\partial}{\partial n} \phi_{\rm 1RSB}(n, m) = \underset{q_1, q_0, \widehat{q}_1, \widehat{q}_0}{\rm Extr} \left\{ \frac{\beta^2}{4} ((m-1) q_1^p - m q_0^p) + \frac{\beta^2}{4} \right.$$
$$\left. - \frac{1}{2} \widehat{q}_1 - \frac{1}{2} (m-1) \widehat{q}_1 q_1 + \frac{1}{2} m \widehat{q}_0 q_0 + \frac{1}{m} \int Dz_0 \log \left(\int Dz_1 (2 \cosh h)^m \right) \right\}. \tag{2.44}$$

The extremization condition re-derives eqs. (2.41)-(2.43) with the condition $n = 0$. Although the physical meaning of m is unclear at this moment, we here treat m as an artificial parameter and take the extremization condition to erase the m-dependence of the free energy at the final step of calculations. We will come back to this problem later after deriving the correct solution of the REM in the 1RSB level.

2.3.2 The 1RSB solution in the $p \to \infty$ limit

It is time to solve the REM in the framework of the replica theory. What we should do at first is to find the solution of eqs. (2.41)-(2.43). There are three solutions for these equations in the limit $p \to \infty$, namely $(q_1, q_0) = (0, 0), (1, 1)$ and $(1, 0)$. For the 1RSB solution to be non-trivial, an inequality $q_0 < q_1$, $(\widehat{q}_0 < \widehat{q}_1)$ must hold, which means that $(q_1, q_0) = (1, 0)$ is the appropriate solution. Substituting this solution, we get

$$-\beta f_{\rm 1RSB}(m) = \frac{\beta^2}{4} m + \frac{1}{m} \log 2. \tag{2.45}$$

Variation with respect to m gives

$$(m\beta)^2 = 4 \log 2. \tag{2.46}$$

Substituting this value, we obtain

$$f_{SG} = -\sqrt{\log 2}, \tag{2.47}$$

which is identical to the microcanonical solution (2.31) below the the transition temperature T_c. In the replica theory, the transition temperature is determined by the direct

comparison of the free energy value $f_{SG} = f_P$, which is surely identical to that of the microcanonical approach. Hence, for the REM, the 1RSB solution gives the exact result.

The above is the conventional construction of the 1RSB solution without recent perspectives about the physical meaning of m. Actually, the RSB solution has more information about the phase space structure of the system. We elucidate this point in the next section.

2.4 Pure state statistics of the 1RSB level

As already mentioned in chapter 1, in the mean-field description of spin glasses, there are many pure states in a spin-glass system and the partition function becomes the summation over contributions from all the pure states. Each pure state γ has its own free energy $-\beta f_\gamma = (\log Z_\gamma)/N$ and the number of pure states having the free energy value f, $\mathscr{N}(f)$, is scaled as

$$\mathscr{N}(f) \sim e^{N\Sigma(f)}, \tag{2.48}$$

where $\Sigma(f) \sim O(1)$ is called the complexity. Note that an inequality $\Sigma(f) \geq 0$ must hold, because the complexity is the logarithm of the number of pure states, which cannot become negative. This is the same reason as the entropy cannot become negative. Under these assumptions, we can write the partition function as

$$Z = \sum_\gamma Z_\gamma \sim \int df e^{N(-\beta f + \Sigma(f))}, \tag{2.49}$$

where γ is the index of pure states and

$$Z_\gamma = \mathop{\mathrm{Tr}}_{\boldsymbol{S}\in\gamma} e^{-\beta H(\boldsymbol{S}|\boldsymbol{J})} = \mathop{\mathrm{Tr}}_{\boldsymbol{S}} e^{-\beta H(\boldsymbol{S}|\boldsymbol{J})}\delta_\gamma(\boldsymbol{S}), \tag{2.50}$$

where $\delta_\gamma(\boldsymbol{S})$ is the indicator function where $\delta_\gamma(\boldsymbol{S}) = 1$ when $\boldsymbol{S} \in \gamma$ and $\delta_\gamma(\boldsymbol{S}) = 0$ otherwise. Equation (2.49) indicates that the partition function is dominated by the saddle point of $(-\beta f + \Sigma(f))$. For convenience, we define another generating function $g(x|J)$ as

$$e^{Ng(x|\boldsymbol{J})} = \sum_\gamma Z_\gamma^x \sim \int df e^{N(-\beta x f + \Sigma(f))} \Rightarrow g(x|J) = \max_{f_- \leq f \leq f_+} \{-\beta x f + \Sigma(f)\}, \tag{2.51}$$

where the bounds f_- and f_+ for the range of f come from the constraint $\Sigma(f) \geq 0$. Equation (2.51) implies that, when the complexity $\Sigma(f)$ is a convex upward function, the complexity can be calculated from the generating function $g(x|\boldsymbol{J})$ in the parameterized form as follows:

$$-\beta f(x) = \frac{\partial g(x|J)}{\partial x},\ \Sigma(f(x)) = g(x|J) - x\frac{\partial g(x|J)}{\partial x}. \tag{2.52}$$

So far, we are discussing about one sample of quenched disorder. We here assume that $g(x|J)$ is a self-averaging quantity and we can replace $g(x|J)$ by $g(x) = [g(x|J)]_{\boldsymbol{J}}$. This

averaged function $g(x)$ can be expressed by the replica method as

$$Ng(x) = [Ng(x|J)]_{\boldsymbol{J}} = \left[\log\left(\sum_{\gamma} Z_{\gamma}^{x}\right)\right]_{\boldsymbol{J}} = \lim_{y\to 0}\frac{\partial}{\partial y}\log\left[\left(\sum_{\gamma} Z_{\gamma}^{x}\right)^{y}\right]_{\boldsymbol{J}} \tag{2.53}$$

Although exact evaluation of the right-hand side of eq. (2.53) is difficult, for $x, y \in \mathbb{N}$ we can derive the following expression:

$$\left[\left(\sum_{\gamma} Z_{\gamma}^{x}\right)^{y}\right]_{\boldsymbol{J}} = \sum_{\gamma^{1}\cdots\gamma^{y}} \mathrm{Tr}\left[\exp\left(-\beta\sum_{\nu=1}^{y}\sum_{\mu=1}^{x} H(\boldsymbol{S}^{\nu\mu}|\boldsymbol{J})\right)\prod_{\nu=1}^{y}\prod_{\mu=1}^{x}\delta_{\gamma^{\nu}}(\boldsymbol{S}^{\nu\mu})\right]_{\boldsymbol{J}}. \tag{2.54}$$

For the evaluation of this equation, the following observations are important.

- The summation is taken over all possible configurations of xy replica spins.
- However, the factor $\prod_{\nu=1}^{y}\prod_{\mu=1}^{x}\delta_{\gamma^{\nu}}(\boldsymbol{S}^{\nu\mu})$ allows only contributions from configurations in which xy replicas are equally assigned to y pure states by x.

These observations are nothing more than the physical situation of the 1RSB ansatz, in assessing $[Z^{n}(\boldsymbol{J})]_{\boldsymbol{J}}$ with substitution of $n = xy$ and $m = x$ (fig. 2.4). Accepting this

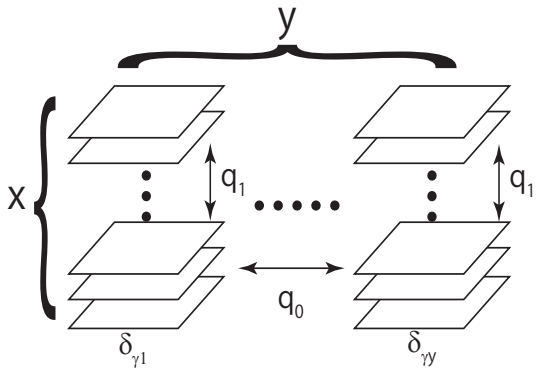

Figure 2.4: Schematic diagram of the 1RSB description of the factor $\prod_{\nu=1}^{y}\left(\prod_{\mu=1}^{x}\delta_{\gamma^{\nu}}(\boldsymbol{S}^{\nu\mu})\right)$

interpretation, we obtain the following expression:

$$\frac{1}{N}\log\left[\left(\sum_{\gamma} Z_{\gamma}^{x}\right)^{y}\right]_{\boldsymbol{J}} = \phi_{\mathrm{1RSB}}(xy, x), \tag{2.55}$$

where $\phi_{\mathrm{1RSB}}(n, m)$ is the 1RSB solution considered in the previous section. Then, combining eqs. (2.53) and (2.55), we obtain the generating function $g(x)$ in the form

$$g(x) = \lim_{y\to 0}\frac{\partial}{\partial y}\phi_{\mathrm{1RSB}}(n = xy, m = x) = -x\beta f_{\mathrm{1RSB}}(x), \tag{2.56}$$

where $f_{\rm 1RSB}(x)$ is the 1RSB free energy shown in the previous section. Hence, the RSB breaking parameter m corresponds to the parameter x which controls the generating function $g(x)$ of complexity, which leads to the following relations from eq. (2.52);

$$-\beta f(x) = -\beta \frac{\partial (x f_{\rm 1RSB}(x))}{\partial x},\ \Sigma(f(x)) = -\beta x f_{\rm 1RSB}(x) + \beta x \frac{\partial (x f_{\rm 1RSB}(x))}{\partial x}. \tag{2.57}$$

2.4.1 Pure states of the limit $p \to \infty$

Here, let us see the complexity of the REM as an example. According to eqs. (2.44) and (2.57), the generating function of the p-spin model is given by

$$\begin{aligned} g(x) = &\frac{1}{4}x(x-1)\beta^2 q_1^p - \frac{1}{2}x(x-1)q_1\widehat{q}_1 + \frac{1}{4}\beta^2 x \\ &-\frac{1}{2}x\widehat{q}_1 + \log \int Dz \left(2\cosh\sqrt{\widehat{q}_1}z\right)^x, \end{aligned} \tag{2.58}$$

where we put $q_0 = 0$ because the nontrivial 1RSB solution exists only under this condition. The value of q_1 is determined by eq. (2.41). Taking the limits $p \to \infty$ and $q_1 \to 1$, we obtain

$$g(x) = \frac{1}{4}x^2\beta^2 + \log 2. \tag{2.59}$$

The parameterized free energy and the complexity are derived from eq. (2.52) as

$$-\beta f(x) = \frac{1}{2}x\beta^2,\ \Sigma(f(x)) = \log 2 - \frac{1}{4}x^2\beta^2 = \log 2 - f^2. \tag{2.60}$$

Clearly, this complexity $\Sigma(f)$ is identical to the microcanonical entropy $s(u)$ if we identify $u = f$. This can be understood if we remember the construction of the REM. For this model, each spin configuration is completely independent of each other as we see the independence of each energy level in section 2.2.2. This means that each pure state of the REM is constructed from only one configuration, which indicates that the entropy of a pure state defined as the logarithm of the number of configurations belonging to the state, is 0. Hence, the free energy of a pure state corresponds to the energy of the state, which leads to the agreement between the complexity $\Sigma(f)$ and the entropy $s(u)$. As might be expected, this is a peculiar property of the REM, and in general the complexity $\Sigma(f)$ is different from the entropy $s(u)$.

In the microcanonical approach, the phase transition and free energy in each phase were easily derived by the pictorial interpretation of eq. (2.29). We here reexamine this derivation from a view point of the complexity. The form of $\Sigma(f)$ is identical to that of $s(u)$ given in fig. 2.1 by reading $u = f$ and $s(u) = \Sigma(f)$. There are two things which we should do. One is to derive the phase transition and the equilibrium value of the free energy $f_{\rm eq} \equiv -T(\log Z)/N$ in each phase. The other is to elucidate relations between the derivation of $f_{\rm eq}$ and the conventional prescription of the 1RSB. We start from the first point. The equilibrium free energy $f_{\rm eq}$ is obviously equal to $-g(1)/\beta$ from the definition.

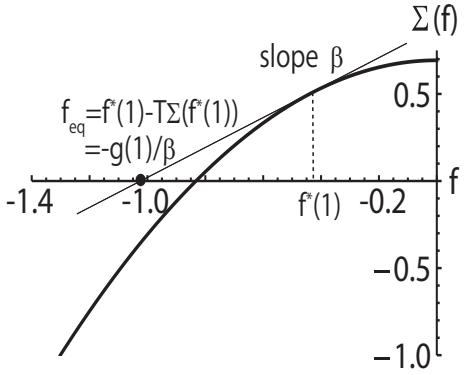

Figure 2.5: An expression of the derivation of $f_{\rm eq}$ for $T > T_c$. The free energy is given by the f-intercept of the tangent to the curve $\Sigma(f)$ with slope β.

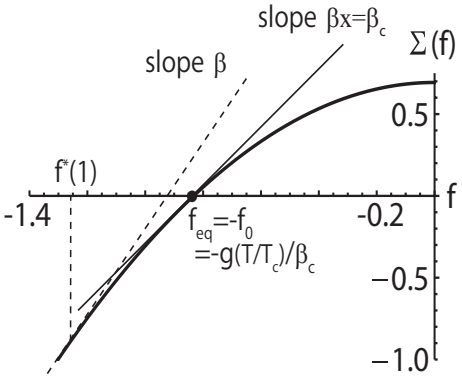

Figure 2.6: An expression of the derivation of $f_{\rm eq}$ for $T \leq T_c$. The point $-f_0$ where $\Sigma(f)$ vanishes yields $f_{\rm eq}$, which is determined by the tangent to $\Sigma(f)$ with the slope $\beta x = \beta_c$. The value $x = \beta_c/\beta$ is identical to the extremization of $f_{\rm 1RSB}(x)$ with respect to x.

The relation between $g(x)$ and the complexity $\Sigma(f)$ is derived from eq. (2.51) and (2.60) as

$$g(x) = \max_{f_- \leq f \leq f_+} \{-\beta x f + \Sigma(f)\} = \max_{|f|<f_0} \left\{-\beta x f + \log 2 - f^2\right\}, \tag{2.61}$$

where f_0 is equal to $\sqrt{\log 2}$. As mentioned in section 2.4, the complexity is the logarithm of the number of pure states and cannot be negative. Keeping $x = 1$, for $T > T_c$ we can easily see that the maximum of eq. (2.61) is given by $f^*(1) = -\beta/2$, which is identical to the abscissa of the curve $\Sigma(f)$ with slope β as given in fig. 2.5. For $T \leq T_c$, that abscissa $f^*(1)$ is out of the range $|f| < f_0$ and the maximum of eq. (2.61) is given by $-f_0 = -\sqrt{\log 2}$ as the microcanonical case, which leads to the correct result $f_{\rm eq} = -f_0$.

The free energies are correctly reproduced from the viewpoint of the complexity. Next, we see the relation with the conventional 1RSB prescription. The inequality $x = m \leq 1$ in the 1RSB construction is naturally understood from the specialty of $x = 1$. For $x = 1$, the generating function $g(1)$ directly relates to the correct $f_{\rm eq}$ unless the corresponding complexity becomes negative. Hence, in the usual case we should keep $x = 1$ and calculate $g(1)$, which gives the correct solution for $T > T_c$. For $T \leq T_c$, however, a naive calculation of $g(1)$ leads to the negative complexity, but this inconsistency is overcome in the 1RSB construction as follows. An important point is that the point $f = -f_0$ where the complexity vanishes is determined by a tangent to $\Sigma(f)$ with the slope $\beta_c = 2\sqrt{\log 2}$. Hence, to select $f = -f_0$ below $T \leq T_c$, we can modify x of $g(x)$ as $x = T/T_c$. This artificial prescription is just the extremization condition of $f_{\rm 1RSB}(x) = -g(x)/(\beta x)$ with respect to x. In fact,

$$\operatorname*{Extr}_x \{f_{\rm 1RSB}(x)\} \Rightarrow -\frac{1}{\beta}\frac{\partial}{\partial x}\frac{g(x)}{x} = \frac{1}{\beta x^2}\left(g(x) - x\frac{\partial g}{\partial x}\right) = \frac{\Sigma(f(x))}{\beta x^2} = 0, \tag{2.62}$$

which means that the extremization condition of $f_{\rm 1RSB}(x)$ with respect to x leads to the

point where the complexity vanishes. The equilibrium free energy $f_{\rm eq}$ is expressed in the 1RSB prescription as

$$f_{\rm eq} = f_{\rm 1RSB}\left(x = \frac{T}{T_c}\right) = -\frac{g\,(x)}{\beta x}\bigg|_{x=\frac{T}{T_c}} = -\frac{\max_f\left\{-\beta_c f + \Sigma(f)\right\}}{\beta_c} = -f_0. \tag{2.63}$$

Hence, the correct solution is reproduced. These procedures are also illustrated in fig. 2.6.

2.5 Viewpoint from the large deviation theory

In the previous sections, we gave the replica analysis with the RSB and its interpretation from the pure state statistics. In this section, we reexamine this result from the viewpoint of the large deviation theory, which treats asymptotic small probabilities of rare events in the large system limit.

For disordered systems, the probability that the free energy, $-(1/N\beta)\log Z$, will take a certain value f, $P(f)$, fluctuates from sample to sample. The large deviation theory tells us that, in most cases for large N, this probability $P(f)$ can be scaled as

$$P(f) \sim \exp\left\{NR(f)\right\}, \tag{2.64}$$

where $R(f)(\leq 0)$ is referred to as the rate function. The rate function relates to the generating function $\phi(n)$ as

$$\begin{aligned} e^{N\phi(n)} \equiv [Z^n]_{\boldsymbol{J}} = \int d\boldsymbol{J} P(\boldsymbol{J}) e^{-N\beta n f(\boldsymbol{J})} = \int df P(f) e^{-N\beta n f} \sim \int df e^{N(-\beta n f + R(f))} \\ \Rightarrow \phi(n) = \max_{f_- \leq f \leq f_+} \{-\beta n f + R(f)\}, \end{aligned} \tag{2.65}$$

where the bounds f_+ and f_- are required to satisfy the constraint $R(f) \leq 0$, as in the case of pure state statistics. If the rate function is a convex upward function, we can express the free energy and the rate function in forms parameterized by n

$$-\beta f(n) = \frac{\partial \phi(n)}{\partial n}, \quad R(f(n)) = \phi(n) - n\frac{\partial \phi(n)}{\partial n}. \tag{2.66}$$

This equation and the constraint $R(f) \leq 0$ require that the following equation holds for $\forall n$:

$$\frac{\phi(n)}{n} \leq \frac{\partial \phi(n)}{\partial n}. \tag{2.67}$$

Equations (2.65) and (2.66) indicate that the *typical* value of f, which is characterized by the condition $R(f) = (1/N)\log P(f) = 0$, can be evaluated as

$$-\beta f_{\rm typ} = \frac{1}{N}[\log Z]_{\boldsymbol{J}} = \lim_{n\to 0}\frac{\partial \phi(n)}{\partial n}, \tag{2.68}$$

which is the basic identity of the replica method. The above discussion indicates that $n = 1, 2, \ldots > 0$ corresponds to *atypical* samples of $R(f) < 0$ representing a small probability. This means that the replica method can be regarded as a formula that infers the behavior of typical samples by extrapolating the behavior for atypical samples.

2.5.1 Re-derivation of the 1RSB transition

Again we treat the REM as an example. As mentioned in section 2.2, there are two solutions for the equations of states (2.18) in the limit $p \to \infty$, namely the paramagnetic $q = 0$ and spin-glass $q = 1$ solutions. Hence, there are corresponding two solutions for $\phi(n)$ as

$$\phi_{\rm RS}(n; q = 0) \equiv \phi_{\rm RS1}(n) = \frac{1}{4}\beta^2 n + n \log 2, \tag{2.69}$$

$$\phi_{\rm RS}(n; q = 1) \equiv \phi_{\rm RS2}(n) = \frac{1}{4}\beta^2 n^2 + \log 2. \tag{2.70}$$

The RS1 and RS2 solutions correspond to the paramagnetic and RS spin-glass solutions, f_P and $f_{{\rm RS}SG}$ given in section 2.2, respectively[1]. If we follow the concept of the saddle-point method, the correct solution is given by larger $\phi(n)$, but naive application of this criterion yields incorrect results. To treat this problem precisely, we should distinguish regions $T > T_c$ and $T \leq T_c$.

We first treat the high temperature region $T > T_c$. The correct solution of $\phi(n)$ in this region is given by

$$\phi(n) = \begin{cases} \phi_{\rm RS2}(n) & (n > n_P(T) \equiv (4 \log 2)/\beta^2 = \beta_c^2/\beta^2) \\ \phi_{\rm RS1}(n) & (n \leq n_P(T)) \end{cases}, \tag{2.71}$$

which gives the correct free energy $-\beta f_P = \lim_{n\to 0} (\partial \phi_{\rm RS1}(n)/\partial n)$. Note that the boundary $n_P(T) > 1$ is determined by equating two solutions $\phi_{\rm RS1}$ and $\phi_{\rm RS2}$, which agrees with the concept of the saddle-point method, but another intersection at $n = 1$ is ignored in the solution (2.71) even though the RS2 solution exceeds the RS1 below $n = 1$. The correctness of this prescription in the present case can be understood from the following criteria which should be satisfied by the correct $\phi(n)$:

1. The generating function $\phi(n)$ is a convex downward function with respect to n.
2. The rate function $R(f(n)) = \phi(n) - n(\partial \phi(n)/\partial n)$ is nonpositive.
3. An equality $\lim_{n\to 0} \phi(n) = 0$ should hold basically[2].
4. The entropy $s = (\partial/\partial T)(\lim_{n\to 0}(\partial \phi(n)/\partial n)/\beta)$ cannot be negative.

The RS2 solution clearly violates the third criterion which comes from a fact that for finite N the generating function $\phi_N(n) = \log[Z^n]_{\boldsymbol{J}}/N$ necessarily becomes 0 at $n = 0$. Hence, we choose the RS1 solution as the correct one in the whole range of $n \leq 1$. This solution is illustrated in the left panel of fig. 2.7. Empirically, it is known that an intersection at $n = 1$ should be neglected in most cases, but the general reason is not found and we only point out this fact here.

[1] Two limits $(q, \widehat{q}) \to (1, \infty)$ and $n \to 0$ are not exchangeable and the values of free energy are different between $-\beta f_{{\rm RS}SG}$ and $\lim_{n\to 0}(\partial \phi_{\rm RS2}/\partial n)$.

[2] In some cases, the identity $\lim_{n\to 0} \phi(n) = 0$ can be broken even though the similar equality for finite N, $\phi_N(0) = 0$, holds, due to taking the thermodynamic limit first. We will see such an example in chapter 3.

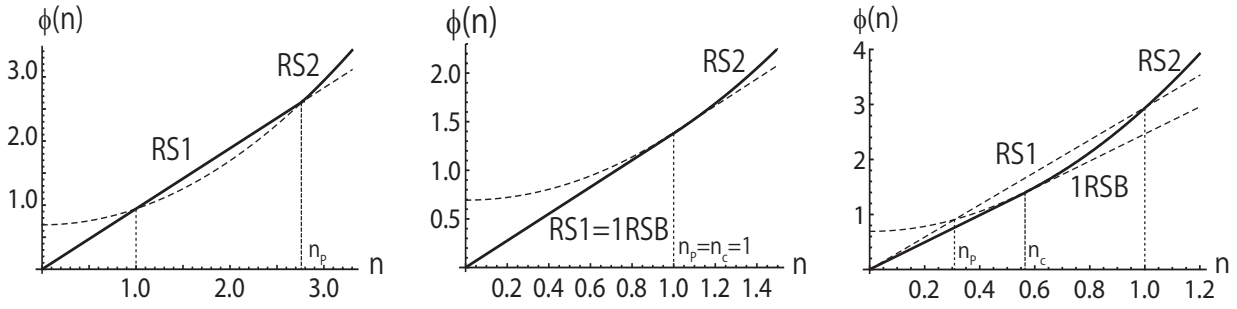

Figure 2.7: Behavior of $\phi(n)$. The solid lines represent the correct $\phi(n)$ and dotted lines are the RS and RSB branches. The corresponding values of temperature T are $1, T_c \approx 0.6$ and 0.333, from left to right.

On the other hand, for the low temperature region $T \leq T_c$, we need to construct another solution for $\phi(n)$ since the solution (2.71) gives incorrect results. It is known that the correct solution is given by

$$\phi(n) = \begin{cases} \phi_{\rm RS2}(n) & (n > n_c(T) \equiv (2\sqrt{\log 2})/\beta = \beta_c/\beta) \\ \frac{\phi_{\rm RS2}(n_c)}{n_c} n & (n \leq n_c(T)) \end{cases} , \tag{2.72}$$

and is illustrated in the right panel of fig. 2.7. The content of this solution is as follows. For large n, the larger RS solution, $\phi_{\rm RS2}(n)$, is correct as the high temperature region. Decreasing n, we find an intersection of the RS1 and RS2 solutions at $n = 1$, but as mentioned in the previous paragraph this intersection should be neglected. Actually, if we adopt the RS1 solution, we obtain the negative entropy at $n = 0$, which violates the fourth criterion in the previous paragraph. Proceeding to the range of $n < 1$, we can find that the rate function $R(f(n))$ becomes positive below $n_c(T)$, which violates the constraint $R(f(n)) \leq 0$. A natural prescription to avoid this inconsistency is keeping the value of $R(f(n))$ as 0 below n_c, which leads to the solution (2.72). This prescription can be proved to be correct in more mathematically proper procedures which focus on the convexity of $\phi(n)$ and the monotonicity of $\phi(n)/n$ [38].

The solution (2.72) relates to the 1RSB solution. In fact, if we set $q_0 = 0$ in eq. (2.40), which is a necessary condition for the nontrivial 1RSB in the current case solution[3], the functional form of $\phi_{\rm 1RSB}(n, m)$ can be expressed by using the RS solution as[4]

$$\phi_{\rm 1RSB}(n, m) = \frac{n}{m} \phi_{\rm RS}(m). \tag{2.73}$$

The interpretation of this equation is simple. The equality $q_0 = 0$ means that each pure state is perfectly uncorrelated. Thus, $\phi_{\rm 1RSB}(n, m)$ becomes proportional to n/m, as we can see in fig. 2.4, which comes from the independent $y = n/m$ sets of replicas. In each set of the replicas, $x = m$ replicas are included and the overlap q_1 takes a value, which is the same situation as the RS one. These considerations naturally lead to eq. (2.73).

[3]The nontrivial solution of equations of states (2.41)-(2.43) is only given by $q_1 > 0$ and $q_0 = 0$ in the present model.

[4]Another 1RSB order parameter q_1 is identified with the RS one q.

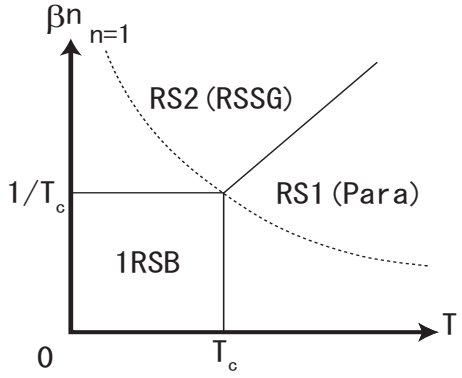

Figure 2.8: Phase diagram of the REM on the T-βn plane. The solid lines denote the phase boundaries and the dotted line represents the line $n = 1$.

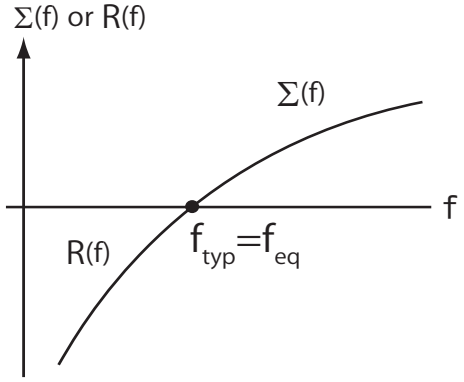

Figure 2.9: Schematic diagram of the complexity $\Sigma(f)$ and rate function $R(f)$. The complexity and rate function have disjointed domains of definition but their functional forms are identical, which leads to that the rate function is naturally continued to the complexity by using the RS generating function $\phi_{\rm RS}(n)$.

Taking the extremization condition of eq. (2.73) with respect to m with fixing $T < T_c$, we find that the breaking parameter m becomes equal to n_c, and the solution (2.72) is reproduced. Hence, the solution $\phi(n) = (\phi_{\rm RS2}(n_c)/n_c)n$ can be regarded as the 1RSB solution. Using eqs. (2.71) and (2.72), we can depict a phase diagram of the REM on the T-βn plane and the result is given in fig. 2.8. If we see the complexity and rate function, the relation between the 1RSB construction and large deviations becomes clearer. Using eqs. (2.57) and (2.73), we can express the complexity as

$$\Sigma(f(m)) = \phi_{\rm RS}(m) - m\frac{\partial \phi_{\rm RS}(m)}{\partial m}, \tag{2.74}$$

the functional form of which is obviously identical to that of the rate function $R(f(n)) = \phi_{\rm RS}(n) - n(\partial\phi_{\rm RS}(n)/\partial n)$, though their domains of definition are disjointed except for a point of typical value of free energy $f_{\rm typ}$ (which is identified with the equilibrium free energy $f_{\rm eq}$ in the context of pure state statistics), where the complexity and rate function become 0. This is also illustrated in fig. 2.9.

Summarizing the above discussions, we have seen the physical significance of the RSB from various perspectives by treating the REM as an example. In the remaining sections of this chapter, we treat the finite p cases by utilizing the above discussions. In addition, we present some arguments about the microscopic description of pure states, which becomes important when we treat problems requiring microscopic information like the optimization problems.

2.6 Finite p cases

In this section, we treat the finite p cases of the fully-connected p-spin interacting model. Especially, we concentrate on the $p = 2$ and 3 cases, since it is known that the qualitative behavior for $p \geq 4$ is similar to either one of those cases. To treat the $p = 2, 3$ cases, we need to consider the transition to the FRSB. Although the 1RSB transition can be observed by calculating the complexity in the 1RSB framework, the FRSB is signaled by the local instability of the RS solution, which is called the de Almeida-Thouless (AT) instability [39]. Hence, we first explain the AT instability, and then present the phase diagrams of the $p = 2, 3$ cases.

2.6.1 de Almeida-Thouless instability

Let us remember that the generating function $\phi(n)$ has the following form

$$\phi(n) = \underset{q^{\mu\nu}, \widehat{q}^{\mu\nu}}{\mathrm{Extr}} \left\{ \frac{\beta^2}{2} \sum_{\mu<\nu} (q^{\mu\nu})^p - \sum_{\mu<\nu} q^{\mu\nu} \widehat{q}^{\mu\nu} + \frac{1}{4}\beta^2 n + \log \mathrm{Tr}\, e^{\sum_{\mu<\nu} \widehat{q}^{\mu\nu} S^\mu S^\nu} \right\}. \tag{2.75}$$

We consider the deviations of the order parameter $q^{\mu\nu}$ around the RS saddle-point

$$q^{\mu\nu} = q + \Delta^{\mu\nu}, \tag{2.76}$$

and expand $\phi(n)$ with respect to $\Delta^{\mu\nu}$ to second order. The conjugate order parameter $\widehat{q}^{\mu\nu}$ becomes

$$\widehat{q}^{\mu\nu} = \frac{1}{2} p\beta^2 (q^{\mu\nu})^{p-1} \approx \frac{1}{2} p\beta^2 \left\{ q^{p-1} + (p-1) q^{p-2} \Delta^{\mu\nu} + \frac{1}{2}(p-1)(p-2) \left(\Delta^{\mu\nu}\right)^2 \right\}, \tag{2.77}$$

hence the leading two terms in eq. (2.75) become

$$\frac{\beta^2}{2} \sum_{\mu<\nu} (q^{\mu\nu})^p - \sum_{\mu<\nu} q^{\mu\nu} \widehat{q}^{\mu\nu} \approx -\frac{1}{4}\beta^2 p(p-1)^2 q^{p-2} \sum_{\mu<\nu} (\Delta^{\mu\nu})^2, \tag{2.78}$$

where we leave only the second order terms because the zeroth order terms are irrelevant to the variation of $\phi(n)$, $\Delta\phi(n)$, and the first order terms become 0 since we take the saddle-point condition with respect to q. Similarly, we can expand the last term of eq. (2.75) as

$$\begin{aligned} \log \mathrm{Tr}\, e^{\sum_{\mu<\nu} \widehat{q}^{\mu\nu} S^\mu S^\nu} &\approx \frac{1}{4} p(p-1)(p-2)\beta^2 q^{p-3} \sum_{\mu<\nu} (\Delta^{\mu\nu})^2 \left\langle S^\mu S^\nu \right\rangle_{\mathrm{RS}} \\ &+ \frac{1}{8} p^2 (p-1)^2 \beta^4 q^{2p-4} \sum_{\mu<\nu} \sum_{\delta<\omega} \Delta^{\mu\nu} \Delta^{\delta\omega} \left(\left\langle S^\mu S^\nu S^\delta S^\omega \right\rangle_{\mathrm{RS}} - \left\langle S^\mu S^\nu \right\rangle_{\mathrm{RS}} \left\langle S^\delta S^\omega \right\rangle_{\mathrm{RS}} \right), \end{aligned} \tag{2.79}$$

where the brackets $\langle \cdots \rangle_{\mathrm{RS}}$ denote the average over the RS weight $e^{\widehat{q} \sum_{\mu<\nu} S^\mu S^\nu}$. Regarding that an equality $\langle S^\mu S^\nu \rangle_{\mathrm{RS}} = q$ holds, we eventually derive the variation of the generating

function $\Delta\phi(n)$ as

$$\Delta\phi(n) = -\frac{1}{4}\beta^2 p(p-1)q^{p-2}\sum_{\mu<\nu}\sum_{\delta<\omega}\Delta^{\mu\nu}\Delta^{\delta\omega}\Bigg\{\delta_{(\mu\nu),(\delta\omega)} \\ -\frac{1}{2}p(p-1)\beta^2 q^{p-2}\left(\left\langle S^\mu S^\nu S^\delta S^\omega\right\rangle_{\rm RS} - \left\langle S^\mu S^\nu\right\rangle_{\rm RS}\left\langle S^\delta S^\omega\right\rangle_{\rm RS}\right)\Bigg\}, \quad (2.80)$$

where $\delta_{(\mu\nu),(\delta\omega)}$ is the Kronecker delta function which yields 1 when $(\mu\nu) = (\delta\omega)$ and 0 otherwise. We denote the matrix of coefficients of $\Delta^{\mu\nu}$ by G which is called the *Hessian* matrix. The local stability of the RS solution requires all the eigenvalues of G be positive. Here we classify the elements of G by using the following notations

$$G_{(\mu\nu)(\mu\nu)} = 1 - \frac{1}{2}p(p-1)\beta^2 q^{p-2}(1 - \left\langle S^\mu S^\nu\right\rangle_{\rm RS}) \equiv P, \quad (2.81)$$

$$G_{(\mu\nu)(\mu\delta)} = -\frac{1}{2}p(p-1)\beta^2 q^{p-2}\left(\left\langle S^\nu S^\delta\right\rangle_{\rm RS} - \left\langle S^\mu S^\nu\right\rangle^2_{\rm RS}\right) \equiv Q, \quad (2.82)$$

$$G_{(\mu\nu)(\delta\omega)} = -\frac{1}{2}p(p-1)\beta^2 q^{p-2}\left(\left\langle S^\mu S^\nu S^\delta S^\omega\right\rangle_{\rm RS} - \left\langle S^\mu S^\nu\right\rangle^2_{\rm RS}\right) \equiv R. \quad (2.83)$$

Eigenvalues of the Hessian and the AT condition

Let us find the eigenvectors of G by a heuristic approach found by Almeida and Thouless. The first eigenvector $\boldsymbol{s}_1$ is obtained by assuming $\Delta^{\mu\nu} = a$ for any μ, ν. In this condition, from the eigenvalue equation $G\boldsymbol{s}_1 = \lambda_1\boldsymbol{s}_1$ we can easily derive the first eigenvalue λ_1 as

$$\lambda_1 = P + 2(n-2)Q + \frac{1}{2}(n-2)(n-3)R. \quad (2.84)$$

The next type of solution $\boldsymbol{s}_2$ is obtained by treating a replica θ as a special one. We assume $\theta = 1$ without loss of generality. This solution $\boldsymbol{s}_2$ has $\Delta^{\mu\nu} = b$ when μ or ν is equal to 1, $\Delta^{\mu\nu} = c$ otherwise. The first row of the eigenvalue equation $G\boldsymbol{s}_2 = \lambda_2\boldsymbol{s}_2$ gives

$$(P + (n-2)Q)b + \left((n-2)Q + \frac{1}{2}(n-2)(n-3)R\right)c = \lambda_2 b. \quad (2.85)$$

We here impose the orthogonal condition of the solutions $\boldsymbol{s}_2$ and $\boldsymbol{s}_1$, which leads to

$$(n-1)b + \frac{1}{2}(n-1)(n-2)c = 0, \quad (2.86)$$

Solving eqs. (2.85) and (2.86) under the condition $b, c \neq 0$, we get

$$\lambda_2 = P + (n-4)Q - (n-3)R. \quad (2.87)$$

The third mode $\boldsymbol{s}_3$ is obtained by treating two replicas θ, ω as special ones. This solution $\boldsymbol{s}_3$ has $\Delta^{\theta\omega} = d$, $\Delta^{\theta\mu} = e$ when $\mu \neq \omega$ and $\Delta^{\mu\nu} = f$ otherwise. Without loss of generality, we put $\theta = 1$ and $\omega = 2$. The orthogonal condition of $\boldsymbol{s}_1$ and $\boldsymbol{s}_3$ yields

$$d + 2(n-2)e + \frac{1}{2}(n-2)(n-3)f = 0, \quad (2.88)$$

and the orthogonal condition of $\boldsymbol{s}_2$ and $\boldsymbol{s}_3$ also gives

$$d + (n-2)e = 0,\ e + \frac{1}{2}(n-3)f = 0. \tag{2.89}$$

The first row of the eigenvalue equation $G\boldsymbol{s}_3 = \lambda_3 \boldsymbol{s}_3$ leads to

$$Pd + 2(n-2)Qe + \frac{1}{2}(n-2)(n-3)Rf = \lambda_3 d., \tag{2.90}$$

Solving eqs. (2.88)-(2.90), we obtain

$$\lambda_3 = P - 2Q + R. \tag{2.91}$$

The eigenvectors $\boldsymbol{s}_1$, $\boldsymbol{s}_2$ and $\boldsymbol{s}_3$ construct $n(n-1)/2$-dimensional space, hence all the eigenvalues are exhausted by these three modes.

For the stability of the saddle point, all of the eigenvalues must be non-negative. We hereafter concentrate on a region $n \leq 1$. In this region, from simple algebras we can see that inequalities $\lambda_1, \lambda_2 \geq \lambda_3$ hold, which means that the mode $\boldsymbol{s}_3$ is the relevant mode for the stability of the RS solution and is called the *replicon* mode. To obtain an explicit form of λ_3, we calculate the factor $r \equiv \left\langle S^\mu S^\nu S^\delta S^\omega \right\rangle$ in R and the result is

$$r \equiv \left\langle S^\mu S^\nu S^\delta S^\omega \right\rangle_{\rm RS} = \frac{\int Dz \cosh^n \sqrt{\widehat{q}} z \tanh^4 \sqrt{\widehat{q}} z}{\cosh^n \sqrt{\widehat{q}} z}. \tag{2.92}$$

Remembering $\langle S^\mu S^\nu \rangle_{\rm RS}$ in P, Q and R is equal to q given in eq. (2.18), we finally obtain

$$\lambda_3 = P - 2Q + R = 1 - \frac{1}{2}p(p-1)\beta^2 q^{p-2} \frac{\int Dz (\cosh \sqrt{\widehat{q}} z)^{n-4}}{\int Dz (\cosh \sqrt{\widehat{q}} z)^n} \geq 0, \tag{2.93}$$

as the AT stability condition of the RS solution. Once the AT stability breaks, it is believed that the FRSB solution is required to describe the behavior of the system.

Connection to the divergence of the spin-glass susceptibility

As we can expect, the AT condition is related to the divergence of the spin-glass susceptibility χ_{SG} which is defined in section 1.1. To elucidate this point, we here calculate the spin-glass susceptibility for the fully-connected p-spin interacting model. The following calculations are based on those in reference [40].

We first introduce the modified generating function $\widetilde{\phi}(n, m, \boldsymbol{F})$, in which we introduce the RS interaction $\boldsymbol{F}$ among m out of n replicas,

$$\begin{aligned} N\widetilde{\phi}_N(n, m, \boldsymbol{F}) &= \log \left[\left(\mathrm{Tr}\, e^{-\beta H} \right)^{n-m} \left(\mathrm{Tr}\, e^{\beta \sum_{a=1}^m H^a + \sum_i^N F_i \sum_{a<b} S_i^a S_i^b} \right) \right]_{\boldsymbol{J}} \\ &= \log \left[\left(\mathrm{Tr}\, e^{\beta \sum_{i_1 < \ldots < i_p} J_{i_1 \ldots i_p} \sum_{\mu=1}^n S_{i_1}^\mu \ldots S_{i_p}^\mu + \sum_i^N F_i \sum_{a<b} S_i^a S_i^b} \right) \right]_{\boldsymbol{J}}. \end{aligned} \tag{2.94}$$

We hereafter assume that the indices a, b run only among m replicas, while μ, ν run all n replicas. Note that not only the limit $\boldsymbol{F} \to 0$ but also the limit $m \to 1$ reproduce the

normal generating function $\phi(n)$ from eq. (2.94). The limit $m \to 1$ can be taken by using the analytic continuation from $m \in \mathbb{N}$ to $\mathbb{C}$

$$N\widetilde{\phi}(n,m,\boldsymbol{F}) = \log\left[\prod_{i=1}^{N}\int Dz_i \left(\mathrm{Tr}\, e^{-\beta H+\sum_{i=1}^{N}\sqrt{F_i}z_iS_i}\right)^m \left(\mathrm{Tr}\, e^{-\beta H}\right)^{n-m}\right]_{\boldsymbol{J}}, \tag{2.95}$$

where we have used the Hubbard-Stratonovich transformation. To see the stability of the system against introduction $\boldsymbol{F}$, let us expand $\widetilde{\phi}(n,m,\boldsymbol{F})$ with respect to $\boldsymbol{F}$. Denoting $Z(\boldsymbol{J}) = \mathrm{Tr}\, e^{-\beta H(\boldsymbol{S}|\boldsymbol{J})}$, we can express the first derivative as

$$N\frac{\partial\widetilde{\phi}}{\partial F_k} = \frac{\left[Z^{n-m}(\boldsymbol{J})\left(\mathrm{Tr}\left(\sum_{a<b}S_k^aS_k^b\right)e^{\beta\sum_{a=1}^{m}H^a+\sum_i^N F_i\sum_{a<b}S_i^aS_i^b}\right)\right]_{\boldsymbol{J}}}{\left[Z^{n-m}(\boldsymbol{J})\left(\mathrm{Tr}\, e^{\beta\sum_{a=1}^{m}H^a+\sum_i^N F_i\sum_{a<b}S_i^aS_i^b}\right)\right]_{\boldsymbol{J}}} = \left[\sum_{a<b}\left\langle S_k^aS_k^b\right\rangle_{m,\boldsymbol{F}}\right]_{n,\boldsymbol{F}}, \tag{2.96}$$

where the brackets $\langle(\cdots)\rangle_{m,\boldsymbol{F}}$ and $[(\cdots)]_{n,\boldsymbol{F}}$ denote the following averages

$$\langle(\cdots)\rangle_{m,\boldsymbol{F}} = \frac{1}{Z^m(\boldsymbol{J},\boldsymbol{F})}\mathrm{Tr}\,(\cdots)\,e^{\beta\sum_{a=1}^{m}H^a+\sum_i^N F_i\sum_{a<b}S_i^aS_i^b} \tag{2.97}$$

$$[(\cdots)]_{n,\boldsymbol{F}} = \frac{\left[(\cdots)\,Z^{n-m}(\boldsymbol{J})Z^m(\boldsymbol{J},\boldsymbol{F})\right]_{\boldsymbol{J}}}{\left[Z^{n-m}(\boldsymbol{J})Z^m(\boldsymbol{J},\boldsymbol{F})\right]_{\boldsymbol{J}}} \tag{2.98}$$

where we define $Z(\boldsymbol{J},\boldsymbol{F}) = \mathrm{Tr}\, e^{\beta\sum_{a=1}^{m}H^a+\sum_i^N F_i\sum_{a<b}S_i^aS_i^b}$, and the second derivative becomes

$$N\frac{\partial^2\widetilde{\phi}}{\partial F_k\partial F_l} = \left[\sum_{a<b}\sum_{c<d}\left\langle S_k^aS_k^bS_l^cS_l^d\right\rangle_{m,\boldsymbol{F}}\right]_{n,\boldsymbol{F}} - \left[\sum_{a<b}\left\langle S_k^aS_k^b\right\rangle_{m,\boldsymbol{F}}\right]_{n,\boldsymbol{F}}\left[\sum_{c<d}\left\langle S_l^cS_l^d\right\rangle_{m,\boldsymbol{F}}\right]_{n,\boldsymbol{F}} \tag{2.99}$$

The first term of this equation gives the following three contributions

$$\begin{aligned}&\frac{m(m-1)}{2}\left[\left\langle S_k^aS_l^aS_k^bS_l^b\right\rangle_{m,\boldsymbol{F}}\right]_{n,\boldsymbol{F}} + m(m-1)(m-2)\left[\left\langle S_k^aS_l^aS_k^bS_l^d\right\rangle_{m,\boldsymbol{F}}\right]_{n,\boldsymbol{F}}\\ &+\frac{m(m-1)(m-2)(m-3)}{4}\left[\left\langle S_k^aS_l^bS_k^cS_l^d\right\rangle_{m,\boldsymbol{F}}\right]_{n,\boldsymbol{F}},\end{aligned} \tag{2.100}$$

Hereafter, we concentrate on the case where m is slightly larger than unity $m = 1+\epsilon$. In this case, eq. (2.100) yields $O(m-1)$ terms. On the other hand, the second term in eq. (2.99) is negligible because the order is $O((m-1)^2)$. Taking the limit $\boldsymbol{F} \to 0$, we can find that the m replicas become completely independent and $\langle(\cdots)\rangle_{m,\boldsymbol{F}}$ is reduced to the thermal average $\langle(\cdots)\rangle_m$ with respect to the m-replicated original Hamiltonian $\sum_{a=1}^{m}H^a$, which yields the following expressions of the derivatives up to the order $O(m-1)$,

$$N\frac{\partial\widetilde{\phi}}{\partial F_k}\bigg|_{\boldsymbol{F}=0} \approx \frac{(m-1)}{2}q, \quad N\frac{\partial^2\widetilde{\phi}}{\partial F_k\partial F_l}\bigg|_{\boldsymbol{F}=0} \approx \frac{m-1}{2}\left[\left(\langle S_lS_k\rangle - \langle S_l\rangle\langle S_k\rangle\right)^2\right]_n, \tag{2.101}$$

where the brackets $[(\cdots)]_n$ denote $[(\cdots)]_n = \lim_{\boldsymbol{F}\to 0}[(\cdots)]_{n,\boldsymbol{F}} = [Z^n(\cdots)]_{\boldsymbol{J}}/[Z^n]_{\boldsymbol{J}}$. Hence, we obtain the modified generating function as

$$N\widetilde{\phi}(n,1+\epsilon,\boldsymbol{F}) \approx N\phi(n) + \frac{\epsilon}{2}q\sum_i F_i + \frac{\epsilon}{2}\boldsymbol{F}^{\mathrm{T}}\widehat{\chi}_{SG}\boldsymbol{F} + O(\epsilon^2), \tag{2.102}$$

where $\boldsymbol{F}^{\mathrm{T}}$ denotes the transpose matrix of $\boldsymbol{F}$ and $\widehat{\chi}_{SG}$ represents the spin-glass susceptibility matrix having the component $(\widehat{\chi}_{SG})_{lk} = \left[(\langle S_l S_k\rangle - \langle S_l\rangle \langle S_k\rangle)^2\right]_n$. Equation (2.102) implies that the largest eigenvalue of the matrix $\widehat{\chi}_{SG}$ is related to the stability of the system against introduction $\boldsymbol{F}$. We can expect that the system statistically has the translational invariance, which implies that the eigenvector of the largest eigenvalue is given by $\mathbf{1} = (1, 1, \cdots, 1)/\sqrt{N}$. Hence, the largest eigenvalue becomes

$$\frac{1}{N}\mathbf{1}^{\mathrm{T}}\widehat{\chi}_{SG}\mathbf{1} = \frac{1}{N}\sum_{l,k}\left[(\langle S_l S_k\rangle - \langle S_l\rangle \langle S_k\rangle)^2\right]_n = \chi_{SG}. \tag{2.103}$$

This gives a natural extension of the spin-glass susceptibility to the finite replica case and implies the relation between the divergence of the spin-glass susceptibility and the instability against introduction of interactions between replicas.

Next, we express $\widetilde{\phi}(n, m, \boldsymbol{F})$ in a more tractable form. Using the replica method and following the calculations in section 2.1, we can obtain

$$\widetilde{\phi}(n) = \underset{q^{\mu\nu},\widehat{q}^{\mu\nu}}{\mathrm{Extr}}\left\{\frac{\beta^2}{2}\sum_{\mu<\nu}(q^{\mu\nu})^p - \sum_{\mu<\nu} q^{\mu\nu}\widehat{q}^{\mu\nu} + \frac{1}{4}\beta^2 n + \frac{1}{N}\log \mathrm{Tr}\, e^L\right\}, \tag{2.104}$$

where

$$L = \sum_{i=1}^{N}\left\{\sum_{\mu<\nu}\widehat{q}^{\mu\nu}S_i^\mu S_i^\nu + F_i\sum_{a<b}S_i^a S_i^b\right\}. \tag{2.105}$$

The interaction $\boldsymbol{F}$ breaks the replica symmetry and we should choose the appropriate form of $q^{\mu\nu}$ to take the saddle point. Without loss of generality, we can assume that the RS interaction $\boldsymbol{F}$ is introduced into the first m replicas, $(1, \cdots, m)$. A natural form of $q^{\mu\nu}$ is then expressed as

$$(q^{\mu\nu}, \widehat{q}^{\mu\nu}) = \begin{cases} (q_1, \widehat{q}_1) & (\,\mu \in (1, \cdots, m) \text{ and } \nu \in (1, \cdots, m)\,) \\ (q_0, \widehat{q}_0) & (\,\text{otherwise}\,) \end{cases}. \tag{2.106}$$

Under this ansatz, we get

$$\widetilde{\phi}(n, m, \boldsymbol{F}) = \underset{q^1,q^0,\widehat{q}^1,\widehat{q}^0}{\mathrm{Extr}}\left\{\frac{1}{4}n\beta^2 + \frac{1}{2}(n(n-1) - m(m-1))\left(-\widehat{q}_0 q_0 + \frac{1}{2}\beta^2 q_0^p\right)\right.$$
$$\left. + \frac{1}{2}m(m-1)\left(-\widehat{q}_1 q_1 + \frac{1}{2}\beta^2 q_1^p\right) + \frac{1}{N}\log \mathrm{Tr}\, e^{L_0}\right\}, \tag{2.107}$$

where

$$L_0 = \sum_{i=1}^{N}\left\{\widehat{q}_0\sum_{\mu<\nu}S_i^\mu S_i^\nu + (\widehat{q}_1 - \widehat{q}_0 + F_i)\sum_{a<b}S_i^a S_i^b\right\}. \tag{2.108}$$

The saddle-point condition gives

$$q_1 = \frac{2}{m(m-1)} \frac{1}{N} \sum_{i=1}^{N} \left\langle \sum_{a<b} S_i^a S_i^b \right\rangle_{L_0}, \tag{2.109}$$

$$q_0 = \frac{1}{N} \sum_{i=1}^{N} \frac{\left\langle \sum_{\mu<\nu} S_i^\mu S_i^\nu \right\rangle_{L_0} - \left\langle \sum_{a<b} S_i^a S_i^b \right\rangle_{L_0}}{n(n-1)/2 - m(m-1)/2} \tag{2.110}$$

$$\widehat{q}_1 = \frac{1}{2} p\beta^2 q_1^{p-1}, \quad \widehat{q}_0 = \frac{1}{2} p\beta^2 q_0^{p-1}, \tag{2.111}$$

where

$$\langle (\cdots) \rangle_{L_0} = \frac{1}{\mathrm{Tr}\, e^{L_0}} \mathrm{Tr} (\cdots) e^{L_0}. \tag{2.112}$$

In this expression, the derivatives of $\widetilde{\phi}$ are given by

$$\frac{\partial \widetilde{\phi}}{\partial F_l} = \frac{1}{2N} m(m-1) q_1, \quad \frac{\partial^2 \widetilde{\phi}}{\partial F_k \partial F_l} = \frac{1}{2N} m(m-1) \frac{\partial q_1}{\partial F_k}. \tag{2.113}$$

For obtaining the eigenvalue of the Hessian $\partial^2 \widetilde{\phi} / (\partial F_k \partial F_l)$, we should calculate $\partial q_1 / \partial F_k$. The (statistically) translational invariance of the system enables us to simplify the calculation by putting $F_l = F$ for $\forall l$. Differentiating eq. (2.109) with respect to F, we get

$$\frac{\partial q_1}{\partial F} = C + \frac{\partial \widehat{q}_1}{\partial F} \frac{2}{m(m-1)} \left\{ \left\langle \sum_{a<b} \sum_{c<d} S^a S^b S^c S^d \right\rangle_{L_0} - \left\langle \sum_{a<b} S^a S^b \right\rangle_{L_0} \left\langle \sum_{c<d} S^c S^d \right\rangle_{L_0} \right\}, \tag{2.114}$$

where the particular form of the factor C is irrelevant for our current purpose and is omitted here. The second term in the braces $\{\cdots\}$ is again negligible if we consider the case $m = 1 + \epsilon$ because it is $O(\epsilon^2)$. In addition, in the limit $F \to 0$ we can expect that q_1 and q_0 become the RS spin-glass order parameter q, which leads to that the average $\langle (\cdots) \rangle_{L_0}$ becomes identical to the average $\langle (\cdots) \rangle_{\mathrm{RS}}$ in the limit $F \to 0$. These conditions yield

$$\begin{aligned} \left\langle \sum_{a<b} \sum_{c<d} S^a S^b S^c S^d \right\rangle_{L_0} &\to \frac{m(m-1)}{2} + m(m-1)(m-2) \left\langle S^a S^b \right\rangle_{\mathrm{RS}} \\ &+ \frac{m(m-1)(m-2)(m-3)}{4} \left\langle S^a S^b S^c S^d \right\rangle_{\mathrm{RS}} \approx \frac{\epsilon}{2} \left\{ 1 - 2q + r \right\}, \end{aligned} \tag{2.115}$$

where q and r are defined in eqs. (2.18) and (2.92), respectively. Substituting these conditions and $\partial \widehat{q}_1 / \partial F = p(p-1)\beta^2 q^{p-2} (\partial \widehat{q}_1 / \partial F)/2$ into eq. (2.114), we finally get

$$\left. \frac{\partial q_1}{\partial F} \right|_{F=0} \propto \left(1 - \frac{1}{2} \beta^2 p(p-1) q^{p-2} (1 - 2q + r) \right)^{-1}. \tag{2.116}$$

Using eqs. (2.18) and (2.92), we find that this condition is identical to the AT condition. From (2.101) and (2.113), the spin-glass susceptibility is proportional to $\partial q_1 / \partial F$ and hence the AT condition coincides with the divergence of the spin-glass susceptibility.

2.6.2 Phase diagrams for the $p = 2, 3$ cases

As mentioned in section 2.5.1, the 1RSB solution can be calculated by the RS solution as $\phi_{\rm 1RSB}(n, m) = (n/m)\phi_{\rm RS}(m)$ in the present model[5]. The AT condition is also assessed by the RS solution and hence the RS solution is sufficient to derive phase diagrams for finite p. The resultant plots for $p = 2$ and 3 are given in figs. 2.10 and 2.11, respectively. The

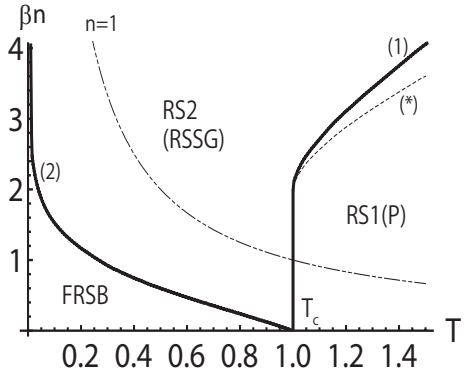

Figure 2.10: Phase diagram of the SK model T-βn plane. The solid lines denote phase boundaries. The boundary between RS2 and FRSB phases is the AT line and is labeled (2). The line $n = 1$ is drawn dashed.

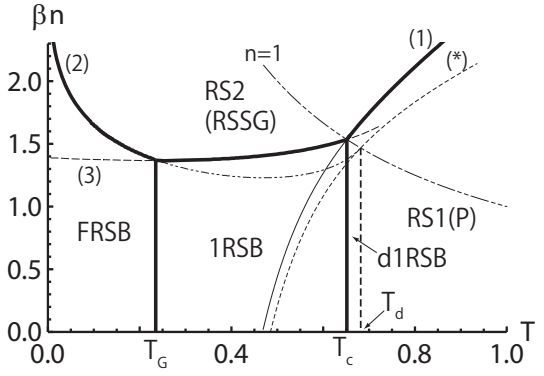

Figure 2.11: Phase diagram of the $p = 3$ case on T-βn plane. The solid lines denote phase boundaries. Above the line indicated by (*), there are two RS saddle points ($q = 0, q > 0$). The dynamical transition temperature T_d exists above the equilibrium transition T_c.

solid lines in figs. 2.10 and 2.11 represent phase boundaries. We see the contents of these phase diagrams in the following.

First, let us consider the $p = 2$ case. In this case, the transition temperature T_c at $n = 0$ is assessed by the perturbative approach because the transition is of second order. We expand the right-hand side of eq. (2.18) with respect to $\widehat{q} = \beta^2 q$ to second order and get

$$q \approx \beta^2 q + (n-2)\beta^4 q^2. \tag{2.117}$$

This equation indicates that for $n \leq 2$ the transition is of second order and the transition temperature is $T_c = 1$ and a phase boundary exists in a vertical form at T_c from $n = 0$ to $n = 2$. For larger n, the transition is of first order and it is required to numerically solve eq. (2.18). Above the line labeled by $(*)$ in fig. 2.10, there are two stable solutions $q = 0$ and $q > 0$, and we call them the RS1 and RS2 solutions, respectively, similarly to the REM case. For large n the RS2 solution dominates the system in the whole range of temperature. For small n, at high temperatures $T > T_c$ we can draw a phase boundary between the RS1 and RS2 phases by equating $\phi_{\rm RS1}(n)$ and $\phi_{\rm RS2}(n)$ and the actual boundary is indicated by the line (1) in fig. 2.10. On the other hand, at low

[5]This is a particular property of models with $q_0 = 0$. If the external field is introduced into the present model, the equality $q_0 = 0$ does not hold any more, and we must consider the 1RSB solution directly. We will treat such a model with $q_0 \neq 0$ in chapter 3.

temperatures $T \leq T_c$, we must consider the RSB of the RS2 solution. The line where the AT stability breaks is the AT line which indicated by (2) in fig. 2.10. Below the AT line, the system requires the FRSB solution. Although there exists a region where the rate function assessed by the RS2 solution becomes positive below the AT line, that region is irrelevant because the RS solution does not hold any meaning below the AT line. In the low temperature limit $\beta \to \infty$, we can analytically derive the asymptotic behavior of the AT line. We here omit the detailed calculations and only give the result

$$\beta n \approx \sqrt{\frac{4}{p} \log \left(\sqrt{\frac{p}{2}} \beta \right)}. \tag{2.118}$$

Hence the AT line diverges in the T-βn plane.

Next, we consider the $p = 3$ case. In this case, transitions are of first order and we need numerical calculations to determine phase boundaries. Unlike the SK ($p = 2$) case, there is a region where the 1RSB solution is relevant, which is signaled by the behavior of the rate function $R(f(n))$. The line indexed by (3) denotes the critical condition $R(f(n)) = 0$ and below this line the rate function is naturally continued to the positive complexity, which means the emergence of the 1RSB phase. The meaning of other symbols in fig. 2.11 are the same as in the $p = 2$ case. The equilibrium transition from the paramagnetic to 1RSB phases occurs at T_c and the equilibrium free energy $f_{\rm eq}$ shows a singularity at this temperature. In addition, at lower temperatures the AT line (2) exceeds the line (3), which leads to another phase transition at T_G. The system is dominated by the FRSB solution below the AT line, and the transition from the 1RSB to FRSB is sometimes called the Gardner transition [41].

Another important fact for the $p = 3$ case is that a non-equilibrium transition, the so-called dynamical transition, occurs at T_d. At this temperature, the equilibrium free energy does not show any singularity, but the phase structure of the system drastically changes. For $T > T_d$, only the paramagnetic solution $q = 0$ exists for $n = 1$[6], which means that the complexity takes 0 at $f = f_P$ and $-\infty$ otherwise. On the other hand, for $T_c \leq T \leq T_d$, there are two solutions $q > 0$ and $q = 0$, which indicates that the nontrivial 1RSB saddle point exists and many pure states appear, which yields the complexity in a certain range of free energy. These pure states affect the dynamics of the system and the system cannot reach the equilibrium states, although the equilibrium value of free energy $f_{\rm eq}$ is completely the same as the paramagnetic one f_P for $T > T_d$. This transition is sometimes called the dynamical 1RSB transition (d1RSB). In the REM, there exist two solutions $q = 1$ and $q = 0$ in the whole temperature region and we did not realize the existence of this dynamical transition[7]. This dynamical transition revealed by the complexity analysis is also confirmed by some numerical approaches [10, 11, 42] which directly investigate dynamical properties. The complexity is nowadays considered to be

[6] Remember the 1RSB-RS correspondence (2.73), i.e. the replica number n of the RS solution corresponds to the 1RSB breaking parameter m, and the specialty of $m = 1$.

[7] We can also interpret as that the dynamical transition temperature of the REM is $T_d = \infty$.

one of the most important concepts to understand not only dynamical behaviors of various systems but also the replica method itself.

2.7 Microscopic description of pure states

In this final section of this chapter, we present the microscopic description of pure states of spin glasses. A basis of this attempt is the so-called TAP equation which is a set of equations with respect to the local magnetizations $\{m_i\}$ and is first derived by Thouless et al. [27].

2.7.1 TAP method

We here treat the SK model, the $p = 2$ case, as an example. The TAP equation for the SK model is given by

$$m_i = \tanh\beta\left\{\sum_{j\neq i} J_{ij}m_j + h_i - \beta(1-q)m_i\right\}. \tag{2.119}$$

For readers interested in the derivation of this equation, we refer to [43]. The corresponding TAP free energy $f_{\mathrm{TAP}}(\{m_i\})$ is expressed as

$$Nf_{\mathrm{TAP}}(\{m_i\}) = -\sum_{i<j} J_{ij}m_i m_j - T\sum_i s_0(m_i) \tag{2.120}$$

where

$$\begin{aligned} s_0(q, m_i) &= -\frac{1+m_i}{2}\log\left(\frac{1+m_i}{2}\right) - \frac{1-m_i}{2}\log\left(\frac{1-m_i}{2}\right) + \frac{\beta^2}{4}(1-q)^2 \\ &= -\frac{1}{2}\log(1-m_i^2) - m_i\tanh^{-1}(m_i) + \log 2 + \frac{\beta^2}{4}(1-q)^2. \end{aligned} \tag{2.121}$$

where q is the spin-glass order parameter and equals to $(\sum m_i^2)/N$. Taking variation of $f_{\mathrm{TAP}}(\{m_i\})$ with respect to m_i, we again obtain eq. (2.119).

In the TAP context, pure states are identified with the solutions of eq. (2.119)[8]. The number of TAP solutions with the free energy value f, $\mathcal{N}_{\mathrm{TAP}}(f)$, is hence given by

$$\mathcal{N}_{\mathrm{TAP}}(f) = \int\prod_i\left\{dm_i\delta\left(\frac{\partial f_{\mathrm{TAP}}(\{m_i\})}{\partial m_i}\right)\right\}|\det G|\,\delta(f_{\mathrm{TAP}}(\{m_i\}) - f), \tag{2.122}$$

where G is the Hessian of the TAP free energy

$$G_{ij} = \frac{\partial^2 f_{\mathrm{TAP}}(\{m_i\})}{\partial m_i\partial m_j} = -J_{ij} + \left(\beta(1-q) + \frac{1}{\beta}\frac{1}{1-m_i^2}\right)\delta_{ij}. \tag{2.123}$$

[8]Historically, the notion of pure state was first founded through analyzing the TAP equation.

The TAP complexity is defined by $\Sigma_{\rm TAP}(f) = (\log \mathscr{N}_{\rm TAP}(f))/N$ and is assumed to be self averaging, which leads to the quantity to be calculated as

$$\Sigma_{\rm TAP}(f) = \frac{1}{N}[\log \mathscr{N}_{\rm TAP}(f)]_{\boldsymbol{J}}. \tag{2.124}$$

This was first formulated by Bray and Moore [44] and is reexamined many times [37, 45–47]. The calculations are straightforward but rather involved and we only give a sketch of actual calculations and refer the results of [47]. The evaluation procedure is as follows:

1. Replace $[\log \mathscr{N}(f)]_{\boldsymbol{J}}$ by $\log[\mathscr{N}^n(f)]_{\boldsymbol{J}}$ by using the replica method.
2. The modulus of $|\det G|$ is removed to simplify the calculation (there is no *a priori* justification of this assumption) and $\det G$ is expressed by using Grassmann variables ψ_i in an integral form $\det G = \int \prod_i \left(d\psi_i d\bar{\psi}_i\right) \exp\left(\sum_{i,j} \psi_i \bar{\psi}_j G_{ij}\right)$.
3. The delta functions in eq. (2.122) are transformed into the Fourier expressions as $\delta(f_{\rm TAP}(\{m_i\}) - f) = \int du/(2\pi i) \exp\{u(f_{\rm TAP}(\{m_i\}) - f)\}$, and all the relevant factors are expressed in an exponential form $\exp(A)$ with an effective action A.
4. The configurational average is performed and then the RS and the Becchi-Rouet-Stora-Tyutin (BRST) supersymmetry are imposed on the effective action A.
5. Finally, the complexity is assessed by using the saddle-point method and taking the $n \to 0$ limit.

Note that it is known that the RS assumption usually yields the same result with the annealed approximation $[\log \mathscr{N}_{\rm TAP}(f)]_{\boldsymbol{J}} \approx \log[\mathscr{N}_{\rm TAP}(f)]_{\boldsymbol{J}}$, and actual calculations are also performed in this approximation in [47] as other references [44–46]. Leaving a parameter u which determines the value of TAP free energy $f_{\rm TAP}$, we can express the TAP complexity as

$$\begin{aligned}\Sigma_{\rm TAP}(f;u) = &\frac{1}{4}\beta^2 u(-u-1)q^2 + \frac{\beta^2}{2}uq - \frac{1}{4}\beta^2 u \\ &+ \log \int Dz \left(2\cosh\sqrt{\beta^2 q}z\right)^{-u} - \beta u f\end{aligned} \tag{2.125}$$

Taking the maximization with respect to u gives the TAP complexity for a free energy value f, $\Sigma_{\rm TAP}(f)$. Comparing eqs. (2.58) with $p = 2$ and (2.125), we can find a formal correspondence between the TAP complexity and the generating function $g(x)$ assessed in the 1RSB level as

$$\Sigma_{\rm TAP}(f; u = -x) = g(x) + \beta x f. \tag{2.126}$$

Taking the minimization with respect to x of the right-hand side yields the complexity in the replica theory of the 1RSB level, hence the TAP and replica theories completely give the same result. This fact supports not only the consistency of different methods but also the correctness of microscopic description of pure states based on the TAP equation.

2.7.2 Zero temperature limit

In the previous discussion, we have seen that pure states statistics based on the microscopic description, the TAP method, gives the same result as the replica one. To investigate the microscopic description of pure states in more detail, we here concentrate on the zero temperature limit. In this limit, pure states are related to stable configurations against single spin flips.

Although it is possible to propose some stabilities of a spin configuration at zero temperature, the stability against single spin flip can be considered as the most natural one. Consider a spin S_i at site i and the effective field $h_i^{\rm eff}$

$$h_i^{\rm eff} = \sum_{j \neq i} J_{ij} S_j. \tag{2.127}$$

The stability condition of $\{S_i\}$ against any single spin flip is that inequalities

$$h_i^{\rm eff} S_i \geq 0 \tag{2.128}$$

hold for all i. This is the same condition as equalities

$$S_i = {\rm sgn}\left(\sum_{j \neq i} J_{ij} S_j \right) \tag{2.129}$$

hold for all i. Since m_i can be identified with the spin S_i in the limit $\beta \to \infty$, eq. (2.129) is nothing but the TAP equation at zero temperature with a condition[9]

$$\beta(1-q) \to 0. \tag{2.130}$$

Equation (2.129) and the discussion in the previous subsection imply that pure states at zero temperature are connected to stable spin configurations against any single spin flip.

Note that this simple relation is, however, considered to be peculiar to the fully-connected models. This important fact was first pointed out by Biroli and Monasson [29]. In order to follow their discussion, we here define a *k-stable* configuration as the configuration the energy of which cannot be decreased by flipping any subset of k (or less than k) spins. In this context, pure states of fully-connected models at zero temperature correspond to 1-stable spin configurations. Denoting the number of k-stable configurations with the energy density e as $\mathscr{N}_k(e)$, we can define a kind of entropy of k-stable configurations, $s_k(e)$, as $s_k(e) \equiv (\log \mathscr{N}_k(e))/N$ in the $N \to \infty$ limit. Biroli and Monasson have shown that the TAP complexity $\Sigma_{\rm TAP}(e)$ is identical to $s_\infty(e)$ by treating a hybrid system of one dimensional and fully-connected models. They have also alleged that the k-stable entropy $s_k(e)$ does not depend on k in the fully-connected models, which leads to an accidental correspondence between $\Sigma_{\rm TAP}(e)$ and $s_1(e)$. This peculiar property to the fully-connected models can be understood as follows: Let us denote the energy deviation

[9] This condition has some delicate points as pointed out in [47], but we do not treat this problem and only adopt the condition $\beta(1-q) \to 0$ in the limit $\beta \to \infty$.

induced by flipping a spin S_i as ΔE_i. If we flip two spins S_i and S_j, the energy deviation ΔE_{ij} equals to $\Delta E_{ij} = \Delta E_i + \Delta E_j - 2J_{ij}S_iS_j$. This energy deviation ΔE_{ij} becomes, however, $\Delta E_{ij} = \Delta E_i + \Delta E_j$ in the $N \to \infty$ limit because J_{ij} is scaled as $O(1/\sqrt{N})$, which means that a 1-stable configuration is also 2-stable, and the same holds for all k. Therefore, $s_k(e)$ does not depend on k and $s_1 = \cdots = s_\infty = \Sigma_{\rm TAP}$.

In conclusion, the microscopic description of pure states is given by the TAP equation. The TAP method gives a simple description of pure states for the fully-connected models, but for more realistic models there still remain some unclear points about the existence and the properties of pure states.

2.8 Summary

In this chapter, we reviewed the replica method in detail by treating the fully-connected p-spin interacting model as an example. The relation between the replica symmetry breaking (RSB) and the emergence of many pure states was closely explained and the distribution of pure states, the complexity $\Sigma(f)$, was calculated in the 1-step RSB (1RSB) level. This description of the 1RSB was also reexamined from a viewpoint of the large deviation theory, and the 1RSB transition was interpreted from the rate function $R(f(n))$. In our particular model, the complexity and rate function share the same functional form, which implies a close relation between these quantities. In addition, the microscopic description of pure states was presented from the TAP context. At zero temperature it was explained that stable spin configurations against ∞-spin flips correspond to pure states, but for the fully-connected models pure states are also identical to the stable spin configurations against single spin flip. It was shown from a simple discussion about the energy balance that this property is peculiar to the fully-connected models.

Viewpoints from pure state statistics and the large deviation theory proposed in this chapter are rather recent results. In past days the RSB formulation was performed without realizing these backgrounds and some confusing discussions were proposed. This chapter is written to clarify these points by comparing conventional and modern operations of the RSB.

Pure states at zero temperature generally correspond to spin configurations stable against ∞-spin flips after taking the thermodynamic limit $N \to \infty$, but for the fully-connected models such configurations are the same as 1-stable spin configurations. This peculiar property is useful for identifying pure states to numerically evaluate the complexity. In the next chapter, we will utilize this property and calculate the complexity numerically to verify the prediction of the replica result.

Chapter 3

Analyses of weight space structure and rare events in the Ising perceptron

In the previous chapter, we introduced the replica method and also elucidated its aspects as a tool to obtain the pure state statistics and large deviations. In this chapter, we reexamine these aspects extensively by treating a model of a neuron, namely the so-called Ising perceptron.

As seen in sec. 2.5, the rate function $R(f)$, which represents a small probability of atypical samples, and the complexity $\Sigma(f)$, which represents a large number of pure states that appear for typical samples, share not only the similar mathematical structure but also the same functional form for the fully-connected p-spin interacting model. This fact naturally motivates us to further explore more general relationships between $R(f)$, and $\Sigma(f)$, including cases for which the formal accordance of functional forms between $R(f)$ and $\Sigma(f)$ does not hold.

The Ising perceptron considered here is a simple model of a neuron and stores random input-output patterns. There are two reasons for considering this system. First, the Ising perceptrons can be macroscopically characterized by a few sets of order parameters and are relatively easier to handle. Despite the simplicity, it is known that this model exhibits rich behavior in the phase space involving nontrivial RSB phenomena [48, 49] and is considered to show different functional forms of $R(f)$ and $\Sigma(f)$, which is highly suitable for our purpose. The second reason is that the meaning of complexity for the Ising perceptrons of finite size is clearer. For the Ising perceptrons, a pure state at zero temperature can be identified with a stable cluster, the definition of which will be given in section 3.4, with respect to single spin flips [28, 29, 50]. For samples of small systems, the size of the clusters can be numerically evaluated by exhaustive enumeration without any ambiguity. This property is extremely useful for justifying theoretical predictions through numerical experiments.

Our investigations reveal that the generating function $g(x)$ of the complexity $\Sigma(f)$ shows an extraordinary behavior, the origin of which is that $\Sigma(f)$ and $R(f)$ of the Ising

perceptron are not convex upward functions, which is assumed in usual analyses. The results presented in this chapter are summarized in reference [51].

3.1 Model

A simple perceptron is a model of a neuron, the function of which is a map from $\mathbb{R}^N$ to $\{+1, -1\}$ as

$$y = \begin{cases} +1, & \boldsymbol{S} \cdot \boldsymbol{x}/\sqrt{N} > 0, \\ -1, & \boldsymbol{S} \cdot \boldsymbol{x}/\sqrt{N} < 0, \end{cases} \tag{3.1}$$

where $\boldsymbol{x} \in \mathbb{R}^N$ is the input pattern and $y \in \{+1, -1\}$ is the output label. The vector $\boldsymbol{S}$ denotes the synaptic weights. We hereafter focus on the Ising weight case, in which each

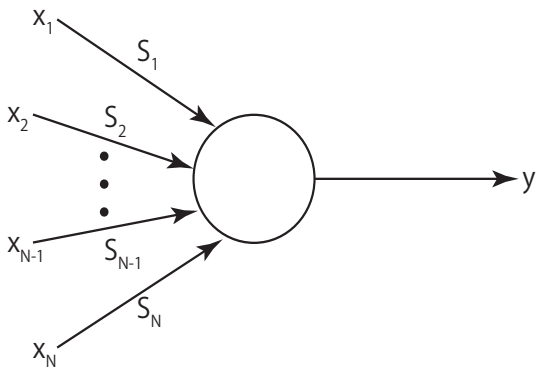

Figure 3.1: A conceptual picture of a simple perceptron.

synaptic weight only takes $S_i = \pm 1$. In a general scenario, the perceptron stores a given set of M labeled patterns

$$D^M = \{(\boldsymbol{x}_1, y_1), \cdots, (\boldsymbol{x}_M, y_M)\}, \tag{3.2}$$

by adjusting the weight $\boldsymbol{S}$ so as to completely reproduce the given label y_μ for the input $\boldsymbol{x}_\mu$ for $\mu = 1, 2, \ldots, M$.

In the following, we consider a situation in which the patterns are independently and identically distributed (i.i.d.). In the conventional situations of the neural networks, a network consisting from Ising perceptrons is considered and in that situation the input $\boldsymbol{x}$ is a set of outputs of other perceptrons [24]. This means that the input $\boldsymbol{x}$ is usually chosen as random signs $x_i = \pm 1$, but in the thermodynamic limit we can regard $\boldsymbol{S} \cdot \boldsymbol{x}$ as multivariate Gaussian random variables due to the central limit theorem. Hence, it is convenient to assume the following distributions

$$P(\boldsymbol{x}) = \left(\frac{1}{\sqrt{2\pi}}\right)^N \exp\left(-\frac{\boldsymbol{x}^2}{2}\right), \tag{3.3}$$

$$P(y) = \frac{1}{2}\left(\delta(y-1) + \delta(y+1)\right), \tag{3.4}$$

from the beginning of the analysis. The question we address here is how the space of the weights that store D^M is characterized macroscopically when the pattern ratio $\alpha = M/N \sim O(1)$ is fixed as M and N tend to infinity. In order to express this problem in the statistical mechanical context, we define the Hamiltonian as

$$\mathscr{H}(\boldsymbol{S}|D^M) = \sum_{j=1}^{M} \Theta\left(-y_j \frac{\boldsymbol{S}\cdot\boldsymbol{x}_j}{\sqrt{N}}\right), \tag{3.5}$$

which counts the number of patterns which are incompatible with the weight $\boldsymbol{S}$. The function $\Theta(x)$ is the step function where $\Theta(x) = 1\,(x > 0)$ and $\Theta(x) = 0$ otherwise. Using the Hamiltonian we can define the partition function

$$Z(D^M) = \operatorname*{Tr}_{\boldsymbol{S}} e^{-\beta\mathscr{H}(\boldsymbol{S}|D^M)}, \tag{3.6}$$

The quantity $Z(D^M)$ varies randomly depending on the quenched randomness D^M, which naturally leads us to evaluate the generating function $\phi(n) = (1/N)\log\left[Z^n(D^M)\right]_{D^M}$, where $[\cdots]_{D^M}$ represents the operation of averaging with respect to D^M.

3.2 Formalism

The generating function $\phi(n)$ can be evaluated by using the replica method. Following the standard prescription of the replica method, we calculate the averaged nth moment in $n \in \mathbb{N}$

$$[Z^n]_{D^M} = \operatorname{Tr}\left[\exp\left(-\beta\sum_{\mu=1}^{n}\sum_{j=1}^{M}\Theta\left(-y_j\frac{\boldsymbol{S}^\mu\cdot\boldsymbol{x}_j}{\sqrt{N}}\right)\right)\right]_{D^M} \tag{3.7}$$

where the brackets $[\cdots]_{D^M}$ denote the average over the quenched randomness D^M. According to eq. (3.3), the variable $u_j^\mu = -y_j\boldsymbol{S}^\mu\cdot\boldsymbol{x}_j/\sqrt{N}$ $(\mu = 1, 2, \ldots, n; j = 1, 2, \ldots, M)$ can be regarded as multivariate Gaussian random variable, which is characterized as

$$\left[u_j^\mu\right]_{D^M} = 0,\ \left[u_j^\mu u_k^\nu\right]_{D^M} = \delta_{jk}\left(\delta_{\mu\nu} + (1-\delta_{\mu\nu})q^{\mu\nu}\right), \tag{3.8}$$

where $q^{\mu\nu} = (1/N)\sum_{i=1}^{N} S_i^\mu S_i^\nu$ $(\mu, \nu = 1, 2, \ldots, n)$. This observation yields the following expression

$$\begin{aligned}
&\left[\exp\left(-\beta\sum_{\mu=1}^{n}\sum_{j=1}^{M}\Theta\left(-y_j\frac{\boldsymbol{S}^\mu\cdot\boldsymbol{x}_j}{\sqrt{N}}\right)\right)\right]_{D^M} \\
&= \int\prod_{\mu<\nu} dq^{\mu\nu}\,\delta\left(\boldsymbol{S}^\mu\boldsymbol{S}^\nu - Nq^{\mu\nu}\right)\left(\left[\exp\left(-\beta\sum_{\mu=1}^{n}\Theta\left(u^\mu\right)\right)\right]_{\boldsymbol{u}}\right)^M
\end{aligned} \tag{3.9}$$

where $[\cdots]_{\boldsymbol{u}}$ denotes the average with respect to the multivariate Gaussian variables the moments of which are given by eq. (3.8), and the independency of M examples is reflected

in eq. (3.9). Using the Fourier expression of the delta function, we get

$$[Z^n]_{D^M} = \int \prod_{\mu<\nu} \frac{dq^{\mu\nu} d\widehat{q}^{\mu\nu}}{2\pi} \exp N \Bigg(- \sum_{\mu<\nu} q^{\mu\nu}\widehat{q}^{\mu\nu} + \log \mathrm{Tr}\, e^{\sum_{\mu<\nu} \widehat{q}^{\mu\nu} S^\mu S^\nu} + \alpha \log \left[e^{-\beta \sum_\mu \Theta(u^\mu)} \right]_{\boldsymbol{u}} \Bigg), \tag{3.10}$$

where we put $\alpha = M/N$. Using the saddle point method, we obtain the generating function as

$$\phi(n,\beta) = \underset{q^{\mu\nu},\widehat{q}^{\mu\nu}}{\mathrm{Extr}} \left\{ - \sum_{\mu<\nu} q^{\mu\nu}\widehat{q}^{\mu\nu} + \log \mathrm{Tr}\, e^{\sum_{\mu<\nu} \widehat{q}^{\mu\nu} S^\mu S^\nu} + \alpha \log \left[e^{-\beta \sum_\mu \Theta(u^\mu)} \right]_{\boldsymbol{u}} \right\}, \tag{3.11}$$

where the symbol Extr_x expresses to take the extremization condition with respect to x.

3.2.1 The replica symmetric solution

The replica symmetric (RS) ansatz gives

$$\widehat{q}^{\mu\nu} = \widehat{q},\ q^{\mu\nu} = q, \tag{3.12}$$

which leads to

$$\sum_{\mu<\nu} q^{\mu\nu}\widehat{q}^{\mu\nu} = \frac{1}{2} n(n-1)\widehat{q}q, \tag{3.13}$$

$$\mathrm{Tr}\, e^{\sum_{\mu<\nu} \widehat{q}^{\mu\nu} S^\mu S^\nu} = e^{-\frac{1}{2}n\widehat{q}} \int Dz (2\cosh \sqrt{\widehat{q}} z)^n, \tag{3.14}$$

where $Dz = dz e^{-z^2/2}/\sqrt{2\pi}$ and we assume that the domain of integration of $\int Dz$ is $]-\infty,\infty[$ if there is no explicit indication. Under the RS ansatz, the Gaussian variable u^μ can be decomposed to two independent Gaussian variables of zero mean and unit variance x^μ and z as

$$u^\mu = \sqrt{1-q}x^\mu + \sqrt{q}z. \tag{3.15}$$

It is easy to check that this assumption satisfies eq. (3.8). Applying this expression, we get

$$\begin{aligned}
\left[e^{-\beta \sum_\alpha \Theta(u^\mu)} \right]_{\boldsymbol{u}} &= \int Dz \int \prod_{\mu=1}^n Dx^\mu e^{-\beta\Theta(u^\mu)} = \int Dz \left(\int Dx e^{-\beta\Theta(u)} \right)^n \\
&= \int Dz \left(\int_{-\infty}^{-\sqrt{\frac{q}{1-q}}z} Dx + \int_{-\sqrt{\frac{q}{1-q}}z}^{\infty} Dx e^{-\beta} \right)^n \\
&= \int Dz \left(e^{-\beta} + (1-e^{-\beta}) E\left(\sqrt{\frac{q}{1-q}} z \right) \right)^n,
\end{aligned} \tag{3.16}$$

where we define the complementary error function $E(x)$

$$E(x) = \int_x^\infty Dz. \tag{3.17}$$

Note that the relation $E(x) + E(-x) = 1$ holds. Using the above expressions, we get the RS generating function as

$$\phi_{\rm RS}(n,\beta) = \underset{q,\widehat{q}}{\rm Extr}\Bigg\{ -\frac{1}{2}n(n-1)\widehat{q}q - \frac{1}{2}n\widehat{q} + \log\int Dz(2\cosh\sqrt{q}z)^n$$
$$+\alpha\log\int Dz\left(E_\beta\left(\sqrt{\frac{q}{1-q}}z\right)\right)^n\Bigg\}, \tag{3.18}$$

where

$$E_\beta(x) = e^{-\beta} + (1-e^{-\beta})E\left(x\right). \tag{3.19}$$

The saddle point conditions yield

$$q = \frac{\int Dz\cosh^n\sqrt{\widehat{q}}z\tanh^2\sqrt{\widehat{q}}z}{\cosh^n\sqrt{\widehat{q}}z}, \tag{3.20}$$

$$\widehat{q} = \frac{\alpha}{2\pi}\frac{(1-e^{-\beta})^2}{1-q}\frac{\int Dze^{-\frac{q}{1-q}z^2}\left(E_\beta\left(\sqrt{\frac{q}{1-q}}z\right)\right)^n}{\int Dz\left(E_\beta\left(\sqrt{\frac{q}{1-q}}z\right)\right)^n}, \tag{3.21}$$

the detailed derivation of which is given in appendix A.1. Before discussing the significance of the RS solution, we proceed to the replica symmetry breaking (RSB) solution. Especially, we utilize the 1RSB ansatz for investigating the complexity and the rate function in a unified framework.

3.2.2 The 1RSB solution

The 1RSB ansatz is expressed as

$$(q^{\mu\nu},\widehat{q}^{\mu\nu}) = \begin{cases} (q_1,\widehat{q}_1) & (\text{ in the same block }) \\ (q_0,\widehat{q}_0) & (\text{ otherwise }) \end{cases}. \tag{3.22}$$

This assumption yields

$$\sum_{\mu<\nu} q^{\mu\nu}\widehat{q}^{\mu\nu} = \frac{1}{2}n(m-1)\widehat{q}_1q_1 + \frac{1}{2}n(n-m)\widehat{q}_0q_0, \tag{3.23}$$

$$\mathrm{Tr}\, e^{\sum_{\mu<\nu}\widehat{q}^{\mu\nu}S^\mu S^\nu} = e^{-\frac{1}{2}n\widehat{q}_1}\int Dz_0\left(\int Dz_1(2\cosh h)^m\right)^{n/m}, \tag{3.24}$$

where $h = \sqrt{\widehat{q}_1-\widehat{q}_0}z_1 + \sqrt{\widehat{q}_0}z_0$ and m is the Parisi's breaking parameter and expresses the size of a block. In the 1RSB ansatz, the Gaussian variable u^μ is decomposed to

$$u^\mu = u^{l,\mu_l} = \sqrt{q_1-q_0}x_l + \sqrt{1-q_1}y_{\mu_l} + \sqrt{q_0}z, \tag{3.25}$$

where the variables x_l, y_{μ_l}, z are drawn from the normal distributions and the index l indicates a block and μ_l specifies a replica in the lth block. This transformation enables us to derive

$$\left[e^{-\beta\sum_\mu \Theta(u^\mu)}\right]_{\boldsymbol{u}} = \left[\prod_l \prod_{\mu_l} e^{-\beta\Theta(\sqrt{q_1-q_0}x_l+\sqrt{1-q_1}y_{\mu_l}+\sqrt{q_0}z)}\right]_{\boldsymbol{u}}$$
$$= \int Dz \left(\int Dx \left\{E_\beta(y_0(z,x))\right\}^m\right)^{n/m}, \tag{3.26}$$

where

$$y_0(z,x) = -\sqrt{\frac{q_0}{1-q_1}}z - \sqrt{\frac{q_1-q_0}{1-q_1}}x. \tag{3.27}$$

Finally, we get

$$\phi_{\rm 1RSB}(n,m,\beta) = \underset{q_1,q_0,\widehat{q}_1,\widehat{q}_0}{\rm Extr}\left\{-\frac{1}{2}n(m-1)\widehat{q}_1 q_1 - \frac{1}{2}n(n-m)\widehat{q}_0 q_0\right.$$
$$-\frac{1}{2}n\widehat{q}_1 + \log\int Dz_0\left(\int Dz_1(2\cosh h)^m\right)^{n/m}$$
$$\left.+\alpha\log\int Dz_0\left(\int Dz_1\left\{E_\beta(y_0(z_0,z_1))\right\}^m\right)^{n/m}\right\}. \tag{3.28}$$

The saddle point conditions yield the following equations of state

$$q_1 = I^{-1}\int Dz_0\left(\int Dz_1\cosh^m h\right)^{n/m}\frac{\int Dz_1\cosh^m h\tanh^2 h}{\int Dz_1\cosh^m h}, \tag{3.29}$$

$$q_0 = I^{-1}\int Dz_0\left(\int Dz_1\cosh^m h\right)^{n/m}\left(\frac{\int Dz_1\cosh^m h\tanh h}{\int Dz_1\cosh^m h}\right)^2, \tag{3.30}$$

$$\widehat{q}_1 = \frac{\alpha}{1-q_1}\widehat{I}^{-1}\int Dz_0\left(\int Dz_1 E_\beta^m\right)^{n/m}\frac{\int Dz_1 E_\beta^m\left(\frac{E'_\beta}{E_\beta}\right)^2}{\int Dz_1 E_\beta^m}, \tag{3.31}$$

$$\widehat{q}_0 = \frac{\alpha}{1-q_1}\widehat{I}^{-1}\int Dz_0\left(\int Dz_1 E_\beta^m\right)^{n/m}\left(\frac{\int Dz_1 E_\beta^m\frac{E'_\beta}{E_\beta}}{\int Dz_1 E_\beta^m}\right)^2, \tag{3.32}$$

where

$$E'_\beta = E'_\beta(y_0(z_0,z_1)) \equiv \left.\frac{dE_\beta(x)}{dx}\right|_{x=y_0} = -\frac{1-e^{-\beta}}{\sqrt{2\pi}}e^{-\frac{1}{2}y_0^2}, \tag{3.33}$$

$$I = \int Dz_0\left(\int Dz_1\cosh^m h\right)^{n/m}, \tag{3.34}$$

$$\widehat{I} = \int Dz_0\left(\int Dz_1 E_\beta^m\right)^{n/m}. \tag{3.35}$$

Note that we omit the arguments of $E_\beta(y_0(z_0,z_1))$ and $E'_\beta(y_0(z_0,z_1))$ in eqs. (3.29)-(3.32). Before investigating the equations of state (3.29)-(3.32), we again discuss the physical

meaning of the 1RSB formulation for exploring the relation between the concepts of $\phi(n)$, $\Sigma(f)$, and $R(f)$.

3.2.3 The complexity and 1RSB formulation revisited

Two ways of the zero-temperature limit

Let us focus on the $y \to 0$ (or $n \to 0$) limit as in section 2.4. Remember that the generating function $g(x|D^M)$ of the complexity satisfies the following relation

$$e^{Ng(x|D^M)} = \int df e^{N(-\beta x f + \Sigma(f))}. \tag{3.36}$$

For the perceptron problems, we are mainly interested in the structure of the weight space at zero temperature since it directly relates to the learning process of the perceptrons.

To investigate the weight space, there are two different ways for accessing the limit of $\beta \to \infty$.

One way is to take the $\beta \to \infty$ limit with keeping $m = x \sim O(1)$, and we call this limit the *entropic* limit. For our Hamiltonian (3.5), the ground state energy E_{GS} is given by 0 or positive constant depending on the sample D^M. In such a situation, the xth moment of the partition function of pure state γ, $Z_\gamma^x = e^{-\beta x f_\gamma}$ becomes in the $\beta \to \infty$ limit

$$e^{-\beta x f_\gamma} = \begin{cases} e^{x s_\gamma} & (u_{GS} \equiv E_{GS}/N = 0) \\ 0 & (u_{GS} > 0) \end{cases}, \tag{3.37}$$

where s_γ is the entropy of the pure state γ. Hence, this limit enables to investigate the weight space structure with $u_{GS} = 0$ in detail, while it is ill defined for instances with $u_{GS} > 0$. The corresponding generating function becomes

$$g(x|D^M) = \max_{s_- \le s \le s_+} \{xs + \Sigma(s)\}. \tag{3.38}$$

This entropic limit is appropriate when samples with $u_{GS} = 0$ are typically produced, which corresponds to the low α case. Note that if we want to directly investigate this limit we can choose the Boltzmann factor $\eta(\boldsymbol{S}|D^M)$ as

$$\eta(\boldsymbol{S}|D^M) = \prod_{\mu=1}^{M} \Theta\left(y_\mu \frac{\boldsymbol{S} \cdot \boldsymbol{x}_\mu}{\sqrt{N}}\right), \tag{3.39}$$

which is obtained by taking the limit $\beta \to \infty$ in $e^{-\beta \mathscr{H}(\boldsymbol{S}|D^M)}$ and is equal to the number of patterns that are incompatible with the weight $\boldsymbol{S}$.

The other way is to take the $\beta \to \infty$ limit with the $m \to 0$ limit keeping $\beta m \to \xi \sim O(1)$, and we call this limit the *energetic* limit. Although the entropic limit cannot treat instances with $u_{GS} > 0$, but the energetic limit works well for such instances. For a simple explanation, we here use two arguments for the complexity $\Sigma(u, s)$. In this notation, the generating function $g(x|J)$ becomes

$$g(x|D^M) = \max_{u,s} \{x(s - \beta u) + \Sigma(u, s)\}. \tag{3.40}$$

If we take the limit $\beta \to \infty$ under the condition $u > 0$, the entropic term becomes irrelevant. After that, we take $x \to 0$ limit keeping $\beta x \to \xi$ and obtain the finite result

$$g(\xi|D^M) = \max_{u_- \le u \le u_+} \{-\xi u + \Sigma_u(u)\}, \tag{3.41}$$

where

$$\Sigma_u(u) = \max_{s_- \le s \le s_+} \Sigma(u, s). \tag{3.42}$$

This limit is appropriate for the case that samples with $u_{GS} > 0$ typically produced, which corresponds to the high α region. In such a region, we can investigate the energy landscape by using the energetic limit.

The two limits, entropic and energetic, are in a complementary relation. Both limits can detect the critical capacity α_s, below which typical samples are *separable* ($u_{GS} = 0$) but not separable for $\alpha > \alpha_s$. However, for our present purpose, i.e. to investigate the relation among $\phi(n)$, $\Sigma(f)$, and $R(f(n))$, the entropic limit is more suitable. We can expect that for $\alpha > \alpha_s$ behaviors of separable samples which are atypically generated can be investigated by introducing the finite replica number $n > 0$ into the entropic limit, which naturally extends the applicable range of this limit. On the other hand, for the energetic limit we do not have any clear reason to introduce the finite replica. We can also expect that introducing $n > 0$ into the energetic limit enables to investigate $u > 0$ region for $\alpha < \alpha_s$, but the $u > 0$ region can also be treated by introducing finite temperature $T > 0$ for the typical case $n = 0$. Thus, we cannot probably distinguish the effects of finite replica $n > 0$ and of finite temperature $T > 0$. Hence, we hereafter concentrate on the entropic limit.

The RS and 1RSB solutions in the entropic limit

The entropic limit is easily taken by performing the limit $\beta \to \infty$ in eq. (3.18). In this limit, there are two solutions for eqs. (3.20)-(3.21):
RS1: $0 < q < 1$ and $\widehat{q} < +\infty$.

$$\begin{aligned} \phi_{\rm RS1}(n) &= -\frac{n(n-1)}{2} q\widehat{q} - \frac{1}{2} n\widehat{q} + \log\left(\int Dz \left(2\cosh\left(\sqrt{\widehat{q}} z \right) \right)^n \right) \\ &\quad + \alpha \log\left(\int Dz E^n \left(\sqrt{\frac{q}{1-q}} z \right) \right). \end{aligned} \tag{3.43}$$

RS2: $q = 1$ and $\widehat{q} = +\infty$.

$$\phi_{\rm RS2}(n) = (1-\alpha)\log 2. \tag{3.44}$$

Similarly, we can find three solutions of the 1RSB saddle-point equations (3.29)-(3.32):
1RSB1: $(q_1, q_0) = (1, q)$ and $(\widehat{q}_1, \widehat{q}_0) = (+\infty, \widehat{q})$, where q and $\widehat{q}$ take the same values as those for $\phi_{\rm RS1}(n)$.

$$\phi_{\rm 1RSB1}(n, m) = \phi_{\rm RS1}\left(\frac{n}{m} \right). \tag{3.45}$$

1RSB2: $(q_1, q_0) = (q, q)$ and $(\widehat{q}_1, \widehat{q}_0) = (\widehat{q}, \widehat{q})$, where q and $\widehat{q}$ take the same values as those for $\phi_{\rm RS1}(n)$.

$$\phi_{\rm 1RSB2}(n, m) = \phi_{\rm RS1}(n). \tag{3.46}$$

1RSB3: $(q_1, q_0) = (1, 1)$ and $(\widehat{q}_1, \widehat{q}_0) = (+\infty, +\infty)$.

$$\phi_{\rm 1RSB3}(n, m) = \phi_{\rm RS2}(n) = (1 - \alpha) \log 2. \tag{3.47}$$

In usual analyses, Parisi's 1RSB parameter m is determined by the extremum condition in evaluating $\phi(n) = {\rm Extr}_m \{\phi_{\rm 1RSB*}(n, m)\}$, where $* = 1, 2$ and 3. In addition, there might be no need to classify **1RSB2** and **1RSB3** as 1RSB solutions because **1RSB2** and **1RSB3** are completely reduced to **RS1** and **RS2**, respectively. However, handling these three solutions as 1RSB solutions with leaving the m-dependence of $\phi_{\rm 1RSB}(n, m)$ explicitly, is crucial for the current purpose as we will see in section 3.3.

The formulation relating $\phi(n)$ and $\Sigma(s)$ is easily obtained by following the same discussion as section 2.4. Assuming that the complexity $\Sigma(s)$ is a convex upward function, we can get the parameterized forms

$$s(x) = \frac{\partial}{\partial x} \left(x \left. \frac{\partial \phi_{\rm 1RSB}(n, x)}{\partial n} \right|_{n=0} \right), \tag{3.48}$$

$$\Sigma(s(x)) = -x^2 \left. \frac{\partial^2 \phi_{\rm 1RSB}(n, x)}{\partial x \partial n} \right|_{n=0}. \tag{3.49}$$

On the other hand, the relation $\phi(n) = \phi_{\rm 1RSB}(n, x)|_{x=1}$ also holds in the entropic limit. This means that the rate function can be assessed from $\phi_{\rm 1RSB}(n, m)$ as follows:

$$s_{\rm eq}(n) = \frac{\partial \phi_{\rm 1RSB}(n, 1)}{\partial n}, \tag{3.50}$$

$$R(s_{\rm eq}(n)) = \phi_{\rm 1RSB}(n, 1) - n \frac{\partial \phi_{\rm 1RSB}(n, 1)}{\partial n}, \tag{3.51}$$

where we define the equilibrium value of entropy

$$s_{\rm eq} \equiv \lim_{N \to \infty} \lim_{\beta \to \infty} (1/N) \log Z = \max_{s_- \leq s \leq s_+} \{s + \Sigma(s)\} \tag{3.52}$$

which corresponds to the total number of weights that are compatible with D^M. In eq. (3.49), the parameter x can vary only in such a range that both $s(x) \geq 0$ and $\Sigma(s(x)) \geq 0$ hold. Similarly, the conditions $s_{\rm eq}(n) \geq 0$ and $R(s_{\rm eq}(n)) \leq 0$ restrict the range of n in eq. (3.51). These constitute the main result of this chapter.

Here, three issues are noteworthy. First, for a class of disordered systems, including the p-spin interacting model without external fields, two equalities $\phi_{\rm 1RSB}(n, m) = (n/m)\phi_{\rm RS}(m)$ and $\phi_{\rm 1RSB}(n, m = 1) = \phi_{\rm RS}(n)$, hold in assessing the complexity and rate function, respectively, where $\phi_{\rm RS}(n)$ is an identical RS solution of the generating function $\phi(n)$. Inserting these functions into eqs. (3.49) and (3.51) offers an identical functional form both for the complexity and the rate function, while their domains of definition are

disjointed, except for a point of the typical value of free energy f^* (or entropy s^*), as mentioned in section 2.5. The current system, however, does not possess this property because $\phi_{\rm 1RSB}(n,m) = (n/m)\phi_{\rm RS}(m)$ does not hold for **1RSB1**, **1RSB2**, or **1RSB3** while $\phi_{\rm 1RSB}(n,m=1) = \phi_{\rm RS}(n)$ is always satisfied. Second, eqs. (3.49) and (3.51) are valid only when $\phi_{\rm 1RSB}(n,m)$ are stable against any perturbation for a further RSB. Fortunately, in the present problem, a stable solution against any known RSB instabilities can be constructed for $\forall\alpha > 0$ and $\forall n > 0$. This implies that, in the present analysis, there is no need to consider further RSB. Finally, however, we have to keep in mind that eqs. (3.49) and (3.51) depend on the assumptions that correct $\Sigma(s)$ and $R(s)$ are convex upward functions, respectively. When the convex property does not hold, the estimates of eqs. (3.49) and (3.51) represent not the correct solution, but rather its convex hull. The following analytical and experimental assessment indicates that this is the case for $\Sigma(s)$ of sufficiently low α and $R(s_{\rm eq})$ of sufficiently high α.

3.3 Theoretical predictions

We are now ready to use the formalism developed above to analyze the behavior of the weight space of the Ising perceptron.

3.3.1 Complexity for $\alpha < \alpha_{\rm s} = 0.833\ldots$

In order to perform the analysis, it is necessary to select a certain solution (functional form) among the three candidates of **1RSB1**, **1RSB2**, and **1RSB3**. Analyticity and physical plausibility are two guidelines for this task.

The replica method is a scheme to infer the properties for real replica numbers $n \in \mathbb{R}$ by analytical continuation from those for natural numbers $n = 1, 2, \ldots \in \mathbb{N}$. This indicates that, for examining typical ($n \to 0$) behavior, it is plausible to select the solution of $\phi(n)$ that is dominant around $n \geq 1$, because unity is the natural number that is closest to zero. For $\alpha < \alpha_{\rm s} = 0.833\ldots$, this solution is $\phi_{\rm RS1}(n)$. In addition, the relevant $\phi_{\rm 1RSB}(n,m)$ must agree with this solution at $m = 1$. These considerations offer two candidates of $g(x)$ as

$$g_{\rm 1RSB1}(x) = x\frac{\partial}{\partial n}\phi_{\rm 1RSB1}(n,x)|_{n=0} = \phi'_{\rm RS1}(0), \tag{3.53}$$

and

$$g_{\rm 1RSB2}(x) = x\frac{\partial}{\partial n}\phi_{\rm 1RSB2}(n,x)|_{n=0} = x\phi'_{\rm RS1}(0). \tag{3.54}$$

We combine these solutions to construct an entire functional form of $g(x)$ based on physical considerations. For $x \gg 1$, $g(x)$ should vary approximately linearly with respect to x, because a single pure state of the largest entropy typically dominates $\sum_\gamma Z_\gamma^x$. In addition, $s(x) = (\partial/\partial x)g(x)$ for $x \sim 0$ should be smaller than that for $x \gg 1$ because $s(x)$

should increase monotonically with respect to x. Furthermore, $g(x)$ must be a continuous function. These considerations reasonably yield an entire functional form of $g(x)$ as

$$g(x) = \begin{cases} \phi'_{\mathrm{RS1}}(0), & x \leq 1, \\ x\phi'_{\mathrm{RS1}}(0), & x > 1, \end{cases} \tag{3.55}$$

which yields the complexity as

$$\Sigma(s) = \begin{cases} \phi'_{\mathrm{RS1}}(0) - s, & 0 \leq s \leq \phi'_{\mathrm{RS1}}(0), \\ -\infty, & \text{otherwise.} \end{cases} \tag{3.56}$$

The piecewise linear profile of eq. (3.55) is somewhat extraordinary. This is thought to be because the correct complexity is not convex upward in this system. When $\Sigma(s)$ is convex upward, the current formalism using the saddle-point method defines a one-to-one map between $g(x)$ and $\Sigma(s)$. However, if $\Sigma(s)$ is not convex upward, the functional profile of a region in which the correct complexity is convex downward is lost and only the convex hull is obtained by the transformation from $g(x)$, as shown in figure 3.2. The piecewise linear profile of $g(x)$ presumably signals that this actually occurs in the current problem. Similar behavior of the complexity could also be observed in a certain type of random energy models [52].

The physical implication of eq. (3.56), the profile of which is obtained by connecting two points $(s, \Sigma) = (0, \phi'_{\mathrm{RS1}}(0))$ and $(\phi'_{\mathrm{RS1}}(0), 0)$ with a straight line having a slope of $-x = -1$, is that the weight space is equally dominated by exponentially many clusters of vanishing entropy and a subexponential number of large clusters composed of exponentially many weights. The existence of large clusters may accord with an earlier study which reported that local search heuristics of a certain type manage to find a compatible weight efficiently up to a considerably large value of α near to the capacity α_s [53]. On the other hand, the coexisting exponentially many small clusters may be a major origin of a known difficulty in finding compatible weights by Monte Carlo sampling schemes [54, 55].

3.3.2 Rate function for $\alpha > \alpha_{\mathrm{s}} = 0.833\ldots$ and a transition at $\alpha_{\mathrm{GD}} = 1.245\ldots$

For $\alpha_{\mathrm{s}} < \alpha$, eq. (3.56) becomes negative, which implies that there exist no compatible weights for typical samples of D^M. In such cases, the rate function $R(s)$, which characterizes a small probability that atypical samples that are compatible with the Ising perceptrons are generated, becomes relevant in the current analysis. Therefore, we focus on the assessment of this exponent for this region.

For $\alpha_{\mathrm{s}} < \alpha < \alpha_{\mathrm{GD}} = 1.245\ldots$, $\phi_{\mathrm{RS1}}(n)$ dominates the generating function $\phi(n)$ in the vicinity of $n \geq 1$ as for $\alpha < \alpha_{\mathrm{s}}$. This means that $\phi_{\mathrm{1RSB1}}(n, m = 1) = \phi_{\mathrm{1RSB2}}(n, m = 1) = \phi_{\mathrm{RS1}}(n)$ should be used to assess $R(s)$ of relatively frequent events that correspond to $0 < n < 1$. However, this function is minimized to a negative value at a certain point at which $0 < n_{\mathrm{s}}(\alpha) < 1$, which implies that assessment by naïvely using $\phi_{\mathrm{RS1}}(n)$

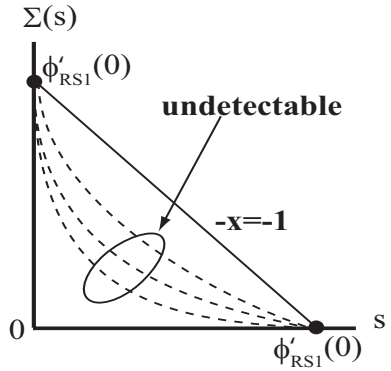

Figure 3.2: Schematic profile of complexity eq. (3.56). The characteristic exponent of the size distribution of pure states cannot be correctly assessed in the current formalism if it is a convex downward function (dashed curves). In such cases, the complexity $\Sigma(s)$ assessed from $g(x)$ (solid line) is the convex hull (black circle) of the correct exponent.

for $n < n_{\rm s}(\alpha)$ leads to incorrect results, which yield a negative equilibrium value of the entropy $s_{\rm eq}(n) = (\partial/\partial n)\phi_{\rm RS}(n) < 0$. In order to avoid this inconsistency, we fix the value of $\phi(n)$ to $\phi_{\rm RS1}(n_{\rm s}(\alpha))$, which is reduced to the conventional construction of a frozen RSB solution. In particular, this yields an assessment of

$$R(0) = \phi_{\rm RS1}(n_{\rm s}(\alpha)) = \min_{n}\{\phi_{\rm RS1}(n)\}, \tag{3.57}$$

which has the physical meaning of a characteristic exponent of a small probability that a given sample set D^M is separable by certain Ising perceptrons. For $\alpha \geq \alpha_{\rm GD} = 1.245\ldots$, on the other hand, the dominant solution of $\phi(n)$ in the vicinity of $n \geq 1$ is updated from $\phi_{\rm RS1}(n)$ to $\phi_{\rm RS2}(n) = (1-\alpha)\log 2$, which yields

$$R(0) = \phi_{\rm RS2}(n) = (1-\alpha)\log 2. \tag{3.58}$$

In order to provide a visual representation of the above discussions, we depict the behaviors of $\phi(n)$ in figure 3.3.

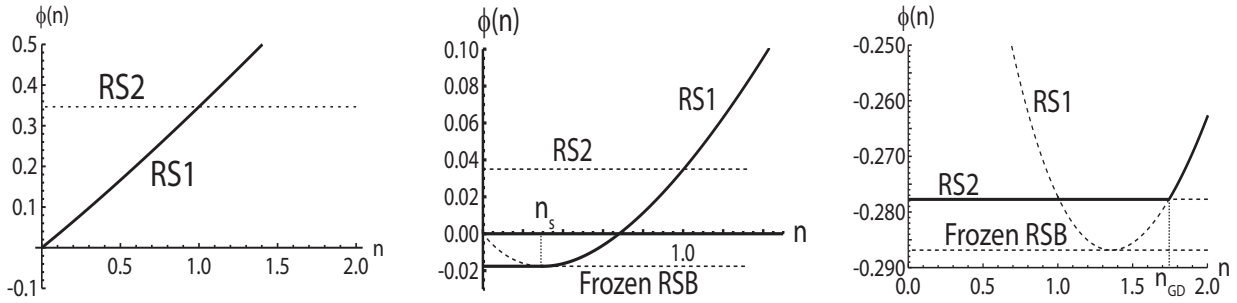

Figure 3.3: Behavior of $\phi(n)$. The solid lines denote the correct $\phi(n)$, and the dotted lines are the RS and frozen RSB branches. The corresponding values of the parameter α are $0.5, 0.95$, and 1.4, from left to right.

The difference in physical behavior between $\alpha_{\rm s} < \alpha < \alpha_{\rm GD}$ and $\alpha > \alpha_{\rm GD}$ is expected to be as follows. For $\alpha_{\rm s} < \alpha < \alpha_{\rm GD}$, the dominant solution around $n > n_{\rm s}(\alpha)$, $\phi(n) = \phi_{\rm RS1}(n)$, varies smoothly. This leads to the following behavior of $R(s_{\rm eq})$ in the vicinity of $s = 0$:

$$R(s_{\rm eq}) = R(0) - As_{\rm eq}^2 + \ldots, \tag{3.59}$$

where $A > 0$ is a certain constant, which implies that large clusters can appear with a relatively large probability although typical samples of D^M are not separable by the Ising perceptrons. On the other hand, for $\alpha > \alpha_{\rm GD}$, $\phi(n) = \phi_{\rm RS2}(n)$ is constant for $n < n_{\rm GD}(\alpha)$, which is characterized by $\phi_{\rm RS2}(n_{\rm GD}(\alpha)) = \phi_{\rm RS1}(n_{\rm GD}(\alpha))$ and $n_{\rm GD}(\alpha) > 1$, and is switched to $\phi(n) = \phi_{\rm RS1}(n)$ for $n > n_{\rm GD}(\alpha)$ at $n = n_{\rm GD}(\alpha)$, which is accompanied by a jump in the first derivative. This indicates that the rate function $R(s_{\rm eq})$ is not convex upword in the region of $0 < s_{\rm eq} < (\partial/\partial n)\phi_{\rm RS1}(n_{\rm GD}(\alpha))$ as was mentioned for $\Sigma(s)$ in the previous subsection, which implies that the events of $s_{\rm eq} = 0$ overwhelm those of $s_{\rm eq} > 0$ in relative probabilities. Therefore, the generation of large clusters should be considerably rare for α of this region.

3.3.3 Phase diagram on the n-α plane

The above considerations are sufficient to draw a phase diagram on the n-α plane, which is depicted in figure 3.4.

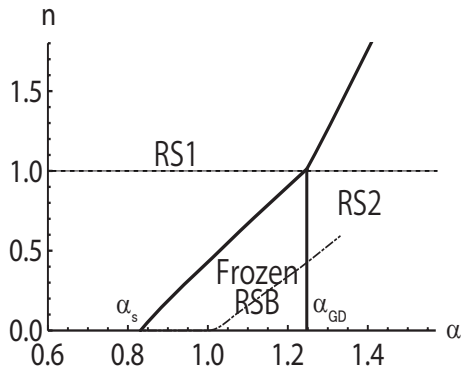

Figure 3.4: Phase diagram on the n-α plane. Solid lines are phase boundaries, and the dotted line denotes $n = 1$. The dotted-dashed line expresses the AT line for the RS1 solution, but is irrelevant. The AT line vanishes at a certain value of α, because the solution for $0 < q < 1$ vanishes at this point. The RS2 solution involves the AT instability only on the $n = 0$ line, which is presumably of no relevance in the replica analysis.

The value of the tricritical point $\alpha_{\rm GD} = 1.245\ldots$ is identical to the critical ratio of the perfect learning of the Ising perceptrons in the teacher-student scenario [56, 57]. Formally, this agreement is explained as follows. The dominant solution for $n < 1$ is determined by whether $\phi_{\rm RS1}(n)$ or $\phi_{\rm RS2}(n)$ dominates around $n \geq 1$. Since $\phi_{\rm RS1}(n = 1) =$

$\phi_{\rm RS2}(n=1)$ is always guaranteed, the critical condition is given as $(\partial/\partial n)\phi_{\rm RS1}(n)|_{n=1} = (\partial/\partial n)\phi_{\rm RS2}(n)|_{n=1} = 0$. On the other hand, $(\partial/\partial n)\phi_{\rm RS1}(n)|_{n=1}$ generally provides the equilibrium value of entropy after learning in the teacher-student scenario, the target of which can be dealt with as an $(n+1)$-replicated system, in which the teacher is handled as an extra replica. Therefore, the condition of perfect learning, which indicates that the weight of the student agrees perfectly with that of the teacher after learning, is identical to the vanishing entropy condition of the $(n+1)$-replicated system in the limit $n \to 0$, which agrees with $(\partial/\partial n)\phi_{\rm RS1}(n)|_{n=1} = 0$, giving the critical value $\alpha_{\rm GD}$ in the current problem. Although the agreement is justified formally in this manner, its physical implication remains somewhat unclear. The line $n = 1$, which passes through the tricritical point, may have an analogous relation to the concept of Nishimori's line in the theory of spin glasses [24, 58].

Finally, we mention the de Almeida-Thouless (AT) condition in this model [39]. The AT (stability) condition of $\phi_{\rm RS}(n)$ with the order parameters q and $\widehat{q}$ is expressed as follows:

$$\frac{\alpha}{(1-q)^2}\frac{\int Dz E^n \left(\frac{E''}{E} - \left(\frac{E'}{E}\right)^2\right)^2}{\int Dz E^n}\frac{\int Dz \cosh^{n-4}\sqrt{\widehat{q}}z}{\int Dz \cosh^n \sqrt{\widehat{q}}z} \leq 1. \tag{3.60}$$

The derivation is given in appendix A.2. This condition for $\phi_{\rm RS1}(n)$ is broken in a certain region on the n-α plane, but is irrelevant because the region is always included in $n < n_s(\alpha)$, for which the relevant solution is already switched to that of the frozen RSB. On the other hand, $\phi_{\rm RS2}$ is stable for $n > 0$ but becomes unstable only on $n = 0$, the deviation of which is also given in appendix A.2, as reported in [59]. The relevance of this instability for $\alpha \geq \alpha_{\rm GD}$ may require more detailed discussions, but we assume herein that this instability can be ignored because only the asymptotic behavior of $\phi(n)$ in the limit $n \to 0$ is relevant in procedures of the replica method.

3.4 Numerical validation

For validating the theoretical predictions obtained in the previous section, we carried out extensive numerical experiments.

In describing the experiments, let us first define the cluster in the present system. The cluster is a set of spin configurations that are stable with respect to single spin flips [28,29]. Clusters have the following properties:

- Any configuration belongs to a cluster.
- When a spin configuration "A" can be moved to another configuration "B" by a single spin flip without changing the number of incompatible patterns, "A" and "B" belong to the same cluster.

In the following, we concentrate on vanishing energy clusters, which are composed of weights that are perfectly compatible with D^M.

Before going into details, we elucidate the relation between the cluster and the pure state. Identifying the microscopic description of a pure state is generally a delicate problem, but in the Ising perceptron a pure state can be identified with a cluster, as mentioned in the opening sentence in this chapter. There is no proof of this statement but it is naturally understood by considering the following aspects of the present problem: The Boltzmann weight of $\eta(\boldsymbol{S}|D^M)$ in eq. (3.39) becomes completely zero if there is any incompatible pattern. This means that accessing from a cluster to a different cluster by single spin flips is impossible because those clusters are completely separated by states with zero probability $\eta(\boldsymbol{S}|D^M) = 0$. This naturally leads to identifying a cluster with a pure state, because a pure state is a set of configurations which cannot be accessed from other sets by natural dynamics. Several earlier studies support this description [28,29,50], and we hereafter admit this assumption.

Now let us return to the experiments. We denote the size of a cluster as Q and the number of size-Q clusters for a sample D^M as $C(Q|D^M)$. The entropy of a cluster s is considered to be identified by $s = (1/N)\log Q$, and the complexity $\Sigma(s|D^M)$ corresponds to $(1/N)\log C(Q|D^M)$. The clusters can be numerically evaluated, and hence we can construct the 1RSB generating function from the numerical data as

$$\phi_{\rm 1RSBnum}(n = xy, m = x) = \frac{1}{N}\log\left[\left(\sum_\gamma Q_\gamma^x\right)^y\right], \tag{3.61}$$

where $[\ldots]$ denotes the sample average operation with respect to D^M. In the typical limit $y \to 0$, this yields the following expression:

$$g_{\rm num}(x) = \lim_{y\to 0}\frac{\partial}{\partial y}\phi_{\rm 1RSBnum}(xy, x) = \frac{1}{N}\frac{\left[\Theta\left(\sum_\gamma Q_\gamma^x\right)\log\left(\sum_\gamma Q_\gamma^x\right)\right]}{\left[\Theta\left(\sum_\gamma Q_\gamma^x\right)\right]}, \tag{3.62}$$

where the step function $\Theta(x)$ comes from the differentiation of $\log\left[\left(\sum_\gamma Q_\gamma^x\right)^y\right]$ with respect to y. This means that if there is no cluster for a sample D^M, then the contribution of $\Theta\left(\sum_\gamma Q_\gamma^x\right)\log\left(\sum_\gamma Q_\gamma^x\right)$ vanishes.

In order to examine the consistency with the replica analysis, we assess eq. (3.62) based on data obtained in extensive numerical experiments. The function $g_{\rm num}(x)$ is evaluated by the exact enumeration of weights that are compatible with D^M, which are referred to hereinafter as *solutions*. The procedure is summarized as follows:

1. Generate M examples $D^M = \{(y_1, \boldsymbol{x}_1)\cdots(y_M, \boldsymbol{x}_M)\}$.
2. Enumerate all solutions.
3. Partition the solutions into clusters, and calculate $\sum_\gamma Q_\gamma^x$ for an appropriate set of x. We actually took 41 points between $x = 0$ and 2.0.
4. Repeat the above procedures until sufficient data are obtained and calculate $\left[\Theta\left(\sum_\gamma Q_\gamma^x\right)\log\left(\sum_\gamma Q_\gamma^x\right)\right]$ by taking the sample average.

The resultant plots of $g_{\rm num}(x)$ for $\alpha = 0.5$ are shown in fig. 3.5. As the system size

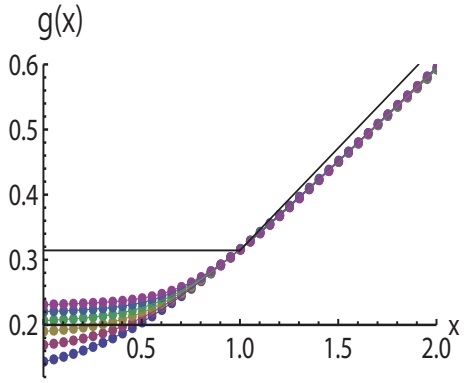

Figure 3.5: Behavior of $g_{\rm num}(x)$ for $\alpha = 0.5$. The system sizes are $N = 14, 16, 18, 20, 22$, and 24, from bottom to top. The solid lines denote $g(x)$ given by eq. (3.55). The number of samples is $32,000$ for each N. Error bars are smaller than the size of markers. As the system size grows, the profiles of $g_{\rm num}(x)$ approach the theoretical prediction.

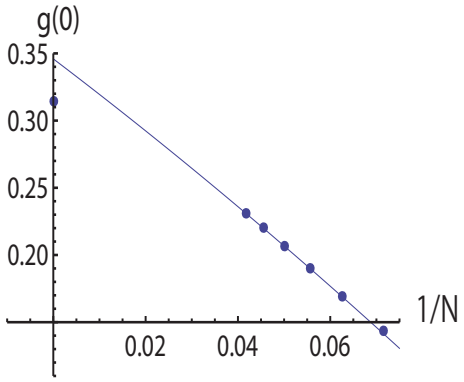

Figure 3.6: Size dependence of $g_{\rm num}(0)$. The data are the same as fig. 3.5. The solid line is provided by quadratic fitting to the data. The point at $1/N = 0$ is the theoretical value derived by the replica method. The data tend to reach this theoretical value as the system size grows.

grows, the numerical data for $x \leq 1$ exhibit flatter slopes approaching the theoretical prediction $g(x) = \phi'_{\rm RS1}(0)$ for $x < 1$. This can also be seen in fig. 3.6 as the systematic approaching of $g_{\rm num}(0)$ to the theoretical value of $g(0) = 0.314\ldots$ derived from the replica analysis. The difference between the numerical extrapolation and the analytical result at $1/N = 0$ is considered to be the systematic error due to higher order contributions of $1/N$. The profiles of $x > 1$, on the other hand, are approximately straight lines, and the gradient of the slopes appear smaller than that of the theoretical prediction $\phi'_{\rm RS1}(0)$. However, the data still slowly move closer to $x\phi'_{\rm RS1}(0)$ $(x > 1)$ as N becomes larger as a whole, implying consistency with the theoretical prediction.

Complexity $\Sigma(s)$ can also be assessed from the numerical data. One scheme for evaluating $\Sigma(s)$ is to use the relation (3.49) with a polynomial interpolation of the numerical data. We determined the order of the polynomial using Akaike's information criteria [60] and eventually selected a 27th degree polynomial, but the obtained results were not so sensitive to details of the choice of the polynomial. The assessed profiles of $\Sigma(s)$ are plotted in fig. 3.7. The curves appear to approach the line predicted in the previous section as N increases, which supports our replica analysis.

However, the complexity curve shown in fig. 3.7 might lose the information about the correct distribution of the clusters, as mentioned in section 3.3.2. In order to examine this possibility, we directly evaluate the distribution of pure states in a rather naive manner. We refer to the result of this assessment as the raw complexity, which is defined as

$$\Sigma_{\rm r}(s = (1/N)\log Q|D^M) = \frac{1}{N}\Theta\left(C(Q|D^M)\right)\log\left(C(Q|D^M)\right). \tag{3.63}$$

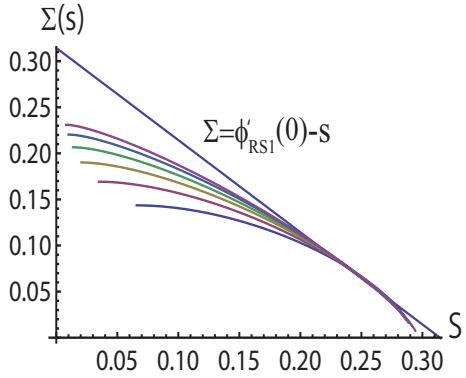

Figure 3.7: $\Sigma(s(x))$ obtained from $g_{\rm num}(x)$ using the relation (3.49) for $\alpha = 0.5$. The system sizes increase from bottom to top. The solid line denotes the asymptotic line in the thermodynamic limit predicted by the replica analysis.

Taking the sample average yields the typical profile of $\Sigma_{\rm r}(s|D^M)$ as $\Sigma_{\rm r}(s) = [\Sigma_{\rm r}(s|D^M)]$, the result of which for $\alpha = 0.5$ is shown in fig. 3.8. We took 32,000 samples in the evaluation for each size and joined the plots to obtain smooth curves. This figure indicates

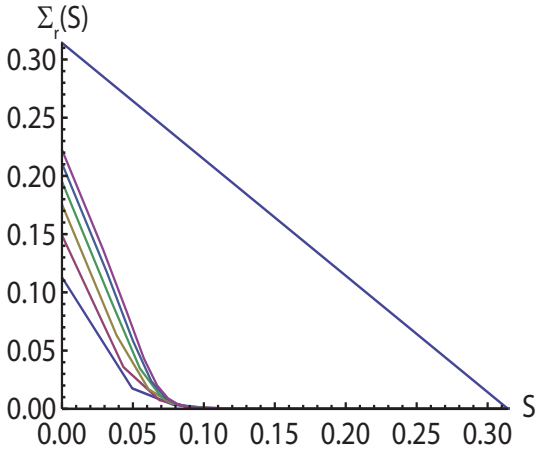

Figure 3.8: Plot of the raw complexity $\Sigma_{\rm r}(s)$ for $\alpha = 0.5$. The system size increases from $N = 14$ to 24 in increments of 2, from bottom to top. The solid line is the same as that shown in fig. 3.7.

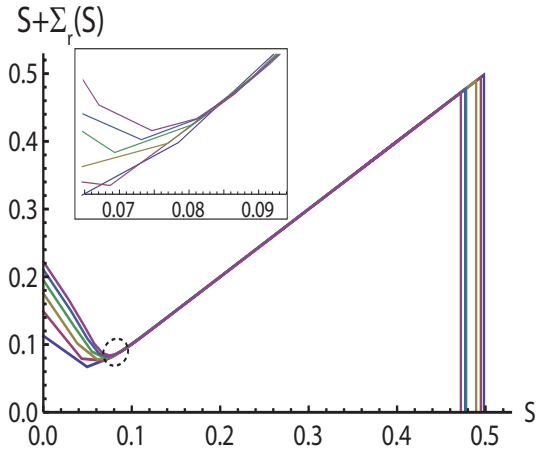

Figure 3.9: Plot of $s + \Sigma_{\rm r}(s)$. As the system size increases, the curve appears to converge to a V-shape function, indicating that $\Sigma_{\rm r}(s)$ is convex downward. The inset shows a close-up of the region enclosed by the dotted ellipse.

that $\Sigma_{\rm r}(0)$ approaches the value of the theoretical prediction $\phi'_{\rm RS1}(0)|_{\alpha=0.5} = 0.314\ldots$ from below as N increases. However, $\Sigma_{\rm r}(x)$ for $x \geq 0.1$ appears to remain approximately constant at zero, indicating that $\Sigma_{\rm r}(x)$ converges to a convex downward function. We also plot the function $s+\Sigma_{\rm r}(s)$ in figure 3.9. This plot shows two peaks and one dip of $s+\Sigma_{\rm r}(s)$, indicating that $\Sigma_{\rm r}(s)$ is convex downward. The position of the right-hand peak tends to move left to the right terminal point $s = 0.314\ldots$ of the theoretical prediction as the

system size increases, while the dip appears to be bounded at the point $x = 0.084$ as shown in the inset. In conclusion, these figures indicate that the exponent that characterizes the size distribution of the pure states, $\Sigma_{\rm r}(s)$, is not a convex upward function in this system and does not agree with $\Sigma(s)$, which is evaluated by the relation (2.52).

Next, we assessed the rate function for the region of $\alpha > \alpha_{\rm s}$. In this region, the generation of samples that are perfectly compatible with the Ising perceptrons rarely occurs and is dominated by $s = 0$. Therefore, we numerically evaluated the probability that a given set of samples D^M could be separated by the Ising perceptron, $P_{\rm sep}$, and estimated $R(0)$ as $R(0) = (1/N) \log P_{\rm sep}$.

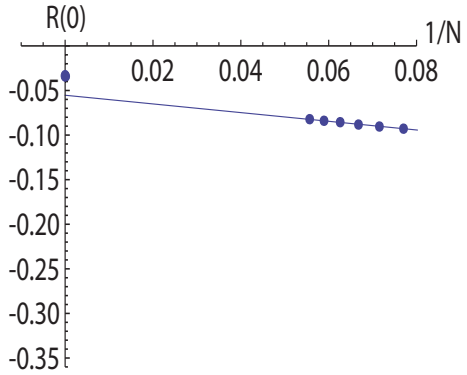

Figure 3.10: Size dependence of the rate function for $\alpha = 1.0$. The point at $1/N = 0$ is the value predicted by the frozen RSB solution. The system size increases from $N = 12$ to 18 in increments of 1. The data from 320,000 samples were evaluated for each N. The statistical errors are smaller than the markers.

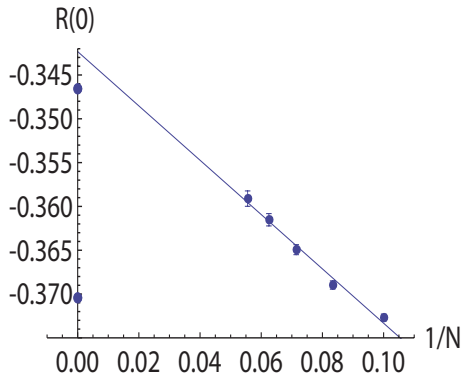

Figure 3.11: Size dependence of the rate function for $\alpha = 1.5$. The upper and lower plots at $1/N = 0$ are given by the RS2 and frozen RSB solutions, respectively. The system size increases from $N = 10$ to 18 in increments of 2. The data from 25,600,000 samples were evaluated for each N.

The resultant plots are given in figures 3.10 and 3.11 for $\alpha = 1.0$ and 1.5, respectively. The solid lines in these figures were obtained by the linear fitting for the numerical data. These figures show that the theoretical predictions are reasonably consistent with the values of extrapolation of the numerical data. The statistical errors are sufficiently small, and hence the differences between the analytical and numerical results should be the systematic errors due to the nonlinearity of the Ising perceptron.

3.5 Summary

In this chapter, we investigated the structure of the weight space of Ising perceptrons in which a set of random patterns is stored using the derivatives of the generating function of the partition function. This was achieved by carrying out a finite-n replica analysis under the assumption of one-step replica symmetry breaking (1RSB) handling Parisi's 1RSB parameter as a control parameter. To directly investigate the weight space structure, we

took the zero-temperature limit and studied the entropy of the zero-energy weight. For $\alpha < \alpha_{\rm s} = 0.833\ldots$, the analysis of $n \to 0$ indicates that the characteristic exponent of the size distribution of pure states is not convex upward, which implies that the weight space is equally dominated by a single large cluster of exponentially many weights and exponentially many clusters of a single weight. For $\alpha > \alpha_{\rm s}$, a set of random patterns is rarely compatible with the Ising perceptron. The $n \to 0$ analysis enables us to assess the rate function that characterizes a small probability that a cluster of a given entropy will emerge after the storage of random patterns. We found that a cluster of finite entropy is generated with a relatively high probability for $\alpha_{\rm s} < \alpha < \alpha_{\rm GD} = 1.245\ldots$, but this is very rare for $\alpha > \alpha_{\rm GD}$. These theoretical predictions have been validated by extensive numerical experiments. We also drew a complete phase diagram on the n-α plane, in which $(n, \alpha) = (1, \alpha_{\rm GD})$ becomes a tricritical point. The line $n = 1$ that passes through the tricritical point is analogous to the Nishimori line in the theory of spin glasses.

Chapter 4

The replica zeros of $\pm J$ Ising spin glass at zero temperature

In the previous chapters, we have seen that the generating function $\phi(n)$ shows the analyticity breaking leading to phase transitions with respect to the replica number n in several models. Employing the Parisi scheme and some discussions based on the physical plausibility, we have detected such transitions and constructed the reasonable solutions after the transitions. These schemes are very powerful and can give physically plausible predictions, but still involve some questions about the mathematical correctness, as pointed out in section 1.4. The possible problems are summarized as follows:

1. The uniqueness of the analytical continuation from natural to real (or complex) numbers.

2. The consistency between the analytical continuation of $\phi(n)$ in the replica prescription and the possible analyticity breaking of $\phi(n) = \lim_{N\to\infty} \phi_N(n)$.

The first problem claims that even if all the moments of $[Z^n]$ are given for $n \in \mathbb{N}$, in general it is impossible to uniquely continue the analytical expressions for $n \in \mathbb{N}$ to $n \in \mathbb{R}$ (or $\mathbb{C}$). The Carlson's theorem guarantees that the analytical continuation from $n \in \mathbb{N}$ to $n \in \mathbb{C}$ is uniquely determined if $[Z^n]^{1/N} < O(e^{\pi|n|})$ holds as $\mathrm{Re}(n)$ tends to infinity [61]. Unfortunately, the moments of the SK model grow as $[Z^n]^{1/N} < O(e^{C|n|^2})$, where C is a constant, and therefore this sufficient condition is not satisfied. van Hemmen and Palmer conjectured that the failure of the RS solution of the SK model might be related to this issue [62], but as we have seen in chapter 2 this is not the case because $\phi(n)$ actually loses its analyticity in a certain region of n and T.

The second issue concerns the possible breaking of the analyticity of $\phi(n)$. The naive premise of the analytical continuation in the replica theory is the analyticity of $\phi_N(n)$ with respect to n. However, even if $\phi_N(n)$ is analytic with respect to n for finite N, the analyticity of $\phi(n) = \lim_{N\to\infty} \phi_N(n)$ can be broken, as we have seen in the previous chapters. Once the analyticity breaking occurs, in general we cannot depend on the analytical continuation from large n to small n to obtain $\phi(n)$; but the Parisi scheme somehow gives the correct behavior of $\phi(n)$ by partly utilizing the analytical continuation.

The question is how the Parisi scheme overcomes the analyticity breaking and reaches the small n region.

For considering this question, in this chapter, we investigate the analyticity breaking of $\phi(n)$ with respect to n in completely different ways. To this end, we propose a method based on the Lee-Yang theory [26] of phase transitions. In particular, we observe the zeros of $[Z^n]_{\boldsymbol{J}}$ with respect to complex $n \in \mathbb{C}$, which will be referred to as "replica zeros" (RZs), and examine how some sequences of the zeros approach the real axis of n as the system size N grows. For some discrete versions of the random energy models [36,63–65], this strategy is known to successfully characterize the 1RSB transition accompanied by the singularity of the rate function $R(f)$ [66]. We extend the scheme to be applicable to other tractable systems, $\pm J$ models with a symmetric distribution on two types of lattices, ladder systems and Cayley trees (CTs) with random fields on the boundary. There are some reasons for treating these models. First, these models can be investigated in a feasible computational time by the cavity method [30, 31]. Especially, at zero temperature this approach gives a simple iterative formula to yield the partition function. Employing the replica method and the cavity method, we can perform symbolic calculations of the moment $[Z^n]_{\boldsymbol{J}}$, which enables us to directly solve the equation of RZs $[Z^n]_{\boldsymbol{J}} = 0$. The second reason is the existence of the spin-glass phase. It is known that the spin-glass phase is present for CTs [32–35] and is absent for ladder systems. Therefore, we can compare the behavior of RZs, which are considered to be dependent on the spin-glass ordering.

Our result indicates that the RZs of CTs are relevant to neither 1RSB nor FRSB. We consider some possible explanations about this fact, and also refer to some relatives of CTs, which are considered to show the RSB, to clarify the properties of the relatives from the RZs of CTs.

The results in this chapter are written in reference [67].

4.1 Fundamental knowledge about models and formulations

We start from reviewing the models and formulations which will be needed in the following sections.

4.1.1 Definition of the Cayley tree and the properties

The definition of the Cayley tree is summarized as follows:

- The Cayley tree (CT): A tree of finite size consisting of an origin and its neighbors. The first generation is built from c neighbors which are connected to the origin. Each site in the gth generation is connected to new $c-1$ sites without overlap and all these new sites comprise the $g+1$th generation. Iterating this procedure to the Lth generation, we obtain the CT, and the Lth generation becomes its boundary.

As an example, we give a picture of a CT in fig. 4.1. Let us consider a general Ising

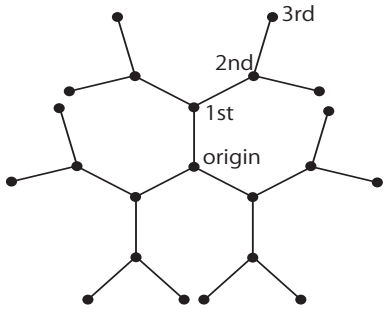

Figure 4.1: A picture of CT with coordination number $c = 3$ and total generation $L = 3$.

system defined on the CT

$$\mathscr{H} = -\sum_{\langle i,j \rangle} J_{ij} S_i S_j - \sum_i H_i S_i. \tag{4.1}$$

For CTs, it is possible to efficiently assess the partition function by an iterative method, *i.e.* the cavity method[1]. The basis of the cavity method for a CT is a formula for evaluating an effective field by a partial trace:

$$\sum_{S_j} \exp\left\{\beta(J_{ij} S_i S_j + H_i S_i + h_j S_j)\right\} = A \exp(\beta h_i S_i). \tag{4.2}$$

A simple algebra offers

$$h_i = H_i + \widehat{h}_j(J_{ij}, h_j), \;\; A(J_{ij}, h_j) = \frac{2 \cosh \beta J_{ij} \cosh \beta h_j}{\cosh \beta \widehat{h}_j}, \tag{4.3}$$

where

$$\beta \widehat{h}_j(J_{ij}, h_j) = \tanh^{-1}(\tanh \beta J_{ij} \tanh \beta h_j). \tag{4.4}$$

The fields h_j and $\widehat{h}_j$ are sometimes termed the cavity field and cavity bias, respectively.

For CTs, iterating the above equations from the boundary gives the series of cavity fields and biases $\{h_j, \widehat{h}_j\}$. In general, a cavity field becomes a summation of the cavity biases from its $c-1$ descendants (c is the coordination number):

$$h_i = H_i + \sum_{j=1}^{c-1} \widehat{h}_j(J_{ij}, h_j). \tag{4.5}$$

For simplicity, we mainly concentrate on the $c = 3$ case, the local structure of which is given in fig. 4.2, but the generalization to general c is straightforward. Let us denote the

[1]The term 'cavity method' is usually used in a different meaning and is considered to be a generalized Bethe approximation [25, 43]. Mathematical and physical aspects about the cavity method in this sense are very fruitful, but in this thesis we only use this term to indicate the generic name of the iterative methods to calculate the partition function.

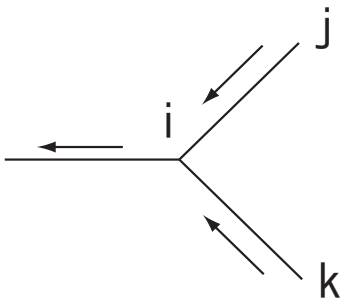

Figure 4.2: Local structure of a CT with coordination number $c = 3$.

partition function in the absence of i's ascendants as Z_i. Equations (4.2)–(4.5) imply that the partition function is updated as

$$Z_i = \sum_{S_i,S_j,S_k} Z_j Z_k \exp\{-\beta(-H_i S_i + \Delta H_{ij} + \Delta H_{ik})\}\rho_j(S_j)\rho_k(S_k), \tag{4.6}$$

where

$$\rho_j(S_j) = \frac{\exp(\beta h_j S_j)}{2\cosh\beta h_j}, \tag{4.7}$$

is the one-site marginal in the absence of j's ascendants and $\Delta H_{ij} = -J_{ij}S_iS_j$ is the bond Hamiltonian added by a propagation procedure. As a final step, the contribution from the origin of the tree is calculated as

$$Z = Z_1 Z_2 Z_3 \prod_{i=1}^{3}(2\cosh\beta J_i)\frac{2\cosh\beta(H_0 + \sum_{i=1}^{3}\widehat{h}_i)}{\prod_{i=1}^{3}(2\cosh\beta\widehat{h}_i)}, \tag{4.8}$$

where H_0 is the external field on the origin and the whole partition function Z is derived.

For the sake of simplicity, we consider pure ferromagnets $J_{ij} = J$ and $H_i = H$ for a while. In this case each cavity field depends only on the generation g and the recursion relation becomes

$$h_g = H + (c-1)\widehat{h}_{g-1}, \quad \widehat{h}_{g-1} = \frac{1}{\beta}\tanh^{-1}(\tanh(\beta J)\tanh(\beta h_{g-1})) \tag{4.9}$$

where g is the index of the generation, but for simplicity of notation, we labeled the boundary as $g = 0$ and the origin as $g = L$, which is in the inverse relation to fig. 4.1. The partial partition function Z_g, which represents the partition function of a branch consisting from a gth-generation spin and its descendants, is also calculated by

$$Z_g = Z_{g-1}^{c-1}(2\cosh\beta J)^{c-1}\frac{2\cosh\beta h_g}{(2\cosh\beta\widehat{h}_{g-1})^{c-1}}. \tag{4.10}$$

At the origin, we need to merge c branches, which yields the whole partition function Z

$$Z = Z_{L-1}^{c}(2\cosh\beta J)^{c}\frac{2\cosh\beta(H + c\widehat{h}_{L-1})}{(2\cosh\beta\widehat{h}_{L-1})^{c}}. \tag{4.11}$$

These formulas enable us to efficiently assess the partition function.

4.1.2 Bulk properties of Cayley trees

Usually, phase transitions are related to the bulk properties of the system. Contributions from the boundary condition are negligible and the inside part of the system dominates the whole behavior. Unfortunately, this is not the case for a CT, because the CT is extraordinary in that the number of the boundary spins N_B are comparable to the whole number of the spins N. Due to this peculiarity, the CTs are known to show some extraordinary critical behaviors [68–70]. This problem may be also interesting but we are not involved in this topic.

On the other hand, considering the bulk part of a CT is also meaningful. For this, we define the following two systems which are closely related to CTs:

- The Bethe lattice (BL): A lattice consisting of the first L' generations of a CT, for which $L \to \infty$ is taken. Alternatively, we can define a BL as a finite CT of L' generation, the boundary condition of which is given by the convergent cavity field distribution of the infinite CT. Unlike for a CT, the boundary condition depends on the external parameters, e.g. the temperature T and the external field$H$.

- The regular random graph (RRG): A randomly generated graph under the constraint of a fixed connectivity c. There exist many cycles in this lattice, which makes it difficult to calculate the partition function for finite N. In the limit $N \to \infty$ under appropriate conditions, however, the contribution coming from the loops becomes negligible and the RRG becomes an exactly solvable model. Moreover, it is known that the RRG and the BL share many identical properties [30, 71, 72].

As examples, we give diagrams of a BL and RRG in figs. 4.3 and 4.4, respectively. The

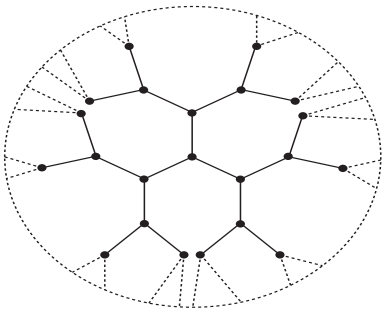

Figure 4.3: Schematic diagram of a BL with coordination number $c = 3$.

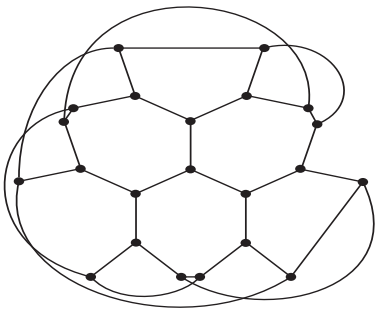

Figure 4.4: A sample of RRG with coordination number $c = 3$ and $N = 22$.

RRG is sometimes identified with the BL, but we here distinguish these two systems. That is because the main purpose of this chapter is to clarify the asymptotic properties of $\phi_N(n)$ from finite N to infinite N, and our definition of the BL is useful to compare these limits. Here, the term "RRG" is used only to refer to systems of infinite size.

A BL is the deep inside part of a CT and the behavior is determined by the limit $g \to \infty$ in eq. (4.9). In this limit, we can easily derive the self-consistent equations

satisfied by the converging cavity field h^* and bias $\widehat{h}^*$

$$h^* = H + (c-1)\widehat{h}^*, \quad \widehat{h}^* = \frac{1}{\beta}\tanh^{-1}(\tanh(\beta J)\tanh(\beta h^*)), \tag{4.12}$$

Note that this equation is identical to the 'Bethe approximation'. The name of 'Bethe lattice' comes from this fact that the Bethe approximation is exact on this lattice. When the external field is zero $H = 0$, these self-consistent equations have the paramagnetic solution $h = 0$ at high temperatures and the ferromagnetic solution $h > 0$ at low temperatures. Expanding eq. (4.12) with respect to h, we can obtain the following equation determining the critical temperature

$$\tanh \beta J = \frac{1}{c-1}. \tag{4.13}$$

For general tree systems, it is known that the free energy can be expressed as the following form [30, 31, 43, 73–75]

$$F = \sum_{\langle i,j \rangle} f_{ij}^{(2)} - \sum_i (c_i - 1) f_i^{(1)}, \tag{4.14}$$

where $f_{ij}^{(2)}$ and $f_i^{(1)}$ is the bond and site contributions of the free energy, respectively and c_i is the number of bonds that site i has. For regular CTs, $c_i = c$ holds if i is inside the tree, while $c_i = 1$ for the boundary sites. The explicit forms of f_{ij} and f_i are

$$-\beta f_{ij}^{(2)} = \log \sum_{S_i, S_j} \exp \beta \left\{ J_{ij} S_i S_j + \left(H_i + \sum_{k \in \lambda_i - j} \widehat{h}_k \right) S_i + \left(H_j + \sum_{k \in \lambda_j - i} \widehat{h}_k \right) S_j \right\}, \tag{4.15}$$

$$-\beta f_i^{(1)} = \log \sum_{S_i} \exp \left\{ \beta \left(H_i + \sum_{k \in \lambda_i} \widehat{h}_k \right) S_i \right\}, \tag{4.16}$$

where H_i denotes the external field applied on site i and $\widehat{h}_k$ denotes the cavity bias. The symbol λ_i denotes the neighbors of site i and $\lambda_i - j$ represents the neighbors of site i except for site j. These are expressed in the pictorial forms in figs. 4.5 and 4.6. For pure

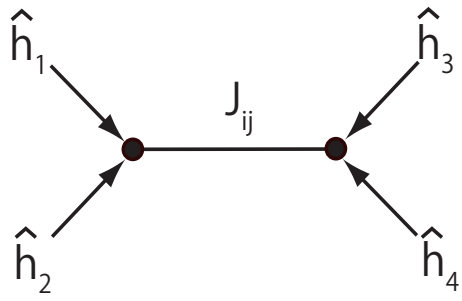

Figure 4.5: A pictorial representation of f_{ij} for $c = 3$.

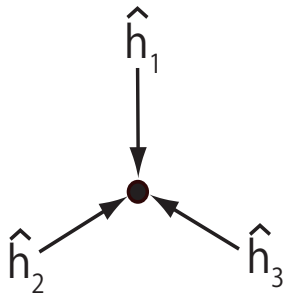

Figure 4.6: A pictorial representation of f_i for $c = 3$.

ferromagnets on CTs, the cavity bias takes different values depending on the generation,

and we cannot obtain a simple form of the free energy. On the other hand for BLs, the cavity bias takes an identical value $\widehat{h}^*$, which leads to the Bethe free energy $F/N = f^{\rm BL}$ as

$$f^{\rm BL} = \frac{r_{\rm I} + r_{\rm B} - 1}{r_{\rm I} + r_{\rm B}} f^{(2)} - r_{\rm I}(c-1) f^{(1)} = r_{\rm I} f_{\rm I} + r_{\rm B} f_{\rm B}. \tag{4.17}$$

where $r_{\rm I} = \left(1 + c(c-2)^{-1}\left((c-1)^{L'-1} - 1\right)\right) / \left(1 + c(c-2)^{-1}\left((c-1)^{L'} - 1\right)\right)$ and $r_{\rm B} = 1 - r_{\rm I}$ represent the fractions of the number of sites inside the tree and on the boundary, respectively, and

$$f_{\rm I} = \frac{c}{2} f^{(2)} - (c-1) f^{(1)}, \tag{4.18}$$

and

$$f_{\rm B} = \frac{1}{2} f^{(2)}. \tag{4.19}$$

The explicit expressions of bond and site contributions, $f^{(2)}$ and $f^{(1)}$, are derived from eqs. (4.15) and (4.16), respectively, by putting $\widehat{h}_i = \widehat{h}^*$, $J_{ij} = J$ and $H_i = H$. These formulas give the free energy of the BL.

Although the uniformness of the cavity fields is recovered in the BL by applying the convergent cavity field to the boundary spins, the BL still has a distinctive feature as a tree system, which appears in the existence of the boundary free energy (4.19). Nevertheless, the complete separation of contributions between the inside and the boundary in the equation (4.17) implies that it is physically plausible to use $f_{\rm I}$, instead of $f^{\rm BL}$, in handling problems concerning the bulk part of the CT. In general, $f_{\rm I}$ agrees with the free energy of an RRG which can be derived by using the replica method and the derivation is given in appendix B.1. This fact provides the basis of the correspondence between BLs and RRGs.

Using the relations between CTs, BLs, and RRGs discussed so far, we compare the analytical results of RRGs with the numerical plots of RZs of CTs for exploring possible links between them. The BL will be also useful to connect those distinctive results. According to this advantage, we clearly distinguish the three systems, CTs, BLs, and RRGs, throughout this thesis.

4.1.3 Zeros and singularities

Phase transitions are generally reflected as the singularities of the free energy $-\beta f = (1/N)\log Z$. Lee and Yang pointed out that those singularities are related to the zeros of the partition function with respect to the complex parameters [26]. For simplicity of explanation, let us consider an Ising system with an complex external field H. The partition function for finite N becomes the following polynomial

$$Z(H) = e^{N\beta H} \sum_{k=0}^{N} \Omega(k) Y^k, \tag{4.20}$$

where $\Omega(k)$ is the partition function of the system with the fixed magnetization $M = \sum_i S_i = N - 2k$, and Y equals to $e^{-2\beta H}$. The partition function is the polynomial of Y and has its zeros. Of course, these zeros are distributed in the complex H plane and never on the real axis of H for finite N. However, as the system size N grows, in several cases some sequences of the zeros approaches the real axis, and finally a part of the zeros touch the real axis in the limit $N \to \infty$. Roughly speaking, Lee and Yang proved that these zeros on the real axis are directly related to the phase transition of the system, and that if the zeros never touch the real axis, the system never shows the phase transition. They also showed that for several models the existing region of the zeros is strongly limited and the phase transitions of those systems are well observed by the behavior of the zeros of Z for finite N.

The discussion by Lee and Yang that the zeros of the partition function are closely related to the singularities of $\log Z$ is quite general and we can apply this to our problem, which motivates us to investigate the RZs given by the equation $[Z^n]_{\boldsymbol{J}} = 0$ for studying the singularities of $\phi(n) = \lim_{N\to\infty}(1/N)\log[Z^n]_{\boldsymbol{J}}$

4.1.4 Energetic zero-temperature limit for replica zeros

Solving

$$[Z^n]_{\boldsymbol{J}} = 0 \tag{4.21}$$

with respect to n is our main objective. Unfortunately, this is, in general, a hard task even by numerical methods because eq. (4.21) is a transcendental equation unlike eq. (4.20), and becomes highly complicated as the system size N grows. In the $T \to 0$ limit, however, the main contributions to the partition function only come from the ground state and eq. (4.21) becomes

$$[Z^n]_{\boldsymbol{J}} \approx [d_{\mathrm{g}}^n e^{-\beta n E_{\mathrm{g}}}]_{\boldsymbol{J}} = 0, \tag{4.22}$$

where E_{g} is the energy of the ground state and d_{g} is the degeneracy. If n is finite when $\beta \to \infty$, the term $e^{-\beta n E_{\mathrm{g}}}$ diverges or vanishes and there is no meaningful result. Therefore, we suppose that non-trivial solutions exist only in the limit $n \to 0, \beta \to \infty$, and $y = \beta n \sim O(1)$. This is the same limit as the energetic zero temperature limit referred to in section 3.2.3. Under this condition, eq. (4.22) becomes

$$[e^{-yE_{\mathrm{g}}}]_{\boldsymbol{J}} = 0. \tag{4.23}$$

In the following, we focus on the $\pm J$ model whose Hamiltonian is given by

$$\mathscr{H} = -\sum_{\langle i,j\rangle} J_{ij} S_i S_j, \tag{4.24}$$

and the distribution of interactions is

$$P(J_{ij}) = \frac{1}{2}\delta(J_{ij} - 1) + \frac{1}{2}\delta(J_{ij} + 1), \tag{4.25}$$

assuming that the total number, N_B, of interacting spin pairs $\langle i, j\rangle$ is proportional to N, which is the case for ladder systems and CTs. This limitation restricts the energy of any

state to an integer value. As a result, eq. (4.23) can always be expressed as a polynomial of $x = e^y$, which significantly reduces the numerical cost for searching for RZs.

4.2 General formula for ladders and Cayley trees

4.2.1 The cavity method

We have already demonstrated the cavity method for pure ferromagnetic systems on CTs in section 4.1, and we here only give a simple explanation of its generalization to treat random systems, k-body interactions, and ladder systems.

Equations (4.2)–(4.5) are applicable to random systems in the unchanged forms. Generalizing these equations to k-spin interacting CTs (k-CTs) is straightforward; the only necessity is to replace the partial trace (4.2) with that for a k-spin interaction, as

$$\sum_{\{S_j\}} \exp\left\{\beta\left(S_i J_l \prod_{j=1}^{k-1} S_j + \sum_{j=1}^{k-1} h_j S_j + H_i S_i\right)\right\} = A\exp(\beta h_i S_i), \tag{4.26}$$

where

$$h_i = H_i + \widehat{h}_l,\ A = \frac{2^{k-1}\cosh\beta J_l \prod_{j=1}^{k-1}\cosh\beta h_j}{\cosh\beta\widehat{h}_l}, \tag{4.27}$$

$$\widehat{h}_l = \frac{1}{\beta}\tanh^{-1}\left(\tanh\beta J_l \prod_{j=1}^{k-1}\tanh\beta h_j\right). \tag{4.28}$$

The 3-CT's local structure with $c = 3$ is shown in fig. 4.7 as an example.

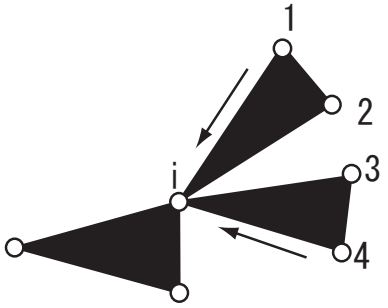

Figure 4.7: Local structure of a 3-CT with coordination number $c = 3$.

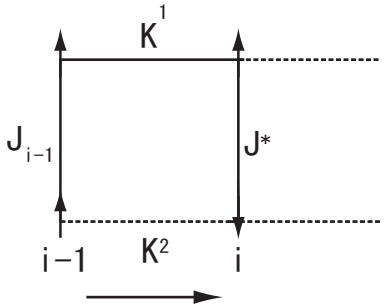

Figure 4.8: Local structure of a ladder with the width 2.

For ladder systems, similar relations can be derived with some slight modifications. We treat the width 2 ladder as an example. Summation over the two spins of i's previous layer as in fig. 4.8, we can obtain an expression corresponding to eq. (4.2) of the CT as

$$\sum_{S_{i-1}^{1,2}} \exp\{\beta(J_{i-1}S_{i-1}^1 S_{i-1}^2 + K^1 S_{i-1}^1 S_i^1 + K^2 S_{i-1}^2 S_i^2 + J^* S_i^1 S_i^2)\} = A\exp\left\{\beta(J^* + \widehat{J}_{i-1})S_i^1 S_i^2\right\}. \tag{4.29}$$

From simple algebras we get

$$\widehat{J}_{i-1}(J_{i-1},K^1,K^2)=\frac{1}{\beta}\tanh^{-1}(\tanh\beta K^1\tanh\beta K^2\tanh\beta J_{i-1}), \tag{4.30}$$

$$A(J_{i-1},K^1,K^2)=4\frac{\cosh\beta J_{i-1}\cosh\beta K^1\cosh\beta K^2}{\cosh\beta\widehat{J}_{i-1}(J_{i-1},K^1,K^2)}, \tag{4.31}$$

which means that the effective bonds J_i between S_i^1 and S_i^2 becomes

$$J_i=J^*+\widehat{J}_{i-1}(J_{i-1},K^1,K^2). \tag{4.32}$$

As eq. (4.6) in the CT case, the partition function is also updated as

$$Z_i=\sum_{S_{i-1}^{1,2},S_i^{1,2}}Z_{i-1}e^{-\beta\Delta H_{i,i-1}}\rho(S_{i-1}^1,S_{i-1}^2) \tag{4.33}$$

where

$$\rho(S_{i-1}^1,S_{i-1}^2)=\frac{e^{\beta J_{i-1}S_{i-1}^1S_{i-1}^2}}{4\cosh\beta J_{i-1}} \tag{4.34}$$

and $\Delta H_{i,i-1}=-K^1S_{i-1}^1S_i^1-K^2S_{i-1}^2S_i^2-J^*S_i^1S_i^2$ is the partial Hamiltonian added by an iterative procedure. The above formulas for the CTs and ladders enable us to assess the partition function of a given bond configuration $\{J_{ij}\}$ in a feasible computational cost.

Taking the $T\to 0$ limit yields the ground-state energy for a given bond configuration. For the $c=3$ CT, eqs. (4.4) and (4.6) become

$$\widehat{h}_j\to\mathrm{sgn}\,(J_{ij}h_j)\min(|J_{ij}|,|h_j|), \tag{4.35}$$

and

$$E_i=E_j+E_k-J_{ij}-J_{ik}+\begin{cases}0 & (\ \mathrm{sgn}\,(J_{ij}J_{ik}h_jh_k)\geq 0\ )\\ 2\min(|J_{ij}|,|J_{ik}|,|h_j|,|h_k|) & (\ \text{otherwise}\ )\end{cases}. \tag{4.36}$$

where we put the ground-state energy as $E_i=\lim_{\beta\to\infty}-(1/\beta)\log Z_i$ and assume $\mathrm{sgn}\,(0)\equiv 0$. The extension to general c and k-body interactions is straightforward and we here omit. Similarly, for the ladder, we can derive

$$\widehat{J}_{i-1}\to\mathrm{sgn}\left(J_{i-1}K^1K^2\right)\min(|J_{i-1}|,|K^1|,|K^2|), \tag{4.37}$$

and

$$E_i=E_{i-1}-K^1-K^2-J^*+\begin{cases}0 & (\ \mathrm{sgn}\,(J_{i-1}J^*K^1K^2)\geq 0\ )\\ 2\min(|J_{i-1}|,|J^*|,|K^1|,|K^2|) & (\ \text{otherwise}\ )\end{cases}. \tag{4.38}$$

For a given single sample of interactions and boundary conditions, a simple application of the cavity method enables us to evaluate the partition function in a feasible computational time. Unfortunately, this does not fully resolve the problem of the computational cost for assessing the moments (4.21) since the cost for evaluating the average over all possible samples of interactions and boundary conditions grows exponentially with respect to the number of spins.

4.2.2 Use of the replica method

To overcome the difficulty mentioned immediately above, we perform the configurational average for $n \in \mathbb{N}$ and use the analytical continuation of the obtained expressions to $n \in \mathbb{C}$ in the level of the cavity recursions, the method of which may be considered as a generalization of the replica method.

For this purpose, we first evaluate the nth moment of the partition function Z

$$\Xi(n) \equiv [Z^n]_{\boldsymbol{J}} = \mathrm{Tr} \prod_{\langle i,j \rangle} \left[\exp\left(\beta J_{ij} \sum_{\mu=1}^{n} S_i^\mu S_j^\mu \right) \right]_{\boldsymbol{J}}, \tag{4.39}$$

for $n \in \mathbb{N}$, where μ is the replica index. Let us denote the effective Hamiltonian as

$$H_{\mathrm{eff}} = \sum_{\langle i,j \rangle} H_{ij} = \sum_{\langle i,j \rangle} -\frac{1}{\beta} \log \left[\exp\left(\beta J_{ij} \sum_{\mu=1} S_i^\mu S_j^\mu \right) \right]_{\boldsymbol{J}}, \tag{4.40}$$

where $[\cdots]_{\boldsymbol{J}}$ stands for the configurational average with respect to the interactions $\{J_{ij}\}$. This means that eq. (4.39) is simply the partition function of an n-replicated system, which is defined on the same lattice as the original system, and is free from quenched randomness. Therefore, we can again use the cavity method to calculate $\Xi(n)$.

The case of the CT

For the $c = 3$ CT, we can derive the following recursion relation for $\Xi(n)$ as

$$\Xi_i(n) = \sum_{\boldsymbol{S}_i, \boldsymbol{S}_j, \boldsymbol{S}_k} \left[\exp\left\{ \beta \left(J_{ij} \sum_{\mu=1}^{n} S_i^\mu S_j^\mu + J_{ik} \sum_{\mu=1}^{n} S_i^\mu S_k^\mu \right) \right\} \right]_{\boldsymbol{J}} \rho_j \rho_k \Xi_j(n) \Xi_k(n) \tag{4.41}$$

$$= \sum_{\boldsymbol{S}_i} \rho_i(\boldsymbol{S}_i) \Xi_i(n), \tag{4.42}$$

where ρ_i is the one-site marginal distribution of site i. The expressions (4.41) and (4.42) define the updating rules of ρ_i and $\Xi_i(n)$.

So far, we have made no assumptions or approximations and therefore eq. (4.42) yields exact assessments for $n \in \mathbb{N}$, but to practically calculate $\Xi(n)$, we need to specify the form of ρ_i. In the present case, the form of ρ_i can be determined as follows. First, we assume the RS which requires that the correlation functions are independent of combinations of replica indices

$$\left\langle S_i^1 S_i^2 \right\rangle_{\rho_i} = \left\langle S_i^\mu S_i^\nu \right\rangle_{\rho_i} = q^{(2)}, \tag{4.43}$$

where the brackets $\langle (\cdots) \rangle_\rho$ denote the average over the distribution ρ_i. This assumption is correct for $n \in \mathbb{N}$ because the replicated Hamiltonian eq. (4.40) is invariant under the permutation of the replica indices. Moreover, in our case as long as the number of spins N is finite, the RS is exact even for real $n \in \mathbb{R}$. This is because the $\pm J$ model satisfies

the necessary conditions of the Carlson's theorem [61], as explained in section 4.2.4. With the RS, the expression of ρ_i is uniquely determined as

$$\rho_i(\boldsymbol{S_i}) = \frac{\sum_{l=0}^{n} q_i^{(l)} \sum_{\{a_1 \ldots a_l\}} S_i^{a_1} \cdots S_i^{a_l}}{2^n}, \tag{4.44}$$

where the symbol $\sum_{\{a_1 \ldots a_l\}}$ stands for a summation over all combinations of l choices from n replicas and $q^{(l)}$ denotes the correlation functions among l replica spins. It is easy to check that the normalization condition is satisfied and all the moments are recovered in this expression. Generally, eq. (4.44) can be transformed as follows

$$\rho_i(\boldsymbol{S}_i) = \int P_i(x) \prod_{\mu=1}^{n} \left(\frac{1 + x S^\mu}{2} \right) dx, \tag{4.45}$$

where the distribution function $P_i(x)$ must be defined to satisfy relations

$$\int x^l P_i(x) dx = q_i^{(l)}. \tag{4.46}$$

If $|x|$ is bounded by 1, the nonnegativity of the distribution ρ_i is satisfied. Under this assumption, we can perform a variable transformation $x = \tanh \beta h$ as

$$\rho_i = \int \pi_i(h) \prod_{\mu=1}^{n} \left(\frac{1 + \tanh(\beta h) S_i^\mu}{2} \right) dh = \int \pi_i(h) \frac{e^{\beta h \sum_\mu S_i^\mu}}{(2 \cosh \beta h)^n} dh. \tag{4.47}$$

This expression can be interpreted as that the cavity field h fluctuates by the randomness and has the distribution $\pi_i(h)$.

Inserting eq. (4.47) into eq. (4.42) and performing some simple algebraic steps give

$$\begin{aligned} \Xi_i &= \sum_{\boldsymbol{S}_i} \Xi_j \Xi_k (2 \cosh \beta)^{2n} \int dh_i \frac{e^{\beta h_i \sum_\mu S_i^\mu}}{(2 \cosh \beta h_i)^n} \Bigg\{ \iint \pi_j(h_j) \pi_k(h_k) \\ &\times \left[\delta(h_i - \widehat{h}_j - \widehat{h}_k) \left(\frac{2 \cosh \beta h_i}{2 \cosh \beta \widehat{h}_j 2 \cosh \beta \widehat{h}_k} \right)^n \right]_{\boldsymbol{J}} dh_j dh_k \Bigg\} \qquad (4.48) \\ &= \sum_{\boldsymbol{S}_i} \int dh_i \pi_i(h_i) \frac{e^{\beta h_i \sum_\mu S_i^\mu}}{(2 \cosh \beta h_i)^n} \Xi_i. \qquad (4.49) \end{aligned}$$

Equations (4.48) and (4.49) provide the cavity equation of $\pi_i(h_i)$:

$$\pi_i(h_i) \propto \iint \pi_j(h_j) \pi_k(h_k) \left[\delta(h_i - \widehat{h}_j - \widehat{h}_k) \left(\frac{2 \cosh \beta h_i}{2 \cosh \beta \widehat{h}_j 2 \cosh \beta \widehat{h}_k} \right)^n \right]_{\boldsymbol{J}} dh_j dh_k, \tag{4.50}$$

$$\Xi_i = \Xi_j \Xi_k (2 \cosh \beta)^{2n} \iint dh_j dh_k \, \pi_j(h_j) \pi_k(h_k) \left[\left(\frac{2 \cosh \beta (\widehat{h}_j + \widehat{h}_k)}{2 \cosh \beta \widehat{h}_j 2 \cosh \beta \widehat{h}_k} \right)^n \right]_{\boldsymbol{J}}, \tag{4.51}$$

which are applicable to $\forall n \in \mathbb{C}$. When the algorithm reaches the origin of the CT, the moment of eq. (4.39) is assessed as

$$\Xi(n) = [Z^n]_{\boldsymbol{J}} = \Xi_1\Xi_2\Xi_3(2\cosh\beta)^{3n}\iiint dh_1dh_2dh_3\,\pi_1(h_1)\pi_2(h_2)\pi_3(h_3)$$
$$\times\left[\left(\frac{1+\tanh\beta J_1\tanh\beta J_2\tanh\beta h_1\tanh\beta h_2+R}{4}\right)^n\right]_{\boldsymbol{J}}, \tag{4.52}$$

where R is two terms with the indices $1,2,3$ rotated.

The case of the ladder

For the width-2 ladder, the moment $\Xi(n)$ is updated as

$$\Xi_i = \sum_{\boldsymbol{S}_{i-1}^{1,2},\boldsymbol{S}_i^{1,2}}\left[\exp\left\{\beta\sum_{\mu=1}^{n}\left(J_{i-1}S_{i-1}^{1,\mu}S_{i-1}^{2,\mu}+K^1S_{i-1}^{1,\mu}S_i^{1,\mu}+K^2S_{i-1}^{2,\mu}S_i^{2,\mu}+J^*S_i^{1,\mu}S_i^{2,\mu}\right)\right\}\right]_{\boldsymbol{J}}$$
$$\times\Xi_{i-1}\rho_{i-1}(\boldsymbol{S}_{i-1}^1,\boldsymbol{S}_{i-1}^2) \tag{4.53}$$
$$=\sum_{\boldsymbol{S}_i^{1,2}}\Xi_i\rho_i(\boldsymbol{S}_i^1,\boldsymbol{S}_i^2) \tag{4.54}$$

These equations also define the recursion rule of the two-site marginal distribution $\rho_i(\boldsymbol{S}_i^1,\boldsymbol{S}_i^2)$. As in the CT case, we can specify the form of $\rho_i(\boldsymbol{S}_i^1,\boldsymbol{S}_i^2)$ from symmetries of the present problem as

$$\rho_i(\boldsymbol{S}_i^1,\boldsymbol{S}_i^2) = \int dJ_i\pi_i(J_i)\frac{e^{\beta J_i\sum_\mu S_i^{1,\mu}S_i^{2,\mu}}}{(4\cosh\beta J_i)^n}, \tag{4.55}$$

which can be interpreted as that the effective bond fluctuates by quenched randomness. The equation of the moment Ξ_i then becomes

$$\Xi_i = \Xi_{i-1}\int dJ_{i-1}\pi_{i-1}(J_{i-1})\left[(4\cosh\beta K^1\cosh\beta K^2)^n\left(\frac{\cosh\beta(J^*+\widehat{J}_{i-1})}{\cosh\beta\widehat{J}_{i-1}}\right)^n\right]_{\boldsymbol{J}}. \tag{4.56}$$

Equations (4.53)-(4.55) imply that the recursion relation of $\pi_i(J_i)$ becomes

$$\pi_i(J_i)\propto\int dJ_{i-1}\pi_{i-1}(J_{i-1})\left[\delta(J_i-J^*-\widehat{J}_{i-1})\left(\frac{\cosh\beta(J^*+\widehat{J}_{i-1})}{\cosh\beta\widehat{J}_{i-1}}\right)^n\right]_{\boldsymbol{J}}. \tag{4.57}$$

These relations yield the algorithm to calculate $\Xi(n)$ for the width-2 ladder.

4.2.3 Energetic zero-temperature limit in the cavity recursions

Let us take the energetic zero-temperature limit $\beta\to\infty$, $n\to 0$ keeping $y=\beta n\approx O(1)$ in the iterative procedures of the cavity method.

We first focus on the width-2 ladder. In our present model, the interaction J_{ij} takes ±1 with an equal probability $1/2$, which means that the initial condition of the recursion relation (4.57), $\pi_0(J_0)$, takes the following form

$$\pi_0(J_0) = \frac{1}{2}(\delta(J_0-1)+\delta(J_0+1)), \tag{4.58}$$

and the initial condition of the moment Ξ_0 becomes in the energetic zero-temperature limit as

$$\Xi_0(n) = (2\cosh\beta)^n \to e^y. \tag{4.59}$$

The relation (4.37) and the fact that $|J_{ij}|$ equals to 1 mean that for $\forall i$ J_i only takes five integers $0, \pm 1, \pm 2$ at zero temperature. This condition considerably simplify the current problem. The cavity equation (4.57) becomes

$$\pi_i(J_i) \propto \int dJ_{i-1}\pi_{i-1}(J_{i-1}) \Bigg[\delta(J_i - J^* - \mathrm{sgn}\left(K^1K^2J_{i-1}\right)) \times e^{y\left(\left|J^*+\mathrm{sgn}\left(K^1K^2J_{i-1}\right)\right|-\left|\mathrm{sgn}\left(K^1K^2J_{i-1}\right)\right|\right)} \Bigg]_{\boldsymbol{J}}, \tag{4.60}$$

and the distribution $\pi_i(J_i)$ takes the following form

$$\pi_i(J_i) = p_{i;0}\delta(J_i) + \sum_{f=1}^{2} p_{i;f}(\delta(J_i - f) + \delta(J_i + f)), \tag{4.61}$$

where $\boldsymbol{p}_i = (p_{i;0}, p_{i;1}, p_{i;2})$ represents a probability vector satisfying $p_{i;0} + 2\sum_f p_{i;f} = 1$ and $p_{i;f} \geq 0$. The symmetry $p_{i;f} = p_{i;-f}$ comes from the symmetric distribution of $\{J_{ij}\}$. Equations (4.60) and (4.61) offer the simple recursion equations as follows;

$$(p_{i;2}, p_{i;1}, p_{i;0}) \propto \left(\frac{(1 - p_{i-1;0})}{2},\ p_{i-1;0},\ (1 - p_{i-1;0})e^{-2y} \right), \tag{4.62}$$

and the recursion relation of the moment Ξ_i (4.53) is also simplified as

$$\Xi_i = \Xi_{i-1}e^{3y} \left\{ p_{i-1;0} + \frac{1}{2}(1 + e^{-2y})(1 - p_{i-1;0}) \right\}. \tag{4.63}$$

Equations (4.62) and (4.63) indicate that only $p_{i;0}$ is relevant for the evaluation of the moment. This is a peculiar property to the symmetric distribution of $J_{ij} = \pm 1$. We here write down the explicit form of the cavity equation of $p_{i;0}$

$$p_{i;0} = \frac{1 - p_{i-1;0}}{1 - p_{i-1;0} - (1 + p_{i-1;0})e^{2y}}. \tag{4.64}$$

The formulas (4.63) and (4.64) enable us to assess the moment $\Xi(y)$ in a feasible computational time and therefore offer a useful scheme for examining the RZs.

Next, we proceed to the CT case. Unlike the ladder case, for the CT we should choose the boundary conditions appropriately. This is because the CT has no cycle in the graph and hence the frustration cannot be introduced into the system unless the boundary condition is appropriately chosen.

The boundary condition we here treat is the random external field $h_i = \pm 1$, the sign of which is determined with an equal probability of $1/2$. As the result of this boundary

condition, the cavity field distribution and the moment at the boundary, $\pi_0(h_0)$ and Ξ_0, become

$$\pi_0(h_0) = \frac{1}{2}\left(\delta(h_0 - 1) + \delta(h_0 + 1)\right) \tag{4.65}$$

and

$$\Xi_0 = (2\cosh\beta)^n \to e^y, \tag{4.66}$$

respectively, which yield the initial conditions of the cavity recursions. The relevance of the boundary condition to the current objective systems is discussed later.

Equation (4.65) in conjunction with the property $|J_{ij}| = 1$ again restrict the functional form of $\pi_i(h_i)$ in eq. (4.50) as

$$\pi_i(h_i) = p_{i;0}\delta(h_i) + \sum_{f=1}^{c-1} p_{i;f}\left(\delta(h_i - f) + \delta(h_i + f)\right). \tag{4.67}$$

The symmetry $\pi_i(h_i) = \pi_i(-h_i)$ comes from the symmetry of the boundary-field distribution (4.65) as in the ladder case.

After the configurational average is performed, the cavity-field distribution $\pi_i(h_i)$ depends only on the distance, g, from the boundary. Therefore, we hereafter denote $\pi_i(h_i)$ as $\pi_g(h_i)$ and represent the distance of the origin from the boundary as $g = L$. The current scheme assesses $\boldsymbol{p}_{g+1}$ using its descendents $\boldsymbol{p}_g$ For the $c = 3$ case, the actual formula is derived from eq. (4.50) as

$$(p_{g+1;2}, p_{g+1;1}, p_{g+1;0}) \propto \left(\left(\frac{(1 - p_{g;0})}{2}\right)^2,\ p_{g;0}(1 - p_{g;0}),\ p_{g;0}^2 + 2\left(\frac{1 - p_{g;0}}{2}\right)^2 e^{-2y}\right). \tag{4.68}$$

Similarly to the ladder case, the relevant part to the assessment of $\Xi(n)$ is only for $p_{g;0}$, the precise recursion relation of which is given by

$$p_{g+1;0} = \frac{p_{g;0}^2 + 2\left(\frac{1-p_{g;0}}{2}\right)^2 e^{-2y}}{1 - 2(1 - e^{-2y})\left(\frac{1-p_{g;0}}{2}\right)^2}, \tag{4.69}$$

being accompanied by an update of the moment

$$\Xi_{g+1} = \Xi_g^2 e^{2y}\left\{1 - 2(1 - e^{-2y})\left(\frac{1 - p_{g;0}}{2}\right)^2\right\}. \tag{4.70}$$

After evaluating $p_{g;0}$ and Ξ_g using this algorithm up to $g = L - 1$, the full moment, $\Xi(y)$, in the current limit $n \to 0$ and $\beta \to \infty$ keeping $y = n\beta \sim O(1)$ is finally assessed as

$$\Xi(y) = \Xi_{L-1}^3 e^{3y}\left\{1 - 3(1 - e^{-2y})\left(\frac{1 - p_{L-1;0}}{2}\right)^2 (1 + p_{L-1;0})\right\}. \tag{4.71}$$

As eqs. (4.62) and (4.63) for the ladder case, eqs. (4.69)–(4.71) enable us to calculate the moment $\Xi(y)$ in a feasible time, which constitute the main result of this chapter.

4.2.4 Uniqueness of the analytic continuation

The analytical continuation from $n \in \mathbb{N}$ to $n \in \mathbb{C}$ cannot be determined uniquely in general systems. However, in the present system, we can show the uniqueness of the continuation. Therefore, the RS solution assumed above is correct.

For this, let us consider the modified moment $[(Ze^{-\beta N_B})^n]_{\boldsymbol{J}}^{1/N}$, where N_B is the total number of bonds. This quantity satisfies the inequality

$$\begin{aligned}\left|\left[\left(Ze^{-\beta N_B}\right)^n\right]_{\boldsymbol{J}}^{1/N}\right| &\leq \left[\left(Ze^{-\beta N_B}\right)^{\mathrm{Re}(n)}\right]_{\boldsymbol{J}}^{1/N} \\ &\leq \left[\left(\mathrm{Tr}\,1\right)^{\mathrm{Re}(n)}\right]_{\boldsymbol{J}}^{1/N} = 2^{\mathrm{Re}(n)} < O(e^{\pi|n|}),\end{aligned} \tag{4.72}$$

for finite N. Suppose that we have an analytic function $\psi(n;N)$ that satisfies the condition $|\psi(n;N)| < O(e^{\pi|n|})$. The Carlson's theorem guarantees that if the equality $|\psi(n;N) - [(Ze^{-\beta N_B})^n]_{\boldsymbol{J}}^{1/N}| = 0$ holds for $\forall n \in \mathbb{N}$, $\psi(n;N)$ is identical to $[(Ze^{-\beta N_B})^n]_{\boldsymbol{J}}^{1/N}$ for $\forall n \in \mathbb{C}$. Because $e^{-\beta N_B}$ is a non-vanishing constant, this means that the analytic continuation of $[Z^n]_{\boldsymbol{J}}^{1/N}$ is uniquely determined. This indicates that expressions in the above subsections, which analytically continued under the RS ansatz, are correct for finite N (or equivalently, finite L). Hence, in the current problem, the possible problem of the analytic continuation of $\phi(n) = \lim_{N\to\infty}(1/N)\log[Z^n]_{\boldsymbol{J}}$ is summarized into the point whether the analyticity breaking on the real axis occurs or not in the limit $N \to \infty$.

4.3 Results for the ladders

The concrete procedure to obtain RZs for the width-2 ladder with the length L is summarized as follows:

1. To obtain a series of $p_{i;0}$, eq. (4.64) is recursively applied under the initial condition $p_{0;0} = 0$ until i reaches L. This can be symbolically performed by using computer algebra systems such as *Mathematica*.

2. Using the series $\{p_{i;0}\}$, the moment Ξ_i is recursively calculated by using eq. (4.63) under the initial condition $\Xi_0 = e^y$ until i becomes L. Then, the full moment $\Xi(y) = \Xi_L$ is obtained.

3. Solving $\Xi_L = 0$ with respect to $x = e^y$ numerically.

Although the right hand side of eq. (4.64) is expressed as a rational function, the moment $\Xi(y)$ is guaranteed to be certain polynomials of x since the contribution from the denominator is canceled in each step of eqs. (4.63) and (4.64). The procedures of 1, 2 and 3 can be performed in a polynomial time with respect to the number of spins. Figure 4.9 shows the plot for a $2 \times L$ ladder. Notice that all RZs lie on a line $\mathrm{Im}(y) = \pi/2$. This fact can be mathematically proven, as detailed in B.2. The physical significance of this

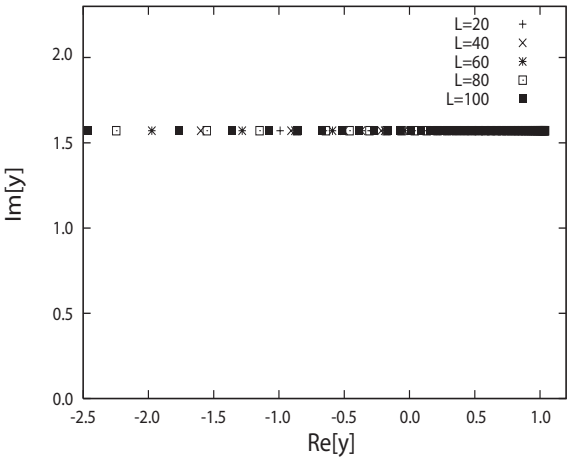

Figure 4.9: RZs for ladders with $2 \times L$. All the zeros lie on $\mathrm{Im}(y) = \pi/2$ and never reach the real axis of $y = \beta n$. The inequality $\mathrm{Re}(y) \leq \log 2\sqrt{2}$ holds, as shown in appendix B.2.

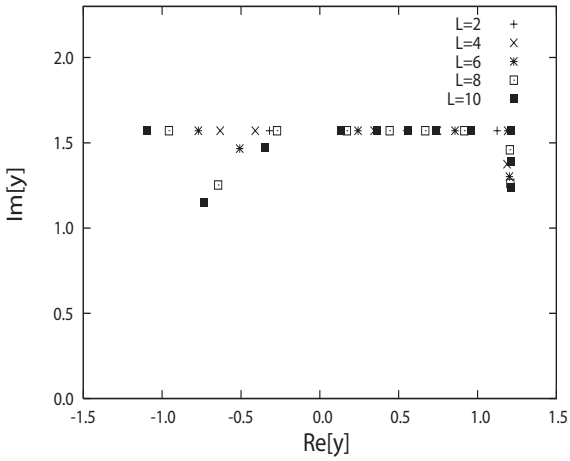

Figure 4.10: Zeros of width-4 ladders. Some of the zeros approach the real axis around $\mathrm{Re}(y) \approx 1.2$ and -0.8, but the rate of approach rapidly decreases as L grows.

behavior is that the generating function $g_N(n)$ is analytic with respect to real y even for the $N \to \infty$ limit.

We also investigated larger-width ladders. However, the larger-width systems requires many-body interactions to calculate the marginal distribution ρ. It makes the problem complicated and simple relations like (4.55) cannot be obtained. Hence, when treating larger-width ladders, we directly use the cavity method for a given sample $\{J_{ij}\}$ to obtain the ground state energy [76], which is just the use of the cavity method we mentioned in the end of section 4.2.1. In this prescription, we numerically assess the distribution of the ground state energies $P(E_g)$ by enumerating all the bond configurations $\{J_{ij}\}$. Using the distribution $P(E_g)$, the RZs equation is derived as

$$\sum_{E_g} P(E_g) e^{-yE_g} = 0. \tag{4.73}$$

This equation is solved numerically in the same way as the width-2 case. Note that computational times required in the counting process to obtain $P(E_g)$ exponentially increases as L grows, which makes it infeasible to obtain Ξ_L for large L, unlike the width-2 case.

The RZs for $3 \times L$ ladder were calculated and found qualitatively similar results as for the width-2 case. For a width-4 ladder, the RZ plot is given in fig. 4.10. We can observe that some zeros approach the real axis around $\mathrm{Re}(y) \approx 1.2$ and -0.8, but the rate of approach decreases rapidly as L grows. This implies that the RZs do not reach the real axis, which agrees with a naive speculation that ladders are essentially one-dimensional systems and therefore do not involve any phase transitions as long as the width is kept finite. These results indicate that the RZs for the ladders do not reach the real axis of y in the limit $N \to \infty$. This means that the analyticity breaking of $\phi(n)$ does not occur for the ladder systems, which accords with an intuition that the ladders are essentially

one-dimensional systems in the thermodynamic limit and should not exhibit the spin-glass ordering.

4.4 Results for the CTs

As for the ladder case, we first summarize the concrete procedure to obtain RZs for the CT:

1. Recursively applying (4.69) under the initial condition $p_{0;0} = 0$ until g reaches $L-1$ to obtain the series$\{p_{g;0}\}$.
2. The moment Ξ_g is recursively assessed from eq. (4.70) by using the series $\{p_{g;0}\}$ until g becomes $L-1$.
3. The full moment $\Xi(y) = \Xi_L$ is derived from eq. (4.71) using Ξ_{L-1} and $p_{L-1;0}$
4. Solving $\Xi_L = 0$ with respect to $x = e^y$ numerically.

The procedures 1–4 can be performed in a polynomial time with respect to the number of spins, which is the same as the ladder case.

On the other hand, for CTs the number of spins and the degree of the polynomial Ξ_L increase exponentially as $O\left(((k-1)(c-1))^L\right)$ as L grows, which makes it infeasible to solve $\Xi_L = 0$ for large L. For instance, it is computationally difficult to evaluate RZs beyond $L = 7$ for $(k, c) = (2, 3)$ and $L = 4$ for $(k, c) = (3, 4)$ by use of today's computers of reasonable performance. This prevents us from accurately examining the convergence of RZs to the real axis in the limit $L \to \infty$ by means of numerical methods.

However, the data of small L still strongly indicate that the qualitative behavior of RZs can be classified distinctly depending on whether certain bifurcations occur for the cavity field distribution in the limit of $L \to \infty$, which implies that the RZs of the CTs reflect the phase transitions with respect to y. Unfortunately, we also clarify that the transitions are related to no RSB by some analytical discussions. In the following subsections, we give detailed discussions to lead this conclusion presenting plots of RZs.

4.4.1 Plots of the replica zeros for CTs

We here present the results for CTs. The plots for a CT and for a 3-CT with $c = 3$ are shown in figs. 4.11 and 4.12, respectively. It is known that the FRSB and 1RSB transitions occur in RRGs with $(k, c) = (2, 3)$ and $(k, c) = (3, 3)$, respectively [10, 30, 72, 77].

Figure 4.11 shows that RZs of the $c = 3$ CT lie on a line $\mathrm{Im}(y) = \pi/2$. Interestingly, this behavior is the same as the $2 \times L$ ladder case in fig. 4.9. This result indicates that there is no phase transition or breaking of analyticity of $\phi(n)$ with respect to real y. This strongly suggests that the RZs of CTs cannot detect the FRSB transitions in RRGs.

On the other hand, for the 3-CT case in fig. 4.12, a sequence of RZs approaches a point y_c on the real axis from the line $\mathrm{Im}(y) = \pi/2$ as the number of generations L increases,

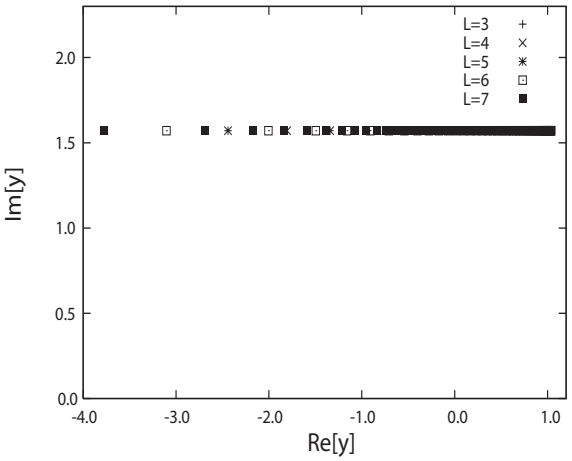

Figure 4.11: Plot of RZs for a CT with $c = 3$. All the zeros lie on the line $\mathrm{Im}(y) = \pi/2$, as for a $2 \times L$ ladder.

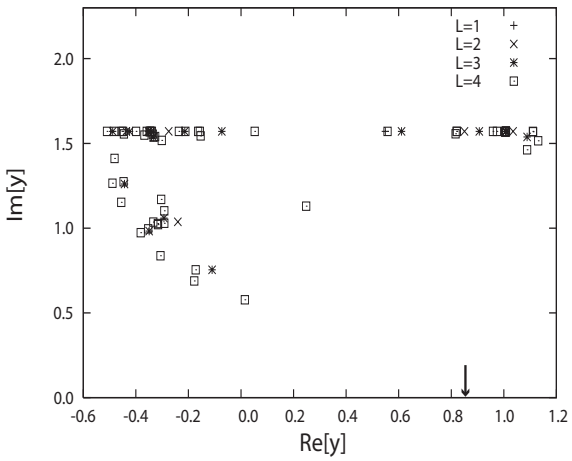

Figure 4.12: RZs plot for a 3-CT with $c = 3$. A sequence of zeros approaches the real axis as the number of generations L increases. The arrow indicates the collision point expected from the study of the $L \to \infty$ limit in section 4.4.2.

although the value of y_c is far from $y_s = \infty$ where the corresponding RRG occurs the 1RSB transition. The arrow in fig. 4.12 represents the speculated value of y_c from the analysis of the corresponding BL, the detail of which is given in the next subsection.

A similar tendency is also observed for a CT and 3-CT with $c = 4$, plots of which are presented in figs. 4.13 and 4.14, respectively. The 1RSB critical values are $y_s = 0.38926$ for the CT and $y_s = 1.41152$ for the 3-CT. Again, these values are far from the values of y_c, which can be observed in figs. 4.13 and 4.14.

These results indicate that certain phase transitions occur for some CTs, although they are irrelevant to 1RSB and FRSB. It is difficult to identify the critical value y_c from the plots because of the computational limits. Instead, in the following subsection we investigate the $L \to \infty$ limit of these models. The arrows in figs. 4.12–4.14 represent the transition points y_c determined by this investigation.

4.4.2 The thermodynamic limit and phase transitions of BLs

In order to identify the value of y_c, we here consider the thermodynamic limit. Direct investigation of CTs in this limit is difficult, and we employ BLs to speculate the behavior of CTs.

Transitions of the convergent cavity-field distribution

The first step is to take the $L \to \infty$ limit by equating $p_{g+1;0}$ and $p_{g;0}$ in the iterative equation of $p_{g;0}$, which yields the boundary condition p_* of the BL. For a $c = 3$ 3-CT, the

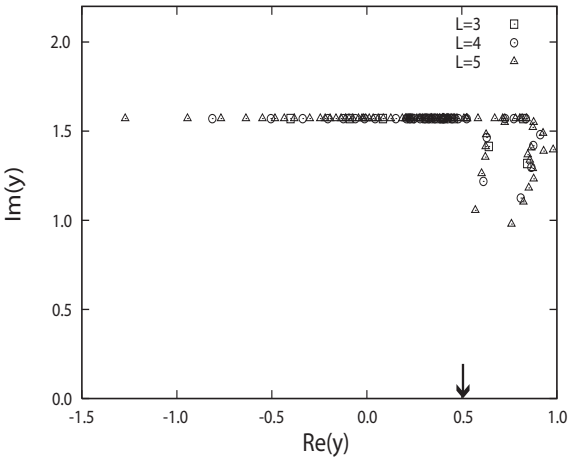

Figure 4.13: RZs of a CT with $c = 4$. We consider only an L-generation branch in this case because of computational limits. RZs approach the real axis as L increases around $y_c \approx 0.5$. The arrow indicates the location of the singularity of the cavity-field distribution.

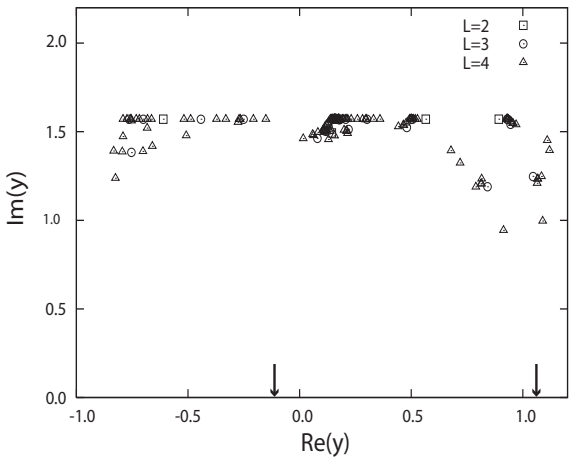

Figure 4.14: RZs of a 3-CT with $c = 4$. We consider only an L-generation branch. The zeros approach the real axis around $y_c \approx 1.1$. There are two singular points of the cavity field distribution in this case, both of which are indicated by arrows.

iterative equation is given by

$$p_{g+1;0} = \frac{\left\{p_{g;0}^2 + 2p_{g;0}(1-p_{g;0})\right\}^2 + \frac{1}{2}e^{-2y}(1-p_{g;0})^4}{1 - \frac{1}{2}(1-p_{g;0})^4(1-e^{-2y})}. \tag{4.74}$$

A return map of the recursion of $p_{g;0}$ and the convergent solution p_* in the initial condition $p_{0;0} = 0$ are presented in figs. 4.15 and 4.16, respectively. The return map shows that there are three fixed points for $x \gtrsim 2.35$, while $p = 1$ is the only fixed point for $x \lesssim 2.35$. This situation is in contrast to the $c = 3$ CT case, in which the cavity-field distribution uniformly converges to an analytic function:

$$p_* = \frac{2 + x^2 - \sqrt{x^4 + 8x^2}}{2(1-x^2)}, \tag{4.75}$$

which can be derived from eq. (4.69). This implies that when eq. (4.65) is put on the boundary of the CT, the boundary condition of the BL, which was obtained by an infinite number of recursions $L - L' \to \infty$, exhibits a discontinuous transition from $p_* < 1$ to $p_* = 1$ at $x \approx 2.35 \Leftrightarrow y_c \approx 0.86$ as y is reduced from the above. Actually, in fig. 4.12, RZs of the $c = 3$ 3-CT seem to approach $y_c \approx 0.86$, marked by an arrow. This indicates that RZs obtained by our framework are relevant to the phase transition of the boundary of a BL, which is not related to 1RSB. This can be also confirmed from the initial condition dependence of the RZs behavior. Equation (4.74) implies that the fixed point $p = 1$ is always stable, which can be seen from fig. 4.15, and a sufficiently large initial condition $p_{0;0} > 0$ leads to the convergence to this fixed point. In that case, it is reasonable that RZs do not approach the real axis of y. The actual plot of RZs for a $c = 3$ 3-CT with the initial

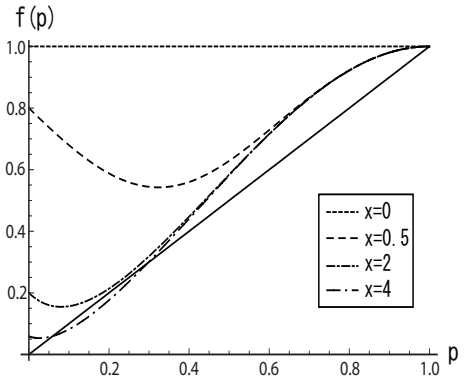

Figure 4.15: Return map of a 3-CT with $c = 3$. The convergent point of the recursion discontinuously changes depending on x. The solid line represents the function $f(p) = p$.

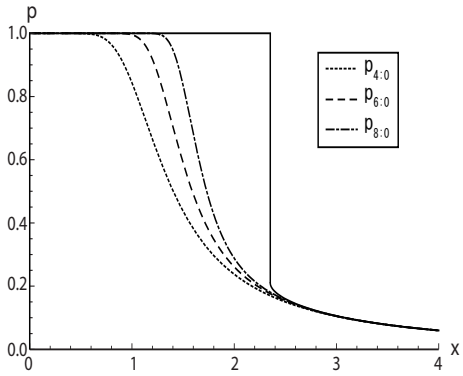

Figure 4.16: Asymptotic behavior of $p_{g;0}$ of a 3-CT with $c = 3$. A finite jump of p occurs at $x \approx 2.35$. The solid line denotes the Ł $\to \infty$ solution p_*.

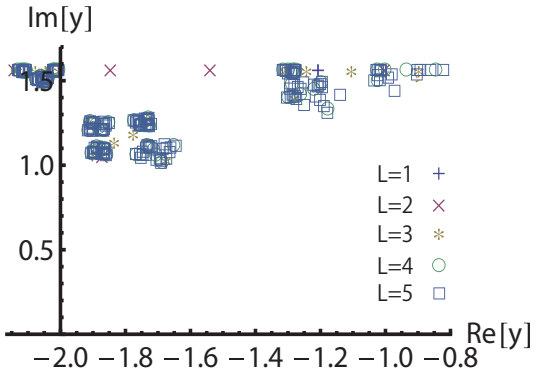

Figure 4.17: Plot of RZs of a $c = 3$ 3-CT with the initial condition $p_{0;0} = 1/2$. The RZs do not approach the real axis even as L grows.

condition $p_{0;0} = 1/2$ is given in fig. 4.17. This figure clearly shows that the RZs do not approach the real axis. It can be also observed that as the initial condition $p_{0;0}$ becomes close to 1, RZs tend to go to the limit $\mathrm{Re}(y) \to -\infty$ and $\mathrm{Im}(y) = \pi/2$, and become to never approach the real axis. These observations support the present description that the RZs of CTs correspond to the transition at the boundary of BLs.

The same analysis for a $c = 4$ CT shows that bifurcation of another type can occur for even c. For this model, the recursive equation of $p_{g;0}$ has a trivial solution $p_* = 0$ for $\forall x$, which is always the case when $c - 1$ is odd. The return map and plots of p_* are shown in figs. 4.18 and 4.19, respectively. These figures indicate that there exists a continuous transition from $p_* = 0$ to $p_* > 0$ at a certain value of x, which can be assessed as $x_c = \sqrt{3} \Rightarrow y_c \approx 0.5$. This is consistent with a certain sequence of RZs approaching the real axis around $y_c \approx 0.5$ in fig. 4.13, which supports the analytical assessment of the critical points.

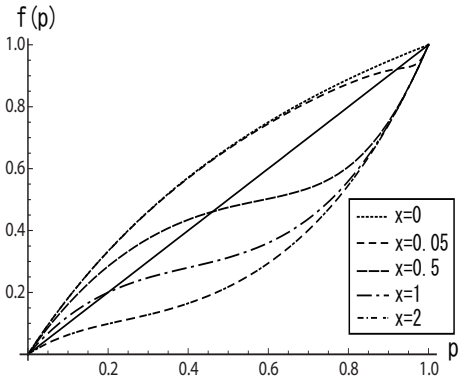

Figure 4.18: Return map of a CT with $c = 4$. The stable fixed point is unique but shows a singularity at $x = e^y = \sqrt{3}$.

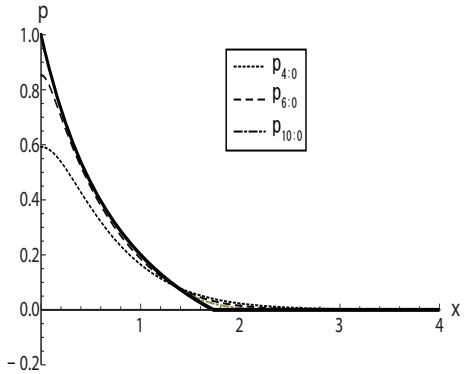

Figure 4.19: Asymptotic behavior of $p_{g;0}$ of a CT with $c = 4$. In the thermodynamic limit, $p_{g;0}$ is continuous but the derivative becomes discontinuous at $x = \sqrt{3}$.

In general, the discontinuous transition appears for cases of $k \geq 3$ spin interactions and the continuous transition occurs when c is even. Actually, for a $c = 4$ 3-CT, both discontinuous and continuous transitions occur at $x \approx 0.86 \Rightarrow y \approx -0.15$ and $x = 3 \Rightarrow y \approx 1.1$, respectively. Figure 4.14 shows a sequence of RZs approaching $y \approx 1.1$, while it is difficult to clearly identify a sequence converging to the other critical point $y \approx -0.15$. We consider that this is because the system size is not large enough, since a portion of the RZs in the left shows a tendency to approach the real axis, though further increase of the system size is practically unfeasible due to the limitations of current computational resources.

In conclusion, the RZs of CTs are related to the phase transitions on the boundary of the corresponding BLs. Regardless of the type of transition, a sequence of RZs approaches a critical point on the real axis when the BL provided from a CT in the limit $L \to \infty$ exhibits a phase transition on the boundary.

Relevance of the boundary condition and bulk properties of CTs

Equations (4.69)–(4.71) imply that the generating function $\phi_N(y) = N^{-1} \log \Xi(y)$ for CTs can also be separated into the bond and site contributions as eq. (4.14) in the case of free energy

$$\phi_N(y) = \frac{1}{N} \sum_{\langle ij \rangle} \phi^{(2)}_{\langle ij \rangle}(y) - \frac{1}{N} \sum_i (c_i - 1) \phi^{(1)}_i(y). \tag{4.76}$$

As discussed in section 4.1.2, for a BL, the boundary condition given by the convergent solution of eq. (4.69), p_*, which becomes a function of y, simplifies the expression of eq. (4.76) as

$$\phi^{\mathrm{BL}}_N(y) = r_{\mathrm{I}} \phi_{\mathrm{I}}(y) + r_{\mathrm{B}} \phi_{\mathrm{B}}(y). \tag{4.77}$$

and

$$\phi_{\rm I}(y) = \frac{c}{2}\phi^{(2)}(y) - (c-1)\phi^{(1)}(y), \tag{4.78}$$

$$\phi_{\rm B}(y) = \frac{1}{2}\phi^{(2)}(y), \tag{4.79}$$

where $\phi_{\rm I}(y)$ and $\phi_{\rm B}(y)$ represent contributions from a site inside the tree and on the boundary, respectively. In general, $\phi^{(2)}(y)$ and $\phi^{(1)}(y)$ are expressed as

$$\phi^{(2)}(y) = \log\left\{ {\rm Tr}\left[\widehat{\rho}(\boldsymbol{S}_1)^{c-1}\widehat{\rho}(\boldsymbol{S}_2)^{c-1} e^{\beta J\sum_\mu S_1^\mu S_2^\mu}\right]_{\boldsymbol{J}}\right\}, \tag{4.80}$$

$$\phi^{(1)}(y) = \log\left\{ {\rm Tr}\,\widehat{\rho}(\boldsymbol{S})^c\right\}, \tag{4.81}$$

where

$$\widehat{\rho}(\boldsymbol{S}) = \int d\widehat{h}\widehat{\pi}(\widehat{h})\frac{e^{\beta\widehat{h}\sum_\mu S_\mu}}{(2\cosh\beta\widehat{h})^n} \tag{4.82}$$

and $\widehat{\pi}(\widehat{h})$ is the distribution of the cavity bias, which is related to $\pi(h)$ as

$$\widehat{\pi}(\widehat{h}) = \int dh\pi(h)\left[\delta\left(\widehat{h} - \frac{1}{\beta}\tanh^{-1}(\tanh\beta J\tanh\beta h)\right)\right]_{\boldsymbol{J}}. \tag{4.83}$$

These can be interpreted that cavity biases fluctuate due to the average over the quenched randomness. These formulas are generalizations of eqs. (4.14)–(4.16) to the generating function $\phi(n)$. For $c = 3$ in the limit $\beta n \to y$, we have

$$\phi^{(2)}(y) = \log e^y\left(1 - \frac{1}{2}(1-e^{-2y})(1-p_*)^2\right)^3, \tag{4.84}$$

$$\phi^{(1)}(y) = \log\left(1 - \frac{3}{4}(1-e^{-2y})(1-p_*)^2(1+p_*)\right). \tag{4.85}$$

In general, $\phi_{\rm I}(y)$ agrees with $\phi(y)$ of an RRG, which is the same as the free energy case.

In spin-glass problems on cycle-free graphs, the replacement of $\phi_N^{\rm BL}(y)$ with $\phi_{\rm I}(y)$ is crucial. To see this, let us investigate the rate function $R(f)$ as in section 2.5. We denote the boundary condition as $P_{\rm B}(\boldsymbol{h}) = \prod_{i\in{\rm boundary}}\pi_i(h_i)$. Since CTs and BLs have no cycle, for the $\pm J$ model defined on those lattices the boundary condition is the only relevant factor determining the property of the model. Combining this fact with eq. (4.23), we can express the moment $\Xi(y)$ of CTs and BLs as

$$\Xi(y) = \int d\boldsymbol{h}P_{\rm B}(\boldsymbol{h})\exp\left(-yE_g(\boldsymbol{h})\right), \tag{4.86}$$

where $E_g(\boldsymbol{h})$ is the ground state energy when $\boldsymbol{h}$ is imposed on the boundary. This yields the following equation with respect to the rate function for finite N, $R_N(y)$,

$$-R_N(y) = y^2\frac{\partial}{\partial y}\left(\frac{\phi_N(y)}{y}\right) = \frac{1}{N}\int dh\widetilde{P}_{\rm B}(\boldsymbol{h})\log\frac{\widetilde{P}_{\rm B}(\boldsymbol{h})}{P_{\rm B}(\boldsymbol{h})} \equiv \frac{1}{N}D(\widetilde{P}_{\rm B}|P_{\rm B}) \geq 0, \tag{4.87}$$

where we define the probability distribution $\widetilde{P}_{\rm B}(\boldsymbol{h})$ as $\widetilde{P}_{\rm B}(\boldsymbol{h}) \equiv P_{\rm B}(\boldsymbol{h}) \exp\left(-yE_g(\boldsymbol{h})\right) / \Xi(y)$ and introduce the so-called Kullback–Leibler (KL) divergence $D(\widetilde{P}_{\rm B}|P_{\rm B})$ between $\widetilde{P}_{\rm B}(\boldsymbol{h})$ and $P_{\rm B}(\boldsymbol{h})$, which takes a positive value unless $\widetilde{P}_{\rm B}(\boldsymbol{h})$ becomes identical to $P_{\rm B}(\boldsymbol{h})$. This equation guarantees the non-positivity of the rate function $R_N(y)$. The constraint $R_N(f) \leq 0$ is always satisfied even when $N \to \infty$. However, as discussed in section 2.5, this is not necessarily the case when we first take the thermodynamic limit $\lim_{N\to\infty} \phi_N(y) = \phi(y)$ and then calculate the rate function by using the analytically continued $\phi(y)$ as $R(y) = -y^2(\partial/\partial y)\left(y^{-1}\phi(y)\right)$. This function $R(y)$ can be positive, and the condition $R(y_s) = 0$ signals the onset of 1RSB as shown in section 2.5.

The condition $R(y_s) = 0$ has already been investigated for RRGs and indicates that 1RSB transitions occur for some types of RRGs [10, 72]. However, it is considered that such a symmetry breaking cannot be detected by an investigation based on eqs. (4.69)–(4.71) because the boundary contribution is inevitably taken into account for a BL as well as for a CT.

An example will clearly illustrate this point. Let us calculate the generating function of the $c = 3$ BL and RRG. The generating function of the RRG (assessed only in the thermodynamic limit) is given by substituting eqs. (4.69), (4.84), and (4.85) into $\phi_{\rm I}(y)$, and the plot is given in fig. 4.20. This shows a 1RSB critical value $R(y_s) = 0$ at $y_s =$

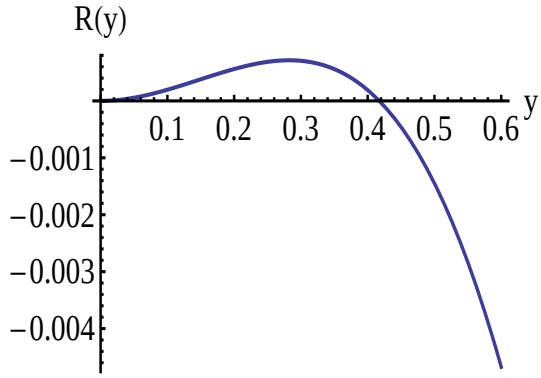

Figure 4.20: The rate function of a $c = 3$ RRG. The 1RSB critical value is $y_s = 0.41741$.

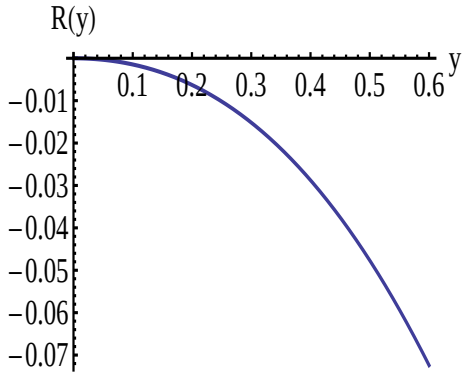

Figure 4.21: The rate function of a $c = 3$ BL in the limit $L \to \infty$. The constraint $R(f) \leq 0$ is completely held.

0.41741 and demonstrates the failure of the analytic continuation of $\phi(y)$. On the other hand, the generating function of the BL for finite N is given by eq. (4.77) with the conditions (4.69), (4.84), and (4.85). Clearly, the N-dependence of $\phi_N^{BL}(y)$ only appears in two factors $r_{\rm I} = \left(1 + c(c-2)^{-1}\left((c-1)^{L'-1} - 1\right)\right) / \left(1 + c(c-2)^{-1}\left((c-1)^{L'} - 1\right)\right)$ and $r_{\rm B} = 1 - r_{\rm I}$ through the total generation L. These factors are analytic with respect to L even in the limit $L \to \infty$, which guarantees the uniform convergence of $\phi_N^{\rm BL}(y)$ to $\lim_{L\to\infty} \phi_L^{\rm BL}(y) = \phi^{\rm BL}(y)$. Hence, the analytic continuation of $\phi(y)$ is successfully performed and the resultant rate function $R(f)$ never violates $R(f) \leq 0$, which can be actually seen in fig. 4.21. Also, we can prove the absence of the 1RSB transition for CTs by showing the uniform convergence of $\phi_N(y)$. We succeeded to prove this for a $c = 3$ CT

and the details are shown in appendix B.3.

In summary, the RZs of CTs provided by the current scheme are irrelevant to the 1RSB because it does not appear in BLs and CTs due to the huge boundary effect. However, this does not mean the absence of another RSG, FRSB, in BLs and CTs. Next we examine this point.

4.4.3 Possibility of the full-step replica symmetry breaking

The AT condition, which is critical for the FRSB, has not yet been characterized for sparsely connected spin models [77–79]. In fact, a previous research has found that critical values of the continuous transitions from $p_* = 0$ to $p_* > 0$ are candidates for those of the AT condition for systems of even c [10]. This motivates us to further explore a possible link between RZs and the AT instability.

As discussed in section 2.6.1, the AT condition is identical to the divergence of the spin-glass susceptibility χ_{SG} in the fully-connected p-spin interacting model. Hence, it is reasonable to adopt the divergence of χ_{SG} as the critical condition of the FRSB for BLs and RRGs [80–82]. Using the (statistical) uniformness of BLs and RRGs, it is sufficient to see the susceptibility of only the root site 0. The spin-glass susceptibility of BLs for finite replica n is generally written as

$$\chi_{SG} = \sum_i \left[\left(\frac{\partial \langle S_0 \rangle}{\partial h_i} \right)^2 \right]_n . \tag{4.88}$$

where $[(\cdots)]_n$ means an average with respect to a modified distribution of coupling and boundary field

$$P_n(\{J_{ij}\}, \{h_i\}) = \frac{P(\{J_{ij}\}, \{h_i\}) Z^n(\{J_{ij}\}, \{h_i\})}{\sum_{\{J_{ij}\}} P(\{J_{ij}\}, \{h_i\}) Z^n(\{J_{ij}\}, \{h_i\})}. \tag{4.89}$$

In a cycle-free graph, an arbitrary pair of nodes is connected by a single path. Let us assign node indices from the origin of the graph 0 to a node of distance G along the path as $g = 1, 2, \ldots, G$. For a fixed set of couplings and boundary fields, the chain rule of the derivative operation indicates that

$$\begin{aligned} \frac{\partial \langle S_0 \rangle}{\partial h_G} &= \frac{\partial \langle S_0 \rangle}{\partial h_0} \frac{\partial h_0}{\partial \widehat{h}_0} \frac{\partial \widehat{h}_0}{\partial h_1} \cdots \frac{\partial h_G}{\partial \widehat{h}_G} = \frac{\partial \langle S_0 \rangle}{\partial h_0} \frac{\partial h_0}{\partial \widehat{h}_0} \prod_{g=1}^{G} \frac{\partial \widehat{h}_{g-1}}{\partial h_g} \frac{\partial h_g}{\partial \widehat{h}_g} \\ &= \frac{\partial \langle S_0 \rangle}{\partial \widehat{h}_0} \prod_{g=1}^{G} \frac{\partial \widehat{h}_{g-1}}{\partial \widehat{h}_g}, \end{aligned} \tag{4.90}$$

as h_g depends linearly on $\widehat{h}_g$ as $h_g = \widehat{h}_g + r_g$, where r_g represents a sum of the cavity biases from other branches that flow into node g. For a BL of $(k, c) = (2, 3)$, the cavity equation yields an evolution equation of the cavity bias

$$\widehat{h}_{g-1} = \frac{1}{\beta} \tanh^{-1} \Big(\tanh(\beta J_g) \tanh(\beta(\widehat{h}_g + r_g)) \Big)$$

$$\rightarrow \begin{cases} \mathrm{sgn}\left(J_g(\widehat{h}_g + r_g)\right) & (\ |\widehat{h}_g + r_g| \geq 1\ ) \\ J_g(\widehat{h}_g + r_g) & (\ \text{otherwise}\ ) \end{cases} \quad (\ \beta \to \infty\ ), \tag{4.91}$$

where J_g denotes the coupling between nodes $g-1$ and g, and similarly for other cases.

To assess eq. (4.88), we take an average of the square of eq. (4.90) with respect to the modified distribution $P_n(\{J_{ij}\}, \{h_i\})$. Here, r_g can be regarded as a sample of a stationary distribution determined by the convergent solution of eq. (4.69) for the BL. As r_g is limited to being an integer and $|J_g| = 1$, eq. (4.91) gives

$$\left|\frac{\partial \widehat{h}_{g-1}}{\partial \widehat{h}_g}\right| = \begin{cases} 0 & (\ |\widehat{h}_g + r_g| > 1\ ) \\ 0 \text{ or } 1 & (\ |\widehat{h}_g + r_g| = 1\ ) \\ 1 & (\ \text{otherwise}\ ) \end{cases}, \tag{4.92}$$

where the value of 0 or 1 for the case of $|\widehat{h}_g + r_g| = 1$ is determined depending on the value of $\widehat{h}_g$. When $\widehat{h}_g$ eqauls 0 (and $|r_g| = 1$), the values 0 and 1 are chosen with equal probability 1/2 since the sign of the infinitesimal fluctuation of $\widehat{h}_g$, $\delta\widehat{h}_g$, is determined in an unbiased manner due to the mirror symmetry of the distribution of couplings. On the other hand, under the condition of $\prod_{k=g+1}^{G} \left|\partial\widehat{h}_{k-1}/\partial\widehat{h}_k\right| \neq 0$, the case of $|\widehat{h}_g| = 1$ (and $r_g = 0$) always yields $\left|\partial\widehat{h}_{g-1}/\partial\widehat{h}_g\right| = 1$. This is because $\widehat{h}_g\delta\widehat{h}_g < 0$ is guaranteed for $|\widehat{h}_g| = 1$ under this condition.

Equation (4.92) indicates that the assessment of eq. (4.90) is analogous to an analysis of a random-walk which is bounded by absorbing walls. We denote by $P_{(G\to 0)}$ the probability that $\left|\partial\widehat{h}_{g-1}/\partial\widehat{h}_g\right|$ never vanishes during the walk from G to 0 and the value of $\prod_{g=1}^{G} |\partial\widehat{h}_{g-1}/\partial\widehat{h}_g|$ is kept to unity. This indicates that

$$\left[\left(\frac{\partial \langle S_0\rangle}{\partial h_G}\right)^2\right]_n \propto P_{(G\to 0)} \tag{4.93}$$

holds. Summing all contributions up to the boundary of the BL yields the expression

$$\chi_{SG} \propto \sum_{G=0}^{L'} (k-1)^G (c-1)^G P_{(G\to 0)}. \tag{4.94}$$

The critical condition for convergence of eq. (4.94) in the limit $L' \to \infty$ is

$$\log\left((k-1)(c-1)\right) + \lim_{G\to\infty} \frac{1}{G} \log P_{(G\to 0)} = 0. \tag{4.95}$$

This serves as the "AT" condition in the current framework.

For a BL, eq. (4.95) can be assessed by analyzing the random walk problem of eq. (4.92), as shown in appendix B.4. We evaluated the critical y_{AT} values of eq. (4.95) for several pairs of (k, c), shown in Table 4.1 along with other critical values. These results show that the values of y_c, which signal the phase transitions of the boundary condition of the BL, agree with neither y_{AT} or y_s for $c = 3$ implying irrelevance of RZs of CTs to

(k,c)	y_{AT}	y_c	y_s
$(2,3)$	0.54397	none	0.41741
$(2,4)$	0.54931	$\log\sqrt{3} \approx 0.54931$	0.38926
$(3,3)$	1.51641	0.85545	∞
$(3,4)$	1.09861	-0.15082, $\log 3 \approx 1.09861$	1.41152

Table 4.1: Relevant values of y. Note that each kind of y is calculated using different models. The 1RSB transition point y_s is for RRGs and y_{AT} is for RRGs or BLs. The singularity of the cavity-field distribution y_c is common for all the models. Note that the value of y_{AT} in the case $(k,c) = (3,4)$ is the same as the one in [10].

the replica symmetry breaking, while for $c = 4$ the values y_{AT} and y_c agree each other. We consider that the correspondence for the $c = 4$ cases is accidental since the case $(k,c) = (2,3)$ offers strong evidence that the AT instability cannot be detected by the current RZs. This point may require more detailed discussions but we here leave it as a future work.

To investigate the irrelevance of RZs to the AT instability further, let us examine the singularities of RZs of a $(k,c) = (2,3)$ BL. The moment of the BL for finite generation L', $\Xi_{L'}(y)$, is easily derived from eqs. (4.70), (4.71) and (4.75), and the result is

$$\Xi_{L'}(y) = \Xi_0^{3\cdot 2^{L'-1}} \left(x^2 - \frac{1}{2}(x^2-1)(1-p_*)\right)^{3\cdot(2^{L'-1}-1)} \left(x^3 + \frac{3}{4}(1-x^2)(1-p_*)^2(1+p_*)\right), \tag{4.96}$$

where $\Xi_0 = p_* + x p_*^1 + x^2 p_*^2$ is the moment of a boundary spin, and the quantities p_*^1 and p_*^2 represent the probabilities that the convergent cavity field takes ± 1 and ± 2, respectively. The explicit forms of p_*^2 and p_*^1 are obtained from eq. (4.68)

$$(p_*^2, p_*^1) = \frac{2}{2-(1-p_*)^2(1-x^{-2})} \left(\left(\frac{1-p_*}{2}\right)^2, p_*(1-p_*)\right). \tag{4.97}$$

The RZs of the BL is easily derived as

$$\Xi_L(y) = 0 \Rightarrow y = \pm\frac{\pi}{2}i, \;\; 0.369207 \pm 1.02419i, \;\; 0.23664 \pm 1.80591i. \tag{4.98}$$

This result implies that RZs of BLs are also irrelevant to the FRSB, because there is no RZ on the real axis of y.

The irrelevance of RZs to the AT instability may be interpreted as follows. Remember the discussions given in section 2.6.1. We can link the spin-glass susceptibility to $\phi_N(n)$ by considering the modified generating function

$$N\widetilde{\phi}_N(n,m,\boldsymbol{F}) = \log\left[\left(\mathrm{Tr}\exp\left(-\beta\sum_{a=1}^{m} H(S^a) + \sum_{l=1}^{N} F_l \sum_{a<b} S_l^a S_l^b\right)\right)\left(\mathrm{Tr}\, e^{-\beta H}\right)^{n-m}\right]_n, \tag{4.99}$$

in which the interaction $\boldsymbol{F} = (F_1, F_2, \ldots, F_N)$ are introduced among m out of n replica systems. Analytically continuing eq. (4.99) to $n, m \in \mathbb{R}$ and expanding the obtained expression around $\boldsymbol{F} = 0$ for $m \simeq 1$ yield

$$N\widetilde{\phi}_N(\boldsymbol{F}; m, n) \approx N\phi_N(n) + \frac{m-1}{2} q \sum_i F_i + \frac{m-1}{2} \boldsymbol{F}^T \widehat{\chi}_{SG} \boldsymbol{F} + (\text{higher orders}), \quad (4.100)$$

where $\widehat{\chi}_{SG} = \left(\left[(\langle S_l S_k \rangle - \langle S_l \rangle \langle S_k \rangle)^2 \right]_n \right)$ represents the spin-glass susceptibility matrix. Equation (4.100) implies that the divergence of the spin-glass susceptibility is linked to analytical singularities of $\lim_{N\to\infty} \widetilde{\phi}_N(n, m, \boldsymbol{F})$ for $m \neq 1$. However, for $m = 1$, which corresponds to $\phi_N(n)$ examined in this chapter, it is difficult to detect the singularity because the factor $m-1$ with $\boldsymbol{F}^T \widehat{\chi}_{SG} \boldsymbol{F}$ makes the divergence of the spin-glass susceptibility irrelevant to the analyticity breaking of $\phi(n) = \lim_{N\to\infty} \phi_N(n)$. This explains the irrelevance of the RZs to the AT instability in the current framework. Considering systems of $m \neq 1$ may enable us to detect the AT instability by the RZs formula, but such an investigation is beyond the current purpose and we leave it as a future work.

4.4.4 Physical implications of the obtained solutions

We concluded that bifurcations of the fixed point solutions of the cavity-field equation correspond to phase transitions of the boundary condition of a BL and are not relevant to either 1RSB or FRSB. Before closing this section, we discuss the physical implications of the obtained solutions.

A naive consideration finds that the solution of $p_{\infty;0} = p_* = 1$ corresponds to a paramagnetic phase implying that any cavity fields vanish and therefore all spin configurations are equally generated. Note that this phase is of the ground states in the limit $\beta \to \infty$ and is different from the usual temperature-induced phase.

For finite $p_* < 1$, relevant fractions of the spins can take any direction without energy cost because the cavity field on the site is 0. This implies that the ground state energy is highly degenerate, which means that this solution describes a RS spin-glass phase. Actually, it is easy to confirm that the following equality holds:

$$q_{\mu\nu} = \frac{[\mathrm{Tr}\, S_g^\mu S_g^\nu e^{-\beta \sum_\mu H^\mu}]_{\boldsymbol{J}}}{[Z^n]_{\boldsymbol{J}}} = \mathrm{Tr}\, S_g^\mu S_g^\nu \rho_g(\boldsymbol{S}) = 1 - p_{g;0}. \quad (4.101)$$

Hence, the singularity of the cavity-field distribution in the limit $g \to \infty$ can be regarded as the transition of the spin-glass order-parameter. A finite jump of p_* for the $k = 3$ case is the first-order transition from the RS spin glass to paramagnetic phases, and such a transition is also observed in the mean-field models. The transitions from $p_* = 0$ to finite-p_* for the $c = 4$ case can be regarded as a saturation of q to $q_{EA} = 1$. We infer that these are the transitions from RS to RS phases. Notice that such a transition has not been observed for infinite-range models. Our results indicate that this $q = 1$ phase appears only when c is even. This means that such a phase is highly sensitive to the geometry of the objective lattice. This may be a reason why such a transition has not been observed in other models.

4.5 RZs for RRGs

In section 4.4.3, we have investigated the AT instability for BLs and RRGs and concluded that the instability cannot be detected by RZs of CTs and BLs. We have also inferred that the AT instability is difficult to observe in the systems without interactions among replicas. To examine this proposition, we present RZs for $c = 3$ RRGs in this section.

Constructing the RZ equation $[Z^n]_{\boldsymbol{J}} = 0$ for a RRG is a rather involved work because the average $[(\cdots)]_{\boldsymbol{J}}$ requires not only the calculations of configurations of $J_{ij} = \pm 1$ but also the geometrical structure of the graph. To overcome this difficulty, we fix a geometrical structure and only treat the configurations of the bond value $J_{ij} = \pm 1$ when constructing the RZ equation $[Z^n]_{\boldsymbol{J}} = 0$. This prescription is not faithful to the definition of the RRG but we can expect that gaps coming from the difference of the definitions vanish in the thermodynamic limit.

Actual procedures we performed for calculating the RZs of RRGs are rather simple:

1. Generate a $c = 3$ RRG with a size N.
2. Set a bond configuration $\boldsymbol{J}$ and calculate the ground-state energy by exploring all the spin configurations.
3. Continue the procedure 2 until all the bond configurations are completed and make the distribution of the ground-state energy $P(E_g)$.
4. Construct the RZ equation $\sum_{E_g} P(E_g) e^{-yE_g} = 0$ and solve it.
5. Generate other RRGs with the same size N and compare the results (actually we generate 16 samples for a size).

Clearly, these procedures require huge computational times, which makes it infeasible to calculate for $N > 16$.

Some typical behavior of RZs of RRGs for the sizes $N = 14$ and 16 are given in figs. 4.22 and 4.23, respectively. We can see that the RZs lie on the line $\mathrm{Im}(y) = i\pi/2$ for $N = 14$. Actually for $N \leq 14$, we could not find any samples which show RZs approaching to the real axis. For the $N = 16$ case, some sequences of the zeros exist apart from the line $\mathrm{Im}(y) = i\pi/2$. This result implies that RZs of RRGs approach the real axis as the system size grows, which may signal the AT instability of the RRGs. However, it is difficult to draw any distinct conclusion from figs. 4.22 and 4.23 because the system sizes are not sufficiently large. For further investigation, we need some other idea to overcome the computational difficulty of large systems, and leave this problem as a future work.

4.6 Summary

In this chapter, we have investigated RZs for CTs and ladders in the limit $T, n \to 0,\ \beta n \to y \sim O(1)$. Most of the zeros exist near the line $\mathrm{Im}(y) = \pi/2$ in all cases investigated;

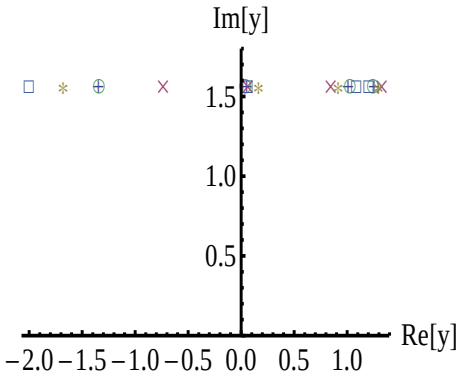

Figure 4.22: Plot of RZs for five samples of $c = 3$ RRG of the size $N = 14$. All of the RZs lie on the line $\mathrm{Im}(y) = i\pi/2$.

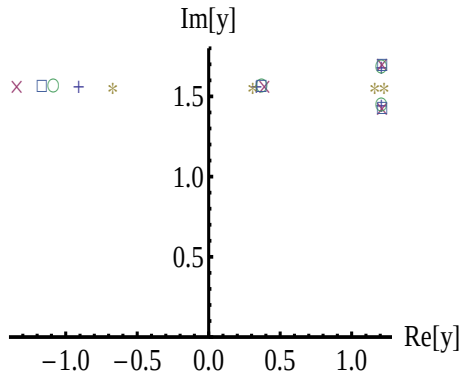

Figure 4.23: Plot of RZs for five samples of $c = 3$ RRG of the size $N = 16$. For some samples, some sequences of the zeros exist apart from the line $\mathrm{Im}(y) = i\pi/2$.

in particular, for the $(k, c) = (2, 3)$ CT and the width-2 ladder all the zeros lie on this line. For the width-2 ladder we have proved that the generating function is analytic with respect to y in this model. On the other hand, for some CTs, a relevant fraction of the RZs spreads away from the line $\mathrm{Im}(y) = \pi/2$ and approaches the real axis as the generation number L grows. This implies that $\phi(n)$ has a singularity at a finite real y in the thermodynamic limit. A naive observation finds that the RZs collision points correspond to phase transitions of the boundary condition of the BL. We have compared them with known critical conditions of the 1RSB and FRSB and concluded that these conditions are irrelevant to the behavior of RZs. This is consistent with the absence of RSB in CTs reported in some earlier studies [32–35].

The irrelevance of RZs to the 1RSB and FRSB has been considered in many aspects. By considering the boundary effect of CTs and BLs, we have concluded that the 1RSB cannot be observed by the current framework. On the other hand, the AT instability, the critical condition of the FRSB, has required some delicate discussions. We have inferred that the AT instability cannot be detected by the current formula without introducing the interaction among several replicas and the peculiarity of CTs and BLs is not essential. We have examined this statement by considering RZs of $c = 3$ RRG but any distinct conclusion could not be obtained because the system sizes are not sufficiently large, which is caused by the computational difficulty of the moment $[Z^n]_{\boldsymbol{J}}$ of RRGs. Overcoming this difficulty needs some more idea and is left as a future work. Another possible way to examine the statement is considering the replicated systems with interactions among replicas. This strategy seems to be more hopeful but here we leave this problem as a future work too.

Chapter 5

The replica symmetry breaking and the partition function zeros for Bethe lattice spin glasses

In the previous chapter, we have investigated replica zeros of Cayley trees and discussed the possible links to the RSB. Our conclusion is that the replica zeros of Cayley trees and Bethe lattices cannot detect any RSB. According to some discussions about the boundary condition of Bethe lattices we have clarified that the peculiarity of Cayley trees and Bethe lattices makes it difficult to identify the 1RSB transition by the replica zeros. On the other hand, the FRSB has required more delicate discussions and we have finally inferred that the replica zeros are essentially not able to detect the FRSB, not due to the peculiarity of Cayley trees and Bethe lattices. To examine this conclusion, we investigate the partition function zeros of Bethe lattices with respect to the external field H and temperature T in this chapter.

As mentioned in chapter 1, the spin-glass susceptibility is directly related to the non-linear susceptibility as eq. (1.5). This fact implies that singularities with respect to the external field H well signal the AT condition, which is expected to be the same as the divergence of the spin-glass susceptibility.

Utilizing the cavity method, we can accurately calculate the partition function zeros of Bethe lattices of infinite sizes. Our result implies that the FRSB is related to the continuous zeros of the partition function and can be detected in Bethe lattices despite the peculiarity, which supports our conclusion in the previous chapter. In addition, this result directly confirms a common belief that the AT instability leads to the continuous singular behavior of the system [83].

The results given in this chapter is in reference [84]. Note that most of numerical calculations in this chapter was done by Yoshiki Matsuda and he has the priority of those results. The zeros formulation given in section 5.2.1 was mainly investigated by Antonello Scardicchio and Markus Müller. The contributions of the author of this thesis to the results are mainly on investigating the formulation of the AT instability based on the divergence of the spin-glass susceptibility. Especially, the zero-temperature analysis of

the AT instability given in appendix C.1 was performed exclusively by the present author.

5.1 Phase boundaries and critical properties of Bethe lattice spin glasses

Before proceeding to the formulation of the partition function zeros, we first review some critical properties of Bethe lattice spin glasses in this section. When the external field H is absent, the critical conditions of Bethe lattice spin glasses are given by

$$(c-1)[\tanh(\beta J)]_{\boldsymbol{J}} = 1, \tag{5.1}$$

$$(c-1)[\tanh^2(\beta J)]_{\boldsymbol{J}} = 1. \tag{5.2}$$

The first relation gives the boundary between the paramagnetic and ferromagnetic phases, and the latter corresponds to the transition from the paramagnetic to spin-glass phases. We here derive these relations by using the cavity method. Taking the $n \to 0$ limit in eq. (4.50), we can find the equation of the cavity-field distribution (CFD) $P_i(h) = \lim_{n\to 0} \pi_i(h)$ as

$$P_i(h) = \int \prod_{j=1}^{c-1} (dh_j P_j(h_j)) \left[\delta \left(h - H - \sum_{j=1}^{c-1} \widehat{h}_j(J_{ij}, h_j) \right) \right]_{\boldsymbol{J}}. \tag{5.3}$$

If the external field H is absent, this equation always has the paramagnetic solution $P(h) = \delta(h)$. Instability of this paramagnetic solution signals phase transitions to other phases. To perform the stability analysis, we expand the relation (4.5) with respect to h_i and get

$$h_i = \sum_{j=1}^{c-1} t_{ij}(h_j - \frac{1}{3}(1-t_{ij}^2)h_j^3), \tag{5.4}$$

where $t_{ij} = \tanh(\beta J_{ij})$. Near the phase boundary, we can expect that the moments $\langle h^n \rangle$ decrease rapidly as n grows, which validates to ignore higher order terms. Here, we treat up to the third order. Taking powers of eq. (5.4) and averaging with respect to P_i which is denoted by the brackets $\langle \cdots \rangle$, we get

$$\langle h \rangle = (c-1)(2p-1) \left(\langle h \rangle - \frac{1}{3}(1-t^2) \langle h^3 \rangle \right), \tag{5.5}$$

$$\langle h^2 \rangle = (c-1)t^2 \langle h^2 \rangle + (c-1)(c-2)(2p-1)^2 t^2 \langle h \rangle^2, \tag{5.6}$$

$$\langle h^3 \rangle = (c-1)(2p-1)t^3 \left\{ \langle h^3 \rangle + 3(c-2) \langle h^2 \rangle \langle h \rangle + (c-2)(c-3)(2p-1)^2 \langle h \rangle^3 \right\}, \tag{5.7}$$

where we assume the $\pm J$ model

$$P(J_i) = p\delta(J_i - J) + (1-p)\delta(J_i + J), \tag{5.8}$$

and denote $t = \tanh(\beta J)$. To investigate the stability of the paramagnetic solution $\langle h \rangle = \langle h^2 \rangle = \langle h^3 \rangle = 0$, we linearize eqs. (5.5)–(5.7) to yield

$$\begin{pmatrix} \langle h \rangle \\ \langle h^2 \rangle \\ \langle h^3 \rangle \end{pmatrix} = \begin{pmatrix} (c-1)(2p-1)t & 0 & -\frac{1}{3}(c-1)(2p-1)t(1-t^2) \\ 0 & (c-1)t^2 & 0 \\ 0 & 0 & (c-1)(2p-1)t^3 \end{pmatrix} \begin{pmatrix} \langle h \rangle \\ \langle h^2 \rangle \\ \langle h^3 \rangle \end{pmatrix}. \tag{5.9}$$

This matrix has three eigenvalues $((c-1)(2p-1)t, (c-1)t^2, (c-1)(2p-1)t^3)$. It is quite straightforward to rewrite these eigenvalues for general distribution $P(J)$, and the explicit form is $((c-1)[\tanh(\beta J)]_{\boldsymbol{J}}, (c-1)[\tanh^2(\beta J)]_{\boldsymbol{J}}, (c-1)[\tanh^3(\beta J)]_{\boldsymbol{J}})$. When an eigenvalue exceeds unity, the paramagnetic solution becomes unstable, which yields the critical conditions (5.1) and (5.2). In this chapter, we treat the $\pm J$ model with $J = 1$ on a $c = 3$ Bethe lattice, and here present the phase diagram in fig. 5.1. Symbols P, F, SG

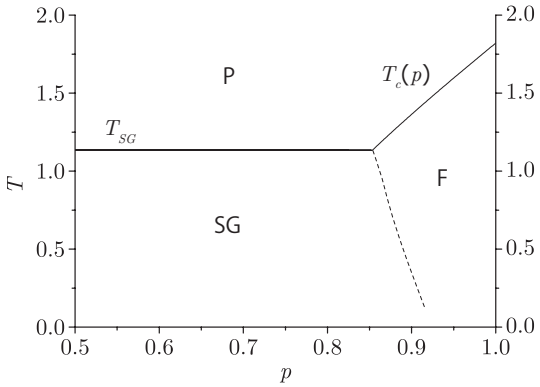

Figure 5.1: A T-p phase diagram of the $\pm J$ model without the external field on a $c = 3$ Bethe lattice. Symbols P, F, SG in the figure represent the paramagnetic, ferromagnetic, and spin-glass phases, respectively. The dashed line is the AT line. The boundary between the ferromagnetic and spin-glass phases is not determined. The critical temperature between the paramagnetic and spin-glass phases is given by $T_{SG} = 1/\tanh^{-1}\left[1/\sqrt{2}\right] \simeq 1.13$. The critical line $T = T_c(p)$ denotes the boundary between the paramagnetic and ferromagnetic phases.

in fig. 5.1 represent the paramagnetic, ferromagnetic, and spin-glass phases, respectively. The boundary between the ferromagnetic and spin-glass phases is not given in this figure because there is no known method to calculate this boundary. Although we did not discuss the AT condition so far, we provide the AT line as the dashed line in fig. 5.1. The detailed derivation of the AT line will be given in section 5.3.4.

From eqs. (5.5)–(5.7), we can also obtain the critical exponents. Near the phase boundary between the paramagnetic and ferromagnetic phases, we can define a small parameter ϵ by $(c-1)[\tanh \beta J]_{\boldsymbol{J}} = (c-1)(2p-1)t = 1 + \epsilon$. For $\epsilon < 0$, the paramagnetic solution is stable but for $\epsilon > 0$ it becomes unstable and the ferromagnetic solution emerges.

For the lowest order with respect to ϵ, we find the ferromagnetic solution as follows;

$$\langle h \rangle = \sqrt{3}\sqrt{\frac{(c-1)(1-(c-1)t^2)}{(c-2)\{c-3-t^2(c(c-7)+9)\}}}\epsilon^{1/2}, \tag{5.10a}$$

$$\left\langle h^2 \right\rangle = \frac{3}{c-3-t^2(c(c-7)+9)}\epsilon, \tag{5.10b}$$

$$\left\langle h^3 \right\rangle = \frac{3\sqrt{3}}{1-t^2}\sqrt{\frac{(c-1)(1-(c-1)t^2)}{(c-2)\{c-3-t^2(c(c-7)+9)\}}}\epsilon^{3/2}. \tag{5.10c}$$

Equations (5.10) indicate that the critical exponent β, which yields the temperature dependence of spontaneous magnetization $m \sim (T - T_c)^{\beta}$, equals to 1/2. Near the P-SG boundary, similar calculations are possible. In this case, we need the moments up to the fourth order. Assuming the absence of the ferromagnetic order $\langle h^1 \rangle = \langle h^3 \rangle = 0$, we get

$$\left\langle h^2 \right\rangle = (c-1)t^2(\left\langle h^2 \right\rangle - \frac{2}{3}(1-t^2)\left\langle h^4 \right\rangle), \tag{5.11a}$$

$$\left\langle h^4 \right\rangle = (c-1)t^4\left\langle h^4 \right\rangle + 3(c-1)(c-2)t^4\left\langle h^2 \right\rangle^2. \tag{5.11b}$$

Putting $(c-1)t^2 = 1+\epsilon$, we find the solution of eqs. (5.11) in powers of ϵ

$$\left\langle h^2 \right\rangle = \frac{c-1}{2(c-2)}\epsilon + \frac{(c-1)(2t^2-3)}{2(c-2)(1-t^2)}\epsilon^2 + O(\epsilon^3), \tag{5.12a}$$

$$\left\langle h^4 \right\rangle = \frac{3(c-1)}{4(c-2)(1-t^2)}\epsilon^2 + O(\epsilon^3). \tag{5.12b}$$

This implies that the spin-glass order parameter q is proportional to $\epsilon \propto T - T_{SG}$, which is known to be the same property as the SK model.

5.2 Formulations

Next, we present the formulation to yield the zeros of the partition function. The cavity method again plays a key role for this purpose. Antonello Scardicchio and Markus Müller mainly contributed to the derivation of the zeros formula given in section 5.2.1. Actual implementation of the formula was done by Yoshiki Matsuda and the author of this thesis.

5.2.1 The partition function zeros of Bethe lattices

Let us first consider the zeros of the partition function with respect to the uniform external field H, the Lee-Yang zeros [26]. The Lee-Yang zeros are known to be related to the magnetization of the system, and here we start from illustrating this point. In general, the partition function of an Ising system in the external field H is expressed as degree N polynomial with respect to $e^{-2\beta H}$ as

$$Z(H) = e^{N\beta H}\sum_{k=0}^{N}\Omega(k)\,e^{-2k\beta H} = \xi e^{N\beta H}\prod_{i}^{N}\left(e^{-2\beta H} - e^{-2\beta H_i}\right), \tag{5.13}$$

where N is the system size and $\Omega(k)$ is the partition function for a fixed magnetization $M = N - 2k = \sum_i S_i$. In the last equation, we factorize the polynomial and introduce the zeros $e^{-2\beta H_i}$. The leading factor ξ is an irrelevant constant and hereafter omitted. Taking the logarithm of eq. (5.13) and dividing by N, we get

$$\frac{1}{N}\log Z(H) = -\beta f(H) = \beta H + \iint d^2H' g_z(H') \log\left(e^{-2\beta H} - e^{-2\beta H'}\right). \tag{5.14}$$

where $g_z(H)$ is the density of zeros on the complex H plane. The magnetization $m(H) = -\partial f/\partial H$ is then expressed as

$$m(H) = 1 + \iint d^2H' g_z(H') \frac{2}{e^{2\beta(H-H')} - 1}. \tag{5.15}$$

Taking an infinitesimal closed line integral with respect to complex H, we can derive $g_z(H)$ from the magnetization as

$$g_z(H) = \frac{\beta}{2\pi i} \lim_{r\to 0} \frac{1}{\pi r^2} \oint_{|H-H'|=r} m(H')dH'. \tag{5.16}$$

This relation enables us to evaluate the density of zeros from the magnetization.

Next let us turn to discuss the properties of Bethe lattices. We have defined a Bethe lattice as an interior part of an infinitely large Cayley tree. This means that a Bethe lattice is statistically uniform and the typical magnetization is represented by the magnetization of the central spin, which is expressed by using the CFD of the central spin, $P^{(c)}(h^{(c)})$, as

$$m = \int d^2h^{(c)} P^{(c)}\left(h^{(c)}\right) \tanh\left(\beta h^{(c)}\right). \tag{5.17}$$

Note that the domain of integration is two-dimensional (as $d^2h^{(c)}$) because we are now treating the complex cavity field. The central CFD $P^{(c)}(h^{(c)})$ is derived from the convergent CFD $P(h) = \lim_{g\to\infty} P_g(h)$[1], where $P_g(h)$ denotes the CFD of the gth generation of a Cayley tree, as

$$P^{(c)}\left(h^{(c)}\right) = \int \left[\delta\left(h^{(c)} - H - \sum_{j=1}^{c} \widehat{h}_j\left(J_{ij}, h_j\right)\right) \prod_{j=1}^{c} P(h_j)\, d^2h_j\right]_{\boldsymbol{J}}. \tag{5.18}$$

Substituting eq. (5.17) to eq. (5.16), we obtain

$$\begin{aligned}
g_z(H) &= \frac{\beta}{2\pi i} \lim_{r\to 0} \frac{1}{\pi r^2} \oint_{|H-H'|=r} dH' \int d^2h^{(c)} P^{(c)}\left(h^{(c)}\right) \tanh\left(\beta h^{(c)}(H')\right) \\
&= \lim_{r\to 0} \frac{1}{\pi r^2} \int_{|H-H'|\le r} d^2H' \int d^2h^{(c)} P^{(c)}\left(h^{(c)}\right) \sum_{n\in\mathbb{N}} \delta\left(\beta h^{(c)}(H') - \frac{2n-1}{2}\pi i\right) \\
&= \lim_{r\to 0} \frac{1}{\pi r^2} \int_{|H-H'|\le r} d^2H' \sum_{n\in\mathbb{N}} P^{(c)}\left((2n-1)\pi i/2\beta\right) \\
&= \sum_{n\in\mathbb{N}} P^{(c)}\left((2n-1)\pi i/2\beta\right).
\end{aligned} \tag{5.19}$$

[1]The convergence of the CFD is shown rigorously in [32] for the real cavity-field case. Although this proof is not directly applicable to our case of complex cavity field, we numerically observed the convergence for $p < 1$ and hereafter assume it.

In the second line, we used the residue theorem under the condition that the radius r is sufficiently small. Equation (5.19) enables us to calculate the density of zeros from the central CFD $P^{(c)}(h^{(c)})$.

For a Bethe lattice, eq. (5.19) can also be interpreted as follows. Remember that the partition function of the whole system of a Bethe lattice is given by

$$Z = 2\cosh\left(\beta h^{(c)}\right)\prod_{j=1}^{c}\left(\frac{\cosh\left(\beta J_{ij}\right)}{\cosh\left(\beta\widehat{h}_j\right)}Z_j\right). \tag{5.20}$$

This implies that the equation of zeros $Z = 0$ becomes identical to[2]

$$2\cosh\left(\beta h^{(c)}\right) = 0 \Rightarrow \beta h^{(c)} = \frac{2n-1}{2}\pi i. \quad (\forall n \in \mathbb{N}). \tag{5.21}$$

Equations (5.19) and (5.21) provide a simple interpretation of the zeros of the Bethe lattice. That is the probability distribution that the partition function of a central spin becomes 0 is identical to the distribution of zeros of the whole Bethe lattice. This interpretation is useful for evaluating the density of zeros with respect to complex temperature. What we should do is to evaluate $P^{(c)}(h^{(c)})$ at the temperature $T = 1/\beta$ fixed on a complex value and to calculate $g_z(\beta)$ using the relation (5.19). This prescription is one of the advantages by considering Bethe lattices and constitutes the main result of this chapter.

5.2.2 Population method to evaluate the CFD

In the previous subsection, we have derived the relation to obtain the distribution of zeros from the central CFD $P^{(c)}(h)$. The next step is to actually calculate the CFD. A widely-used numerical method for this purpose is the "population method", the main idea of which is to represent the distribution by a population of N_{pop} cavity fields h_i. The actual procedure is as follows:

1. Set the initial population of N_{pop} cavity fields.
2. Choose $c-1$ fields randomly and compute a new field according to eqs. (4.4) and (4.5).
3. Replace a randomly chosen field with the new field.

These procedures define a Markov chain on the space of the N_{pop} fields. Usually, it is known that this chain has a stationary distribution and the stationary distribution satisfies the self-consistent equation of the convergent CFD $P(h)$ in the limit $N_{\text{pop}} \to \infty$ [30]. This population method is usually employed to evaluate the real CFD but we here apply this to the complex CFD case.

[2]Note that eq. (5.20) seems to diverge when the factor $\cosh\beta\widehat{h}_j$ becomes 0, but this is not the case. That is because the condition $\cosh\beta\widehat{h}_j = 0$ always involves $Z_j = 0$ and the factor $(\cosh\beta\widehat{h}_j)^{-1}Z_j$ yields a finite value.

We should here notice that there are two delicate points in applying the population method to complex $P(h)$.

One is related to the relevance of the boundary condition. Even in the real parameter case, the boundary condition is very important to correctly consider the spin-glass problem on Cayley trees and Bethe lattices, as discussed in the previous chapter. The selection of the boundary condition is directly related to the selection of the convergent CFD or the selection of the saddle-point of the corresponding regular random graph. Moreover for the complex parameter case, there is a possibility that other additional solutions of $P(h)$ appear depending on the boundary condition. To avoid confusions coming from such a situation, we choose the boundary condition by referring to an "adiabatic" criterion, which is based on an intuition that the physically relevant complex $P(h)$ should be smoothly continued to the real solution. This means that in principle the correct complex $P(h)$ is derived by gradually increasing the imaginary part of the parameter during the cavity update. As one of the simplest choices according to this adiabatic criterion, we choose the fixed boundary condition, which yields the initial cavity bias as $\widehat{h}_i = J_i$ where J_i is the bond between the outermost site i and its ascendant.

The other is the dimensionality of the zeros distribution g_z. Hereafter let us focus on the $\pm J$ model, the bond distribution of which is given by eq. (5.8). For the $p = 1$ ferromagnetic case, the Lee-Yang zeros are distributed only in a one-dimensional subspace of the complex field plane, which is also the case for the zeros with respect to the complex temperature [26,85]. On the other hand, for several spin-glass systems the zeros are known to two-dimensionally spread in the complex plane [63, 64, 86–91]. These facts imply that the existence region of the zeros gradually spread as the ferromagnetic bias p decreases and the zeros distribution g_z has its one and two-dimensional parts, g_{z1} and g_{z2}, respectively, in a certain range of p. The problem is the one-dimensional part is difficult to detect by the population method because we use the two-dimensionally distributed population. For the Lee-Yang zeros case, however, we can expect that g_{z1} takes non-zero values only on the imaginary axis, which enables us to calculate $g_{z1}(H = i\theta)$ from the the following relation[3] [85]

$$\mathrm{Re}\left(\lim_{H_r \to 0} m(H = H_r + i\theta)\right) = 2\pi g_{z1}(\theta). \tag{5.22}$$

In general, if the region where g_{z1} takes non-zero values is exactly known, the evaluation of g_{z1} is possible by using a similar relation to eq. (5.22). Unfortunately, however, the exact location of such region of g_{z1} is not known in general situations. In the remainder of this thesis, we calculate g_{z1} only on the imaginary axis of the external field $H = i\theta$, and ignore other possible region of g_{z1}.

[3]This relation is easily understood by regarding the relation (5.14) between the free energy and the zeros distribution is the same as the one between the electrostatic potential and the charge distribution in a two-dimensional space. In this context, the magnetization corresponds to the electric field, which has the discontinuous jump on the line density of the charge. This analogy leads to eq. (5.22).

5.2.3 Numerical procedures

In the previous subsections we present the conceptual explanation of the procedures to obtain g_z and the convergent CFD $P(h)$. However, the implementation of those procedures is also involved and we here summarize actual numerical procedures.

To this end, we first write down the update rule of the cavity bias $\widehat{h}_i$, which is more numerically tractable than the cavity field, as

$$\widehat{h}_i = \frac{1}{\beta}\tanh^{-1}\left(\tanh\left(\beta J_i\right)\tanh\left(\beta\left(H+\sum_{j=1}^{c-1}\widehat{h}_j\right)\right)\right), \tag{5.23}$$

where J_i is the bond between the site i and its ascendant. We hereafter assume that the function $\tanh^{-1}$ takes the principal branch, which restricts the value of the imaginary part of the bias to a range $[-\pi/\beta, \pi/\beta]$. The cavity bias distribution (CBD) for the gth generation $\widehat{P}_g(\widehat{h})$ is represented by a population and is updated by eq. (5.23) until $\widehat{P}_g(\widehat{h})$ converges.

After the convergence, the central CFD $P^{(c)}(h^{(c)})$ is calculated from the convergent CBD $\widehat{P}(\widehat{h}) = \lim_{g\to\infty}\widehat{P}_g(\widehat{h})$ as

$$P^{(c)}(h^{(c)}) = \int\prod_{j=1}^{c} d^2\widehat{h}_j\widehat{P}(\widehat{h}_j)\delta\left(h^{(c)} - H - \sum_{j=1}^{c}\widehat{h}_j\right). \tag{5.24}$$

and g_z is calculated from $P^{(c)}(h^{(c)})$ by using eqs. (5.19) and (5.22).

Before closing this subsection, we summarize the actual steps of the algorithm:

1. Generate the initial population $\left\{\widehat{h}_i\right\}_{i=1}^{N_{\rm pot}}$ as $\widehat{h}_i = J_i = \pm 1$ according to the distribution (5.8).
2. Update the population by the relation (5.23) until $\widehat{P}_g(\widehat{h})$ converges.
3. Calculate the central CFD $P^{(c)}(h^{(c)})$ by eq. (5.24).
4. Estimate the two-dimensional part of the zeros density g_{z2} by

$$g_{z2}(H,T) = \sum_{n\in\mathbb{N}} P^{(c)}\left(h^{(c)} = (2n-1)\pi i\right), \tag{5.25}$$

for a given H and T.

   (a) When the external field is pure imaginary $H = i\theta$, estimate $g_{z1}(H = i\theta, T)$ separately by

$$\begin{aligned} g_{z1}(H = i\theta, T) &= \frac{1}{2\pi}\mathrm{Re}\left(m(H = i\theta)\right) \\ &= \frac{1}{2\pi}\mathrm{Re}\left(\lim_{H_R\to 0}\int d^2h^{(c)}P^{(c)}\left(h^{(c)}\right)\tanh\left(h^{(c)}\right)\Big|_{H=i\theta+H_R}\right). \end{aligned} \tag{5.26}$$

In the remainder of this thesis, we assume the conditions $c = 3$ and $N_{\text{pop}} = 10^6$. We performed at least $5000N_{\text{pop}}$ cavity iterations until the population converged. After the convergence, we took the average of the objective quantities (g_{z2} and $m(H = i\theta)$) over additional $5000N_{\text{pop}}$ steps to avoid possible fluctuation due to the finiteness of the population.

5.3 Result

In this section, using the formula given above, we derive the distributions of the zeros of the presented model for several values of temperature T, external field H, and ferromagnetic bias p. The physical significance of the zeros distribution is discussed and the phase diagram of this model is re-derived in terms of the zeros. The relevance of the zeros distribution to the AT instability is also argued, which leads to a conclusion that the AT instability corresponds to the continuous distribution of zeros on the real axes of T and H.

5.3.1 Zeros on the complex field plane

First, we show the density of zeros on the complex field plane, the Lee-Yang zeros, for fixed real temperatures. For simplicity of calculations, we rescale the complex field H as $2\beta H$ when analyzing the Lee-Yang zeros hereafter. Figure 5.2 is the distributions of zeros on

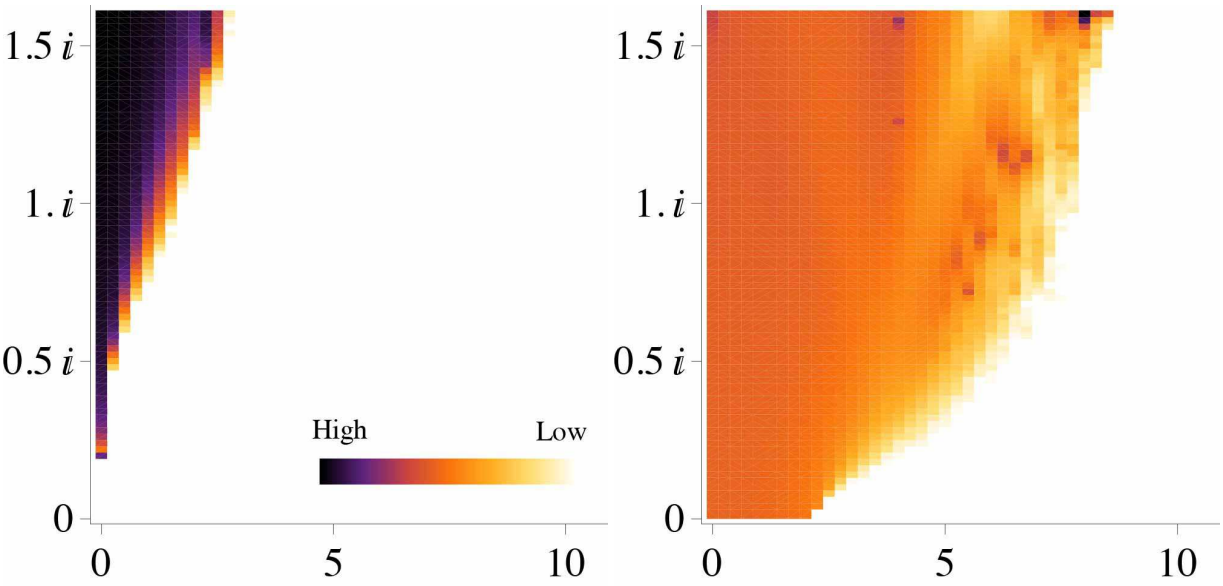

Figure 5.2: Distribution of zeros on the complex $2\beta H$ plane with $p = 0.5$ at $T = 1.43$ (left) and 0.5 (right). Densities are colored in logarithmic scale. Zeros with finite real part approach the real axis at low temperature, whereas g_{z1} is numerically zero.

the complex $2\beta H$ plane with $p = 0.5$ and $T = 1.43 > T_{SG} = 1/\tanh^{-1}\left(1/\sqrt{c-1}\right)$ (left) and $0.5 < T_{SG}$ (right). To draw this figure, we changed the value of $\mathrm{Re}(2\beta H)$ from 0 to 12 with the increment 0.25 and of $\mathrm{Im}\,(2\beta H)$ from 0.02 to $\pi/2$ with the increment of 0.02.

Each evaluated point locates at the center of each cell in fig. 5.2 and the corresponding value of g_z represents the value of the cell. The density out of the range is omitted, since the range is sufficient to see zeros near the real axis which are relevant to the critical phenomena. Both g_{z1} and g_{z2} are plotted in the same figure and colored in logarithmic scale; the black dots show a very high density.

The left panel of fig. 5.2 ($T = 1.43$) is for the paramagnetic phase. In both g_{z1} and g_{z2} parts, the zeros do not reach the real axis, which means there is no phase transition. On the other hand, the right panel of fig. 5.2 is in the spin-glass phase ($T = 0.5$) and the zeros reach the real axis at a certain value $0 < H_{SG} \in \mathbb{R}$. This means that there is a phase transition at $\mathrm{Re}(H) = H_{SG}$ in the Bethe lattice. Besides, below the critical field H_{SG}, zeros continuously touch the real axis, which indicates that the phase transitions continuously occur in the range of $|\mathrm{Re}(H)| < H_{SG}$. This behavior is quite different from usual phase transitions, and seems to be related to the chaos effect of a small change of field. The chaos effect is considered to be the result of the instability of randomly frozen spin configurations in the spin-glass phase and to be one of the characteristic properties of spin glasses. Note that the one-dimensional density $g_{z1}(H = i\theta)$ is numerically zero at all the range of θ in this $p = 1/2$ case, which implies the absence of singularities of the magnetization. This fact suggests that the Griffiths singularity [92], which is the essential singularity of the free energy with respect to the external field H at $H = 0$ and is considered to appear in some diluted ferromagnets and spin glasses, is absent in the current Bethe lattice spin glass without the ferromagnetic bias ($p = 1/2$).

As the ferromagnetic bias p increases, the ferromagnetic phase appears and the situation changes. Figure 5.3 is of the case $p = 0.9$. The right panel of fig. 5.3 is in the

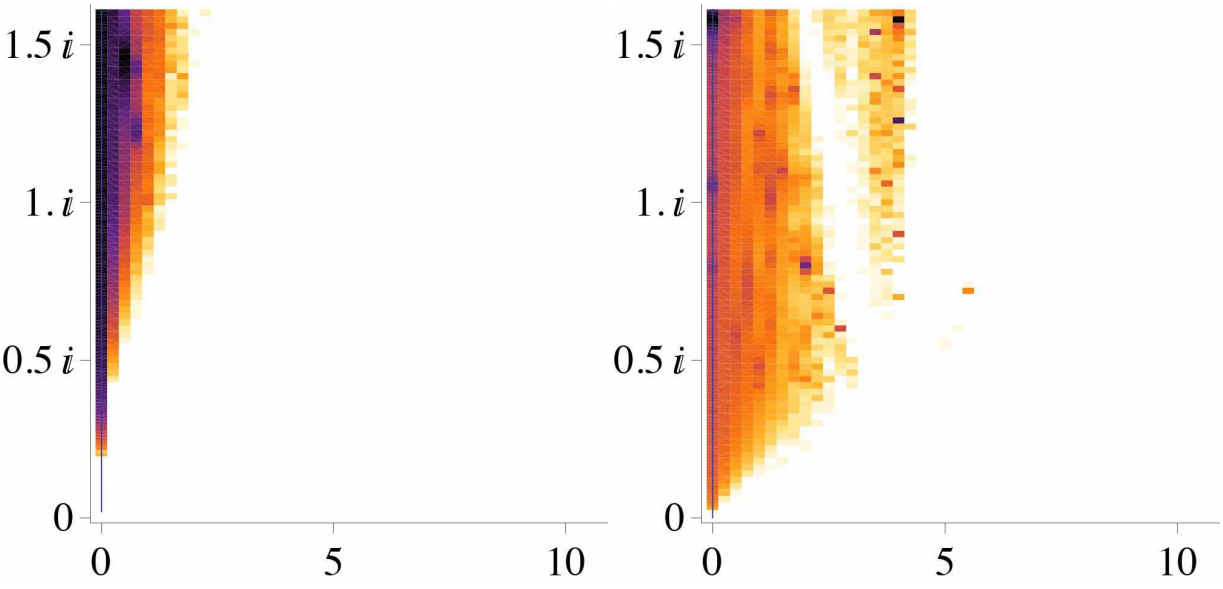

Figure 5.3: Distribution of zeros on the complex $2\beta H$ plane with $p = 0.9$ at $T = 1.5$ (left: para) and 0.5 (right: ferro). Only the one-dimensional part of the zeros on the imaginary axis (thin lines) approaches the origin at the low temperature.

ferromagnetic phase, in which g_{z2} does not reach the real axis but only g_{z1} touches the

origin. Besides, comparing to the left panel of fig. 5.2, we can find that g_{z1} has a finite value on the imaginary axis away from the origin. These observations indicate that the ferromagnetic ordering is characterized by g_{z1}, while g_{z2} signals the spin-glass ordering. According to this distinction of roles of g_{z1} and g_{z2}, we can draw the phase diagram of the current system and will present the result in section 5.3.3.

5.3.2 Zeros on the complex temperature plane

Assuming the temperature is complex, we can also obtain the density of zeros on the complex temperature plane at a fixed $H \in \mathbb{C}$.

Figure 5.4 shows the zeros on the temperature plane at $p = 0.5$ with $H = 0$ (left) and $H = 0.5$ (right). All the (two-dimensional) zeros below the spin-glass transition

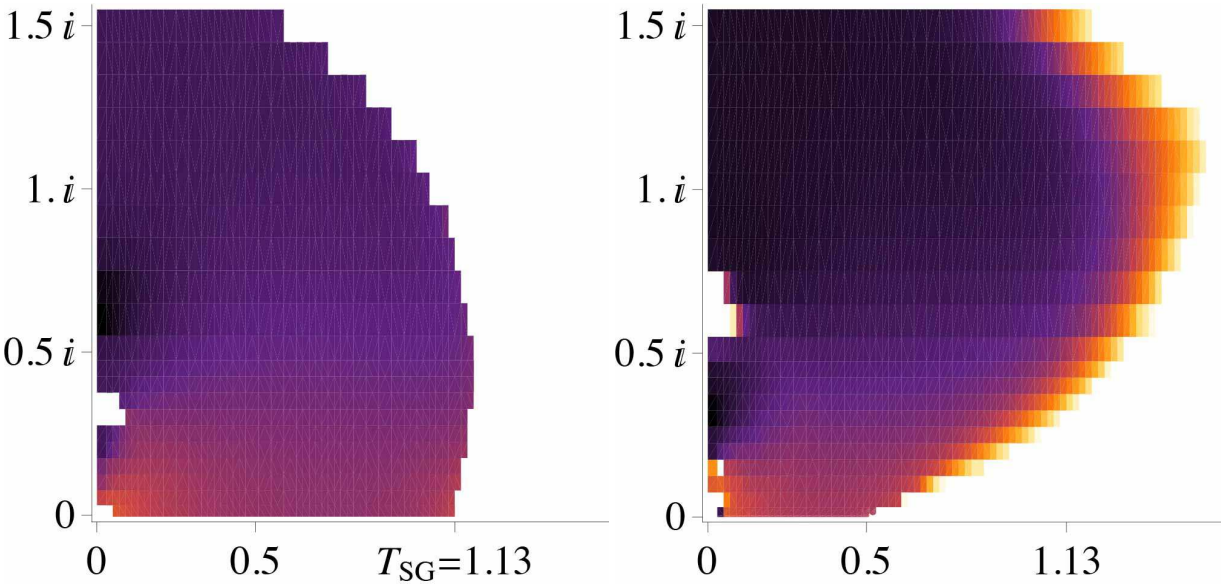

Figure 5.4: Distribution of zeros on the complex T plane with $p = 0.5$ and $H = 0$ (left) and $H = 0.5$ (right). Zeros reach the real axis below the critical temperature $T_{SG} \simeq 1.13$ (left) and 0.5 (right). The apparent absence of zeros near the origin may be due to numerical rounding errors of $\tanh \beta$.

temperature $T_{SG} \simeq 1.13$ also reach the real temperature axis. This result reconfirms that the spin-glass transition differs from usual phase transitions where zeros touch the real axis only at the transition temperature. The continuous singularities in the range of $\mathrm{Re}(T) \leq T_{SG}$ again implies the chaos effect against temperature deviation. The right panel of fig. 5.4 shows that the spin-glass phase is stable under a weak field ($H = 0.5$), which is in accordance with the Lee-Yang zeros result (the right panel of fig. 5.2).

The distributions at high p are also interesting. Figure 5.5 shows the density at $p = 0.9$ with $2\beta H = 0$ (left) and $2\beta H = 10^{-4}i$ (right). The critical temperature between the paramagnetic and ferromagnetic phases is known as $T_c \simeq 1.36$ at $p = 0.9$. We can find that the zeros protrude and tend to distribute in a sharp curve near this critical temperature T_c, which implies the existence of the one-dimensional part of the zeros density near T_c. As

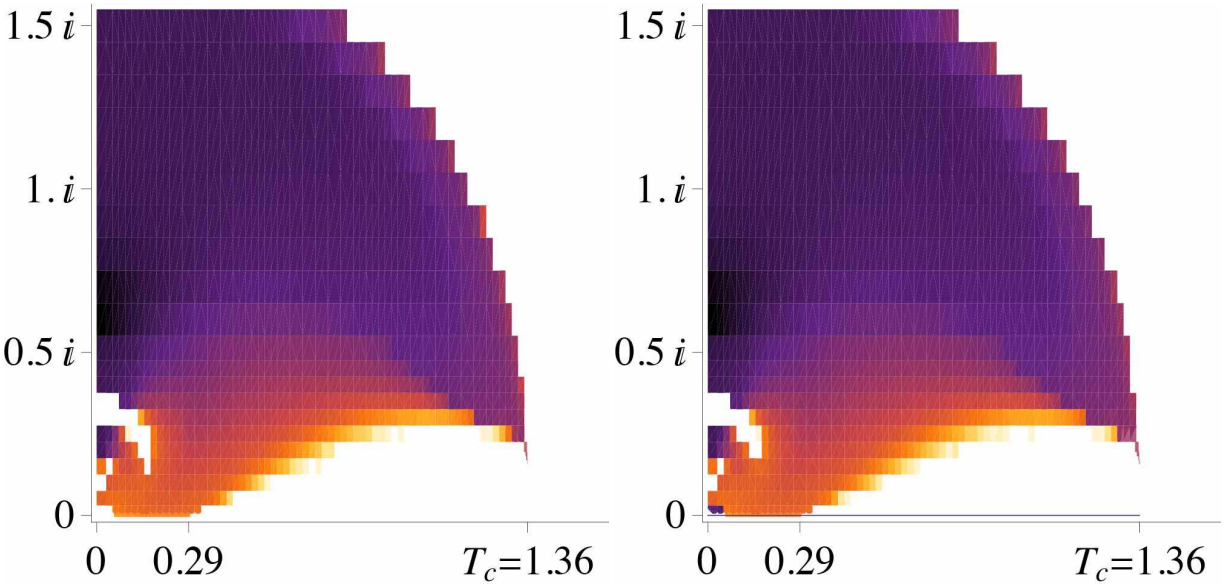

Figure 5.5: Distribution of zeros on the complex T plane with $p = 0.9$ and $2\beta H = 0$ (left) and $2\beta H = 10^{-4}i$ (right). The zeros tend to approach the real axis near $T = T_c$, where $T_c \simeq 1.36$ is the ferromagnetic critical temperature. It can be also observed that zeros reach the real axis at and below another lower critical temperature. This second critical temperature corresponds to the AT line as shown in fig. 5.6. The one-dimensional part of the zeros is revealed by introducing a small imaginary field and lies on the real axis in the right panel.

mentioned in section 5.2.2, however, we cannot directly detect this one-dimensional part by the current formalism using the two-dimensionally distributed population. Instead, we introduce a small pure imaginary field $2\beta H = 10^{-4}i$ and investigate g_{z1}, the result of which is in the right panel of fig. 5.5. This figure clearly shows the presence of a critical temperature near $\mathrm{Re}(T) \simeq 1.36$; zeros have finite densities on the real axis below $\mathrm{Re}(T) \simeq 1.36$, which reflects that $g_{z1}(H = i\theta, T)$ is finite for $\theta \simeq 0$ in the ferromagnetic phase. On the other hand, the two-dimensional part of the zeros distribution, g_{z2}, also touch the real axis at and below $\mathrm{Re}(T) \simeq 0.29$. This situation is the same as fig. 5.4 and indicates that the system is in the spin-glass phase in this region. As shown in later, this critical temperature quantitatively accords with the AT line, which we identify with the divergence point of the spin-glass susceptibility as the chapter 4. This fact strongly supports our speculation that the two-dimensional part of the zeros distribution, g_{z2}, dominates the spin-glass behavior of the system.

5.3.3 Phase diagram

The previous observations lead to an ansatz that two types of transitions are classified by one- and two-dimensional parts of the zeros distribution; the one-dimensional part g_{z1} detects the ferromagnetic phase transition and the two-dimensional part g_{z2} signals the emergence of the spin-glass ordering. According to this ansatz, we can plot the p-T phase

diagram and the result is given in fig. 5.6. Note that the T-H phase diagram is also drawn

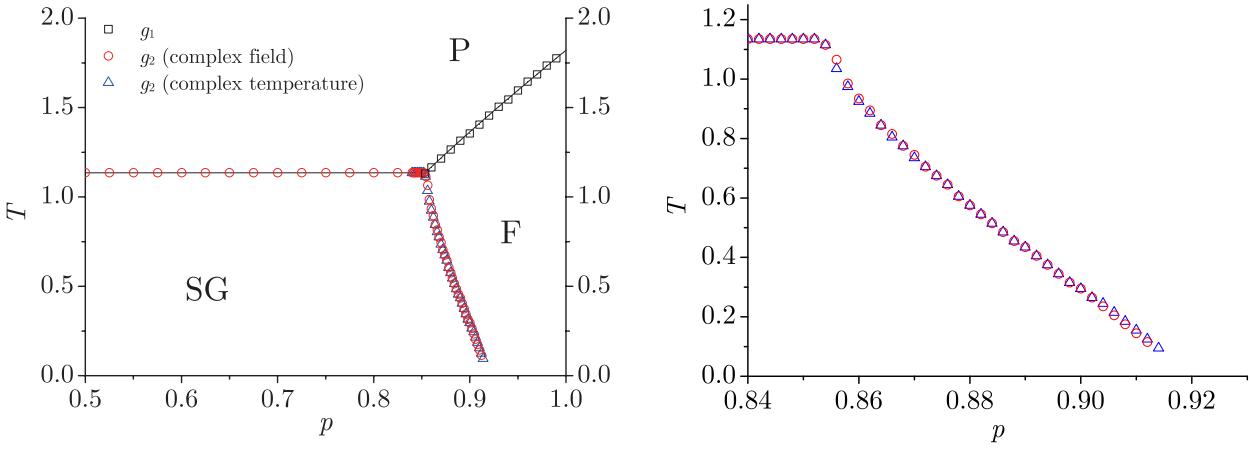

Figure 5.6: Phase diagrams on the p-T plane written by the density of zeros. The solid lines are analytically given as $T_c = 1/\tanh^{-1}\left[1/\left(4p-2\right)\right]$ (para and ferro) and $T_{SG} = 1/\tanh^{-1}\left[1/\sqrt{2}\right]$ (para and spin glass). Left: Circles and triangles are determined by two-dimensional density of zeros g_{z2} on the complex field and temperature planes, respectively, which corresponds to the AT line as shown in section 5.3.4. Squares are phase boundaries calculated by one-dimensional density of zeros g_{z1} indicating the ferromagnetic order. Note that our result does not immediately conclude the phase boundary between mixed and spin-glass phases. Right: Blow up of the critical temperatures derived from g_{z2} on the left panel.

by the same procedure. That diagram has also some interesting features but we here omit it because the p-T phase diagram is sufficient for the current purpose of examining the AT instability of the Bethe lattice spin glass.

The resulting phase boundaries in fig. 5.6 well agree with the analytical ones, $T_c = 1/\tanh^{-1}\left[1/\left(4p-2\right)\right]$ (para and ferro) and $T_{SG} = 1/\tanh^{-1}\left[1/\sqrt{2}\right]$ (para and spin glass). This fact supports our ansatz that g_{z1} and g_{z2} correspond to the ferromagnetic and spin-glass ordering, respectively. To examine the relation between g_{z2} and the AT instability further, in the next subsection we investigate the relation between the boundary obtained from g_{z2} in fig. 5.6 and the AT line, which we identify with the divergence of the spin-glass susceptibility.

5.3.4 The divergence of the spin-glass susceptibility

Let us remember the discussions in section 4.4.3 and develop a similar argument in the limit $n \to 0$. The spin-glass susceptibility is then given by

$$\chi_{SG} = \frac{1}{N}\sum_{i,j}\left[\left(\frac{\partial\left\langle S_i\right\rangle}{\partial h_j}\right)^2\right]_{\boldsymbol{J}} = \sum_{j}\left[\left(\frac{\partial\left\langle S_0\right\rangle}{\partial h_j}\right)^2\right]_{\boldsymbol{J}}, \tag{5.27}$$

Considering the fact that on a Bethe lattice an arbitrary pair of sites is connected by a single path and using the chain rule of the derivative operation, we can rewrite this quantity as

$$\chi_{SG} = \sum_{G=1}^{\infty} c(c-1)^{G-1} \left[\left(\frac{\partial \langle S_0 \rangle}{\partial h_G} \right)^2 \right]_{\boldsymbol{J}} \propto \sum_{G}^{\infty} (c-1)^G \left[\prod_{g=1}^{G} \left(\frac{\partial \widehat{h}_{g-1}}{\partial \widehat{h}_g} \right)^2 \right]_{\boldsymbol{J}}, \tag{5.28}$$

where the factor $c(c-1)^G$ denotes the number of sites of distance G from the central site 0. This yields the divergence condition of χ_{SG} as

$$\log(c-1) + \lim_{G\to\infty} \frac{1}{G} \log \left(\left[\prod_{g=1}^{G} \left(\frac{\partial \widehat{h}_{g-1}}{\partial \widehat{h}_g} \right)^2 \right]_{\boldsymbol{J}} \right) = 0. \tag{5.29}$$

In order to estimate the divergence points of the spin-glass susceptibility at finite temperatures, we numerically implement the calculation of the factor

$$\left[\prod_{g=1}^{G} \left(\frac{\partial \widehat{h}_{g-1}}{\partial \widehat{h}_g} \right)^2 \right]_{\boldsymbol{J}} = \left[\left(\frac{\partial \widehat{h}_0}{\partial \widehat{h}_G} \right)^2 \right]_{\boldsymbol{J}}. \tag{5.30}$$

A naive consideration that the derivative can be estimated by the difference coming from a small deviation yields

$$\frac{\partial \widehat{h}_0}{\partial \widehat{h}_G} \approx \frac{\widehat{h}_0 \left(\widehat{h}_G + \Delta \widehat{h}_G \right) - \widehat{h}_0 \left(\widehat{h}_G \right)}{\Delta \widehat{h}_G}. \tag{5.31}$$

The procedure to evaluate this equation is as follows. We arrange two replicas of an identical population $\{\widehat{h}_i\}_{i=1}^{N_{\rm pop}}$ expressing the convergent CBD $\widehat{P}(\widehat{h})$. In addition, we introduce a uniform perturbation ($\Delta \widehat{h}_G = 10^{-4}$) into only one of two replicas, and then observe the square average of the variation $(1/N_{\rm pop}) \sum_{i=1}^{N_{\rm pop}} (\widehat{h}_i(\widehat{h}_G + \Delta \widehat{h}_G) - \widehat{h}_i(\widehat{h}_G))^2$ after a certain number of the cavity updates.

In particular, we update two populations by $5000 N_{\rm pop}$ iterations with the same set of J_{ij}. A critical line of the divergence of the spin-glass susceptibility is determined whether the square average is numerically zero or much larger than the original perturbation. The result is shown in fig. 5.7 where the spin-glass susceptibility diverges below this line. This result well agrees with the phase boundary drawn by g_{z2} in fig. 5.6, which implies that the continuous distribution of g_{z2} on the real axis corresponds to the divergence of the spin-glass susceptibility. Combining the behavior of g_{z2} and the discussions about the divergence of the spin-glass susceptibility in section 2.6.1, we can expect that the current results reveal a physical aspect of the AT instability or the FRSB. Namely, the FRSB is related to the continuous singularities of the partition function, which is the common belief about the AT instability as mentioned in the beginning of this chapter. Consequently, we can reasonably conclude that the presented results leads to the AT instability of the

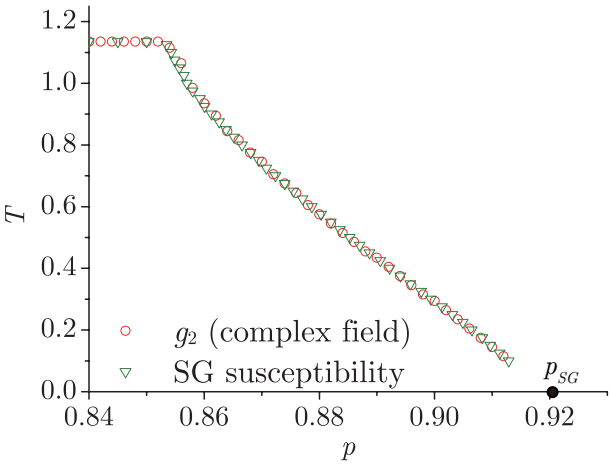

Figure 5.7: The divergence points of spin-glass susceptibility, which is denoted by the inverted triangles. The circles represent the phase boundary estimated by the two-dimensional distribution of zeros (fig. 5.6). They agree well each other. The critical value of the ferromagnetic bias $p_{SG} = 0.92067$ at zero temperature is indicated by the colored circle.

Bethe lattice spin glass as the continuous singularities of the partition function and meets the purpose of this chapter.

Note that at zero temperature, evaluating the condition (5.29) can be performed in a more analytical manner. The result gives the critical value of the ferromagnetic bias $p_{SG} = 0.92067$ which well agrees the estimated value by the finite-temperature results derived by both the zeros and spin-glass susceptibility analyses. The details of the zero temperature analysis are rather involved and presented in appendix C.1.

5.4 Summary

In this chapter, we founded the formulation to investigate the partition function zeros of Bethe lattices by utilizing the cavity method, for the purpose of investigating the AT instability of the Bethe lattice spin glasses. In the formulation, the cavity field distribution, which can be evaluated by using the population method, is directly linked to the density of zeros. This enables us to assess the zeros density in infinite-size Bethe lattices by using the cavity method.

Using this formulation, we investigated the $\pm J$ model on the coordination $c = 3$ Bethe lattice. The density of zeros consisted of two parts: One-dimensional and two-dimensional densities. We found that the two-dimensional density is related to the spin-glass ordering, while the one-dimensional part on the imaginary axis of the external field corresponds to the ferromagnetic transition. These observations were confirmed by comparison with the conventional critical conditions. The resultant p-T phase diagram was drawn by those two different ways, and the accordance between them is excellent.

Our result about the zeros indicates that the system is singular everywhere in the spin-glass phase. This observation and the relation between the AT instability and the divergence of the spin-glass susceptibility enable us to reasonably conclude that the continuous singularities reveals a physical aspect of the AT instability and the FRSB phase is present in the Bethe lattice spin glass, which meets the purpose of this chapter.

Throughout this thesis, we consider the 1RSB and FRSB transitions separately. A possible further work is to clarify the behavior of zeros of the systems with the 1RSB.

In the random energy model, it is known that the zeros touch the real axis at only the transition point [63, 91], which is in contrast to our result of the FRSB case. The current formalism can treat any RSB in the same framework and can be expected to give useful information about other types of the RSB. Investigation along this line is quite hopeful and is currently under way.

Chapter 6

Conclusion

In this thesis, the replica method was reviewed and examined from several viewpoints. The replica symmetry breaking (RSB) was the central concept about this issue and was investigated by several ways. The generating function of the partition function Z, $\phi(n) = (1/N)\log[Z^n]$ appearing in the replica method, played a key role in the investigation.

In chapter 2, we presented a review of the replica method in a form including recent descriptions of the method. The important concepts for this purpose are the probability distribution of the free energy and the pure states which are disjointed sets of configurations in the phase space. Two characteristic exponents, the complexity characterizing the number of pure states and the rate function characterizing a small probability of the free energy, are naturally embedded in the replica procedures. Practical calculations of those quantities were demonstrated on the fully-connected p-spin interacting model for several values of p. Especially, since the limit $p \to \infty$ makes the calculations easier, many aspects of the RSB in the one-step level (1RSB) were elucidated in this limit. As a result, we found that the transition to the 1RSB phase occurs due to the crisis of the complexity. This consequence was re-derived from the large deviations of the free energy, and it was revealed that the 1RSB is also signaled by the rate function of the probability distribution of the free energy. We also pointed out that the behavior of the rate function is closely related to the analytical properties of the generating function $\phi(n)$ and can be understood by some necessary conditions which should be satisfied by the correct $\phi(n)$.

On the other hand, another RSB, the full-step RSB (FRSB), is characterized by the de Almeida-Thouless (AT) condition which is the local stability condition of the replica symmetric (RS) saddle-point. We demonstrated this point for $p = 2$ and 3 cases. The relation between the AT instability and the divergence of the spin-glass susceptibility was also discussed. In addition, for $p = 3$, we pointed out that the dynamical 1RSB transition exists, which cannot be observed by the RS ansatz and require the 1RSB prescription with the complexity analysis. As a consequence of the above considerations, the phase diagrams for $p = 2, 3$ and ∞ on the T-βn plane were presented.

Besides, in the end of chapter 2, the microscopic description of the pure states were presented. To this end, the formulation by Thouless, Anderson and Palmer (TAP) was discussed and the equivalence with the replica result was shown; the characteristic ex-

ponent of the number of solutions of the TAP equation becomes identical to that of the complexity. We also showed that the solution of the TAP equation at zero temperature can be identified with the spin configurations stable against any single spin flip, which provides a simple interpretation of the pure state and is useful for identifying the pure states by numerical methods.

In chapter 3, we analyzed the Ising perceptron, which is a model of a neuron, by the replica method. To study the structure of the synaptic weight space, we intensively used the concept of the pure states and calculated the complexity in the 1RSB level. The complexity analysis revealed that the weight space consists of many clusters (pure states) for $\alpha \leq \alpha_s = 0.833...$ where $\alpha = M/N$ is the ratio of the number of the embedded patterns M to the system size N. Besides, it was shown that the weight space is equally dominated by a single large cluster of exponentially many weights and exponentially many small clusters of a single weight. This fact means that any information about the middle-size clusters cannot be obtained in the replica method due to the convex downward form of the cluster-size distribution. On the other hand, for $\alpha \geq \alpha_s$, we calculated the rate function to evaluate the small probability that a given set of random patterns is atypically separable by the Ising perceptron. The result showed that for $\alpha_s \leq \alpha \leq \alpha_{GD} = 1.245...$ the rate function takes the minimum for $n_s > 0$ and the system freezes out below n_s, which is a new type of frozen RSB phases and is not directly related the conventional 1RSB ones. For $n \geq n_{GD}$, it was shown that the analyticity of the rate function drastically changes, which implies that the dominant configuration of the atypically separable patterns exhibits a phase transition at this critical ratio. Extensive numerical experiments were also conducted and supported the above theoretical predictions.

In chapter 4, zeros of the nth moment of the partition function $[Z^n]$ were investigated to directly reveal the analyticity breaking of $\phi(n)$ in a vanishing temperature limit $\beta \to \infty$, $n \to 0$ keeping $y = \beta n \sim O(1)$ by combining the replica and cavity methods. In this limit, the moment parameterized by y characterizes the distribution of the ground-state energy. We numerically investigated the zeros for $\pm J$ Ising spin glass models defined on several Cayley trees and ladders. For several Cayley trees, we found that the zeros tend to approach the real axis of y in the thermodynamic limit, which implies that the moment cannot be described by a single analytic function of y as the system size tends to infinity. To explore the possible links of those analyticity breaking to the RSB, we examined the analytical properties of $\phi(n)$ and assessed the spin-glass susceptibility which can be identified with the AT instability. To this end we employed two relatives of Cayley trees, Bethe lattices and regular random graphs. The result revealed that the analyticity breaking indicated by the zeros of Cayley trees is relevant to neither the 1RSB and FRSB. We concluded that the peculiarity of Cayley trees and Bethe lattices makes the 1RSB not appear in those systems. On the other hand, the FRSB required some delicate discussions. According to the analysis of the modified generating function introduced interactions between replicas, we finally inferred that the AT instability cannot be detected by the current formula.

In chapter 5, to remove a possibility that the FRSB does not occur on Cayley trees

and Bethe lattices considered in chapter 4, we investigated the zeros of the partition function of the $\pm J$ model with respect to the external field H and temperature T on a Bethe lattice with the coordination number $c = 3$, by utilizing the cavity method. The result indicates that once the spin-glass phase emerges, the two-dimensional part of the zeros continuously tough the real axis, which means that the system is singular everywhere in the spin-glass phase. Combining this observation and the relation between the AT instability and the divergence of the spin-glass susceptibility, we could reasonably conclude that the continuous singularities of the partition function reveals a physical aspect of the AT instability and the FRSB phase is present in the Bethe lattice spin glass.

Main results of this thesis are summarized as follows:

1. Clarifying the behavior of the generating function when the complexity and rate function are not convex upward (chapter 3).

2. Comparing the analytical value of the rate function with the numerical one qualitatively and supporting the validity of the replica method (chapter 3).

3. Proposing a new method to investigate zeros of the moment $[Z^n]$ with respect to the replica number n and finding the analyticity breaking of $\phi(n)$ by using the zeros (chapter 4).

4. Clarifying the relation among Cayley trees, Bethe lattices, and regular random graphs in the context of the RSB (chapter 4).

5. Drawing a phase diagram of a Bethe lattice spin glass in terms of the partition function zeros and reasonably identifying the FRSB phase by the continuous singularities of the free energy (chapter 5).

Although the spin-glass theory has its long history, the essential comprehension of physics of spin glasses is still lacking. One of the main controversial points in the theory is whether the mean-field description is applicable to finite-dimensional systems or not. To obtain the solution to this problem, much effort have been made not only on directly studying finite-dimensional systems but also on improving the mean-field theory itself. The presented researches in this thesis can be regarded as one of such improvements in that our results provide some new aspects of the replica method being one of the central methods of the mean-field theory of spin glasses.

Besides, our results suggest further possibilities. Deeper understanding about pure states can provide some insights on several other problems, e.g. structural glasses, optimization problems and so on. The zeros formulations given in chapter 4 and 5 are in principle applicable to finite-dimensional systems, which can lead to further comprehension of finite-dimensional spin glasses. Also, our results of the Lee-Yang zeros in chapter 5 can provide a possibility of detecting the RSB in real experiments by observing the response of the system to the external field, like the Griffiths singularities [93].

In the light of the above possibilities, we have several hopeful future works.

Lessons from chapter 3 tell us that in other research fields there probably exist many other systems exhibiting extraordinary behavior of the generating function, complexity and rate function. This implies that investigation of such systems can reveal not only the properties of the systems but also the remaining mysteries of the replica theory. Researches along this line are already one of the rapidly-expanding mainstreams of the current spin-glass theory and will continue to develop at least for the near future.

The replica-zeros formulation in chapter 4 should be improved to be a more tractable form. In the current formulation, the replica zeros require huge computational time which prevents us from treating systems of large sizes. Moreover, we should clarify the relation between the replica zeros and the AT instability to investigate whether the AT instability occurs in finite-dimensional systems or not. The formulation of the inter-replicas interactions may be useful for this purpose and should be developed in the future.

The Lee-Yang zeros in chapter 5 may be most hopeful in clarifying the properties of real spin glasses, since they are directly related to the external field being controllable in real experiments. To give concise predictions for real experiments, we should obtain more detailed information about the distribution of the Lee-Yang zeros. The precise functional form of the distribution may enable to distinguish the RSB response from the normal one in the scaling form of the magnetization with respect to the external field. Obviously, we should find out the behavior of the zeros distribution in different types of RSB. Investigation of this point is a promising research and is currently underway.

It would be expected that the future direction of the spin-glass theory is classified broadly into two lines. One is the mathematical foundation of the mean-field theory in a more rigorous way. The other is the application of the spin-glass theory to a wide variety of different systems; real spin glasses, structural glasses, information processing tasks, and so on. The results presented in this thesis probably contribute to both of the two directions. This is because the mathematical structure of the replica method is closely related to both of the mathematics and physics of spin glasses. We hope that the reviews and results in this thesis become a basis to researches in such directions and inspire further study and understanding of spin glasses and beyond.

Appendix A

Calculations for chapter 3

A.1 Derivation of the RS saddle-point equations and the limit $q \to 1$.

Differentiation of eq. (3.18) with respect to q yields

$$\frac{\partial \phi}{\partial q} = -\frac{1}{2} n(n-1)\widehat{q} + \alpha \frac{\int Dz \frac{\partial}{\partial q} E_\beta^n \left(\sqrt{\frac{q}{1-q}} z \right)}{\int Dz E_\beta^n \left(\sqrt{\frac{q}{1-q}} z \right)} = 0. \tag{A.1}$$

The following integration requires some algebras

$$\int Dz \frac{\partial}{\partial q} E_\beta^n \left(\sqrt{\frac{q}{1-q}} z \right) = n \int Dz E_\beta^{n-1} \frac{\partial E_\beta}{\partial q}. \tag{A.2}$$

The differentiation of E_β with respect to q gives

$$\frac{\partial}{\partial q} E_\beta \left(\sqrt{\frac{q}{1-q}} z \right) = -\frac{1-e^{-\beta}}{2\sqrt{2\pi}(1-q)^2} \sqrt{\frac{1-q}{q}} z e^{-\frac{1}{2}\frac{q}{1-q} z^2} \tag{A.3}$$

Inserting this expression into eq. (A.2) and integrating by parts with respect to z give

$$\begin{aligned} \int Dz E_\beta^{n-1} z e^{-\frac{1}{2}\frac{q}{1-q} z^2} &= (1-q)(n-1) \int \frac{dz}{\sqrt{2\pi}} e^{-\frac{1}{2}\frac{1}{1-q} z^2} E_\beta^{n-2} \frac{\partial E_\beta}{\partial z} \\ &= (1-q)(n-1) \int \frac{dz}{\sqrt{2\pi}} e^{-\frac{1}{2}\frac{1}{1-q} z^2} E_\beta^{n-2} \frac{-(1-e^{-\beta})}{\sqrt{2\pi}} \sqrt{\frac{q}{1-q}} e^{-\frac{1}{2}\frac{q}{1-q} z^2}. \end{aligned} \tag{A.4}$$

Substituting this equation into eq. (A.1) and reducing some factors, we finally get the saddle-point equation (3.21). The other saddle-point equation (3.20) is also derived in a similar way.

Next we take the limit $q \to 1$ in eqs. (3.20-3.21). In this limit, the argument of E, $z\sqrt{q/1-q}$, diverges to ∞ or $-\infty$ depending on the sign of z and we need the asymptotic behavior of $E(x)$

$$E(x) \to \begin{cases} \frac{1}{\sqrt{2\pi}} \left(\frac{1}{x} - \frac{1}{2x^3} \right) e^{-\frac{1}{2}x^2} \to 0, & (x \to \infty) \\ 1, & (x \to -\infty) \end{cases}, \tag{A.5}$$

which leads to $E_\beta(x) \to e^{-\beta}$ for $x \to \infty$ and 1 for $x \to -\infty$. Hence, we can calculate the asymptotic behavior of $\widehat{q}$ as

$$\widehat{q} \to \frac{\alpha}{2\pi}\frac{(1-e^{-\beta})^2}{1-q}\frac{\int_{-\infty}^{0} Dze^{-\frac{1}{1-q}z^2} + \int_{0}^{\infty} Dze^{-\frac{1}{1-q}z^2}e^{-\beta n}}{\int_{-\infty}^{0} Dz + \int_{0}^{\infty} Dze^{-\beta n}}$$

$$= \frac{\alpha}{2\pi}\frac{(1-e^{-\beta})^2}{1-q}\frac{\sqrt{\frac{1-q}{1+q}}(1+e^{\beta n})/2}{(1+e^{\beta n})/2} \to \frac{\alpha}{4\pi}\frac{(1-e^{-\beta})^2}{\sqrt{1-q}} \to \infty. \tag{A.6}$$

This condition $\widehat{q} \to \infty$ enables us to calculate the following integration

$$\int Dz(2\cosh\sqrt{\widehat{q}}z)^n \to \int Dze^{n\sqrt{\widehat{q}}|z|} = \frac{2}{\sqrt{2\pi}}\int_0^\infty e^{-\frac{1}{2}z^2+n\sqrt{\widehat{q}}z} =$$

$$\frac{2}{\sqrt{2\pi}}\int_0^\infty dze^{-\frac{1}{2}\left(z-n\sqrt{\widehat{q}}\right)^2}e^{\frac{1}{2}n^2\widehat{q}} \to 2e^{\frac{1}{2}n^2\widehat{q}}. \tag{A.7}$$

Substituting these results into eq. (3.18), we obtain the RS2 solution (3.44).

A.2 Derivation of the AT condition

We consider small deviations of eq. (3.11) around the RS saddle points. We use the notation $q^{\mu\nu} = q + y^{\mu\nu}$, $\widehat{q}^{\mu\nu} = \widehat{q} + \widehat{y}^{\mu\nu}$ and expand eq. (3.11) with respect to the perturbations $y^{\mu\nu}$ and $\widehat{y}^{\mu\nu}$. The terms of first order of $y^{\mu\nu}$ and $\widehat{y}^{\mu\nu}$ becomes automatically 0 because we impose the saddle-point conditions with respect to q and $\widehat{q}$. Hence, the relevant terms in the first term of eq. (3.11) become

$$-\sum_{\mu<\nu} q^{\mu\nu}\widehat{q}^{\mu\nu} \approx -\sum_{\mu<\nu} y^{\mu\nu}\widehat{y}^{\mu\nu}. \tag{A.8}$$

Similarly, for the second term of eq. (3.11),

$$\log \operatorname*{Tr}_{\{S^\mu\}} e^{\sum_{\mu<\nu}\widehat{q}^{\mu\nu}S^\mu S^\nu} = \log \operatorname*{Tr}_{\{S^\mu\}} e^{\widehat{q}\sum_{\mu<\nu}S^\mu S^\nu + \sum_{\mu<\nu}\widehat{y}^{\mu\nu}S^\mu S^\nu}$$

$$\approx \sum_{\mu<\nu}\sum_{\delta<\omega}\widehat{y}^{\mu\nu}\widehat{y}^{\delta\omega}\left(\left\langle S^\mu S^\nu S^\delta S^\omega\right\rangle - \left\langle S^\mu S^\nu\right\rangle\left\langle S^\delta S^\omega\right\rangle\right), \tag{A.9}$$

where the brackets $\langle(\cdots)\rangle$ denote the following average

$$\langle(\cdots)\rangle = \frac{\mathrm{Tr}_{\{S^\mu\}}(\cdots)e^{\widehat{q}\sum_{\mu<\nu}S^\mu S^\nu}}{\mathrm{Tr}_{\{S^\mu\}}e^{\widehat{q}\sum_{\mu<\nu}S^\mu S^\nu}}. \tag{A.10}$$

To expand the third term of eq. (3.11), we need some more algebras. First, we write down the general form of the probability distribution of $[f(\boldsymbol{u})]_{\boldsymbol{u}}$

$$[f(\boldsymbol{u})]_{\boldsymbol{u}} = \sqrt{\frac{\det(Q^{-1})}{(2\pi)^N}}\int\left(\prod_{\mu=1}^{n}du^\mu\right)e^{-\frac{1}{2}\langle u|Q^{-1}|u\rangle}f(\boldsymbol{u}) \tag{A.11}$$

where $|u\rangle$ expresses the u vector whose μth component is u^μ and Q is the matrix whose elements are spin-glass order parameters

$$Q_{\mu\nu} = q^{\mu\nu}. \tag{A.12}$$

This distribution satisfies relations (3.8). We here employ the following identity

$$e^{-\frac{1}{2}\langle u|Q^{-1}|u\rangle} = \sqrt{\frac{\det Q}{(2\pi)^N}} \int \left(\prod_{\mu=1}^{n} dv^\mu\right) e^{-\frac{1}{2}\langle v|Q|v\rangle - i\langle v|u\rangle}. \tag{A.13}$$

Using these formulas, we get

$$\begin{aligned}
\log[f(\boldsymbol{u})]_{\boldsymbol{u}} &= \log \frac{1}{(2\pi)^N} \int \left(\prod_{\mu=1}^{n} du^\mu dv^\mu\right) e^{-\frac{1}{2}\langle v|Q|v\rangle - i\langle v|u\rangle} f(\boldsymbol{u}) \\
&= \log \frac{1}{(2\pi)^N} \int \left(\prod_{\mu=1}^{n} du^\mu dv^\mu\right) e^{-\frac{1}{2}\langle v|Q_{\rm RS}|v\rangle - \sum_{\mu<\nu} y^{\mu\nu} v^\mu v^\nu - i\langle v|u\rangle} f(\boldsymbol{u}) \\
&\approx \sum_{\mu<\nu} \sum_{\delta<\omega} y^{\mu\nu} y^{\delta\omega} \left([v^\mu v^\nu v^\delta v^\omega]_v - [v^\mu v^\nu]_v [v^\delta v^\omega]_v \right),
\end{aligned} \tag{A.14}$$

where the brackets $[(\cdots)]_v$ denote the following average

$$[(\cdots)]_v = \frac{\int \left(\prod_{\mu=1}^{n} du^\mu dv^\mu\right) (\cdots) e^{-\frac{1}{2}\langle v|Q_{\rm RS}|v\rangle - i\langle v|u\rangle} f(\boldsymbol{u})}{\int \left(\prod_{\mu=1}^{n} du^\mu dv^\mu\right) e^{-\frac{1}{2}\langle v|Q_{\rm RS}|v\rangle - i\langle v|u\rangle} f(\boldsymbol{u})}. \tag{A.15}$$

This average with respect to v can be transformed to the average with respect to u by using the integral by parts

$$\begin{aligned}
&\int \left(\prod_{\mu=1}^{n} du^\mu dv^\mu\right) v^\mu e^{-\frac{1}{2}\langle v|Q_{\rm RS}|v\rangle - i\langle v|u\rangle} f(\boldsymbol{u}) \\
&= \frac{1}{i} \int \left(\prod_{\mu=1}^{n} du^\mu dv^\mu\right) e^{-\frac{1}{2}\langle v|Q_{\rm RS}|v\rangle - i\langle v|u\rangle} \frac{\partial f(\boldsymbol{u})}{\partial u^\mu}.
\end{aligned} \tag{A.16}$$

Hence, we get

$$\begin{aligned}
&\sum_{\mu<\nu} \sum_{\delta<\omega} y^{\mu\nu} y^{\delta\omega} \left([v^\mu v^\nu v^\delta v^\omega]_v - [v^\mu v^\nu]_v [v^\delta v^\omega]_v \right) \\
&= \sum_{\mu<\nu} \sum_{\delta<\omega} \left(y^{\mu\nu} y^{\delta\omega} \frac{[\partial_{\mu\nu\delta\omega} f]_{\boldsymbol{u}}}{[f]_{\boldsymbol{u}}} - \frac{[\partial_{\mu\nu} f]_{\boldsymbol{u}}}{[f]_{\boldsymbol{u}}} \frac{[\partial_{\delta\omega} f]_{\boldsymbol{u}}}{[f]_{\boldsymbol{u}}} \right),
\end{aligned} \tag{A.17}$$

where the symbol $\partial_{x_1^{n_1}\cdots x_l^{n_l}}$ means

$$\partial_{x_1^{n_1}\cdots x_l^{n_l}} = \prod_{i=1}^{l} \frac{\partial^{n_i}}{\partial x_i^{n_i}} \tag{A.18}$$

and note that $[(\cdots)]_{\boldsymbol{u}}$ is the same average as defined in Sec. 3.2. Summarizing above results, we can derive the explicit form of the Hessian G around the RS ansatz

$$G = \sum_{\mu<\nu}\sum_{\delta<\omega}\Bigg(-\delta_{\mu\nu,\delta\omega}\widehat{y}^{\mu\nu}y^{\mu\nu} + \widehat{y}^{\mu\nu}\widehat{y}^{\delta\omega}\left(\left\langle S^\mu S^\nu S^\delta S^\omega\right\rangle - \left\langle S^\mu S^\nu\right\rangle\left\langle S^\delta S^\omega\right\rangle\right)$$
$$+\alpha y^{\mu\nu}y^{\delta\omega}\left(\frac{[\partial_{\mu\nu\delta\omega}f]_{\boldsymbol{u}}}{[f]_{\boldsymbol{u}}} - \frac{[\partial_{\mu\nu}f]_{\boldsymbol{u}}}{[f]_{\boldsymbol{u}}}\frac{[\partial_{\delta\omega}f]_{\{u^\mu\}}}{[f]_{\boldsymbol{u}}}\right)\Bigg) \tag{A.19}$$

Here we classify the elements of G by using the following notations

$$P = \alpha\left([\partial_{\mu^2\nu^2}f]_{\boldsymbol{u}}/[f]_{\boldsymbol{u}} - ([\partial_{\mu\nu}f]_{\boldsymbol{u}}/[f]_{\boldsymbol{u}})^2\right), \tag{A.20}$$
$$Q = \alpha\left([\partial_{\mu^2\nu\delta}f]_{\boldsymbol{u}}/[f]_{\boldsymbol{u}} - [\partial_{\mu\nu}f]_{\boldsymbol{u}}[\partial_{\mu\delta}f]_{\boldsymbol{u}}/[f]_{\boldsymbol{u}}^2\right), \tag{A.21}$$
$$R = \alpha\left([\partial_{\mu\nu\delta\omega}f]_{\boldsymbol{u}}/[f]_{\boldsymbol{u}} - [\partial_{\mu\nu}f]_{\boldsymbol{u}}[\partial_{\delta\omega}f]_{\boldsymbol{u}}/[f]_{\boldsymbol{u}}^2\right), \tag{A.22}$$
$$\widehat{P} = 1 - \left\langle S^\mu S^\nu\right\rangle^2 = 1 - q^2, \tag{A.23}$$
$$\widehat{Q} = \left\langle S^\mu S^\nu\right\rangle - \left\langle S^\mu S^\nu\right\rangle\left\langle S^\mu S^\delta\right\rangle = q - q^2, \tag{A.24}$$
$$\widehat{R} = \left\langle S^\mu S^\nu S^\delta S^\omega\right\rangle - \left\langle S^\mu S^\nu\right\rangle\left\langle S^\delta S^\omega\right\rangle = r - q^2, \tag{A.25}$$

where $r = \left\langle S^\mu S^\nu S^\delta S^\omega\right\rangle$. Using these notations, we can express the Hessian G as

$$G = \left(\begin{array}{ccc|ccc} P & Q\cdots Q & R\cdots R & & & \\ & \ddots & & & I & \\ Q\cdots Q & R\cdots R & P & & & \\ \hline & & & \widehat{P} & \widehat{Q}\cdots\widehat{Q} & \widehat{R}\cdots\widehat{R} \\ & I & & & \ddots & \\ & & & \widehat{Q}\cdots\widehat{Q} & \widehat{R}\cdots\widehat{R} & \widehat{P} \end{array}\right), \tag{A.26}$$

where I is the unit matrix of rank $n(n-1)/2$.

Let us find the eigenvectors of this matrix by a heuristic approach found by de Almeida and Thouless. The first eigenvector $\boldsymbol{s}_1$ is obtained by assuming $y^{\mu\nu} = a$ and $\widehat{y}^{\mu\nu} = \widehat{a}$ for any μ, ν . The upper half of the eigenvalue equation $G\boldsymbol{s}_1 = \lambda_1\boldsymbol{s}_1$ gives

$$\left(P + 2(n-2)Q + \frac{1}{2}(n-2)(n-3)R\right)a + \widehat{a} = \lambda_1 a, \tag{A.27}$$

and the lower half yields

$$a + \left(\widehat{P} + 2(n-2)\widehat{Q} + \frac{1}{2}(n-2)(n-3)\widehat{R}\right)\widehat{a} = \lambda_1\widehat{a}. \tag{A.28}$$

These equations have the eigenvalue λ_1 with non-vanishing $a, \widehat{a}$, which must satisfies the following relation

$$\lambda_1^2 - (X_1 + \widehat{X}_1)\lambda_1 + (X_1\widehat{X}_1 - 1) = 0, \tag{A.29}$$

where $X_1 = P + 2(n-2)Q + (n-2)(n-3)R/2$ and $\widehat{X}_1 = \widehat{P} + 2(n-2)\widehat{Q} + (n-2)(n-3)\widehat{R}/2$. This equation says that this mode constructs a two-dimensional space.

The next type of solution $\boldsymbol{s}_2$ is obtained by treating a replica θ as a special one. We assume $\theta = 1$ without loss of generality. This solution $\boldsymbol{s}_2$ has $y^{\mu\nu} = b$ and $\widehat{y}^{\mu\nu} = \widehat{b}$ when μ or ν is equal to 1, $y^{\mu\nu} = c$ and $\widehat{y}^{\mu\nu} = \widehat{c}$ otherwise. The first low of the eigenvalue equation $G\boldsymbol{s}_2 = \lambda_2 \boldsymbol{s}_2$ gives

$$(P + (n-2)Q)b + \left((n-2)Q\frac{1}{2}(n-2)(n-3)R\right)c + \widehat{b} = \lambda_2 b, \tag{A.30}$$

and the first low of the lower half yields

$$b + \left(\widehat{P} + (n-2)\widehat{Q}\right)\widehat{b} + \left((n-2)\widehat{Q} + \frac{1}{2}(n-2)(n-3)\widehat{R}\right)\widehat{c} = \lambda_2 \widehat{b}. \tag{A.31}$$

We here use the orthogonal condition of the solutions $\boldsymbol{s}_2$ and $\boldsymbol{s}_1$. We expect that the upper half of $\boldsymbol{s}_2$ is orthogonal with that of $\boldsymbol{s}_1$ independent of the lower half space. This leads to

$$(n-1)b + \frac{1}{2}(n-1)(n-2)c = 0, \tag{A.32}$$

and the same relation holds for $\widehat{b}$ and $\widehat{c}$. Substituting these conditions, we get

$$(P + (n-4)Q - (n-3)R)\, b + \widehat{b} = \lambda_2 b, \tag{A.33}$$

$$\left(\widehat{P} + (n-4)\widehat{Q} - (n-3)\widehat{R}\right)\widehat{b} + b = \lambda_2 \widehat{b}, \tag{A.34}$$

and with non-vanishing b and $\widehat{b}$, this leads to

$$\lambda_2^2 - (X_2 + \widehat{X}_2)\lambda_2 + (X_2\widehat{X}_2 - 1) = 0, \tag{A.35}$$

where $X_2 = P + (n-4)Q - (n-3)R$ and $\widehat{X}_2 = \widehat{P} + (n-4)\widehat{Q} - (n-3)\widehat{R}$. There are n possible choices of the special replica θ and there are two eigenvalues for the solutions $\boldsymbol{s}_1$ and $\boldsymbol{s}_2$, which means that $\boldsymbol{s}_1$ and $\boldsymbol{s}_2$ construct $2n$-dimensional space.

The third mode $\boldsymbol{s}_3$ is obtained by treating two replicas θ, ω as special ones. This solution $\boldsymbol{s}_3$ has $y^{\theta\omega} = d$ and $\widehat{y}^{\theta\omega} = \widehat{d}$, $y^{\theta\mu} = e$ and $\widehat{y}^{\omega\mu} = \widehat{e}$, and $y^{\mu\nu} = f$ and $\widehat{y}^{\mu\nu} = \widehat{f}$ otherwise. Following the similar argument to the case of $\boldsymbol{s}_2$, we obtain

$$\lambda_3^2 - (X_3 + \widehat{X}_3)\lambda_3 + (X_3\widehat{X}_3 - 1) = 0, \tag{A.36}$$

where $X_3 = P - 2Q + R$ and $\widehat{X}_2 = \widehat{P} - 2\widehat{Q} + \widehat{R}$. This solution constructs $n(n-3)$-dimensional space and all the eigenvalues are exhausted by these three modes.

For the stability of the saddle point, all of the eigenvalues must be non-negative. This condition corresponds to

$$\forall i, \quad X_i\widehat{X}_i \leq 1. \tag{A.37}$$

Note that the desired condition is $X_i\widehat{X}_i \leq 1$ but not $X_i\widehat{X}_i \geq 1$. That is because $\widehat{q}^{\mu\nu}$ is originally pure imaginary variable, which means that $\delta q^{\mu\nu}\delta\widehat{q}^{\mu\nu}$ is associated with a factor i and $\delta\widehat{q}^{\mu\nu}\delta\widehat{q}^{\mu\nu}$ is with a factor -1. Hence, if we change the variable from $\widehat{q}^{\mu\nu}$ to $i\widehat{q}^{\mu\nu}$, the diagonal block of lower half of G yields a factor -1 and the off-diagonal part becomes iI, which leads to the positivity condition of the eigenvalues as eq. (A.37).

The most relevant mode is $\boldsymbol{s}_3$ and to check this condition we next calculate eqs. (A.20-A.25). The order parameter q is already given by eq. (3.20) and the quantity $\left\langle S^\mu S^\nu S^\omega S^\delta \right\rangle = r$ is calculated in a similar way to the derivation of eq. (3.20). The result is

$$r = \frac{\int Dz \cosh^n \sqrt{\widehat{q}} z \tanh^4 \sqrt{\widehat{q}} z}{\cosh^n \sqrt{\widehat{q}} z}. \tag{A.38}$$

The factor $P - 2Q + R$ requires to assess $[\partial_\theta f]_{\boldsymbol{u}}$. This factor is calculated as

$$\begin{aligned}
[\partial_\theta f]_{\boldsymbol{u}} &= \int Dz \int \prod_{\mu=1}^{n} Dx^\mu \frac{\partial}{\partial u^\theta} f(\boldsymbol{u}) \\
&= \int Dz \prod_{\mu \neq \theta} \left(\int Dx^\mu f(u^\mu) \right) \left(\int Dx^\theta \frac{\partial}{\partial u^\theta} f(u^\theta = \sqrt{1-q} x^\theta + \sqrt{q} z) \right) \\
&= \int Dz \left(E_\beta \left(\sqrt{\frac{q}{1-q}} z \right) \right)^{n-1} \left(\frac{1}{\sqrt{q}} \frac{\partial}{\partial z} E_\beta \left(\sqrt{\frac{q}{1-q}} z \right) \right) \\
&= \frac{1}{\sqrt{1-q}} \int Dz E_\beta^n \left(\sqrt{\frac{q}{1-q}} z \right) \frac{E'_\beta \left(\sqrt{\frac{q}{1-q}} z \right)}{E_\beta \left(\sqrt{\frac{q}{1-q}} z \right)},
\end{aligned} \tag{A.39}$$

where we used the explicit form of the function $f(\boldsymbol{u}) = \exp(-\beta \sum_{\mu=1}^{n} \theta(u^\mu))$ and denoted $E'_\beta(x) = dE_\beta(x)/dx$. All the derivatives in the factor $P - 2Q + R$ can be similarly calculated. The result is

$$P - 2Q + R = \frac{\alpha}{(1-q)^2} \frac{\int Dz E_\beta^n \left(\frac{E''_\beta}{E_\beta} - \left(\frac{E'_\beta}{E_\beta} \right)^2 \right)^2}{\int Dz E_\beta^n}, \tag{A.40}$$

where we omit the argument $\sqrt{q/(1-q)} z$ of the functions E_β, E'_β and E''_β, and the explicit forms of E'_β and E''_β are

$$E'_\beta(x) = -\frac{1 - e^{-\beta}}{\sqrt{2\pi}} e^{-\frac{1}{2}x^2}, \;\; E''_\beta(x) \equiv \frac{d^2 E_\beta(x)}{dx^2} = \frac{1 - e^{-\beta}}{\sqrt{2\pi}} x e^{-\frac{1}{2}x^2}. \tag{A.41}$$

Finally we obtain the AT condition as

$$X_3 \widehat{X}_3 = \frac{\alpha}{(1-q)^2} \frac{\int Dz E_\beta^n \left(\frac{E''_\beta}{E_\beta} - \left(\frac{E'_\beta}{E_\beta} \right)^2 \right)^2}{\int Dz E_\beta^n} \frac{\int Dz \cosh^{n-4} \sqrt{\widehat{q}} z}{\int Dz \cosh^n \sqrt{\widehat{q}} z} \leq 1. \tag{A.42}$$

A.2.1 AT instability of the RS2 solution

The AT condition for the RS2 saddle point is calculated by taking the limits $q \to 1$ and $\widehat{q} \to \infty$. In the limit $\beta \to \infty$, the function $E_\beta(x)$ is reduced to the complementary error

function $E(x)$ defined in eq. (3.17), and we need to calculate the following integral to obtain the explicit form of the AT condition of the RS2 solution

$$\int Dz E^n \left(\frac{E''}{E} - \left(\frac{E'}{E} \right)^2 \right)^2 . \tag{A.43}$$

Remembering the argument of E in the AT condition is $\sqrt{q/(1-q)}z$ and using eq. (A.5), we find that for $z < 0$ the function E goes to 1 and the integrand of eq. (A.43) becomes

$$E^n \left(\frac{E''}{E} - \left(\frac{E'}{E} \right)^2 \right)^2 \to \left(\frac{1}{\sqrt{2\pi}} \sqrt{\frac{q}{1-q}} z e^{-\frac{1}{2}\frac{q}{1-q}z^2} - \frac{1}{2\pi} e^{-\frac{q}{1-q}z^2} \right)^2 , \tag{A.44}$$

This contribution vanishes in a rapid manner for any n. Meanwhile, for $z > 0$ eq. (A.43) becomes

$$4 \int_0^\infty Dz \left(\sqrt{\frac{1-q}{q}} \frac{1}{z} e^{-\frac{1}{2}\frac{q}{1-q}z^2} \right)^n , \tag{A.45}$$

which vanishes for $n > 0$ but a constant 2 remains if $n = 0$. Assuming $0 < n < 4$, we obtain the AT condition in this limit as

$$\frac{\alpha}{(1-q)^2} \frac{4 \int_0^\infty Dz \left(\sqrt{\frac{1-q}{q}} \frac{1}{z} e^{-\frac{1}{2}\frac{q}{1-q}z^2} \right)^n}{1/2} \frac{\sqrt{\frac{2}{\pi}} \frac{1}{(4-n)\sqrt{\widehat{q}}}}{2e^{\frac{1}{2}n^2\widehat{q}}} \leq 1. \tag{A.46}$$

Recalling eq. (A.6) indicating $\widehat{q} \propto 1/\sqrt{1-q}$, we can see that this condition is always satisfied for $n > 0$ but is violated on $n = 0$, which was already pointed out by Gardner [59].

Appendix B

Calculations for chapter 4

B.1 Derivation of the generating function $\phi(n)$ and free energy of regular random graphs

At first, we give the explicit form of the generating function $\phi(n)$ for the k-spin interacting regular random graph with coordination number c, since the derivation requires rather involved calculations. The generating function $\phi(n)$ is given by

$$\phi^{\mathrm{RRG}}(n) = \log[Z^n]_{\boldsymbol{J}}/N = \frac{c}{k}\log I_1 - c\log I_2 + \log I_3, \tag{B.1}$$

where

$$I_1 = \left[(2\cosh\beta J)^n \int \prod_{i=1}^{k}(dh_i\pi(h_i))\left(\frac{1+\tanh\beta J\prod_i^k\tanh\beta h_i}{2^{k+1}}\right)^n\right]_{\boldsymbol{J}}, \tag{B.2}$$

$$I_2 = \int d\widehat{h}dh\widehat{\pi}(\widehat{h})\pi(h)\left(\frac{1+\tanh\beta\widehat{h}\tanh\beta h}{4}\right)^n, \tag{B.3}$$

$$I_3 = \int \prod_{i=1}^{c}(d\widehat{h}_i\widehat{\pi}(\widehat{h}_i))\left(\frac{2\cosh\beta\sum_i^c\widehat{h}_i}{\prod_i^c 2\cosh\beta\widehat{h}_i}\right)^n. \tag{B.4}$$

The functions $\pi(h_i)$ and $\widehat{\pi}(\widehat{h}_i)$ are determined by the saddle-point conditions. The saddle point conditions for π and $\widehat{\pi}$ yield

$$\widehat{\pi}(\widehat{h}) = \int \prod_{i=1}^{k-1}(dh_i\pi(h_i))\left[\delta\left(\widehat{h} - \frac{1}{\beta}\tanh^{-1}(\tanh\beta J\prod_i^{k-1}\tanh\beta h_i)\right)\right]_{\boldsymbol{J}}, \tag{B.5}$$

$$\pi(h) \propto \int \prod_{i}^{c-1}(d\widehat{h}_i\widehat{\pi}(\widehat{h}_i))\delta\left(h - \sum_i^{c-1}\widehat{h}_i\right)\left(\frac{2\cosh\beta h}{\prod_i^{c-1}2\cosh\beta\widehat{h}_i}\right)^n. \tag{B.6}$$

These relations are identical to those of the cavity field h and bias $\widehat{h}$ of BLs. Substituting solutions of eqs. (B.5) and (B.6) to eq. (B.1), we obtain an explicit expression of $\phi(n)$.

Next, we turn to the derivation of eq. (B.1).

The first procedure is to calculate the number of possible configurations of a random graph. Let us define a_μ as a characteristic function which takes 1 when a coupling exists between a k-spin combination $\mu = \{l_1, l_2, \cdots, l_k\}$ and 0 otherwise. The number of possible graphs is expressed by using a_μ as

$$G = \sum_{\{a_\mu\}} \prod_{l=1}^{N} \delta \left(\sum_{a_{\mu_l}} a_{\mu_l} - c \right), \tag{B.7}$$

where $\mu_l = \{l, l_2, \cdots, l_k\}$. This can be transformed as

$$\begin{aligned} G &= \frac{1}{(2\pi i)^N} \oint \prod_{l=1}^{N} \left(\frac{1}{z_l} \right) \sum_{\{a_\mu\}} \prod_{l=1}^{N} z_l^{\sum_{\mu_l} a_{\mu_l} - c} \\ &= \frac{1}{(2\pi i)^N} \oint \prod_{l=1}^{N} \left(\frac{1}{z_l^{c+1}} \right) \exp \left(\sum_{\mu} \log \left(1 + z_{l_1} z_{l_2} \cdots z_{l_k} \right) \right), \end{aligned} \tag{B.8}$$

where we used an identity

$$\frac{1}{2\pi i} \oint dz \frac{1}{z} z^n = \delta_{n,0}, \tag{B.9}$$

for the first formula. We expand $\log \left(1 + z_{l_1} z_{l_2} \cdots z_{l_k} \right)$ and keep only the first-order term $z_{l_1} z_{l_2} \cdots z_{l_k}$ since higher-order terms correspond to multiple interactions for a combination μ. Hence,

$$G = \frac{1}{(2\pi i)^N} \oint \prod_{l=1}^{N} \left(\frac{1}{z_l^{c+1}} \right) \exp \left(\sum_{\mu} z_{l_1} z_{l_2} \cdots z_{l_k} \right). \tag{B.10}$$

We use an asymptotic formula $k! \sum_\mu z_{l_1} z_{l_2} \cdots z_{l_k} \approx (\sum_{l=1}^{N} z_l)^k$ for large N to introduce a variable $q = (\sum_{l=1}^{N} z_l)/N$. Expressing this constraint by a delta function and using the Fourier expression, we get

$$G \approx \frac{1}{(2\pi i)^N} \int dq d\widehat{q} \oint \prod_{l=1}^{N} \left(\frac{1}{z_l^{c+1}} \right) \exp \left(\widehat{q} \left(\sum_{l} z_l - Nq \right) + \frac{N^k}{k!} q^k \right). \tag{B.11}$$

The integration with respect to z_l can be performed and eq. (B.11) reads

$$G \approx \frac{1}{(2\pi i)^N} \int dq d\widehat{q} \exp \left(N \log \frac{\widehat{q}^c}{c!} - N\widehat{q}q + \frac{N^k}{k!} q^k \right). \tag{B.12}$$

The saddle-point method yields the asymptotic behavior of G as

$$\widehat{q} = \frac{N^{k-1}}{(k-1)!} q^{k-1}, \ q = \frac{c}{\widehat{q}}, \tag{B.13}$$

$$\frac{1}{N} \log G = \frac{c}{k} - c + c \log c + \frac{c}{k} \log \frac{N^{k-1}}{c(k-1)!} - \log c!. \tag{B.14}$$

Secondly, we calculate $[Z^n]_{\boldsymbol{J}}$. The expression using a_μ is given by

$$[Z^n]_{\boldsymbol{J}} = \frac{1}{G}\sum_{\{a_\mu\}}\prod_{l=1}^{N}\delta\left(\sum_{a_{\mu_l}} a_{\mu_l} - c\right)\operatorname*{Tr}_{\{\boldsymbol{S}\}}\left[\exp\left(\beta\sum_{\mu} a_\mu J_\mu \sum_{\alpha=1}^{n} S_{l_1}^\alpha S_{l_2}^\alpha \cdots S_{l_k}^\alpha\right)\right]_{\boldsymbol{J}}. \quad \text{(B.15)}$$

Using the same transformation as eqs. (B.7)-(B.10), we get

$$[Z^n]_{\boldsymbol{J}} = \frac{1}{G}\frac{1}{(2\pi i)^N}\oint\prod_{l}^{N}\left(dz_l\frac{1}{z_l^{c+1}}\right)\operatorname*{Tr}_{\{\boldsymbol{S}\}}\exp\left(\sum_{\mu} z_{l_1}z_{l_2}\cdots z_{l_k}\left[e^{\beta J_\mu\sum_\alpha S_{l_1}^\alpha S_{l_2}^\alpha\cdots S_{l_k}^\alpha}\right]_{\boldsymbol{J}}\right). \quad \text{(B.16)}$$

We introduce the following transformation

$$\left[e^{\beta J_\mu\sum_\alpha S_{l_1}^\alpha S_{l_2}^\alpha\cdots S_{l_k}^\alpha}\right]_{\boldsymbol{J}} = \operatorname*{Tr}_{\{\boldsymbol{\sigma}\}}\left[e^{\beta J_\mu\sum_\alpha \sigma_1^\alpha\sigma_2^\alpha\cdots\sigma_k^\alpha}\right]_{\boldsymbol{J}}\prod_{i=1}^{k}\delta_{(\boldsymbol{\sigma}_i,\boldsymbol{S}_{l_i})}, \quad \text{(B.17)}$$

where $\sigma = \pm 1$ denote the additional spin variable and $\delta(\boldsymbol{\sigma}_i, \boldsymbol{S}_{l_i})$ is the indicator function which takes 1 when the spin variables $\boldsymbol{\sigma}_i$ completely accord with $\boldsymbol{S}_{l_i}$ and 0 otherwise. This formula leads to

$$\sum_{\mu} z_{l_1}z_{l_2}\cdots z_{l_k}\left[e^{\beta J_\mu\sum_\alpha S_{l_1}^\alpha S_{l_2}^\alpha\cdots S_{l_k}^\alpha}\right]_{\boldsymbol{J}} = \operatorname*{Tr}_{\{\boldsymbol{\sigma}\}}\sum_{\mu}\prod_{i}^{k}\left(z_{l_i}\delta_{(\boldsymbol{\sigma}_i,\boldsymbol{S}_{l_i})}\right)\left[e^{\beta J_\mu\sum_\alpha \sigma_1^\alpha\sigma_2^\alpha\cdots\sigma_k^\alpha}\right]_{\boldsymbol{J}} \quad \text{(B.18)}$$

$$\approx \frac{N^k}{k!}\operatorname*{Tr}_{\{\boldsymbol{\sigma}\}}\prod_{i}^{k}\left(Q(\boldsymbol{\sigma}_i)\right)\left[e^{\beta J_\mu\sum_\alpha \sigma_1^\alpha\sigma_2^\alpha\cdots\sigma_k^\alpha}\right]_{\boldsymbol{J}}, \quad \text{(B.19)}$$

where

$$Q(\boldsymbol{\sigma}_i) = \frac{1}{N}\sum_{l} z_l\delta_{(\boldsymbol{\sigma}_i,\boldsymbol{S}_l)}. \quad \text{(B.20)}$$

For each configuration $\boldsymbol{\sigma}$, we impose the constraint (B.20) by a delta function and introduce its Fourier expression by employing the conjugate variable $\widehat{Q}(\boldsymbol{\sigma})$. The result is

$$\begin{aligned}[Z^n]_{\boldsymbol{J}} = \frac{1}{G}\frac{1}{(2\pi i)^2}\oint\prod_{l}^{N}\left(dz_l\frac{1}{z_l^{c+1}}\right)\operatorname*{Tr}_{\{\boldsymbol{S}\}}\int\prod_{\boldsymbol{\sigma}}\left(dQ(\boldsymbol{\sigma})d\widehat{Q}(\boldsymbol{\sigma})\right)\\ \times\exp\left\{\operatorname*{Tr}_{\boldsymbol{\sigma}}\widehat{Q}(\boldsymbol{\sigma})\left(\sum_l z_l\delta_{(\boldsymbol{\sigma},\boldsymbol{S}_l)} - NQ(\boldsymbol{\sigma})\right)\right.\\ \left.+\operatorname*{Tr}_{\{\boldsymbol{\sigma}\}}\frac{N^k}{k!}\prod_{i}^{k}(Q(\boldsymbol{\sigma}_i))\left[e^{\beta J_\mu\sum_\alpha \sigma_1^\alpha\sigma_2^\alpha\cdots\sigma_k^\alpha}\right]_{\boldsymbol{J}}\right\}, \quad \text{(B.21)}\end{aligned}$$

Performing spin trace with respect to $\boldsymbol{S}$ and integration with respect to z_l, we get

$$\begin{aligned}[Z^n]_{\boldsymbol{J}} = \frac{1}{G}\int\prod_{\boldsymbol{\sigma}}\left(dQ(\boldsymbol{\sigma})d\widehat{Q}(\boldsymbol{\sigma})\right)\\ \times\exp\left\{N\log\frac{\operatorname{Tr}_{\boldsymbol{\sigma}}\widehat{Q}(\boldsymbol{\sigma})}{c} - N\operatorname*{Tr}_{\boldsymbol{\sigma}}\widehat{Q}(\boldsymbol{\sigma})Q(\boldsymbol{\sigma}) + \operatorname*{Tr}_{\{\boldsymbol{\sigma}\}}\frac{N^k}{k!}\prod_{i}^{k}(Q(\boldsymbol{\sigma}_i))\left[e^{\beta J_\mu\sum_\alpha \sigma_1^\alpha\sigma_2^\alpha\cdots\sigma_k^\alpha}\right]_{\boldsymbol{J}}\right\} \quad \text{(B.22)}\end{aligned}$$

The saddle-point method is again useful to evaluate this equation. Under the RS ansatz of the saddle-point, Q and $\widehat{Q}$ are generally written in the form

$$Q(\boldsymbol{\sigma}) = q \int dh \pi(h) \prod_{\alpha}^{n} \left(\frac{1 + \tanh \beta h \sigma^{\alpha}}{2} \right), \tag{B.23}$$

$$\widehat{Q}(\boldsymbol{\sigma}) = \widehat{q} \int d\widehat{h} \widehat{\pi}(\widehat{h}) \prod_{\alpha}^{n} \left(\frac{1 + \tanh \beta \widehat{h} \sigma^{\alpha}}{2} \right). \tag{B.24}$$

Substituting these formulas to eq. (B.22), we can calculate all the terms in the argument of exponential. The result is

$$\operatorname*{Tr}_{\{\boldsymbol{\sigma}\}} \frac{N^k}{k!} \prod_{i}^{k} (Q(\boldsymbol{\sigma}_i)) \left[e^{\beta J_{\mu} \sum_{\alpha} \sigma_1^{\alpha} \sigma_2^{\alpha} \cdots \sigma_k^{\alpha}} \right]_{\boldsymbol{J}} = \frac{N^k}{k!} q^k I_1, \ \operatorname*{Tr}_{\{\boldsymbol{\sigma}\}} \widehat{Q}(\boldsymbol{S}) Q(\boldsymbol{S}) = q\widehat{q} I_2, \ \operatorname*{Tr}_{\{\boldsymbol{\sigma}\}} \widehat{Q}(\boldsymbol{S}) = \widehat{q}^c I_3, \tag{B.25}$$

where I_1-I_3 are defined in eqs. (B.2)-(B.4). Then, eq. (B.22) is rewritten as

$$\frac{1}{N} \log [Z^n]_{\boldsymbol{J}} = \operatorname{Extr} \left\{ \frac{N^{k-1}}{k!} q^k I_1 - q\widehat{q} I_2 + c \log \widehat{q} - \log c! + \log I_3 \right\} - \frac{1}{N} \log G. \tag{B.26}$$

Taking the saddle-point conditions with respect to q and $\widehat{q}$, we get

$$\widehat{q} q I_2 = c = \frac{N^{k-1}}{(k-1)!} q^k I_1, \ \ \widehat{q} = \frac{c}{q I_2} = \frac{c}{I_2} \left(\frac{I_1 N^{k-1}}{c(k-1)!} \right)^{1/k}, \tag{B.27}$$

Substituting these conditions and eq. (B.14) into eq. (B.26), we find that irrelevant constants are canceled out and obtain eq. (B.1).

The free energy is easily obtained from eq. (B.1)

$$\left. \frac{\partial \phi^{\mathrm{RRG}}(n)}{\partial n} \right|_{n=0} = -\beta f^{\mathrm{RRG}} = \frac{c}{k} I_1' - c I_2' + I_3', \tag{B.28}$$

where

$$I_1' = \int \prod_{i=1}^{k} (dh_i \pi(h_i)) \log \left(2 \cosh \beta J \frac{1 + \tanh \beta J \prod_i^k \tanh \beta h_i}{2^{k+1}} \right), \tag{B.29}$$

$$I_2' = \int d\widehat{h} dh \widehat{\pi}(\widehat{h}) \pi(h) \log \left(\frac{1 + \tanh \beta \widehat{h} \tanh \beta h}{4} \right), \tag{B.30}$$

$$I_3' = \int \prod_{i=1}^{c} (d\widehat{h}_i \widehat{\pi}(\widehat{h}_i)) \log \left(\frac{2 \cosh \beta \sum_i^c \widehat{h}_i}{\prod_i^c 2 \cosh \beta \widehat{h}_i} \right). \tag{B.31}$$

These distributions $\pi(h)$ and $\widehat{\pi}(\widehat{h})$ satisfy eqs. (B.5) and (B.6) in $n = 0$. Note that the first term in eq. (B.28) corresponds to the bond contribution (4.15) and the second and third terms are the site contribution (4.16), which shows the correspondence between the free energy of an RRG f^{RRG} and that of internal part of a BL f_{I} in eq. (4.18). Although the second and third terms in eq. (B.28) take different mathematical expressions, the saddle-point conditions with respect to $\pi(h)$ and $\widehat{\pi}(\widehat{h})$ guarantee the accordance of these terms.

B.2 Location of replica zeros of the width-2 ladder

We prove that all RZs of a $2 \times L$ ladder lie on the line $\mathrm{Im}(y) = \pi/2$ for any L. We introduce the notation

$$p_l(x) = p_{l;0} = \frac{n_l(x)}{d_l(x)}, \tag{B.32}$$

where d_l and n_l are polynomials of $x = e^y$ and $n_l(x)/d_l(x)$ is assumed to be irreducible. The outline of the proof is as follows. First we present the general solution of p_l and show that the denominator d_l has $2F((l+1)/2)$ roots which are all purely imaginary. The function $F(l)$ is the floor function, which is defined to return the maximum integer i in the range $i \leq l$. Also, we show that the number of nontrivial solutions of $\Xi_l = 0$ is equal to $2F((l+1)/2)$ and Ξ_l can be factorized as $C_l(x)d_l(x)$, where $C_l(x)$ is a polynomial of x. From the correspondence of the numbers of the roots, we conclude that all the zeros of Ξ_l are equivalent to the roots of $d_l(x)$ and $C_l(x)$ takes the form ax^b.

The iteration for p_l (4.64) has a solvable form and its general solution is given by

$$p_l = \frac{2(4^l - h(x)^l)}{4^l(2 + x^2 - x\sqrt{x^2+8}) - (2 + x^2 + x\sqrt{x^2+8})h(x)^l}, \tag{B.33}$$

where

$$h(x) \equiv -4 - x(x + \sqrt{x^2+8}) = 4\frac{x + \sqrt{x^2+8}}{x - \sqrt{x^2+8}}. \tag{B.34}$$

The roots of the numerator in eq. (B.33) can be easily calculated as

$$x = \begin{cases} \pm 2\sqrt{2}i & (l = 2m+1) \\ 0, \pm 2\sqrt{2}i & (l = 2m) \end{cases}, \tag{B.35}$$

where i denotes the imaginary unit and m is a natural number. Then, we concentrate on finding the roots of the denominator in eq. (B.33) except for those of the numerator (B.35). From numerical observations in sec. 4.3, we found that any of the roots x^*, which satisfy $\Xi_l(x^*) = 0$, are purely imaginary and bounded by $|x^*| \leq 2\sqrt{2}$. Hence, we assume these conditions and perform the variable transformation $z = -xi$. Equating the denominator of eq. (B.33) to 0, we get

$$\left(\frac{h(-iz)}{4}\right)^l = \left(\frac{\sqrt{8-z^2} + iz}{\sqrt{8-z^2} - iz}\right)^l = \frac{2 - z^2 - i\sqrt{8-z^2}}{2 - z^2 + i\sqrt{8-z^2}}. \tag{B.36}$$

We now enumerate the number of solutions under conditions that z is real and bounded as $-2\sqrt{2} \leq z \leq 2\sqrt{2}$. Under these conditions, we can transform eq. (B.36) into a simple form by using the polar representation. The result is

$$e^{i(2\theta_1 - \pi)l} = e^{i2\theta_2}, \tag{B.37}$$

where $\sqrt{8-z^2} + iz = r_1 e^{i\theta_1}$ $(-\pi < \theta_1 \leq \pi)$ and $r_2 e^{i\theta_2} = 2 - z^2 - i\sqrt{8-z^2}$ $(-\pi < \theta_2 \leq \pi)$. While z varies from $-2\sqrt{2}$ to $2\sqrt{2}$ continuously, the radius r_1 stays at a constant $2\sqrt{2}$ and

the argument θ_1 varies from $-\pi/2$ to $\pi/2$ in the positive direction. In the same situation, θ_2 changes from $+\pi$ to $-\pi$ in the negative direction. The radius r_2 is not constant, but is finite in this range. The variables θ_1 and θ_2 are obviously continuous and monotonic functions of z. Therefore, the argument of the left-hand side of eq. (B.37) starts from $\theta = 0$ and rotates with angle $2l\pi$ in the positive direction and the counterpart of the right-hand side varies from the same point $\theta = 0$ to -4π. This means that there are $l + 1$ values of z where the factor $(2\theta_1(z) - \pi)l$ becomes equal to $2\theta_2(z)$ except for trivial solutions $z = \pm 2\sqrt{2}$. When l is even, these solutions contain a trivial solution $z = 0$, which can also be confirmed from eq. (B.33). Hence, the number of nontrivial roots of d_l becomes $l + 1$ for odd l and l for even l, which is equivalent to $2F((l + 1)/2)$.

As already noted, the number of nontrivial solutions of $\Xi_l = 0$ is equal to $2F((l+1)/2)$. This can be understood by considering that the number of terms of $[Z^n]_{\boldsymbol{J}}$ is determined by the maximum number of defects n_d. In the $2 \times l$ ladder case, the value of n_d is given by $F((l + 1)/2)$ and the number of terms is $n_d + 1$. The highest degree of the relevant polynomials for RZs comes from the difference between the highest and lowest ground-state energies and is given by $2n_d = 2F((l + 1)/2)$, which yields the number of nontrivial solutions of $\Xi_l = 0$.

Finally, we prove that Ξ_l takes the form $A_l x^{b_l} d_l(x)$ by induction. From eqs. (4.64) and (4.63) with the initial conditions $p_{0;0} = 0,\ \Xi_0 = x$, we derive

$$p_1 = \frac{1}{x^2 + 1},\ \Xi_1 = \frac{1}{2}x^2(x^2 + 1), \tag{B.38}$$

which satisfies the desired form. Assuming that the condition $\Xi_l = Ax^{b_l} d_l(x)$ is true for $l = k$, we substitute this expression into eq. (4.63) to get

$$\begin{aligned}\Xi_{k+1} &= Ax^{b_k} d_k x^3 \left\{ \frac{n_k}{d_k} + \frac{1}{2}\left(1 + \frac{1}{x^2}\right)\left(1 - \frac{n_k}{d_k}\right)\right\} \\ &= \frac{1}{2}Ax^{b_k+1}\left\{(x^2 - 1)n_k + (1 + x^2)d_k\right\}. \end{aligned} \tag{B.39}$$

Equation (4.64) can be written as

$$p_{k+1} = \frac{d_k - n_k}{(x^2 - 1)n_k + (1 + x^2)d_k} = \frac{n_{k+1}}{d_{k+1}}, \tag{B.40}$$

which gives

$$(x^2 - 1)n_k + (1 + x^2)d_k = c_{k+1}(x)d_{k+1}(x), \tag{B.41}$$

where c_{k+1} is a polynomial and satisfies $c_{k+1} = (d_k - n_k)/n_{k+1}$. Substituting this relation, we can rewrite eq. (B.39) as

$$\Xi_{k+1} = \frac{1}{2}Ax^{b_k+1}c_{k+1}(x)d_{k+1}(x). \tag{B.42}$$

As we have already shown, the number of nontrivial zeros of Ξ_{k+1} is equal to that of d_{k+1}. This means that c_{k+1} cannot have nontrivial roots and hence c_{k+1} takes the form Ax^b. This completes the proof by induction and demonstrates our proposition that all RZs for the $2 \times L$ ladder have a constant imaginary part $i\pi/2$.

B.3 Rate function for a CT with $c = 3$

We here calculate the generating function $\phi_L(y)$ for finite L. Consider an L-generation branch of a $c = 3$ CT. An explicit form $\phi_L(y)$ is easily derived from eq. (4.70) as

$$\phi_L(x) = \frac{2^L}{2^{L+1}-1}\phi_0 + \frac{2^{L+1}}{2^{L+1}-1}(1-2^{-L})\log x + \frac{1}{4-2^{-L+1}}\sum_{i=0}^{L-1}\frac{\log f_i}{2^i}, \tag{B.43}$$

where $x = e^y$ and

$$\phi_0 = \log \Xi_0,\ \ f_i = f_i(x, p_{i;0}) = 1 - \frac{1}{2}(1-x^{-2})(1-p_{i;0})^2, \tag{B.44}$$

using the same notations as in section 4.2. The rate function with finite generations L is given by

$$\begin{aligned} R_L(x) = \frac{2^L}{2^{L+1}-1}\left(\phi_0 - x\log x\frac{d\phi_0}{dx}\right) \\ + \frac{1}{4-2^{-L+1}}\sum_{i=0}^{L-1}\frac{1}{2^i f_i}\left(f_i \log f_i - C_i(x) x \log x\right), \end{aligned} \tag{B.45}$$

where the factor $C_i(x)$ is given by

$$C_i(x) = \frac{\partial f_i}{\partial p_{i;0}}\frac{dp_{i;0}}{dx} + \frac{\partial f_i}{\partial x} = (1-x^{-2})(1-p_{i;0})\frac{dp_{i;0}}{dx} - x^3(1-p_{i;0})^2. \tag{B.46}$$

Let us denote $R_\infty(x) = \lim_{L\to\infty} R_L(x)$. Because the inequality $R_\infty \le 0$ always holds, the 1RSB transition does not occur as long as the condition $R_\infty(x) = R(x)$ is satisfied.

In the range $y \ge 0 \Leftrightarrow 1 \le x$, the factor f_i is bounded as $1/2 \le f_i \le 1$. This guarantees the uniform convergence of $\phi_L(x)$. The boundedness of $(dp_{i;0}/dx)$ can also be shown with some calculations. These conditions guarantee that $R_L(x)$ converges to a function R_∞ uniformly. Hence, from elementary calculus, the equality $R(x) = R_\infty(x)$ holds, which implies the absence of 1RSB. The same conclusion is more easily derived for a BL because f_i does not depend on i.

B.4 AT condition for the $(k, c) = (2, 3)$ Bethe lattice

We derive the AT condition for a BL. Especially, we explain the case $(k, c) = (2, 3)$ in detail. The extension to general (k, c) is somewhat involved but straightforward. To evaluate $P_{(G\to 0)}$, we construct the transition matrix of our random-walk problem. For a given $(\widehat{h}_g, \widehat{h}_{g+1})$, the posterior distribution of r_g is given as

$$p(r_g|\widehat{h}_g) = p(r_g, \widehat{h}_g)/p(\widehat{h}_g) \propto e^{y(|r_g+\widehat{h}_g|-|r_g|-|\widehat{h}_g|)}p(r_g), \tag{B.47}$$

where $p(r_g)$ is the prior distribution of r_g. This enables us to derive the concrete expression of $p(r_g|\widehat{h}_g)$, summarized in Table B.1. We can distinguish three states of the walker at the g-step as follows:

$r_g \setminus \widehat{h}_g$	1	0	-1
1	$\dfrac{1-p_b}{(1+p_b)+(1-p_b)e^{-2y}}$	$\dfrac{1-p_b}{2}$	$\dfrac{(1-p_b)e^{-2y}}{(1+p_b)+(1-p_b)e^{-2y}}$
0	$\dfrac{2p_b}{(1+p_b)+(1-p_b)e^{-2y}}$	p_b	$\dfrac{2p_b}{(1+p_b)+(1-p_b)e^{-2y}}$
-1	$\dfrac{(1-p_b)e^{-2y}}{(1+p_b)+(1-p_b)e^{-2y}}$	$\dfrac{1-p_b}{2}$	$\dfrac{1-p_b}{(1+p_b)+(1-p_b)e^{-2y}}$

Table B.1: Values of $p(r_g|\widehat{h}_g)$ for $(k,c)=(2,3)$. The symbol p_b is the probability that the cavity bias takes the value 0.

$|1\rangle$**:** The walker has already vanished.

$|2\rangle$**:** The walker survives and $|\widehat{h}_g|=1$.

$|3\rangle$**:** The walker survives and $|\widehat{h}_g|=0$.

Hence, using the relation (4.92), the transition matrix T can be written as

$$T=\begin{pmatrix} 1 & p_{1,1} & \frac{1}{2}p_{1,0}\times 2 \\ 0 & p_{0,1} & \frac{1}{2}p_{1,0}\times 2 \\ 0 & p_{-1,1} & p_{0,0} \end{pmatrix}, \tag{B.48}$$

where $p_{r_g,\widehat{h}_g}$ represents $p(r_g|\widehat{h}_g)$ and the condition $p_{r_g,\widehat{h}_g}=p_{-r_g,-\widehat{h}_g}$ applies. When $|\widehat{h}_g+r_g|=1$ and $|\widehat{h}_g|=0$, the states $|1\rangle$ and $|2\rangle$ occur with equal probability 1/2, while $|2\rangle$ is always chosen when $|\widehat{h}_g+r_g|=1$ and $|\widehat{h}_g|=1$. This is due to the correlation between $\widehat{h}_g$ and $\delta\widehat{h}_g$. To see this, let us consider the evolutional equations for biases and perturbations. Their explicit forms are

$$\widehat{h}_{g-1}=\mathrm{sgn}\left(J_g(\widehat{h}_g+r_g)\right), \tag{B.49}$$

$$\delta\widehat{h}_{g-1}=\frac{\partial\widehat{h}_{g-1}}{\partial\widehat{h}_g}\delta\widehat{h}_g. \tag{B.50}$$

From eqs. (4.91) and (4.92), we can obtain all possible values of $\widehat{h}_{g-1}$ and $\partial\widehat{h}_{g-1}/\partial\widehat{h}_g$, and summarize the result under the condition $J_g=1$ in Tables B.2 and B.3. A notation $q_g(\pm|u)$ represents the conditional probability for $\mathrm{sgn}\left(\delta\widehat{h}_g\right)=\pm$ under the condition $\widehat{h}_g=u$. Comparing the Tables B.2 and B.3, we can find that when $\widehat{h}_{g-1}=1$, $\delta\widehat{h}_{g-1}=(\partial\widehat{h}_{g-1}/\partial\widehat{h}_g)\delta h_g$ becomes never positive. Similarly, when $\widehat{h}_{g-1}=-1$ holds, $\delta\widehat{h}_{g-1}$ is positive. It is easy to see that these facts hold for $J_g=-1$. Hence, an inequality $\widehat{h}_{g-1}\cdot\delta h_{g-1}\le 0$ is necessarily required, which explains the transition rules between the states $|1\rangle$ and $|2\rangle$.

The matrix T has three eigenvalues: $\lambda_1=1$, λ_2, and λ_3. The eigenvector of the largest eigenvalue $\lambda_1=1$ corresponds to the state $|1\rangle$ or the vanishing state. Hence, the surviving

$r_g \setminus \widehat{h}_g$	1	0	-1
1	1	1	0
0	1	0	-1
-1	0	-1	-1

Table B.2: Values of $\widehat{h}_{g-1}$ with $J_g = 1$.

$r_g \setminus \widehat{h}_g$	1	0	-1
1	0	0 $(q_g(+\|0))$ 1 $(q_g(-\|0))$	1
0	0 $(q_g(+\|1))$ 1 $(q_g(-\|1))$	1	1 $(q_g(+\|-1))$ 0 $(q_g(-\|-1))$
-1	1	1 $(q_g(+\|0))$ 0 $(q_g(-\|0))$	0

Table B.3: Values and probabilities $(q_g(\pm|u))$ of $\partial\widehat{h}_{g-1}/\partial\widehat{h}_g$ with $J_g = 1$.

probability $P_{(G\to 0)}$ is given by $1 - \langle 1|G\rangle$, where $|G\rangle$ is the state of the walker at the G step. For large G, the relevant state is of the second-largest eigenvalue λ_2, and we get

$$P_{(G\to 0)} \approx \lambda_2^G. \tag{B.51}$$

Using the stationary solution (4.75), we obtain $P_{(G\to 0)}$ as a function of $x = e^y$. The AT condition becomes

$$\chi_{SG} \propto \sum_G (k-1)^G (c-1)^G P_{(G\to 0)} \to \infty \Leftrightarrow (k-1)(c-1)\lambda_2 > 1. \tag{B.52}$$

This condition is easily examined numerically and we can verify that the AT instability occurs at $y_{AT} \approx 0.54397$ for $(k, c) = (2, 3)$.

Before closing this section, we give some brief comments on general (k, c). For general c under the case $k = 2$, the evolution equation of the cavity bias becomes

$$\begin{aligned}\widehat{h}_{g-1} = \frac{1}{\beta}\tanh^{-1}\left(\tanh(\beta J_g)\tanh\left\{\beta\left(\widehat{h}_g + \sum_{j=1}^{c-1} r_{g,j}\right)\right\}\right) \\ \to \mathrm{sgn}\left(J_g\left(\widehat{h}_g + \sum_{j=1}^{c-1} r_{g,j}\right)\right) \quad (\beta\to\infty)\end{aligned} \tag{B.53}$$

This equation implies that the table B.3 is modified and becomes a new table between $\widehat{h}_g$ and $r_g = \sum_{j=1}^{c-1} r_{g,j}$. Other discussions are almost the same as the case $c = 3$. Using the notation $p(r_g|\widehat{h}_g) = p_{r_g,\widehat{h}_g}$ and the symmetry $p_{r_g,\widehat{h}_g} = p_{-r_g,-\widehat{h}_g}$ as the $c = 3$ case, the transition matrix T can be written as

$$T = \begin{pmatrix} 1 & \sum_{r=1}^{c-1} p_{r,1} + \sum_{r=2}^{c-1} p_{-r,1} & \sum_{r=2}^{c-1}(p_{r,0} + p_{-r,0}) + \frac{1}{2}(p_{1,0} + p_{-1,0}) \\ 0 & p_{0,1} & \frac{1}{2}(p_{1,0} + p_{-1,0}) \\ 0 & p_{-1,1} & p_{0,0} \end{pmatrix}. \tag{B.54}$$

Note that the term $p_{-2,1}$ in the second column is included in the transition rate from $|2\rangle$ to $|1\rangle$. This is because the inequality $\widehat{h}_{g-1} \cdot \delta h_{g-1} \le 0$ holds in the general c cases. The second largest eigenvalue λ_2 of T determines the AT condition by $(c-1)\lambda_2 = 1$.

For the $k = 3$ case, the update rule of the cavity bias is

$$\widehat{h}_{g-1} = \frac{1}{\beta}\tanh^{-1}\left(\tanh(\beta J_g)\tanh(\beta f_g)\tanh\left\{\beta\left(\widehat{h}_g + \sum_{j=1}^{c-1} r_{g,j}\right)\right\}\right)$$
$$\to \mathrm{sgn}\left(J_g f_g\left(\widehat{h}_g + \sum_{j=1}^{c-1} r_{g,j}\right)\right) \quad (\beta \to \infty), \tag{B.55}$$

where f_g denotes the cavity field coming from the other branch of the tree and r_g again represents $\sum_{j=1}^{c-1} r_{g,j}$. Since the cavity field f_g is uncorrelated with the biases $(\widehat{h}_g, \{r_{g,j}\})$, it is sufficient to consider the correlation among the biases $(\widehat{h}_g, \{r_{g,j}\})$ as eq. (B.47). This fact leads to a similar list to table B.3. Difference between the $k = 2$ and 3 cases appears in the transition matrix. According to eq. (B.55), when the cavity field f_g equals to 0, $\partial\widehat{h}_{g-1}/\partial\widehat{h}_g$ becomes 0 and the walker vanishes independently of the values of $(\widehat{h}_g, \{r_{g,j}\})$. This yields the transition matrix as

$$T = \begin{pmatrix} 1 & 1-(1-p_f)(p_{0,1}+p_{-1,1}) & 1-(1-p_f)\left(\frac{1}{2}(p_{1,0}+p_{-1,0})+p_{0,0}\right) \\ 0 & (1-p_f)p_{0,1} & (1-p_f)\frac{1}{2}(p_{1,0}+p_{-1,0}) \\ 0 & (1-p_f)p_{-1,1} & (1-p_f)p_{0,0} \end{pmatrix}, \tag{B.56}$$

where p_f denotes the probability that the cavity field f_g becomes 0[1]. The second largest eigenvalue of this matrix λ_2 again gives the AT condition by $(3-1)(c-1)\lambda_2 = 1$.

[1]For the $(k, c) = (3, 3)$ case, the probability p_f is already given as the convergent solution of eq. (4.74), or the solid line in fig. 4.16.

Appendix C

Calculations for chapter 5

C.1 Divergence point of the spin-glass susceptibility at zero temperature

Our starting point is the self-consistent equation satisfied by the convergent CBD $\widehat{P}(\widehat{h})$ in the absence of the external field

$$\widehat{P}(\widehat{h}_i) = \int \prod_{j=1}^{c-1} \left(d\widehat{h}_j \widehat{P}(\widehat{h}_j) \right) \left[\delta \left(\widehat{h} - \frac{1}{\beta} \tanh^{-1} \left\{ \tanh \beta J \tanh \left(\beta \sum_{i=1}^{c-1} \widehat{h}_i \right) \right\} \right) \right]_{\boldsymbol{J}}, \quad \text{(C.1)}$$

Analytical assessment of the solution of this equation is possible only at zero temperature as in appendix B.4, which enables us to treat the problem in an analytical manner.

The evolution equation of the cavity bias is given by

$$\begin{aligned} \widehat{h}_{g-1} &= \frac{1}{\beta} \tanh^{-1} \Big(\tanh(\beta J_g) \tanh(\beta(\widehat{h}_g + r_g)) \Big) \\ &\to \begin{cases} \operatorname{sgn}\Big(J_g(\widehat{h}_g + r_g) \Big) & (\ |\widehat{h}_g + r_g| \geq 1 \ ) \\ J_g(\widehat{h}_g + r_g) & (\text{ otherwise }) \end{cases} \quad (\ \beta \to \infty \ ), \end{aligned} \quad \text{(C.2)}$$

where J_g denotes the coupling between sites $g-1$ and g. This relation implies the cavity fields and biases become integers, because we are treating the $\pm J = 1$ model. Hence, the general form of the CBD can be written as

$$\widehat{P}(\widehat{h}) = \sum_{k=-1}^{1} p_k \delta(\widehat{h} - k). \quad \text{(C.3)}$$

For the BL with $c = 3$, eq. (C.1) is rewritten as

$$p_1 = p(p_1^2 + 2p_0p_1) + (1-p)(p_{-1}^2 + 2p_0p_{-1}), \quad \text{(C.4)}$$

$$p_0 = p_0^2 + 2p_1p_{-1}, \quad \text{(C.5)}$$

$$p_{-1} = p(p_{-1}^2 + 2p_0p_{-1}) + (1-p)(p_1^2 + 2p_0p_1). \quad \text{(C.6)}$$

These equations have a ferromagnetic solution for $7/8 \leq p \leq 1$, the explicit form of which is given by

$$p_1 = \frac{4p-3}{2(2p-1)} + \frac{1}{2}\sqrt{\frac{32p^2-52p+21}{(2p-1)^2}}, \tag{C.7}$$

$$p_0 = \frac{1}{2}(2p_1+1) - \frac{1}{2}\sqrt{12p_1^2-4p_1+1}, \tag{C.8}$$

$$p_{-1} = 1 - p_1 - p_0, \tag{C.9}$$

and have another solution $p_{-1} = p_1 = p_0 = 1/3$ for $p < 7/8$, which can be regarded as the RS spin-glass solution.

Equations (C.2) and (C.3) means

$$\left|\frac{\partial \widehat{h}_{g-1}}{\partial \widehat{h}_g}\right| = \begin{cases} 0 & (\ |\widehat{h}_g + r_g| > 1\ ) \\ 0 \text{ or } 1 & (\ |\widehat{h}_g + r_g| = 1\ ) \\ 1 & (\ \text{otherwise}\ ) \end{cases}, \tag{C.10}$$

where the value of 0 or 1 for the case of $|\widehat{h}_g + r_g| = 1$ is determined depending on the value of $\widehat{h}_g$. Equation (C.10) indicates that the assessment of eq. (4.90) is analogous to an analysis of a random-walk which is bounded by absorbing walls. We denote by $P_{(G\to 0)}$ the probability that $\left|\partial \widehat{h}_{g-1}/\partial \widehat{h}_g\right|$ never vanishes during the walk from G to 0 and the value of $\prod_{g=1}^{G} |\partial \widehat{h}_{g-1}/\partial \widehat{h}_g|$ is kept to unity. This indicates that the critical condition at zero temperature becomes

$$\log(c-1) + \lim_{G\to\infty} \frac{1}{G} \log P_{(G\to 0)} = 0. \tag{C.11}$$

To evaluate the surviving probability $P_{(G\to 0)}$, let us formulate this random-walk problem. Since we are now considering the case that the ferromagnetic bias exists, which is different from appendix B.4, we should in principle distinguish the following seven states of the walker at the g-step:

$|1\rangle$**:** The walker has already vanished.

$|2\pm\rangle$**:** The walker survives under the conditions $\widehat{h}_g = 1$ and $\mathrm{sgn}\left(\delta \widehat{h}_g\right) = \pm$.

$|3\pm\rangle$**:** The walker survives under the conditions $\widehat{h}_g = -1$ and $\mathrm{sgn}\left(\delta \widehat{h}_g\right) = \pm$.

$|4\pm\rangle$**:** The walker survives under the conditions $\widehat{h}_g = 0$ and $\mathrm{sgn}\left(\delta \widehat{h}_g\right) = \pm$.

These seven states, however, can be reduced to four states by considering the relation $\widehat{h}_{g-1} \cdot \delta h_{g-1} \leq 0$ which can be derived by the same discussions as in appendix B.4. As a result, the state $|2\pm\rangle$ and $|3\pm\rangle$ are reduced to $|2\rangle \equiv |2-\rangle$ and $|3\rangle \equiv |3+\rangle$, respectively.

On the other hand, when $\widehat{h}_{g-1} = 0$ the sign of $\delta\widehat{h}_g$ does not change with probability p or change with probability $1-p$, which leads to the following equations

$$q_{g-1}(+|0) = pq_g(+|0) + (1-p)q_g(-|0), \tag{C.12}$$
$$q_{g-1}(-|0) = pq_g(-|0) + (1-p)q_g(+|0), \tag{C.13}$$

where $q_g(\pm|u)$ represents the conditional probability for $\mathrm{sgn}\left(\delta\widehat{h}_g\right) = \pm$ under the condition $\widehat{h}_g = u$, which is the same notation as appendix B.4. Under the assumption that the initial perturbation is completely random, we find that $q_g(\pm|0)$ equals to $1/2$ for $\forall g$. Because of this symmetry, we need not to distinguish the states $|4\pm\rangle$ and hereafter write as $|4\rangle$. Considering the above discussions and using the relation (C.10), we can write the transition matrix T of the walker as

$$T = \begin{pmatrix} 1 & p_1 & p_{-1} & \frac{1}{2}(p_1 + p_{-1}) \\ 0 & pp_0 & (1-p)p_0 & \frac{1}{2}(pp_1 + (1-p)p_{-1}) \\ 0 & (1-p)p_0 & pp_0 & \frac{1}{2}(pp_{-1} + (1-p)p_1) \\ 0 & p_{-1} & p_1 & p_0 \end{pmatrix}, \tag{C.14}$$

where T_{ij} denotes the transition probability from $|j\rangle$ to $|i\rangle$. When $|r_g| = 1$ and $\widehat{h}_g = 0$, the probability flow from $|4\rangle$ to $|1\rangle$ exists with the weight $1/2$ while there is no such flow when $r_g = 0$ and $|\widehat{h}_g| = 1$. This is the consequence from the above considerations. This matrix has four eigenvalues $\lambda_1 = 1, \lambda_2, \lambda_3$ and λ_4. The eigenvector of the largest eigenvalue $\lambda_1 = 1$ corresponds to the state $|1\rangle$ or the vanishing state. Hence, the surviving probability $P_{(G\to 0)}$ is given by $1 - \langle 1|g = 0\rangle$, where $|g = 0\rangle$ is the state of the walker at the $g = 0$ step. For large G, the relevant state is of the second-largest eigenvalue λ_2 and $P(G \to 0) \propto \lambda_2^G$, which leads to the critical condition

$$(c-1)\lambda_2 = 1. \tag{C.15}$$

For $c = 3$, this condition is easily examined by using eqs. (C.7)-(C.9) and (C.14). The resultant transition point is $p = 0.92067$, which well agrees with the results given in the main text.

Bibliography

[1] M. A. Ruderman and C. Kittel: Phys. Rev. **96** 99 (1954)

[2] K. Yosida: Phys. Rev. **106** 893 (1957)

[3] S. F. Edwards and P. W. Anderson: J. Phys. F **5** 965 (1975)

[4] T. Taniguchi, H. Matsuyama, S. Chikazawa amd Y. Miyako: J. Phys. Soc. Jpn. **52** 4323 (1983)

[5] S. Nagata, P. H. Keesom and H. R. Harrison: Phys. Rev. B **19** 1633 (1979)

[6] D. Sherrington and S. Kirkpatrick: Phys. Rev. Lett **35** 1792 (1975)

[7] S. Kirkpatrick and D. Sherrington: Phys. Rev. B **17** 4384 (1977)

[8] H. Sompolinsky and A. Zippelius: Phys. Rev. B **25** 6860 (1982)

[9] P. E. Jönsson and H. Takayama: J. Phys. Soc. Jpn. **74** 1131 (2005)

[10] A. Montanari and F. Ricci-Tersenghi: Eur. Phys. J B **33** 339 (2003)

[11] A. Montanari and F. Ricci-Tersenghi: Phys. Rev. B **70** 134406 (2004)

[12] G. Parisi: J. Phys. A **13** L115 (1980) 4384.

[13] G. Parisi: J. Phys. A **13** A 1101 (1980) 4384.

[14] A. P. Young: J. Appl. Phys. **57** 3361 (1985)

[15] E. Vincent: *Lecture notes in Physics* **716** 7-60 (Springer-Verlag, Berlin, 2007)

[16] F. Lefloch, J. Hammann, M. Ocio and E. Vincent: Europhys. Lett **18** 647 (1992)

[17] M. Talagrand: Ann. Math. **163** 221 (2006)

[18] E. Marinari, G. Parisi, F. Ricci-Tersenghi, J. Ruiz-Lorenzo, and F. Zuliani: J. Stat. Phys **98** 973 (2000)

[19] D. S. Fisher and D. A. Huse: Phys. Rev. B **38** 386 (1988)

[20] M. Palassini and A. P. Young: Phys. Rev. lett **85** 3017 (2000)

[21] M. Mézard, G. Parisi, and M. A. Virasoro: *Spin Glass Theory and Beyond* (World Scientific, Singapore, 1987)

[22] J. -L. Barrat et al.: *Slow relaxastions and nonequilibrium dynamics in condenced matter* (Springer-Verlag Berlin Heidelberg, New York, 2003)

[23] F. Sciortino, W. Kob and P. Tartaglia: Phys. Rev. Lett. **83** 3214 (1999)

[24] H. Nishimori: *Statistical Physics of Spin Glasses and Information Processing: An Introduction* (Oxford University Press, Oxford, 2001)

[25] M Mézard and A Montanari: *Information, Physics, and Computation* (Oxford: Oxford University Press, 2009)

[26] C. N. Yang and T. D. Lee: Phy. Rev. **87** 404 (1952), T. D. Lee and C. N. Yang: Phy. Rev. **87** 410 (1952)

[27] D. J. Thouress, P. W. Anderson and R. G. Palmer: Philosophical Magazine **35** 593 (1977)

[28] S. Cocco, R. Monasson and R. Zecchina: Phys. Rev. E **54** 717 (1996)

[29] G. Biroli and R. Monasson: Europhys. Lett. **50** 155 (2000)

[30] M. Mézard and G. Parisi: Euro. Phys. J. B **20** 217 (2001)

[31] D. R. Bowman and K. Levin Phys. Rev. B **25** 3438 (1982)

[32] J. T. Chayes, L. Chayes, J. P. Sethna and D. J. Thouless:Commun. Math. Phys. **106** 41 (1986)

[33] P. Mottishaw: Europhys. Lett. **4** 333 (1987)

[34] J. M. Carlson, J. T. Chayes, L. Chayes, J. P. Sethna and D. J. Thouless: Europhys. Lett. **5** 355 (1998)

[35] P. Lai and Y. Y. Goldschmidt: J. Phys. A **22** 399 (1989)

[36] B. Derrida: Phys. Rev. B **24** 2613 (1981)

[37] R. Monasson: Phys. Rev. Lett. **75** 2847 (1995)

[38] T. Nakajima and K. Hukushima J. Phys. Soc. Jpn. **77** 074718 (2008)

[39] J. R. L. de Almeida and D. J. Thouless: J. Phys. A **11** 983 (1978)

[40] Y. Kabashima: *Replica method and the replica symmetry breaking in single sample systems* (in Japanese), in Proceedings of information physics 1532 (Research Institute for Mathematical Sciences, Kyoto, 2007) p.138, and private communucations

[41] E. Gardner: Nucl. Phys. B **257** 747 (1985)

[42] J. P. Bouchaud, L. Cugliandolo, J. Kurchan, and M. Mézard: Physica A 243 (1996)

[43] M. Opper and D. Saad: *Advanced Mean Field Methods: Theory and Practice* (The MIT Press, Cambridge, Massachusetts, 2001)

[44] A. J. Bray and M. A. Moore: J. Phys. C **13** L469 (1980)

[45] F. Tanaka and S. F. Edwards: J. Phys. F **10** 2769 (1980)

[46] A. Cavagna, J. P. Garrahan and I. Giardina: J. Phys. A **32** 711 (1998)

[47] A. Cavagna, I. Giardina, G. Parisi and M. Mézard: J. Phys. A **36** 1175 (2003)

[48] E. Gardner and B. Derrida: J. Phys. A **22** 1975 (1989)

[49] W. Krauth and M. Mézard: J. Phys. France **50** 3057 (1989)

[50] J. Ardelius and L. Zdeborová: Phys. Rev. E **78** 040101 (2008)

[51] T. Obuchi and Y. Kabashima: J. Stat. Mech. **P12014** (2009)

[52] J. P. Bouchaud and M. Mézard: J. Phys. A **30** 7997 (1997)

[53] A. Braunstein and R. Zecchina: Phys. Rev. Lett **96** 030201 (2006)

[54] H. Horner: Z. Phys. B **86** 291 (1992)

[55] H. Horner: Z. Phys. B **87** 371 (1992)

[56] G. Györgyi: Phys. Rev. A **41** 7097 (1990)

[57] A. Engel and M. Weigt: Phys. Rev. E **53** 2064 (1996)

[58] H. Nishimori: Prog. Theor. Phys. **66** 1169 (1981)

[59] E. Gardner and B. Derrida: J. Phys. A **21** 271 (1988)

[60] H. Akaike: IEEE Trans. on Automatic Control **19** 716 (1974)

[61] E. C. Titchmarsh *The Theory of Functions 2nd. ed.* (Oxford: Oxford University Press, 1939)

[62] J. L. van Hemmen and R. G. Palmer: J. Phys. A **12** 563 (1979)

[63] C. Moukarzel and N. Parga *Physica* A **177** 24 (1991)

[64] C. Moukarzel and N. Parga *Physica* A **185** 305 (1991)

[65] K. Ogure and Y. Kabashima: J. Stat. Mech. (2009) P03010

[66] K. Ogure and Y. Kabashima: J. Stat. Mech. (2009) P05011

[67] T. Obuchi, Y. Kabashima and H Nishimori: J. Phys. A **42** 075004 (2009)

[68] H. Matsuda: Prog. Theor. Phys. **51** 1053 (1974)

[69] E. Müller-Hartmann and J. Zittartz: Z. Physik B **22** 59 (1975)

[70] E. Müller-Hartmann: Z. Physik B **27** 161 (1977)

[71] K. Y. M. Wong and D. Sherrington: J. Phys. A **20** L793 (1987)

[72] M. Mézard and G. Parisi: J. Stat. Phys. **111** 1 (2003)

[73] S. Katsura, S. Inawashiro and S. Fujiki: Physica **99A** 193 (1979)

[74] K. Nakanishi: Phys. Rev. B **23** 3514 (1980)

[75] J. S. Yedidia, W. T. Freeman and Y. Weiss: IEEE Trans. Inform. Theory **51** 2282 (2005)

[76] T. Kadowaki, Y. Nonomura and H. Nishimori: J. Phys. Soc. Jpn. **65** 1609 (1996)

[77] D. J. Thouless: Phys. Rev. Lett. **56** 1082 (1986)

[78] M. Mézard and G. Parisi: J. Physique **46** L771 (1985)

[79] G. Parisi and M. Ratiéville: Eur. J. Phys. B **22** 229 (2001)

[80] O. Rivoire, G. Biroli , O. C. Martin and M. Mézard: Eur. Phys. J. B **37** 55 (2004)

[81] F. Krzakala, A. Montanari, F. Ricci-Tersenghi, G. Semerjian and L. Zdeborova: Proc. Natl. Acad. Sci. **104** 10318 (2007)

[82] O. C. Martin, M. Mézard and O. Rivoire: J. Stat. Mech P09006 (2005)

[83] A. J. Bray and M. A. Moore: J. Phys. C **12** L441 (1979)

[84] Y. Matsuda, M. Müller, H. Nishimori, T. Obuchi and A. Scardicchio: (in preparation)

[85] M. E. Fisher *The Nature of Critical Points (Lectures in Theoretical Physics vol 7C)* (the University of Colorado Press, Boulder,1964)

[86] Y. Ozeki and H. Nishimori: J. Phys. Soc. Jpn. **57** 1087 (1988)

[87] Y. Matsuda, H. Nishimori and K. Hukushima: J. Phys. A: Math. Theor. **41** 324012 (2008)

[88] G. Bhanot and J. Lacki: J. Stat. Phys. **71** 259 (1993)

[89] L. Saul and M. Kardar: Phys. Rev. E **48** R3221 (1993)

[90] P. H. Damgaard and J. Lacki: Int. J. Mod. Phys. **6** 819 (1995)

[91] B. Derrida: Physica A **177** 31 (1991)

[92] R. B. Griffiths: Phys. Rev. Lett. **23** 17 (1969)

[93] P. Y. Chan, N. Goldenfeld, and M. Salamon: Phys. Rev. Lett. **97** 137201 (2006)